Infiltration and Excess Pore Water Pressures in Front of a TBM:
Experiments, Mechanisms and Computational Models

Infiltratie en wateroverspanningen voor een TBM:
experimenten, mechanismen en berekeningen

Tao Xu

Promotor: prof. dr. ir. A. Bezuijen
Proefschrift ingediend tot het behalen van de graad van
Doctor in de ingenieurswetenschappen: bouwkunde

UNIVERSITEIT
GENT

Vakgroep Civiele Techniek
Voorzitter: prof. dr. ir. P. Troch
Faculteit Ingenieurswetenschappen en Architectuur
Academiejaar 2018 - 2019

ISBN 978-94-6355-184-7
NUR 956
Wettelijk depot: D/2018/10.500/102

Members of the examination committee

Chair

Em. Prof. Luc Taerwe, Ghent University, Belgium

Reading Committee

Prof. Wout Broere, Delft University of Technology, Netherlands

Prof. Hans De Backer, Ghent University, Belgium

Prof. Wim Haegeman, Ghent University, Belgium

Prof. Arno Talmon, Delft University of Technology & Deltares, Netherlands

Prof. Markus Thewes, Ruhr University Bochum, Germany

Supervisor

Prof. Adam Bezuijen, Ghent University, Belgium

Acknowledgement

I would like to express my sincere gratitude and appreciation to my supervisor, Prof. Adam Bezuijen, for his expert guidance, continuous encouragement, and selfless support. I learned much about TBM tunnelling practice via the conversation and discussion with him.

Appreciate Prof. Markus Thewes's invitation to work for the second part of this research at Ruhr University Bochum.

Thanks to my examination committee, for their kind helps for improving this thesis.

Thanks to the technicians, Filip and Jan, for their helps for my experiments.

Thanks to the secretaries, Linda and Hilde in Ghent, and Fabiana in Bochum, for their helps for my daily work.

Special thanks go to my friends Zhao in Macau, Xinfeng in Shenzhen and Tongyan and Zhen in Ghent, my research group members and colleagues, Gemmina, Pham, Kristine, Tiago, Ehsan, Hao, Michela, Penglu, Hamzeh, Chenhui, Dongzhu, Quan, Peng (L), Jianguo and Peng (J) in Ghent, and Shengguan, Zdenek, Sascha and Marius in Bochum. Their extensive support and successive encouragement helped me a lot during my research and life.

I would like to thanks to my beloved family and relatives, for their endless love and selfless mental support as always.

The financial support by the China Scholarship Council is sincerely appreciated.

17th December 2018

Ghent

天行健，君子以自强不息！地势坤，君子以厚德载物！

——姬昌

TABLE OF CONTENTS

GLOSSARY OF ABBREVIATIONS

EPB	Earth Pressure Balance
FER	Foam Expansion Ratio
FER_a	Foam Expansion Ratio at atmospheric pressure
FER_m	Effective Foam Expansion Ratio
FER_p	Foam Expansion Ratio at a desired pressure
FIR	Foam Injection Ratio
GHT	Green Heart Tunnel
N/S Line	Amsterdam North/South Metro Line
PPT	Pore Pressure Transducer
TBM	Tunnel Boring Machine

LIST OF NOTATIONS

a	the time at which half the maximum infiltration distance is reached (s)
a	the fitting factor ($m \cdot s^{-0.166}$), Chapter 5
a	the fitting parameter in the VG model (1/cm), Chapter 7
A_s	the cross-sectional area of sand sample (m^3)
A_f	the tunnel face area (m^2)
$\dot{c}$	the hydraulic resistance of the confining layer (s)
c_v	the consolidation coefficient of the clay (m^2/s)
d	the hydraulic pore diameter (m)
d_{10}	the grain diameter of which 10% is finer than (mm)
d_{50}	the grain diameter of which 50 % is finer than (mm)
D_1	the inner diameter of the large cylinder (m)
D_2	the inner diameter of the small cylinder (m)
$d_{particle}$	the mean diameter of sand (m)

g	the acceleration of gravity (m/s^2)
G_s	the specific gravity (-)
h	the matric potential (cm)
H	the height of aquifer (m)
i	the hydraulic gradient (-)
k	the permeability (m/s)
k_b	the permeability of sand for bentonite slurry (m/s)
k_f	the permeability of sand for foam (m/s)
k_w	the permeability of sand for water (m/s)
K_r	the relative permeability (-)
L	the maximum infiltration distance (m)
L_{1s}	the thickness of sand in the large cylinder (m)
L_{2s}	the thickness of sand in the small cylinder (m)
L_b	the length of the bentonite slurry suspension (m)

L_s	the total thickness of sand (m)
m	the fitting parameter in the VG model (-)
m_b	the mass of bentonite (kg)
m_w	the mass of water (kg)
n	the porosity of the saturated sand (-)
n	the fitting parameter in the VG model (-), Chapter 7
n_c	the porosity of the filter cake (-)
n_i	the initial porosity of the fresh bentonite slurry (-)
p	the desired air pressure applied to the foam or soil-foam-mixture (kPa)
p_a	the atmospheric pressure (kPa)
Pe	Peclet number (-)
q	the specific discharge at the tunnel face (m/s)
Q	the discharge (m^3/s)
Q_F	the flow rate of foam (m^3/s)

Q_{FM}	the flow rate of foam in the excavated soil (foaming liquid + residual pore water) (m^3/s)
Q_L	the flow rate of foaming liquid (foaming agent + water) (m^3/s)
Q_{RW}	the flow rate of residual pore water in the excavated soil (m^3/s);
Q_S	the flow rate of excavated soil (m^3/s)
R	the diameter of tunnel (m)
S_s	the coefficient of specific storage (m^{-1})
t	the time (s)
t'	the time of filter cake formation (s)
v_p	the pore fluid velocity (m/s)
v_{TBM}	the advance rate of the TBM (m/s)
V	the volume of pore water that leaves the slurry by pressure filtration (m^3), Chapter 2
V	the volume of water displaced (m^3)
x	the infiltration distance at any time (m)
x_c	the thickness of the filter cake (m)

α	the fitting factor ($2 \leq \alpha \leq 4$)
α	the factor that reflects the effect of infiltrated zone (-), Chapter 7
$\gamma_{particle}$	the specific weight of sand particle (N/m^3)
$\gamma_{suspension}$	the specific weight of slurry suspension (N/m^3)
θ	the angle between the setup and the horizontal plane (°)
λ	the leakage length (m)
μ_a	the apparent viscosity of slurry (Pa)
ρ_w	density of water (kg/m^3)
τ_y	the yield strength of slurry (Pa)
ϕ	the piezometric head at a distance x in front of the tunnel face (m)
ϕ_0	the piezometric head in the sand just beneath the surface of the sand (m)
ϕ_1	the piezometric head in the slurry or foam (m)
ϕ_0	the piezometric head at the tunnel face (m), Chapter 7
ϕ_{mx}	the piezometric head in the excavation chamber (m)

ϕ_∞	the piezometric head far from the tunnel in the soil (m)
ΔL_s	the thickness of sand layer between two adjacent PPTs (m)
Δp	the pressure drop over the sand sample (Pa)
$\Delta \phi$	the difference in piezometric head over the sand (m)
$\Delta \phi'$	the difference in piezometric head between two adjacent PPTs (m)

ABSTRACT

Infiltration and Excess Pore Water Pressures in front of a TBM
Experiments, Mechanisms and Computational models

The Tunnel Boring Machine (TBM) tunneling technique has been developed to construct tunnels that require strict settlement control, for example, in urban areas with a large amount of buildings, historic areas etc., or where the soil is very soft (for example when crossing a river or estuary). When tunnelling with a TBM below the phreatic zone, especially in saturated sandy ground, groundwater flow into the excavation face needs to be impeded. Both stability of the tunnel face and limitation of the groundwater flow are achieved by pressurising the drilling fluid or muck from the excavation chamber of the TBM at the tunnel face. An additional margin for the support pressure is required, depending on the depth of the tunnel, its diameter and the ground conditions.

Due to the pressure difference between the excavation chamber of the TBM and the ground, drilling fluid (slurry or foam) will infiltrate into the ground and thus there will be a flow in front of the tunnel face. In such a situation, part of support pressure applied through the drilling fluid at the tunnel face will be transferred into excess pore water pressure in the ground. As a result, the effective support pressure at the tunnel face and thus the stability of tunnel face will be reduced. The reduction of the effective support pressure depends on the infiltration distance, the infiltration velocity and the drilling speed. However, the infiltration distance of the foam or the slurry, influence of this infiltration on the permeability of the infiltrated ground, and consequently on the excess pore water pressure, are still only partly understood. Finding answers to these questions, therefore, is significantly important for the safety of tunnel.

The purpose of this study is to improve our understanding of the mechanism of drilling fluid infiltration in front of the tunnel face through laboratory experiments, and develop computational models considering such an infiltration process to predict the excess pore water pressures induced by TBM tunnelling. The research concerns both slurry and Earth Pressure

Balance shields (EPB shields). With the results of the experiments, a sounder theoretical basis for the description of infiltration of drilling fluid (slurry or foam), and the computation of excess pore water pressure in front of tunnel face have been established.

In the experiments of infiltration of slurry into the saturated sand, it was found out that the mud spurt (is defined as the process whereby fluid passes through the filtration medium before a filter cake is formed) will stop when an impermeable external filter cake is formed on the sand surface and the infiltration distance during mud spurt is less than 12 cm in the specific experiments in this thesis. The infiltration distance depends on the medium pore diameter, i.e. grain size distribution, as well as properties of the slurry. The permeability of the infiltrated sand is ~ 3×10^5 times lower than the permeability of the original sand. It is essential that the external filter cake makes such a low permeability layer that bentonite particles cannot migrate. When this filter cake is removed and fresh slurry is poured onto the sand surface, and pressure is applied so that the infiltration starts again, there will be two infiltrations before and after removing the filter cake: 1st and 2nd. The infiltration distance in the 2nd infiltration is more or less the same as in the 1st infiltration for low concentrations of bentonite (e.g. 40 and 50 g/l), but is much smaller for high concentrations of bentonite (e.g. 60 g/l). In all cases, the formation of the external filter cake blocks the mud spurt. However, at low concentrations, the mud spurt is much less, than what could occur if there was no external filter cake formation and after removing the external filter cake, the mud spurt starts again until it is again blocked by the internal filter cake. For higher concentrations of bentonite, the mud spurt of the first infiltration is closer to the mud spurt that would occur without external filter cake formation and because there is also some gelling of the bentonite, there will be hardly any further mud spurt and this also prevents the formation of an external filter cake.

Infiltration tests with sand added to the slurry to simulate the spoil of soil in the slurry during the drilling process were performed too. In infiltration of slurry containing sand, there is first mud spurt and after that deep filtration. The bentonite particles and fine sand grains are fixed in the existing sand layer. In this situation, there will a considerable larger infiltration distance than that measured in ‘conventional’ slurry infiltration tests performed with slurry without sand. This is positive for the safety of TBM tunnelling when air intervention is necessary at

the tunnel face, since a low permeable slurry-sand mixture is present over a larger thickness in front of the tunnel face than up to now anticipated based on tests with clean bentonite.

In the experiments of infiltration of foam into the saturated sand, unlike during the infiltration of slurry, no external filter cake will be formed on the sand surface. There will be a low permeable layer formed in the sand. In this layer, the foam bubbles are blocked by the sand grains while the water between the bubbles still flows due to the pressure gradient, resulting in an area with low water content and consequently a low permeability. Like in the slurry experiments, the permeability of the low permeable layer is ~ 2000 times lower than the permeability of the original sand. It was found out that a 'dry' foam (FER (Foam Expansion Ratio) = 20) is not essential for formation of a low permeable layer in the sand, even a 'wet' foam (FER = 5) can form a low permeable layer, because in all cases the water in between the bubbles flows away. The permeability of sand for foam decreased with increasing FER of the foam until FER of approximately 15 in this study. For higher FERs the permeability remains more or less constant.

When adding sand into the foam, as done in the slurry experiments, foam and sand will be deposited on the original sand. There are now 2 sand layers: one of the original sand and one of the deposited sand with a higher porosity. The water permeability of foam-infiltrated sand decreases with increasing air fraction and decreasing liquid fraction with a given solid fraction, or decreases with increasing air fraction and decreasing solid fraction with a given liquid fraction. The permeability of foam-infiltrated sand decreases with Foam Injection Ratio (FIR) and a FIR of 35 - 40 Vol% is recommended for EPB shield tunnelling in sandy soils. Furthermore, with increasing volumetric water content (water fraction), the permeability decreases. The permeability is determined by the water film that is around the bubbles.

Two analytical models are presented to describe the development and decline of the excess pore water pressures in front of a TBM in saturated sandy ground. The first model considers transient flow in a semi-confined aquifer with elastic storage, while the second one assumes different conditions of unconfined steady-state flow governed by the infiltration of slurry into the soil. Based on the experimental data of infiltration of slurry or foam, the input parameters can be obtained, such as, the final infiltration distance, the infiltration distance with time etc.

for the second model. Both models are validated with measurements from the Green Heart Tunnel (GHT) and Amsterdam North/South Metro Line (N/S Line) in the Netherlands. It is shown that both analytical theories can predict the excess pore water pressures in front of slurry shield. The second one seems more appropriate because it reflects the effect of slurry (or foam) infiltration. Furthermore, the measurements seem to indicate that the influence of elastic storage is smaller as assumed in the first theory.

This study has practical consequences for TBM tunnelling in saturated sand:

For drilling with a slurry TBM, the filter cake is beneficial to the stability of tunnel face, but this filter cake is quite thin and thus vulnerable to damage. An external filter cake will not be formed when the density of the slurry is larger than 1100 kg/m^3 or during drilling activity that removes the cake. When a filter cake is formed during a stop in drilling (for example for ring building), this will be almost instantly removed when drilling starts again. When there has been depth infiltration the excess pore water pressures will increase gradually. By measuring the pore water pressure in front of or next to a tunnel face, it is possible to investigate the process that occurs.

During drilling with an EPB shield, the foam bubbles are trapped in the sand grains of the soil-foam-mixture mixture causing a reduction of the permeability. If this is the case, this has consequences when drilling starts after a stop. Most of the low permeable soil will be immediately removed when the cutter head starts drilling.

In most field situations there is no ‘clean foam’ or ‘clean slurry’. In these situations, there is no low permeable ‘foam cake’, but over a larger distance, there is a sand-foam mixture with a low permeability. This is positive for the safety of tunnelling with a TBM when air intervention is necessary at the tunnel face, because it means that a low permeable slurry-sand mixture is present over a larger thickness in front of the tunnel face than up to now anticipated. Determining the necessary support pressure at the tunnel face, it has to be taken into account that this support pressure partly transfers to excess pore water pressure. The analytical models in this study can be used for a first estimation. When it appears that the stability of the tunnel face is critical, additional numerical calculations may be possible.

SAMENVATTING

Infiltratie en Wateroverspanningen voor een TBM

Experimenten, Mechanismen en Berekeningen

De TBM (tunnelboormachine) techniek is ontwikkeld om tunnels te bouwen in gebieden waar slechts een minimale zetting van de grond boven de tunnel is toegestaan, bijvoorbeeld in stedelijke gebieden met een grote hoeveelheid gebouwen, historische gebieden enz., of waar de grond erg zacht is (bijvoorbeeld wanneer de tunnel wordt geboord onder een rivier of estuarium). Bij het boren onder het grondwaterniveau, met name in de verzadigde zandgronden, moet de grondwaterstroming in het graaffront worden belemmerd. Zowel de stabiliteit van het graaffront als een gecontroleerde grondwaterstroming wordt bereikt door de druk van de boorvloeistof of de met schuim geconditioneerde grond in de graafkamer van de TBM te reguleren. Deze dient hoger te zijn dan de waterspanning plus enkele tientallen kPa's (hangt af van de diepte van de tunnel, de diameter en de grondsoort). Vanwege het drukverschil tussen de graafkamer van de boormachine en de grond, zal boorvloeistof (slurry of schuim) in de grond infiltreren en zal er, bij verzadigde grond, dus een grondwaterstroming voor de tunnel zijn. In een dergelijke situatie zal een deel van de ondersteuningsdruk die de boorvloeistof aan het boorfront van de tunnel uitoefent, worden omgezet in wateroverspanningen in de grond. Dientengevolge zal de effectieve steundruk aan het boorfront van de tunnel verminderen en dus de stabiliteit van het boorfront afnemen. De vermindering van de steundruk hangt af van de infiltratieafstand, de infiltratiesnelheid en de boorsnelheid. Maar hoe ver de slurry of schuim in de grond infiltreren, hoe dit de doorlatendheid van de geïnfiltreerde grond verandert en hoe de wateroverspanning wordt beïnvloed, is nog slechts gedeeltelijk bekend. Het vinden van antwoorden op deze vragen is daarom van groot belang voor de veiligheid van een tunnel.

Het doel van deze studie is om het inzicht in de mechanismen van infiltratie van boorvloeistoffen aan het boorfront van de tunnel te verbeteren door middel van laboratoriumexperimenten, en rekenmodellen te ontwikkelen om het infiltratieproces en de

wateroverspanningen geïnduceerd door het boren van een tunnel met een TBM te beschrijven. Het onderzoek heeft betrekking op zowel slurry als EPB-TBM's. Op basis hiervan is een betere beschrijving van de infiltratie van boorvloeistoffen (slurry of schuim) en voor de berekening van de wateroverspanningen voor het boorfront opgesteld.

Bij de infiltratie-experimenten van slurry in verzadigd fijn zand werd gevonden dat de ‘mud spurt’ (gedefinieerd als het proces waarbij de slurry door het filtratiemedium, zand, stroomt) stopt wanneer op het zandoppervlak een ondoordringbare filterkoek gevormd is. In de proeven, met een verschildruk van 50 kPa en uitgevoerd op zand met een d_{50} van 0.15 mm, bleek de infiltratieafstand steeds minder dan 12 cm. De doorlatendheid van het geïnfiltreerde zand is dan ongeveer 3×10^5 keer lager dan de doorlatendheid van het oorspronkelijke zand. Als deze filterkoek verwijderd wordt, een nieuwe slurry op het zandoppervlak wordt gegoten, en de infiltratie opnieuw wordt gestart, zijn er dus twee infiltraties één voor en één na het verwijderen van de filterkoek: de 1e en de 2e. De infiltratie-afstand bij de tweede infiltratie is min of meer dezelfde als bij de eerste infiltratie voor lage concentraties bentoniet (bijvoorbeeld 40 en 50 gr/l), maar is veel kleiner voor hoge concentraties bentoniet (bijvoorbeeld 60 gr/l). Bij lage concentraties bentoniet beperkt de externe filter cake vorming de mud spurt. Wanneer die externe cake wordt verwijderd, kan de mud spurt weer verder gaan. Bij hoge concentraties bentoniet beperkt de externe filter cake ook de mud spurt. Echter, na verwijdering van de externe filter cake, is ook de bentoniet slurry die in het zand zit door gelvorming stijver geworden en blijkt er nauwelijks tot geen verdere mud spurt op te treden.

Als er zand wordt toegevoegd (hetzelfde als waarmee het verzadigde zandmonster gemaakt werd) in de schone suspensie, zal er geen filter cake meer gevormd worden. De mud spurt wordt nu niet belemmerd door de vorming van een externe filter cake en zal daarom dieper in het zandpakket infiltreren. Door voldoende zand toe te voegen (hetzelfde zand als gebruikt om het verzadigde zandmonster te maken) in de schone suspensie, zal er geen externe cakevorming meer zijn. Het zand tussen de bentoniet deeltjes vormt bij infiltratie een korrelskelet boven op het oorspronkelijke zandpakket. Dit voorkomt de grote drukgradiënt over de bentoniet deeltjes die nodig is om een externe filterkoek te vormen. Nadat de mud spurt is gestopt, wordt diepfiltratie waargenomen. Individuele bentoniet deeltjes migreren in

het zandpakket en vullen de nog aanwezige poriën de doorlatendheid van het zand gevuld met bentoniet voor water neemt langzaam af. De grotere infiltratiediepte is positief voor de veiligheid bij het gebruik van TBM's. Wanneer luchtinterventie aan de tunnelzijde noodzakelijk is, aan het boorfront is een laag doorlatend slurry-zand mengsel aanwezig over een grotere dikte dan tot nu toe werd verwacht.

Bij infiltratie experimenten met schuim in verzadigd zand zal, anders dan bij de infiltratie van slurry, geen externe filterkoek op het zandoppervlak worden gevormd. Er zal een slecht doorlatende laag in en op het zand worden gevormd. In deze laag worden de schuimbellen geblokkeerd door de zandkorrels, terwijl in eerste instantie het water van tussen de schuimbellen stroomt. Hierdoor ontstaat een laag met weinig water en met een lage doorlatendheid. Net als bij het met slurry geïnfiltreerde zand, is de doorlaatbaarheid van de met schuim geïnfiltreerde ondoordringbare laag ook veel lager (ongeveer 2000 keer) dan de doorlaatbaarheid van de oorspronkelijke bodem. Er werd gevonden dat een 'droog' schuim (FER = 20) niet essentieel is voor de vorming van een weinig doorlatende laag in het zand, zelfs een 'nat' schuim (FER = 5) kan een weinig doorlatende laag vormen, omdat het water in alle gevallen van tussen de schuimbellen stroomt. De doorlatendheid van zand nam af met toenemende FER van het schuim tot een FER van ongeveer 15 in dit onderzoek. Voor hogere FER's blijft de doorlatendheid min of meer constant. Als er zand in het schuim wordt toegevoegd, zal er, bij een infiltratieproef ook zand en schuimbellen op het oorspronkelijke zandbed komen. Er zijn dan twee zandlagen: het oorspronkelijke zand en het zand uit het schuim dat vaak een hogere porositeit heeft. De doorlatendheid van zand voor waterstroming door het schuim neemt af met toenemende gasfractie en afnemende vloeibare fractie bij een gegeven zand fractie, of neemt af met toenemende gasfractie en afnemende zand fractie bij een gegeven vloeibare fractie. De doorlatendheid van zand voor waterstroming door het schuim neemt af met de FIR en een FIR van 35 tot 40 wordt aanbevolen voor een zanderige ondergrond. Bij een toenemend volumetrisch watergehalte (waterfractie) neemt de doorlatendheid toe. Men kan dus zeggen dat de lucht na de 'schuimspurt' min of meer onbeweeglijk is. De doorlatendheid wordt bepaald door de waterfilm die zich rond de bellen bevindt.

Twee analytische modellen worden gepresenteerd om de ontwikkeling en afname van de wateroverspanningen vóór een TBM in verzadigde zandgrond te beschrijven. Het eerste model beschouwt transiënte stroming in een semi-begrensde watervoerende laag met elastische berging, terwijl de tweede een steady-state stroming veronderstelt, die wordt bepaald door de infiltratie van slurry in de grond. Op basis van de experimentele gegevens van infiltratie van slurry of schuim, kunnen de invoerparameters voor het tweede model worden bepaald, zoals de uiteindelijke infiltratieafstand, de infiltratieafstand met de tijd enz. Beide modellen zijn gevalideerd met metingen van de Groen Hart Tunnel (GHT) en de Noord/Zuid-metrolijn (N/Z Lijn) in Nederland. Aangetoond wordt dat beide analytische theorieën de wateroverspanningen die optreden bij boren met een slurry schild kunnen voorspellen. De tweede theorie lijkt meer geschikt, omdat deze het effect van slurry- (of schuim-) infiltratie weergeeft. Bovendien lijken de metingen erop te wijzen dat de invloed van elastische berging niet zo groot is als in de eerste theorie wordt aangenomen.

Deze studie heeft praktische consequenties voor het boren van een tunnel met een TBM in verzadigd zand:

Voor boren met een TBM-slurry is de filter cake gunstig voor de stabiliteit van het tunnelvlak, maar deze is vrij dun en dus kwetsbaar is voor beschadiging. Een externe filter cake wordt niet gevormd wanneer de dichtheid van de slurry hoger is dan 1300 kg/m^3 of wanneer tijdens het boren de boorsnelheid groter is dan de infiltratiesnelheid. In het laatste geval kan een externe filter cake wel ontstaan tijdens stilstand in het boorproces, bijvoorbeeld wanneer de tunnelringen worden geplaatst.

Wanneer een externe filtercake is gevormd tijdens een boorstop, bijvoorbeeld om een ring te plaatsen, zal deze dunne laag snel verwijderd worden wanneer het boren weer begint en kan de dan waterspanning die dan onstaat voor het boorfront aanleiding geven tot een blow-out. Bij diep-infiltratie zal bij het weer starten van het boorproces de wateroverspanning geleidelijk toenemen. Door het meten van de wateroverspanning voor of naast het boorfront is het dus mogelijk om te zien welk proces optreedt.

Tijdens het boren met een EPB-TBM worden de schuimbellen ingesloten tussen de zandkorrels van het zandige schuimmengsel waardoor de doorlatendheid afneemt. Als dit het

geval is, heeft dit gevolgen wanneer het boren na het stoppen weer opstart. Een groot deel deel van de laagdoorlatende grond zal onmiddellijk worden verwijderd wanneer de snijkop begint te boren.

In de meeste veldsituaties is er geen 'schoon schuim' of 'schone suspensie'. In deze situaties is er geen laag doorlatende 'schuimkoek', er is dan over een grotere afstand een gebied met een lage doorlatendheid. Dit is positief voor de veiligheid van het boren met een TBM, wanneer luchtinterventie nodig is aan de tunnelzijde, omdat het betekent dat een weinig doorlatend mengsel van slurry en zand over een grotere dikte aanwezig is vóór de tunnelzijde dan tot nu toe werd verwacht op basis van experimenten met ‘schoon schuim’.

Bij het bepalen van de druk in de mengkamer, moet rekening gehouden worden met het deel van de druk dat overgaat in wateroverspanning. De analytische modellen in deze studie kunnen worden gebruikt voor een eerste schatting. Wanneer dit kritisch blijkt, kunnen aanvullende numerieke berekeningen nodig zijn.

PART I INTRODUCTION

CHAPTER 1 INTRODUCTION

1.1. BACKGROUND

The human population growth, the urbanization and the increased mobility urge the need for an expanding transport infrastructure. In world's largest cities (more than 1 million population), this will be partly achieved by underground infrastructure. In Europe and North America, systematic underground infrastructures have been set up in largest cities, such as London, Paris and New York. However, in most developing countries, a number of fundamental infrastructures still need to be constructed in the future. As a type of high-capacity public transport, metro is more commonly found in largest cities of these countries. In China, by 2020, according to the National Planning, it is expected that nearly 3000 km new metro lines are to be built up (CURTA, 2016). As a safety, effective method, Tunnelling Boring Machine (TBM) technique, has been widely used in the construction of these metro tunnels in many countries. Apart from these tunnels also high-speed railway tunnels, road tunnels and water tunnels are planned with the TBM technique now.

A TBM, is a machine used to excavate tunnels with a circular cross section through a variety of soil and rock strata. The maximum diameter of TBM is 17.45 metres to date (Fig. 1.1). In soft ground, there are two main types of closed face TBMs: EPB shield and slurry shield. The EPB shield uses the excavated material to balance the pressure at the tunnel face. Pressure is maintained in the cutter head by controlling the rate of extraction of spoil through the screw conveyor and the advance rate. Additives such as bentonite, polymers and foam can be injected ahead of the face to increase the stability of the ground. Additives can also be injected in the cutter head/extraction screw to ensure that the spoil remains sufficiently cohesive to form a plug in the screw conveyor to maintain pressure in the cutter head and restrict water flowing through. In soft ground with very high water pressure, slurry shield is needed. The cutter head is filled with pressurised slurry which applies hydrostatic pressure to the tunnel

face. The slurry also acts as a transport medium by mixing with the excavated material before being pumped out of the cutter head back to a slurry separation plant.

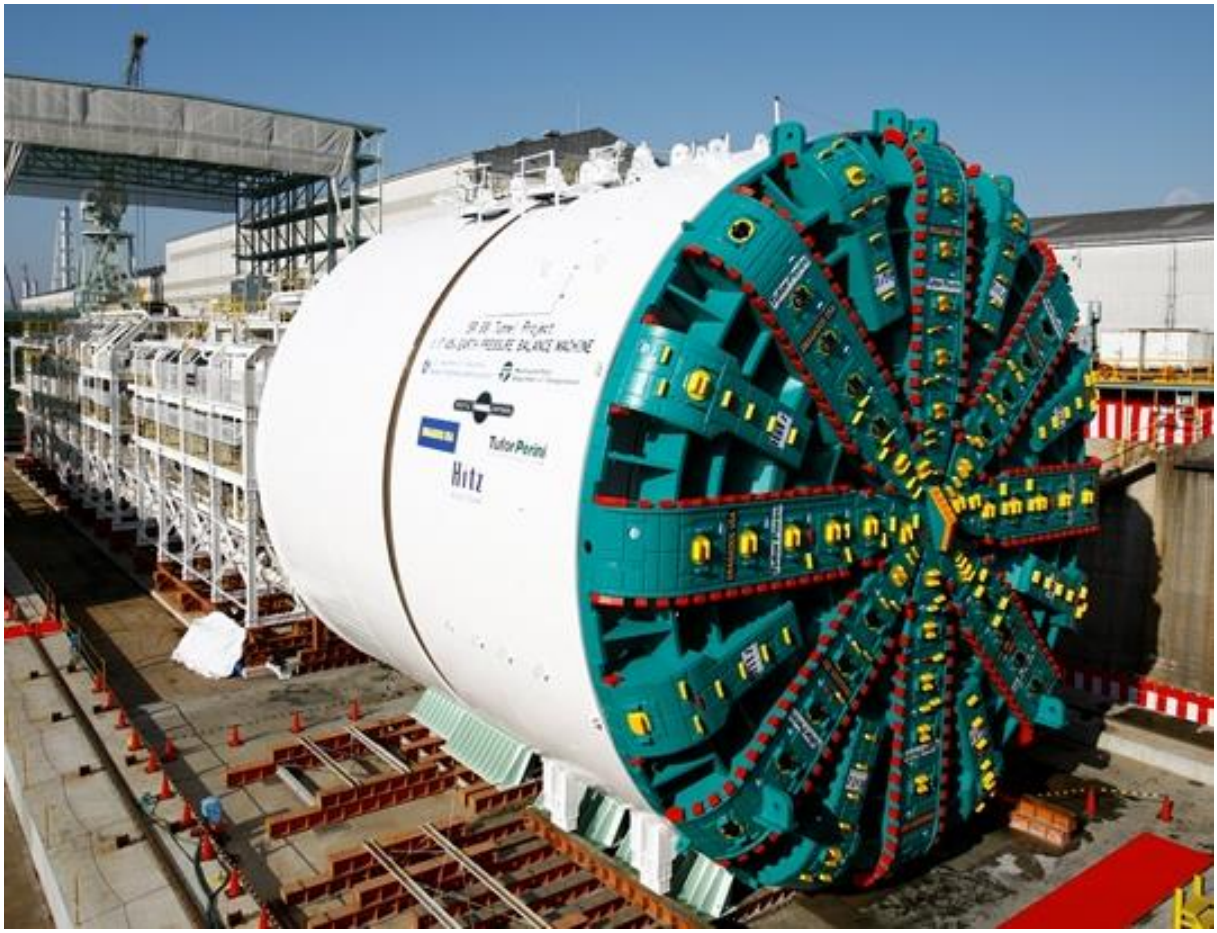

Fig. 1.1. 17.45 m EPB shield tunneling machine for Seattle (Hitachi Zosen Cooperation, 2017).

The metro lines will be built inside largest cities, which are quite often located in deltaic areas, which make it necessary to build these tunnels under the groundwater surface, e.g. in London, New York, Tokyo and Shanghai. When tunnelling with a TBM in these areas, especially in saturated sandy grounds, where the hydraulic pressure is extremely high, and the groundwater flow inward the excavation chamber of the TBM may lead to the collapse of the tunnel face. How to prevent the groundwater flow into the excavation chamber therefore is of great importance. More knowledge on the mechanisms that determine groundwater flow into the excavation chamber and thus the failure of tunnel face will lead to a better estimation of

the failure and ways to reduce the failure. It also helps to reduce the risk on larger failures that may occur during tunnel construction.

1.2. MOTIVATIONS

In practice, pressurised drilling fluid (slurry or foam) is used to prevent the groundwater flow into the excavation chamber when tunnelling with a TBM in saturated sandy soils. In this situation, the pressure in the excavation chamber will be larger than the water pressure in the soil. The drilling fluid (slurry or foam) will therefore infiltrate into the soil and thus there will be a flow in front of the tunnel face. One of the findings from the existing tunnel projects is that part of support pressure applied through the drilling fluid will transfer into excess pore water pressures in the soil due to this flow (COB, 2000; Bakker and Bezuijen, 2008; Kaalberg, et al., 2014). The flow therefore reduces the effective support pressure at the tunnel face and hence the stability of tunnel face. The magnitude of the excess pore water pressure therefore becomes of importance for the stability of the tunnel face. The analytical models of excess pore water pressure induced by TBM tunnelling in an aquifer have been developed by Broere (2001), Bezuijen (2001) and Bezuijen et al. (2016). Broere's model considers transient flow in a semi-confined aquifer with elastic storage, while Bezuijen's model assumes different conditions of unconfined steady-state flow governed by the infiltration of slurry into the soil in front of the tunnel face. But the difference between these models, and most importantly, how the elastic storage of the aquifer and the infiltration determine the development of the excess pore water pressure, have not been addressed. It was also found out that the reduction of the support depends on the infiltration distance and the infiltration velocity (Anagnostou and Kovári, 1994; Bezuijen, 2001). However, the infiltration distance of the foam or the slurry, influence of this infiltration on the permeability of the infiltrated soil, and consequently on the excess pore water pressure, are still only partly understood.

All of these issues need attention in order to improve the safety of the tunnels. Therefore, experiments on slurry and foam infiltration have to be carried out. Based on the data obtained from these experiments, the models of predicting the excess pore water pressure considering

the infiltration can also be established. It is hopeful that this research will contribute to improve the safety of the tunnels in the future.

1.3. OBJECTIVES

In this thesis, the shield of a real TBM will not be modelled. What will be modelled is the infiltration of slurry and foam that is expected in front of a TBM. This research aims to clarify the mechanisms of drilling fluid infiltration in front of both slurry and EPB shields through laboratory experiments, establish computational models for predicting the excess pore water pressures induced by drilling fluid infiltration, and find out how the flow will affect the stability of tunnel face.

Through the laboratory experiments of infiltration of drilling fluids (slurry and foam) into the saturated sand, the mechanisms of both the slurry infiltration for slurry shield and foam infiltration for EPB shield from the experimental data will be clarified.

Apart from the experiments of infiltration, two existing one-dimensional flow models, one considers the pore water pressure by elastic storage and another takes into account the effect of infiltration of slurry or foam, that calculate the excess pore water pressures in front of the TBM are aimed to validate by existing field measurements. The differences among these models and their limitations will also be gained.

This research will also be a good overview of different mechanisms encountered in TBM tunneling and the consequences for the practice of tunneling.

1.4. ORGANIZATION OF THE THESIS

There are totally 8 chapters followed to Chapter 1. Chapters 3, 4 and 7 are the result of published articles.

In Chapter 2, an experiment of infiltration of bentonite slurry in a conventional setup will be performed. A new concept for the mud spurt of bentonite slurry will be proposed. Then the experimental data will be analyzed with the new concept.

In Chapter 3, a modified setup that can provide a comparable hydraulic gradient as in a real tunnel will be introduced, as well as the principle of the pressure infiltration of bentonite slurry into the saturated sand. The new concept in Chapter 2 will also be interpreted with this modified setup.

In Chapter 4, following the experiments in Chapter 3, the experiments of infiltration corresponding with the drilling of TBM and the filter cake formation under various conditions will be presented. A set of experiments simulate the removal of the filter cake formed at the tunnel face. The experimental data obtained before and after removing the filter cake will be analyzed and discussed. Another set of experiments deals with the infiltration of slurry containing sand. These experiments are performed because the excavated soil will be carried into the excavation chamber in real TBM tunnelling and hence the density of slurry will increase. The consequences of these two sets of experiments for the practice will also be discussed.

The former two chapters deal with the slurry TBM. In next two chapters, the EPB TBM will be focused on. Chapter 5 presents the experiments on infiltration of pure foam and Chapter 6 the experiments on infiltration of foam from soil-foam-mixture into saturated sand. The same setup as used in the experiments in Chapter 3 and 4 will be used in the experiments in Chapters 5 and 6.

In Chapter 7, two one-dimensional flow models will be presented: one considering the elastic storage and another taking into account the effect of infiltrated zone. The values predicted by both the models will be compared to the measurements of pore water pressures from two tunnels in semi-confined aquifers. The difference between the two models will also be shown.

In Chapter 8, the conclusions from Chapters 2 to 7 will be presented. The future research will also be recommended.

PART II EXPERIMENTS ON SLURRY INFILTRATION

Pressurised slurry has been extensively used as a drilling fluid to support the face of slurry shield-driven tunnels, specifically in saturated sandy soils. The face stability of slurry shield-driven tunnels depends on the effective support pressure applied through the slurry at the face. Without proper face support, the face may collapse or an uncontrolled and unobserved over excavation may occur over parts of the project, both leading to possible large settlements at the surface (Bezuijen and Talmon, 2008; Broere, 2016). The slurry pressure in the excavation chamber, therefore, must be maintained within predetermined boundaries, to prevent seepage flow, face collapse or blow-out (Broere, 2016). Anagnostou and Kovári (1994) suggested that the slurry pressure must be higher than the pore water pressure in the soil in order to prevent a seepage flow towards the excavation face and for cohesionless soil this is the only way to get a stable excavation face. However, a higher slurry pressure will lead to slurry infiltration into the surrounding soil. Both field research (Bezuijen et al., 2006) and theoretical research (Broere & van Tol, 2000) indicate that the slurry infiltration into soil reduces the effective support pressure at the face. This situation has been found at some tunnel excavations, e.g. the GHT and the N/S Line in the Netherlands (Bakker and Bezuijen, 2008; Kaalberg, et al., 2014). Xanthakos (1979) and Anagnostou and Kovári (1994) demonstrated that the effectiveness of slurry support essentially depends on the infiltration distance into the soil. A larger infiltration distance leads to a lower effective support pressure, and hence a more unstable condition of the face. A larger support pressure is therefore required to stabilise the tunnel face (Bezuijen et al., 2006; Zizka & Thewes, 2016). Other research (COB, 2000; Bezuijen et al., 2006; Zizka and Thewes, 2016) has shown that in saturated sand even limited infiltration will induce excess pore water pressures, decreasing the tunnel face stability. COB (2000), Bezuijen et al. (2006) and Zizka and Thewes (2016) also demonstrated that, due to the infiltration, the support pressure is not transferred directly onto the soil skeleton, but gradually transformed. This is the situation for a permeable soil with significant slurry infiltration. The part of the support pressure that is not transformed to effective stress is present as an excess pore water pressure (compared to the hydrostatic stress) in soil. Consequently, the support

pressure is only partly available to stabilise the tunnel face. This support therefore cannot be simplified as a membrane pushing against the tunnel face, but that during drilling the support pressure can come from a combination of effective support pressure and pore water pressure (Anagnostou & Kovári, 1994; Bezuijen et al. 2006; Bezuijen et al. 2016; Thewes et al., 2016).

Bezuijen et al. (2016) indicate that what kind of support (effective support pressure or pore water pressure) dominates depends on the drilling velocity, the permeability of the soil in front of the tunnel, the porosity of that soil, the diameter of the tunnel, and the infiltration properties of the bentonite slurry. If the infiltration velocity is lower than the drilling velocity, bentonite slurry will only infiltrate over a small distance. Each time a tooth of the cutting wheel passes all bentonite will be removed from that location and the bentonite starts to infiltrate again into the soil at that location. This leads to a continuous flow of slurry into the soil as long as the TBM is drilling. This flow can only exist if there is also a groundwater flow, resulting in an excess pore water pressure. It was shown by Bezuijen et al. (2006) and Broere (2001) that such a groundwater flow leads to a lower effective support pressure, and hence a more unstable condition of the tunnel face. If the infiltration is faster than the drilling, the slurry will infiltrate into the soil in front of the cutting wheel (Bezuijen et al., 2016) and the excess pore water pressure will be lower. The infiltrated slurry is of importance for the face stability of slurry shield-driven tunnel, as it directly transfers the support pressure onto the soil skeleton.

CHAPTER 2 PRESSURE INFILTRATION OF SLURRY, IN A CONVENTIONAL SETUP

The infiltration of bentonite slurry, pressurised against saturated sand, has been investigated in a laboratory setup, to improve the understanding of the mechanisms of two phases of infiltration: mud spurt and filter cake formation. The permeability of sand for bentonite slurry (k_b), the permeability of filter cake for water (k_c) and the Peclet number (Pe) at initiation of filter cake formation were calculated from the experimental results. It appears that the values of k_b and k_c depend on the concentration of bentonite. Adding bentonite to the slurry decreases both k_b and k_c. The estimated Pe is a bit higher than the expected value. It was also found out that filter cake is only formed on the surface of the sand, thus is very vulnerable to damage.

2.1. INTRODUCTION

As pointed out by Talmon et al. (2013), the infiltration process of bentonite slurry in front of the face of shield tunnel is divided into two distinct phases: the mud spurt phase and the filter cake formation phase. They performed slurry infiltration tests, comparable to the ones described later in this chapter, applying a constant pressure on the slurry and measuring how fast the slurry infiltrates into the sand and to what depth. A typical course of discharged fluid in their tests is shown in Fig. 2.1. The volume of displaced fluid (V) was plotted with respect to square root of time ($\sqrt{t}$) rather than time (t) because the displaced fluid in both the initial mud spurt and the subsequent consolidation is, according to theory, proportional to the square root of time. Plotting against square root of time will result in two more or less straight lines as shown in Fig. 2.1. The line just after $t = 0$ represents the phase of mud spurt, which is followed by the phase of filter cake formation (i.e. “consolidation” in Fig. 2.1).

Talmon et al. (2013) suggested that the inflection point between mud spurt and filter cake formation is determined by the Peclet number (Pe), which is defined as the ratio of the time scale of changes in flow velocity and the time scale of consolidation. Since between $1 < Pe$

<10 there is a transition between drained and undrained behaviour of the bentonite in the mud, the filter cake will be formed when $Pe < 10$ (Winterwerp & van Kesteren (2004) and the clay particles have a lower velocity than the water and start to form agglomerates. It was only verified through the result of displaced fluid by Talmon et al. (2013). Hence, further experiments are necessary to confirm its applicability.

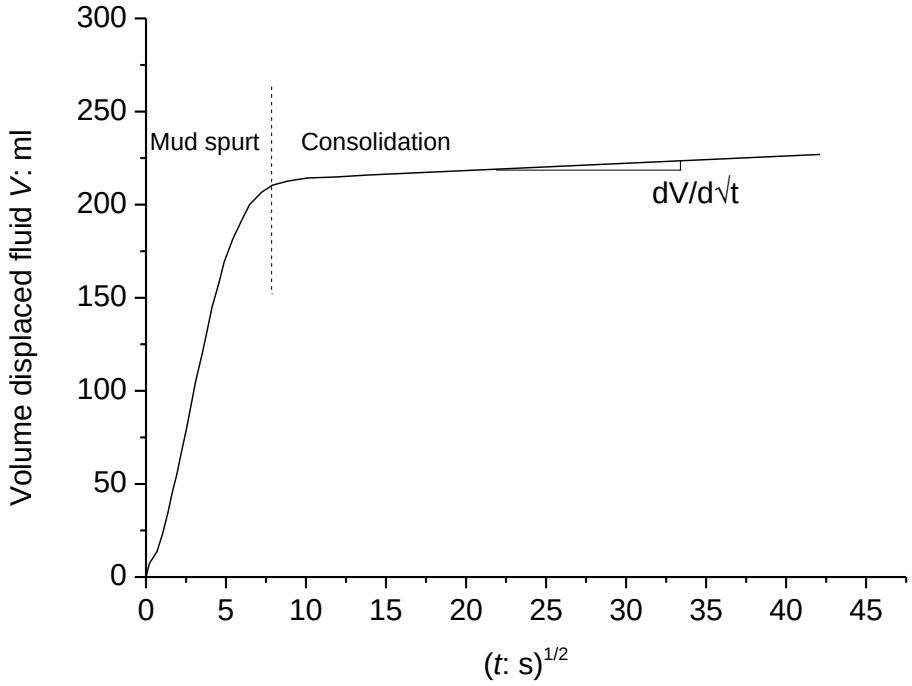

Fig. 2.1. Typical course of displaced fluid in an infiltration test. (Modified after Talmon et al., 2013).

To calculate the infiltration distance during mud spurt, Krause (1987) proposed an empirical time-dependent function. However, Huisman (1998) and Bezuijen et al. (2016) have shown that an empirical constant in this model, is not a real constant, but depends on the setup of the experiments, this was proven experimentally in Chapter 3. Therefore, a more accurate model is needed. Moreover, studies with bentonite grout have described the process of filter cake formation through consolidation theory (Bolton & McKinley, 1997; McKinley & Bolton, 1999; Bezuijen et al., 2009), which indicates the possibility that the same strategy could be used for cases with bentonite slurry.

To study the details of this infiltration process, a series of infiltration tests have been performed. To interpret these tests, a new concept for mud spurt was developed. The test results will be used to check whether it is more accurate than the existing model. The permeability of sand for bentonite slurry (k_b) and the permeability of filter cake for water (k_c) calculated from the test results will be used to interpret the mechanisms of mud spurt and filter cake formation. The results of k_b will be used to further examine the applicability of the *Pe*.

'Infiltration' is defined as the replacement of the original pore water with the mixture in front of the sand (slurry water, bentonite particles), rather than the visual slurry front. The last distance will be less than the first.

2.2. EXISTING THEORIES

2.2.1. PECLET NUMBER

According to Talmon et al. (2013) there is an undrained behaviour in the slurry during mud spurt and a drained behaviour during external cake formation. The transition is determined by the Peclet number (*Pe*), which they define for this situation as:

$$Pe = \frac{v_p d}{c_v} \tag{2.1}$$

Where v_p is the pore fluid velocity (m/s); d the hydraulic pore diameter (m) and c_v the consolidation coefficient of the clay (m^2/s). The hydraulic pore diameter d can be calculated approximately as (Talmon et al., 2013):

$$d = \frac{2}{3}\frac{n}{1-n} d_{15} \tag{2.2}$$

With n the porosity of the soil (-) and d_{15} the 15% percentile of the grain size distribution (m).

The final invasion depth is quantified by an empirical determined relation with the time scale of filter cake formation, time scale of mud invasion and theoretical maximum invasion depth of mud spurt. Following Winterwerp and Van Kesteren (2004), Talmon et al. (2013) assume that undrained behaviour can be expected as long as $Pe > 10$. This would mean that a change

in the slurry velocity implies a change in the slurry infiltration before the cake formation starts. This has consequences for practice since the slurry velocity in laboratory tests is usually much larger than in the field, as will be explained in the next section. A lower slurry velocity in the field compared to the laboratory would mean that also the internal cake is thinner in the field, since the flow velocity decreases during the mud spurt and the situation that $Pe < 10$ is reached after less slurry infiltration than could be assumed based on laboratory tests. A thinner cake means that it is more vulnerable when repairs at the TBM are carried out under air pressure.

2.2.2. MODEL FOR MUD SPURT

Different descriptions have been used to calculate the infiltration distance as a function of time. A well-known one is (Krause, 1987; Broere, 2001):

$$x = \frac{t}{a+t} L \tag{2.3}$$

Where x is the infiltration distance in time (m); t (s) the time, L the maximum infiltration distance (m) and a the time at which half the maximum infiltration distance is reached (s).

According to Huisman (1998), the empirical timespan a can be linked with the different parameters in the setup with a determined value of the maximum infiltration distance L (m) from a column infiltration test:

$$a = \frac{L}{\frac{k_w}{n}\left[\frac{\Delta p}{\rho_w g L_s} + \left(1 + \frac{L_b}{L_s}\right)\sin(\theta)\right]} \tag{2.4}$$

Where k_w is the permeability of the saturated sand sample (m/s), ≈ 4.00×10^{-4} m/s for Mol 32 sand; n the porosity of the sand (-), = 0.37 for Mol 32 sand; Δp the pressure drop over the sand sample (Pa), = 5.00×10^5 Pa in the setup in Fig. 2.2; ρ_w density of water (kg/m^3); g gravitational acceleration (m/s^2); L_b the length of the bentonite slurry suspension (m), = 0.10 m in the setup in Fig. 2.2; L_s the thickness of the sand sample (m), = 0.17 m in the setup; θ the angle between the setup and the horizontal plane (°), = 90° in the setup in Fig. 2.2.

The theoretically maximum infiltration distance L can be estimated through (Broere, 2001):

$$L = \frac{\Delta p d_{10}}{\alpha \tau_y} \tag{2.5}$$

Where d_{10} is the grain diameter (m) of which 10% is finer than d_{10}, = 1.25 × 10^{-3} m for Mol 32 sand; α the fitting factor ($2 \leq \alpha \leq 4$), = 3 in this thesis; τ_y (Pa) the yield stress of slurry, see also Table 2.1.

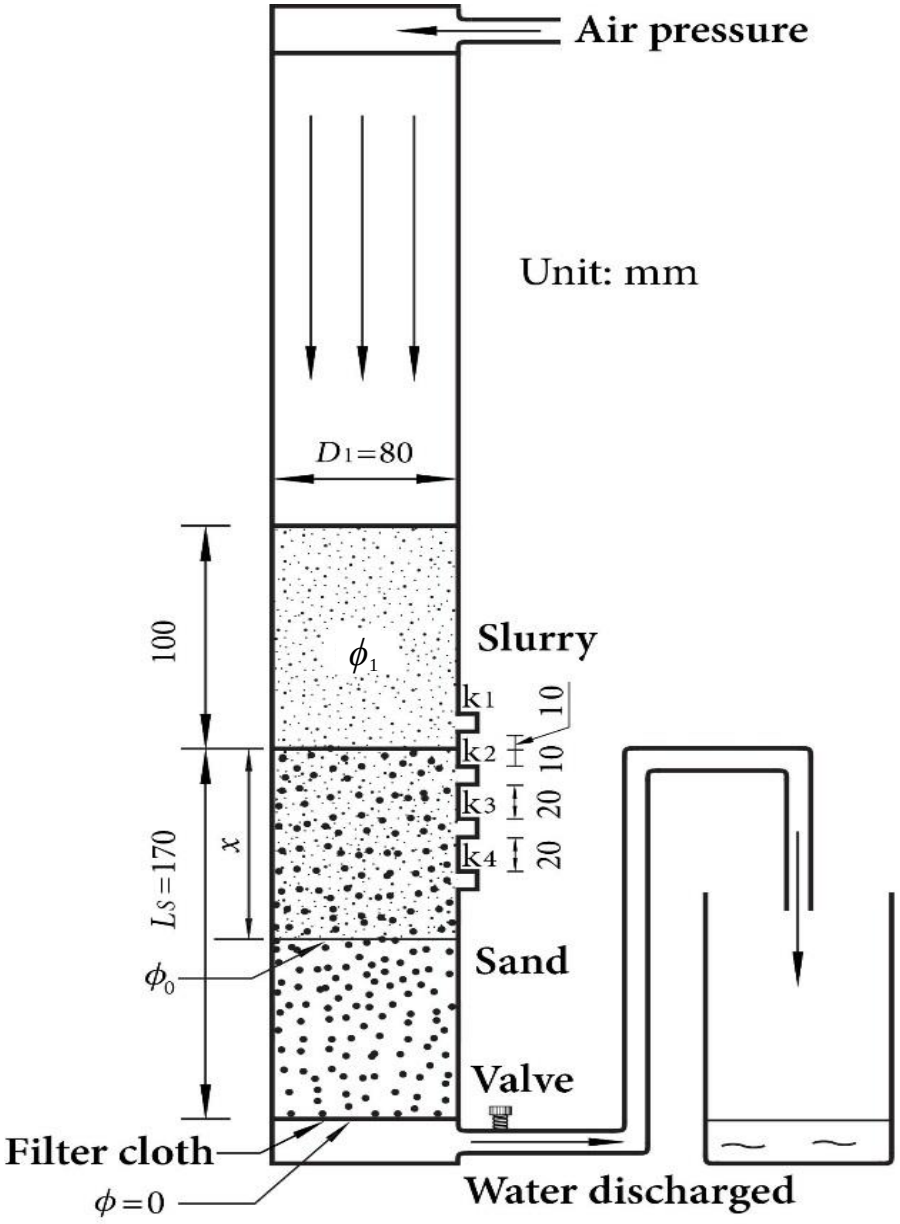

Fig. 2.2. Principle of pressure infiltration of bentonite slurry.

The final infiltration distance in many experiments (see Fig. 2.3) is significantly smaller than the theoretical maximum infiltration distance according to Eq. (2.5). According to Talmon et al. (2013) this may be because, in the majority of the experiments, the mud spurt is stopped by the external filter cake formation before the infiltration distance L is reached. This occurs specifically in fluids with low yield stresses, e.g. low concentration sodium bentonite fluids, for which the infiltration in sand is dominated by the external filter cake formation.

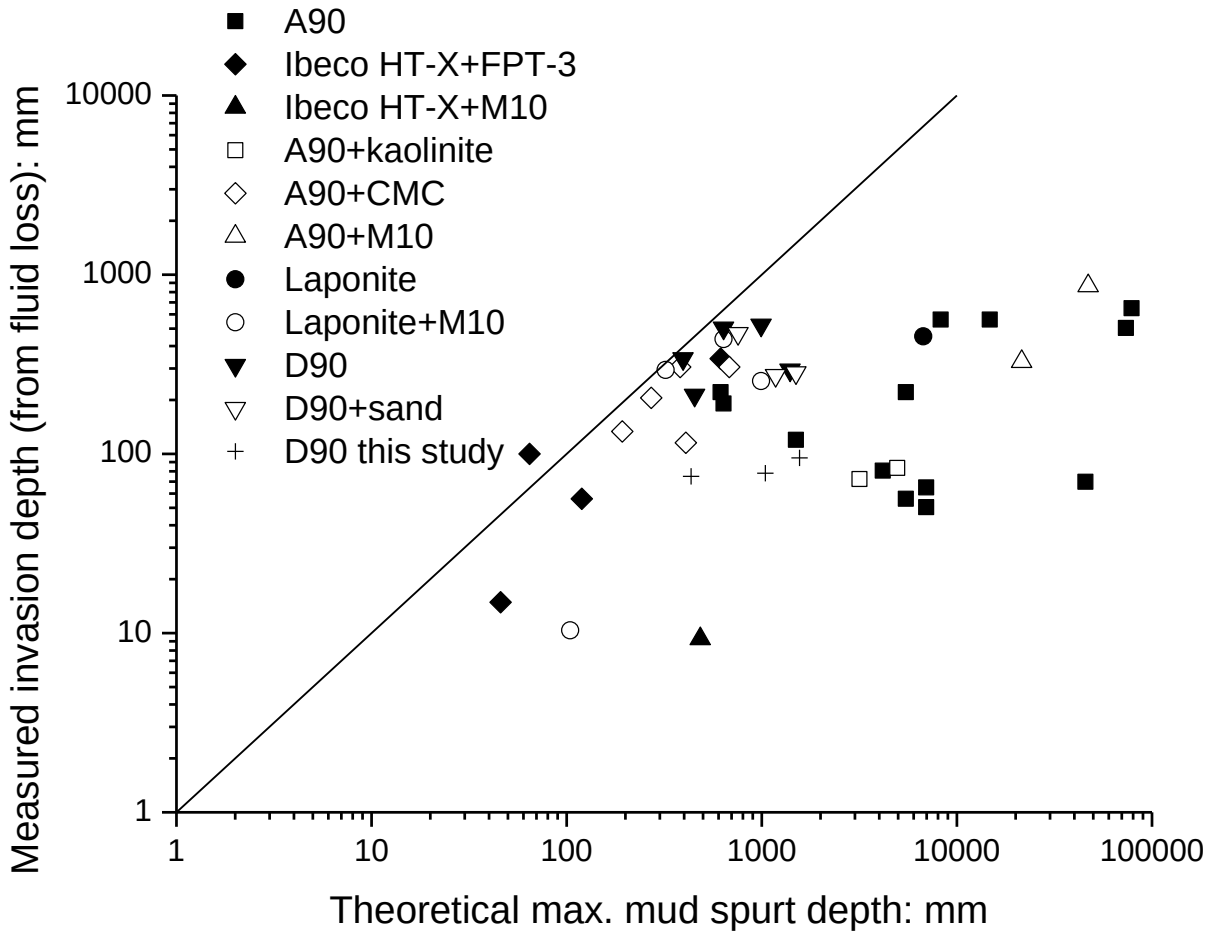

Fig. 2.3. Measured bentonite invasion depth versus theoretical maximum invasion depth mud spurt (i.e., at $t = \infty$). (Modified after Talmon et al., 2013).

2.2.3. Model for filter cake formation

The consolidation of bentonite grout has been described by Mckinley & Bolton (1999) and Bezuijen et al. (2009). As the expression in Bezuijen et al. (2009), using the porosity instead

of void ratio, the thickness of the filter cake due to drainage of the bentonite slurry subjected to a constant pressure gradient can be written as a function of the time of filter cake formation (t'):

$$x_c = \sqrt{2k_c\left(\frac{1-n_i}{n_i-n_c}\right)\Delta\phi \cdot t'} \tag{2.6}$$

Where x_c is the thickness of the filter cake (m); k_c the permeability of the filter cake for water (m/s); n_i the initial porosity of the fresh bentonite slurry (-); n_c (assumed uniform) the porosity of the filter cake (-); $\Delta\phi$ the difference in piezometric head (m) over the grout (but in my application over the filter cake of the bentonite slurry). The thickness of the filter cake can be back calculated by:

$$\frac{V}{A_s} = \left(\frac{n_i-n_c}{1-n_i}\right)x_c \tag{2.7}$$

Where V is the volume of pore water that leaves the slurry by pressure filtration (m^3), and A_s is the area of the sample (m^2).

2.3. IMPROVED MODEL BY CONSIDERING PROPERTIES OF SLURRY AND SOIL

An improved model based on the groundwater flow equations rather than the empirical results as Krause (1987), is developed. Assume the situation sketched as in Fig. 2.2; the difference in piezometric head over the sand is $\Delta\phi$ (m), and the piezometric head in the sand just beneath the surface of the sand is ϕ_0 (m). The relation between $\Delta\phi$ and ϕ_0 can be written as:

$$\Delta\phi = \phi_0 + \frac{nv_p}{k_b}x + \frac{\Delta\phi}{L}x \tag{2.8}$$

Where x (m) is the infiltration distance in any time; v_p (m/s) the pore fluid velocity; k_b (m/s) the permeability of sand for the bentonite slurry. The formula does not take into account the external filter cake formation but only the mud spurt.

The flow in the sand beneath the slurry surface in the sand can be described according to Darcy's law as:

$$\phi_0 = \frac{nv_p}{k_w}(L_s - x) \tag{2.9}$$

With L_s the thickness of sand sample (m), k_w the permeability of sand for water (m/s). The values of v_p are the same in the mud spurt zone and in the sand. This assumes incompressibility, or equal compressibility, and equal porosity of the materials. Also, no impact of slurry infiltration on the porosity is assumed. If the volume of water displaced V (m^3) is known, the infiltration distance then can be calculated by:

$$x = \frac{V}{n \cdot \pi (D_1 / 2)^2} \tag{2.10}$$

With D_1 the diameter of the cylinder (m). Combination of Eq. (2.8) and (2.9), and with $v_p = dx/dt$, we gain:

$$\frac{dx}{dt} = \frac{\Delta\phi\left(1 - x / L\right)}{n\left(L_s - x\right) / k_w + nx / k_b} \tag{2.11}$$

With t the mud spurt time (s).

Integration of Eq. (2.11) leads to:

$$t = -\frac{nL}{\Delta\phi}\left[\left(\frac{L_s - L}{k_w} + \frac{L}{k_b}\right)\ln\left(1 - \frac{x}{L}\right) + x\left(\frac{1}{k_b} - \frac{1}{k_w}\right)\right] \tag{2.12}$$

The formulas above are only valid for the phase of mud spurt. When the bentonite slurry starts to consolidate due to cake formation, the flow will be impeded due to the resistance of the filter cake. The properties of filter cake, such as the permeability (k_c) for water, will control the flow. To address this issue, a related theory that possibly describes the consolidation of bentonite slurry is introduced in next section.

2.3. EXPERIMENTAL STUDY

The objectives of this experiment are: (a) to identify the mechanism of mud spurt and filter cake formation through the measured permeability of sand for the bentonite slurry k_b, (b) to find which mud spurt theory is more accurate to estimate the infiltration distance in time, (c) to confirm the applicability of the Peclet number (Pe) and whether it is comparable to the result of k_b when the filter cake starts to be formed.

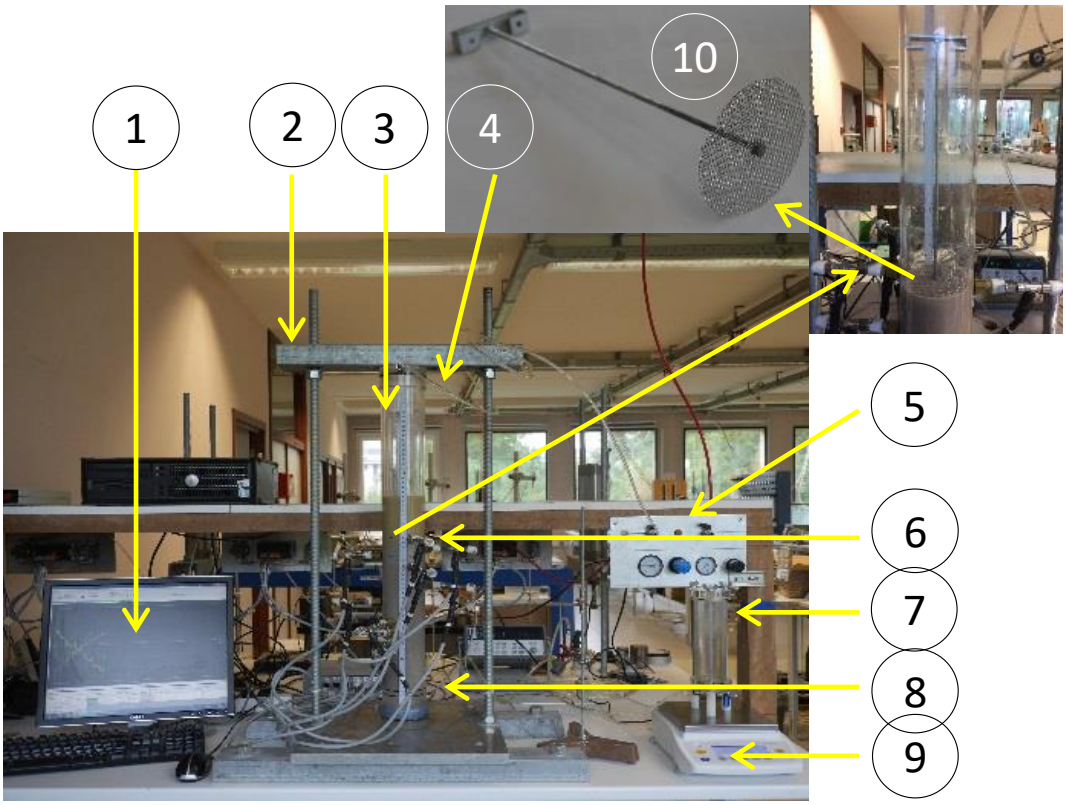

Fig. 2.4. The modified setup. 1. Recording system; 2. Loading frame; 3. PMMA cylinder; 4. Air inlet tube; 5. Air supply system; 6. Pore pressure transducers; 7. Container of discharged water; 8. Water outlet tube; 9. High frequency digital scale; 10. Device of removing the filter cake.

2.3.1. SETUP

The principle of the setup has been shown in Fig. 2.2. Fig. 2.4 shows a picture of the setup. By a valve on the top cap, a constant air pressure was applied on the slurry. Four Honeywell-

26PCCFG6G PPTs (Pore Water Pressure Transducers) numbered k1 to k4 with pressure range of 0 - 100 kPa were installed on the side of the poly (methyl methacrylate) (PMMA) cylinder to measure the pore water pressures in the slurry and sand. PPT k1 was positioned 10 mm above the slurry-sand interface, while k2, k3 and k4 at 10, 30 and 50 mm below the interface, respectively. A filter cloth was placed on top of a perforated plate a few centimeters above the bottom of the PMMA cylinder to avoid that the sand was washed out. The amount of discharged water was measured continuously with an electronic balance. During a test, all data were measured with a frequency of 1 Hz.

2.3.2. TEST MATERIALS

The test materials and the sample preparation procedures in Chapters 2 to 4 are the same. The bentonite and sand used for the experiments of slurry infiltration in were Colclay D90 bentonite, a sodium-activated calcium bentonite which contains more than 85% of montmorillonite, and Sibelco Mol32 sand, a uniform medium fine sand with a d_{15} = 130 μm and d_{50} = 0.154 mm is a poorly graded sand with and permeability, $k_w \approx 4 \times 10^{-4}$ m/s. The grain size distribution curves of Colclay D90 bentonite and Sibelco Mol32 according to the ASTM Unified Soil Classification System (2006) sand are shown in Fig. 2.5.

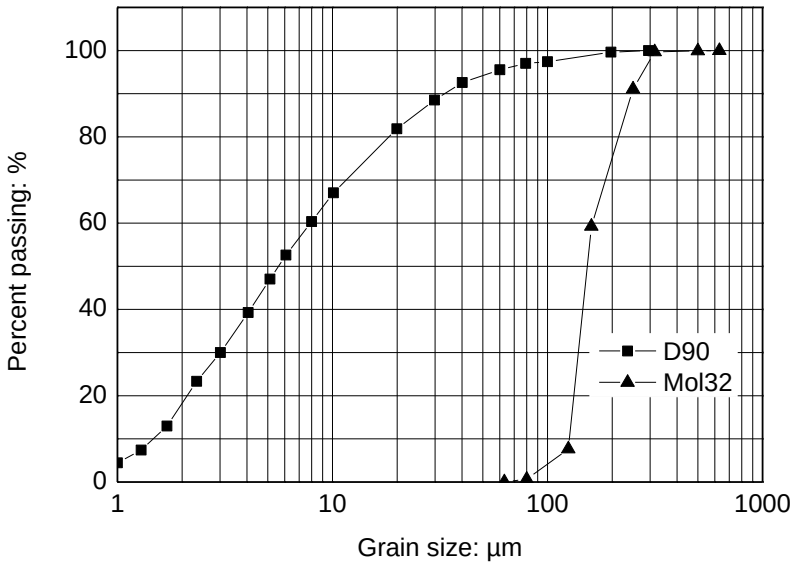

Fig. 2.5. Grain size distribution of Sibelco Mol32 sand (determined by me) and Colclay D90 bentonite (Talmon et al., 2013).

The properties of the bentonite slurry in each test were determined using a Fann Model 35 roto viscometer. Three slurries with various concentrations of bentonite (40, 50 and 60 g/l) were tested. For each test, a 350 ml sample of pre-stirred slurry was added to the cup of the viscometer. All measurements were carried out at the constant temperature of 20 ± 1°C. For each shear rate, the shear stress was recorded when the value of the dial was stable. The flow curves that determined the properties of slurries with various concentrations are shown in Fig. 2.6. The slurry is assumed as a Bingham liquid. The results are shown in Table 2.1.

Table 2.1. Rheological properties of the bentonite slurry in each test.

Concentration of bentonite (g/l)	Apparent viscosity μ_a (mPa:s)	Plastice viscosity μ_p (mPa:s)	Yield Point YP (Pa)	Yield stress τ_y (Pa)	c_v (m^2/s)*
40	4.00	3.00	1.00	0.50	2.50×10^{-8}
50	5.50	4.00	1.50	1.00	2.00×10^{-8}
60	7.50	4.00	1.50	2.00	1.06×10^{-8}

* The values of c_v are constructed by linear interpolation within the data from Talmon et al. (2013).

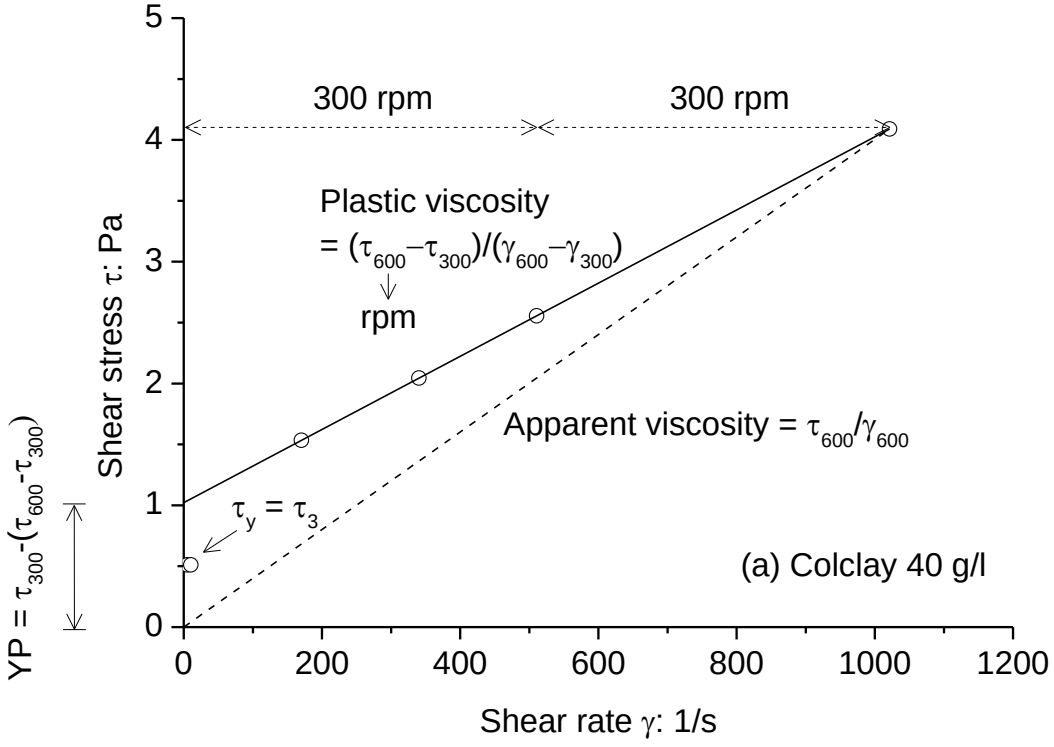

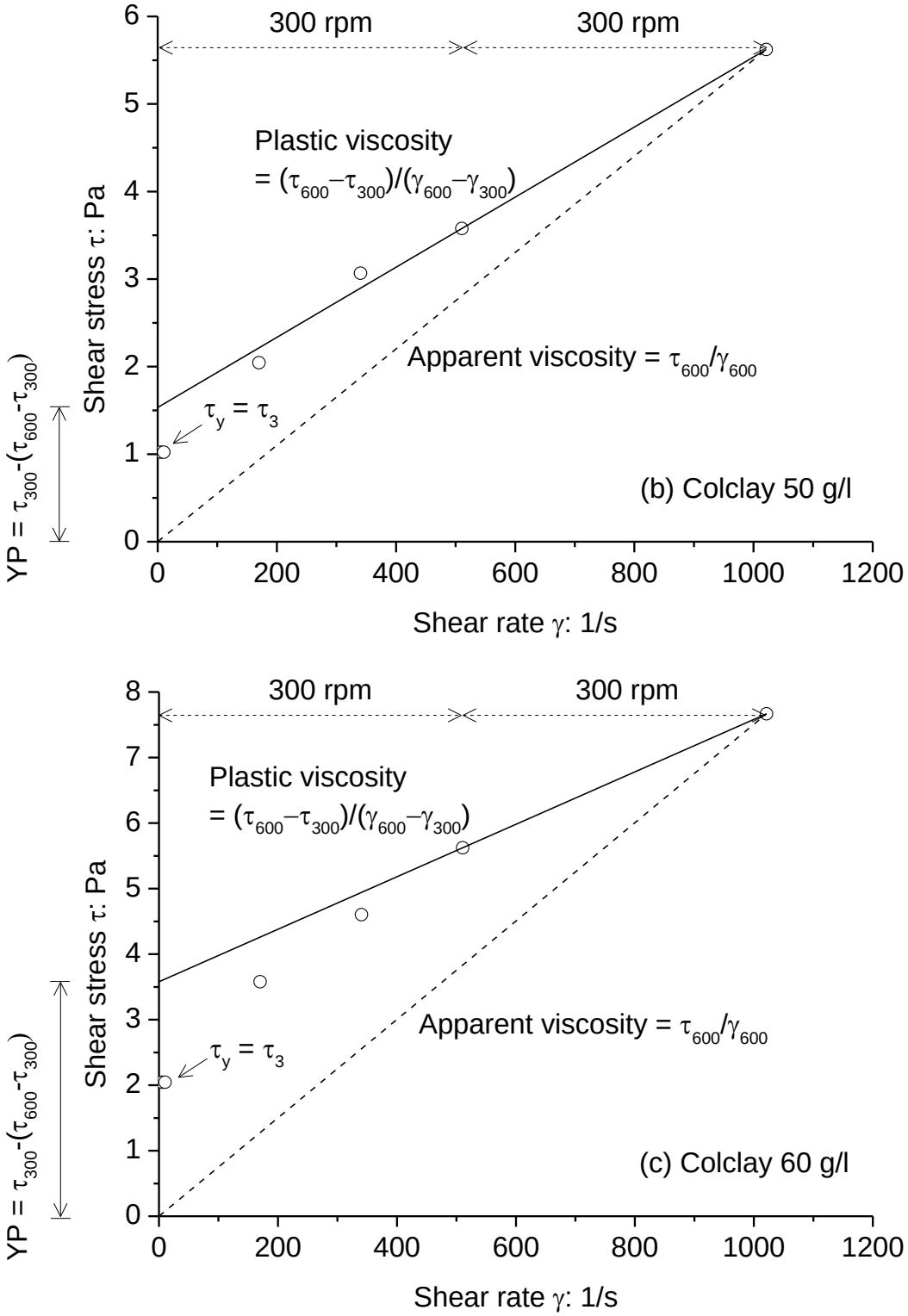

Fig. 2.6. Flow curves slurries with various concentrations of Colclay D90 bentonite: (a) 40 g/l, (b) 50 g/l and (c) 60 g/l.

2.3.3. EXPERIMENTAL PROCEDURE

The sand was compacted in the PMMA cylinder by tamping the saturated sand under water on a filter cloth that allowed water flow but blocked the sand grains, forming a dense layer of 170 mm thickness, with a relative density of approximately 90% and porosity of 0.37.

Then a slurry layer of 10 cm thickness was placed on top of the saturated sand column. The Colclay D90 bentonite and the water were mixed in a high shear Fann mixer (10,000 rpm) for 20 minutes and stiffened for 24 hours as specified by API (2003). The slurry was mixed for 5 minutes, with the same mixer, just before use. Then, a metal wire mesh with a torsion bar was placed on the surface of the sand sample. The possible effect of use of the metal mesh on the test results is that, the metal wire mesh is likely to enhance the formation of filter cakes. Therefore, the metal wire mesh must allow the bentonite grains to pass very smoothly in order to avoid this effect. The grid size of was thus made as 2 mm × 2 mm, which is much larger than the size of bentonite grains. After the test, the filter cake formed on the surface of the metal wire mesh can be taken away by carefully rotating the torsion bar and pull it out.

At the start of the test the slurry layer was pressurised with an air pressure of 50 kPa, which was comparable to the value of the slurry pressure applied in the 2nd Heinenoord tunnel and the GHT in the Netherlands (Talmon et al., 2013). The infiltration of bentonite slurry started immediately with opening the valve at the bottom. The water discharge and the pore water pressures were measured every second (1 Hz). After one hour, the valve was closed and the air pressure was released. At the end of the test, the filter cake was taken out from the cylinder by the metal wire mesh device. The water contents of the fresh bentonite slurry and the filter cake were measured to determine the initial porosity n_i of the fresh bentonite slurry and the porosity n_c of the filter cake in each test.

2.4. RESULTS AND DISCUSSION

Fig. 2.7 gives the plot of the amount of water displaced against the square root of time t for the three tests performed. The results shown are the results of one test with those conditions, but all the tests have been repeated three times and showed similar results. The shape of the curves show a good agreement with the plots provided by Talmon et al. (2013), where the

infiltration is clearly distinguished into two distinct phases: mud spurt and filter cake formation. During the phase of mud spurt, the water leaves the soil rapidly. After some time, because of the formation of the filter cake, the discharge decreases. At this phase there will be only a limited flow caused by the pressure gradient that can push the water into and through the filter cake. The bentonite agglomerations will be deposited at the surface of the sand. The pressure drop will be over this filter cake as can be seen on the pore pressure recordings, see Fig. 2.8. The pore water pressure (k1) above the slurry-sand interface where the filter cake was formed was maintained more or less constant (within 1.5 kPa), whereas the pore water pressures (k2, k3 and k4) beneath the interface drop to hydrostatic pressures, resulted from the build-up of the effective stress onto the soil skeleton due to formation of the filter cake.

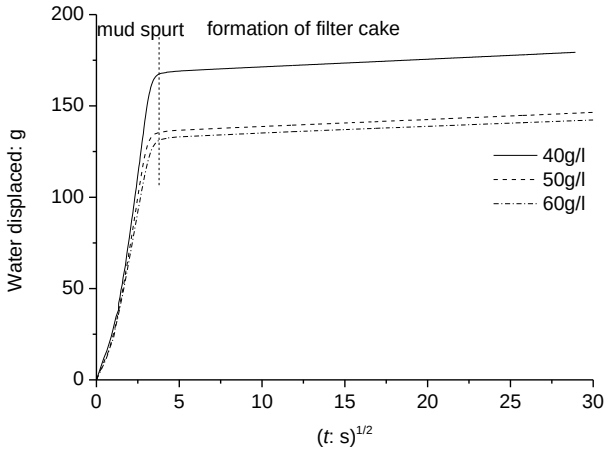

Fig. 2.7. Amount of water displaced against square root of time.

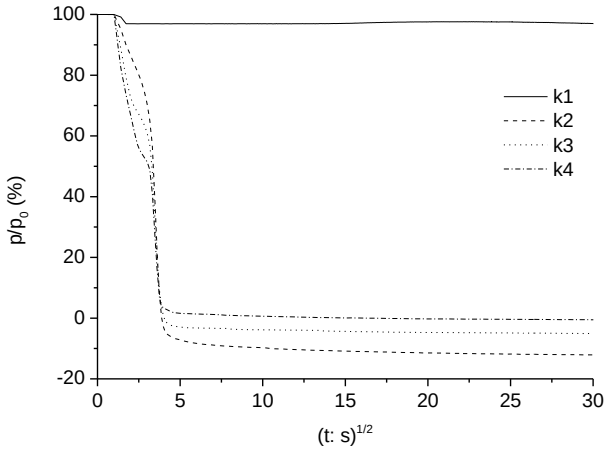

Fig. 2.8. Pore water pressure changes in test of 40 g/l slurry.

2.4.1. MUD SPURT

Fig. 2.9 shows the permeability of sand for bentonite slurry during the phase of mud spurt. The index k1-2 indicates the permeability in the upper part of the sand and 1 cm above it, while k2-3 and k3-4 capture the permeability between 1 – 3, and 3 – 5 cm in the sand, respectively. The permeability (k_b) of sand for bentonite slurry can be determined with:

$$k_b = \frac{\Delta L_s Q}{\Delta \phi' \pi \left(D_1 / 2 \right)^2} \tag{2.13}$$

With ΔL_s the thickness of sand layer between two adjacent PPTs (m) and $\Delta \phi'$ the difference in piezometric head between two adjacent PPTs (m).

Table 2.2 summarizes the results of mud spurt. For the test with 40 g/l bentonite slurry, the sand permeability for water is around 3×10^{-4} m/s, as interpreted from k3-4 at the start of the test. The permeability for bentonite slurry (k_b) is approximately 8.00×10^{-5} m/s (k2-3 at 3 cm of infiltration and k3-4 at 5 cm). After 8.8 cm of infiltration into the sand, the permeability measured in all sections is much lower. It is assumed that the permeability of sand for bentonite slurry remains the same. However, the flow velocity is reduced significantly due to the cake formation and the measurement is not reliable anymore. The calculation was made with only 1 cm to calculate k1-2, because before the cake formation the first 1 cm is just slurry without sand. The fact that the permeability in section k1-2 drops faster than in the other sections is an indication that the filter cake forms at the surface of the sand. Similar results were found in the tests with 50 and 60 g/l concentration. For 50 g/l bentonite slurry the k_b is 5.0×10^{-5} m/s and for 60 g/l bentonite slurry 4.0×10^{-5} m/s. This indicates, as expected, that a higher bentonite concentration causes a decrease of k_b.

Table 2.2. Porosities of the fresh and the consolidated bentonite slurry in each test.

Parameter / Test No.	G_s: g/l	n_i	n_c	k_c: m/s
1	27.50	0.985	0.962	2.80×10^{-9}
2	27.50	0.981	0.947	2.20×10^{-9}
3	27.50	0.978	0.936	2.00×10^{-9}

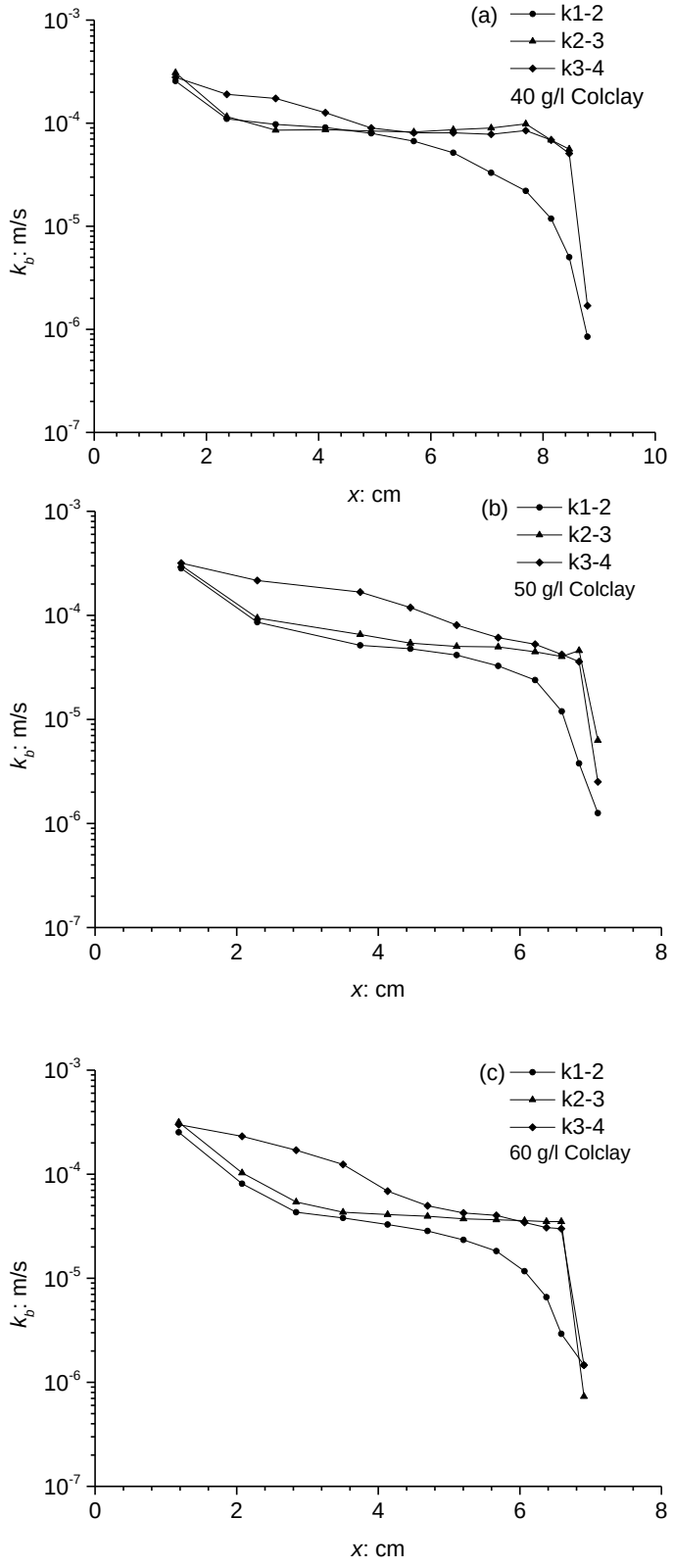

Fig. 2.9. Permeability of sand for Colclay bentonite slurry during the phase of mud spurt.

The Peclet number (*Pe*) was estimated by Eq. (2.1). The pore velocity v_p was calculated by the infiltration distance at every second. The value of the hydraulic pore diameter was estimated as 5.09×10^{-5} m by Eq. (2.2). The values of c_v were gained from Talmon et al. (2013): 1.50×10^{-8} m^2/s, 2.00×10^{-8} m^2/s and 2.80×10^{-8} m^2/s for 40 g/l, 50 g/l and 60 g/l bentonite slurry respectively. Fig. 2.10 shows the calculated *Pe* against the infiltration distance *x*. According to Winterwerp & van Kesteren (2004), the filter cake will be formed if $Pe < 10$. As shown in the graph, for a 40 g/l concentration $Pe < 10$ when $x > 7.8$ cm. It means that the filter cake would start to be formed at $x = 7.8$ cm. However, Fig. 2.9a shows that the filter cake starts to be formed already at $x = 4.0$ cm, indicating that the estimated *Pe* is higher than the expected value in test. This is also found in tests of 50 g/l and 60 g/l bentonite slurries. Fig. 2.10 shows that the filter cake starts to be formed at $x = 6.0$ cm for 50 g/l bentonite slurry and $x = 4.5$ cm for 60 g/l bentonite slurry, while Fig. 2.9b and 2.9c show that the filter cake starts to be formed at $x = 4.5$ cm and for 50 g/l bentonite slurry and $x = 3.5$ cm for 60 g/l bentonite slurry. These values correspond with a Peclet number of 15.5 for 50 g/l slurry and 12.5 for 60 g/l slurry.

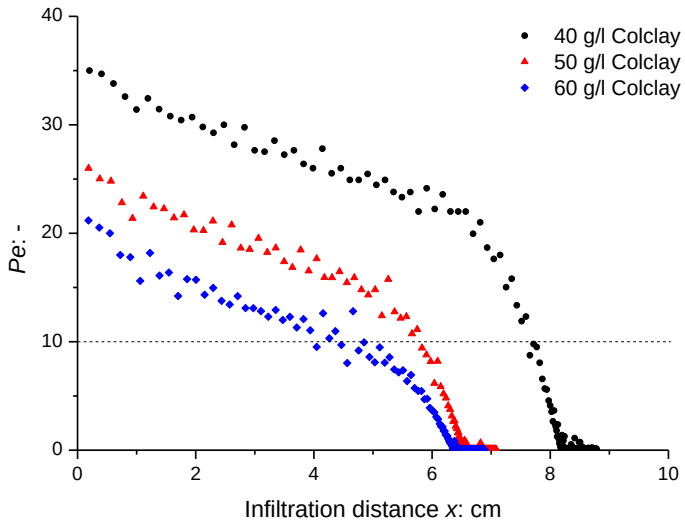

Fig. 2.10. Calculated *Pe* for different tests.

2.4.2. Formation of the filter cake

Assuming the consolidation framework from Section 2.2.3, the permeability (k_c) of the filter cake for water can be determined from the slope of the graph of discharge volume against the

square root of time (Bezuijen et al., 2009). The permeability of the filter cake can be obtained by combining Eqs (2.6) and (2.7):

$$k_c = \frac{1}{2}\frac{\left(\frac{V/A}{\sqrt{t'}}\right)^2 \frac{1-n_i}{n_i-n_c}}{\Delta\phi} \tag{2.14}$$

The initial porosity was calculated from the amount of material used to make the bentonite slurry, that is:

$$n_i = \frac{m_w G_s}{m_b + m_w G_s} \tag{2.15}$$

Where m_w is the mass of water (g); m_b the mass of bentonite (g) and G_s the specific gravity of the Colclay D90 bentonite (-). The final porosity was determined according to the procedure in Section 2.3.3.

The k_c determined by different tests are summarised in Table 2.2. It appears that the permeability of the filter cake for water k_c (~10^{-9} m/s) is four orders of magnitude lower than the sand permeability for bentonite slurry k_b (~10^{-5} m/s). It also indicates that k_c depends on the bentonite concentration in the slurry. Adding bentonite reduces the permeability (k_c) of the filter cake. Table 2.2 also shows that the final porosity decreases with increasing bentonite content. It is expected that the final porosity is determined by the pressure difference and that is more or less the same in all tests. Probably the results were influenced by how the properties of the filter cake were determined. It was found out that there was an apparent boundary between the cake and the original slurry, but no sharp boundary between the cake and the sand. Since there were a little slurry on the cake surface and some sand particles within the cake, it would be very difficult to take away a clean cake from the sand surface and thus the determined properties were not very certain.

To further understand the mechanism of filter cake formation, an additional series of tests was performed. No attempt was made to remove the filter cake in order to leave the filter cake intact. After test, the sample was taken out from the PMMA cylinder and then dried in an oven

at 105 °C for 24 hours. One sample before and after drying is shown in Fig. 2.11. As can be seen clearly from this figure, the real impermeable filter cake was very thin (1.5 ~ 2 mm) and was not in the sand but on top of the sand. This means that the filter cake formed at the real tunnel face is very vulnerable to damage during standstill of the TBM, e.g. ring building or maintenance.

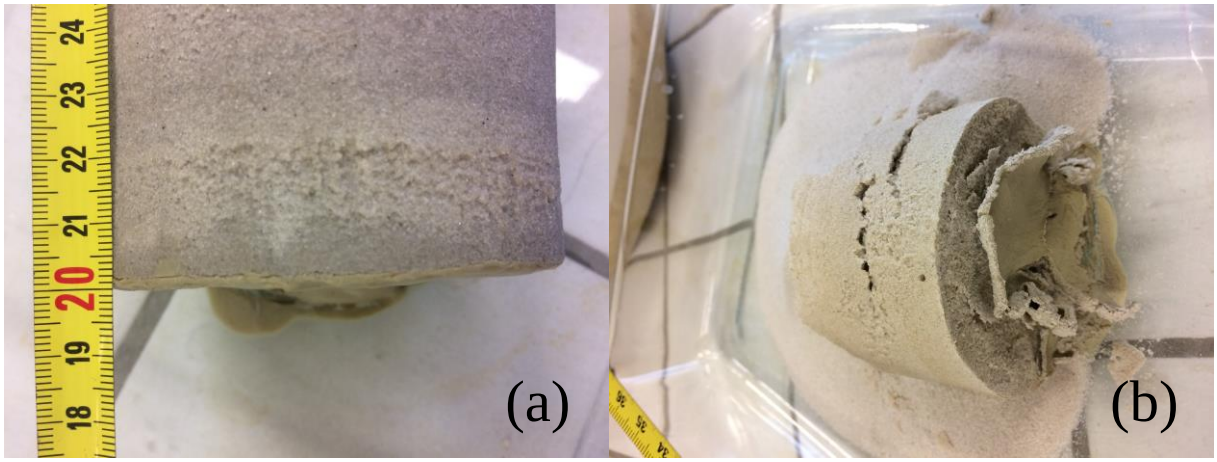

Fig. 2.11. Filter cake (a) before and (b) after drying.

2.4.3. Comparison of models and measurements

Table 2.3 shows that the values of L estimated by Eq. (2.5) are much greater than the measured values, which is consistent with the experimental results of Talmon et al. (2013), see Fig. 2.2. The reason is that the mud spurt is not going to the end, but is stopped by the filter cake formation. The infiltration distance with time can be estimated by two methods:

Eq. (2.3) with the input parameters a determined by Eq. (2.4) and L determined by Eq. (2.5). The values of input parameters for Eqs (2.4) and (2.5) can be found in Section 2.2.1 and Table 2.1 (τ_y).

Eq. (2.12) for the infiltration distance in the phase of mud spurt ($Pe \geq 10$), with input parameters in Table 2.2, and Eq. (2.7) for the infiltration distance in the phase of filter cake formation ($Pe < 10$), with $\Delta\phi$ and input parameters in Table 2.3.

Fig. 2.12 shows the two calculated results with the experimental results. It can be seen that the empirical model apparently underestimated the infiltration distance in the phase of mud spurt,

while the groundwater flow model agreed well with the experimental results. The thicknesses of filter cake were estimated as 3.2 mm, 2.8 mm and 3.0 mm for 40 g/l, 50 g/l and 60 g/l bentonite slurry, respectively, which were very comparable to the observed value.

Table 2.3. Input parameters for calculation of infiltration distance.

Parameter / Test No.	n: -	L: m measured	L: m calculated*	$\Delta\phi$: m	L_s: m	k_w: m/s	k_b: m/s
1	0.37	0.095	4.17	5.00	0.17	4.30×10^{-4}	8.00×10^{-5}
2	0.37	0.078	2.08	5.00	0.17	4.40×10^{-4}	5.00×10^{-5}
3	0.37	0.075	1.04	5.00	0.17	4.40×10^{-4}	4.00×10^{-5}

* The values of this item were calculated by Eq. (2.5) using the yield stresses in Table 2.1.

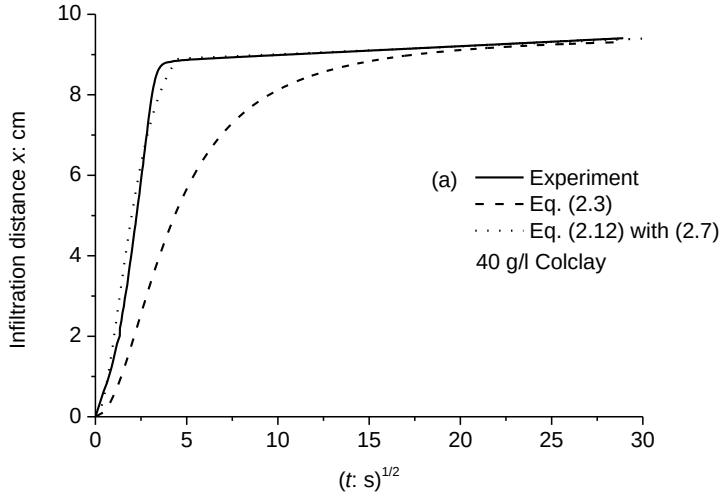

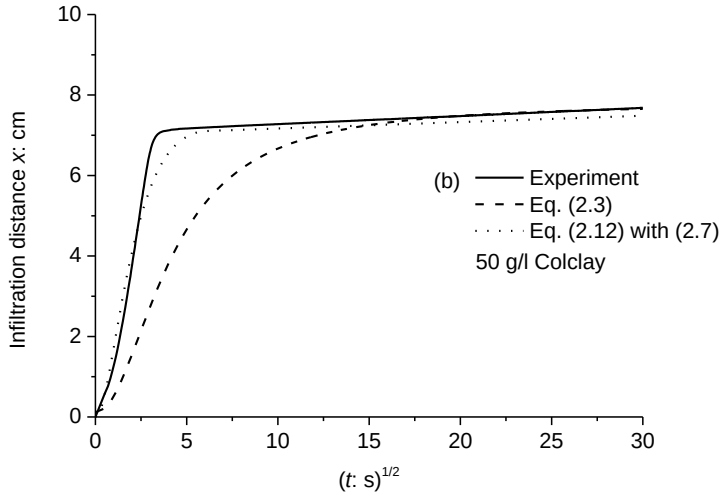

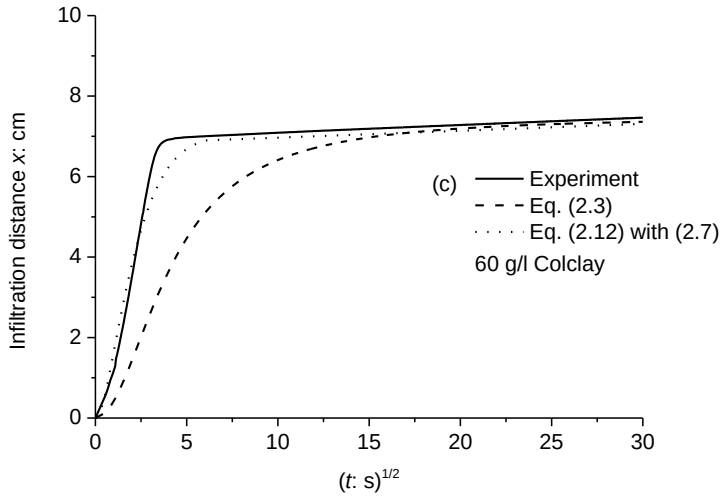

Fig. 2.12. Infiltration distance of bentonite slurry in saturated sand.

Xu et al. (2017) argued that only mud spurt is relevant to calculate the excess pore water pressures in front of a slurry TBM and gained a reasonable agreement between the calculation models with the measurements. In this laboratory study, the improved model based on the groundwater flow equations showed an excellent agreement with the experimental result of mud spurt and it was also shown that the permeability of the filter cake is much smaller than the relevant permeability during mud spurt, which confirms that the excess pore water pressure in the sand in front of the filter cake will be negligible during filter cake formation.

2.5. SUMMARY

An experimental approach to the infiltration of the bentonite slurry at the tunnel face during slurry shield tunneling in saturated sand was presented. The experimental data was analyzed and discussed with the models for mud spurt, groundwater flow and filter cake formation. The following conclusions are possible from the analysis and discussion presented in this chapter.

(a) The filter cake will be formed at the surface of the sand after some time and the permeability (k_b) of sand for bentonite slurry is not affected by this formation of the filter cake. However, the mud spurt will stop when cake formation starts. The excess pore water pressures will dissipate because of the build-up of the effective stress onto the soil skeleton due to formation of the filter cake. However, it should be realized that this

decrease of pore water pressure is a slower process in front of a TBM compared to the decrease measured in this small-scale setup (Bezuijen et al. 2016).

(b) It appears that the permeability (k_b) of sand for bentonite slurry and the permeability (k_c) of filter cake for water differ with several orders of magnitude, slightly depending on the bentonite slurry sample tested. Both the permeability (k_b) of sand for bentonite slurry and the permeability (k_c) of filter cake for water decrease with the increasing concentrations of the bentonite.

(c) It also indicates that adding bentonite decreases k_c as well as the filtration distance, but has minimal influence on the amount of water displaced in the phase of filter cake formation. The experiments also showed that the estimated *Pe* is a bit higher than the expected value ($Pe < 10$) at the initiation of the filter cake formation.

(d) Another finding is that the real impermeable cake is not in the sand but on top of the sand (see Fig. 2.11). Consequently, the filter cake at the tunnel face is very vulnerable to damage during standstill of the TBM, but also during drilling of the TBM because mud spurt will start and thus causes excess pore water pressures.

CHAPTER 3 PRESSURE INFILTRATION OF SLURRY, IN A MODIFIED SETUP

(This chapter is based on the article: Xu, T., Bezuijen, A., 2019. Pressure infiltration characteristics of bentonite slurry. Géotechnique.)

Chapter 2 has presented the experiments on slurry infiltration in a conventional laboratory setup, which is comparable to setups described in the literature. This chapter presents a modified setup which results in a hydraulic gradient in the soil comparable to what can be expected in front of a TBM. The differences in mud spurt and filter cake formation between the two setups will be clearly identified. It is expected that the transition from mud spurt to filter cake formation depends on the infiltration velocity according to the literature. However, this was not found in these tests. The differences between the conventional and modified setups will be discussed too.

3.1. MODIFIED SETUP

For the Setup 1 used in Chapter 2 (Fig. 3.1a): Pressure infiltration of slurry, in a conventional setup, the hydraulic gradient over the sand is, $i = \Delta\phi/L_s$ = 5m/0.17m ≈ 30. However, according to (Bezuijen et al., 2006), for a real tunnel in saturated homogeneous soil, with a diameter of 10 m, the hydraulic gradient at the centre of the tunnel face is approximately, $i = \Delta\phi/R$ = 5m/5m = 1. This was also the result of numerical calculation performed by Zizka and Thewes (2016). To get a comparable hydraulic gradient in the laboratory test as in the field, the Setup 1 was revised. As shown in Fig. 3.1b, a small PMMA cylinder was placed in the bottom of the large PMMA cylinder. The small cylinder (marked in Fig. 3.1b) reduces the discharge. If the bentonite only invades in the large diameter cylinder, the relation between the difference in piezometric head ($\Delta\phi$) and the discharge (Q) can be approximated with:

$$\Delta\phi = \frac{Q}{\pi k_w}\left(\frac{4L_{s1}}{D_1^2} + \frac{4L_{s2}}{D_2^2} + \frac{1}{D_2} - \frac{1}{D_1}\right) \tag{3.1}$$

Where L_{s1} and L_{s2} are the heights of sand in the large cylinder and the small cylinder (m); D_1 and D_2 the inner diameter of the large cylinder and the small cylinder (m). In this case the equivalent length L_s of a homogeneous sand column with the same flow resistance would be:

$$L_s = L_{s1} + L_{s2}\left(\frac{D_1}{D_2}\right)^2 + \frac{D_1^2}{4D_2} - \frac{D_1}{4} \tag{3.2}$$

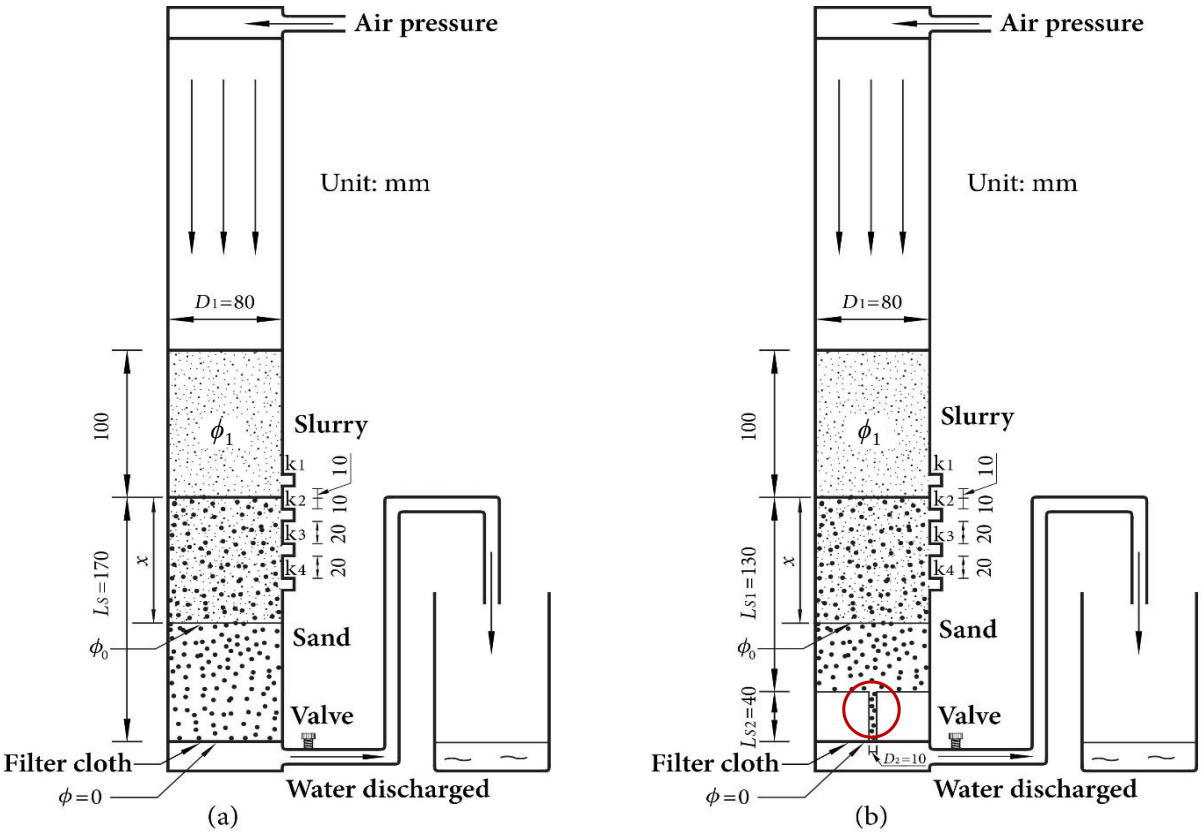

Fig. 3.1. Principle of pressure infiltration of bentonite slurry for (a) setup 1 and (b) setup 2.

In Eq. (3.2), the first 2 terms on the right hand side follow directly from Darcy's law. The last two terms $1/D_2$ and $1/D_1$ describe the resistance that follows from the contraction of the flow lines when the flow has to change from the large diameter cylinder to the small diameter cylinder. The discharge in Setup 2 in Fig. 3.1b is about 1/15 of the discharge for Setup 1 in Fig. 3.1a when flowing with water with the same $\Delta\phi$. This corresponds with a hydraulic

gradient $i = \Delta\phi/L_s$ = 5m/3m ≈ 1.70 in the tube before the constriction, a bit higher but comparable to what can be expected on the jobsite.

In Setup 2, dense layers (40 mm thick in the small diameter cylinder and 130 mm thick in the large diameter cylinder) of Sibelco Mol32 sand were placed. The same procedure as that used for Setup 1 in Chapter 2 was performed.

3.2. RESULTS AND DISCUSSION

There are small differences among the repeated tests with the same conditions, see Table 3.1. The difference in the maximum infiltration found in Setup 1 and Setup 2 is within the experimental variation for the 40 and 50 g/l bentonite slurries. For the 60 g/l bentonite slurry, the infiltration is approximately 35% less in Setup 2.

Table. 3.1. Discharged volumes (ml) after 15 minutes (30 $s^{1/2}$).

Test No.	Concentration of bentonite (g/l)	Setup 1	Test No.	Concentration of bentonite (g/l)	Setup 2
1	40	179.34	10	40	193.82
2	40	173.05	11	40	174.34
3	40	185.05	12	40	195.25
4	50	146.46	13	50	134.87
5	50	150.10	14	50	136.56
6	50	141.96	15	50	138.53
7	60	142.29	16	60	101.98
8	60	139.23	17	60	105.22
9	60	135.86	18	60	102.06

* The procedure of all tests are the same.

Fig. 3.2 gives the plots of discharged volume and infiltration distance against time and the square root of time for Setup 1 and Setup 2. The results show good comparison with the plots provided by Talmon et al. (2013). The process of infiltration is clearly separated into two sub-processes: mud spurt and cake formation. Both test series do not satisfy the Peclet criterion *Pe*

< 10 ($Pe = v_p \cdot d/c_v$) at cake formation (the first series even start cake formation at $Pe \approx 10$), using the consolidation coefficient for D90 bentonite presented by Talmon et al. (2013).

According to Eq. (2.1), in the tests with the same slurry and sand, the Peclet number only depends on the pore fluid velocity (v_p), but cake formation starts at much lower pore velocities in Setup 2 compared to Setup 1, see Fig. 3.2. It seems that the Peclet number was not the determining number for the onset of the external cake formation.

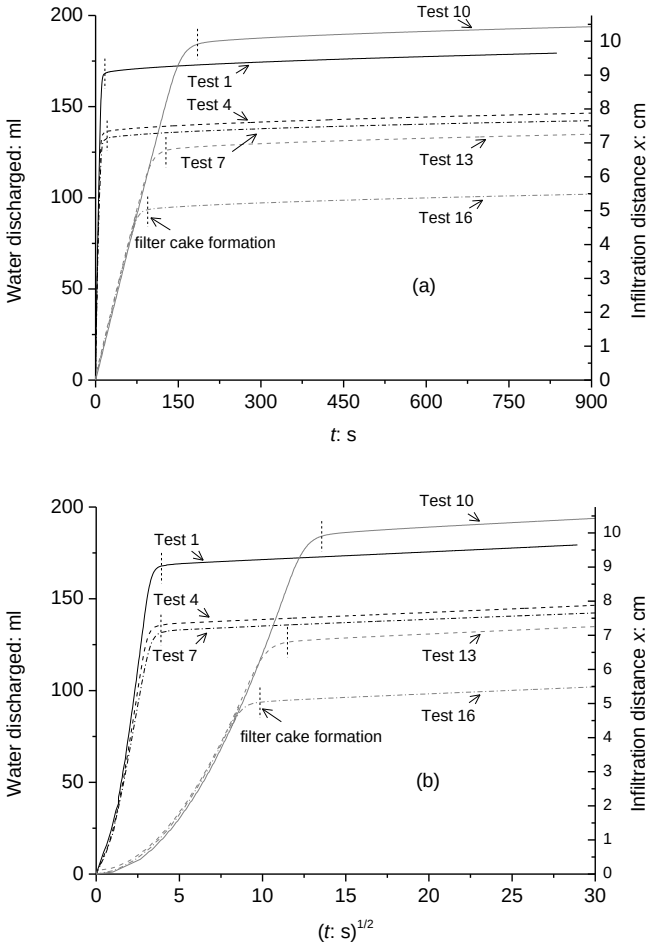

Fig. 3.2. Volumes of discharged water and infiltration distances against (a) linear time and (b) square root of time for Setup 1 and Setup 2.

As mentioned in Chapter 2, the theoretical values of L are 4.17 m, 2.08 m and 1.04 m (with α = 3) for 40, 50 and 60 g/l bentonite slurries, respectively. The theoretical values are much greater than the measured values, which is consistent with the experimental results of Talmon

et al. (2013). The mud spurt is not going to the end, but is stopped after around 10% of the theoretical maximum infiltration distance by the cake formation.

The course of plots during the beginning of the experiment is different for Setups 1 and 2. In Setup 1, the total flow resistance increases during infiltration because the infiltration depth increases with time, leading to an increase of the discharged volume that is proportional to the square root of time. In Setup 2, with a 15 times higher and more realistic flow resistance, the pore water flow in the sand dominates the speed of the infiltration process and the discharged volume increases linearly with time, because the flow resistance is more or less constant.

The permeability of sand for slurry, k_b, can be determined with Eq. (2.13). The calculation was made with only 1 cm to calculate k1-2, because before the cake formation the first 1 cm is just slurry without sand. Between k1 and k2 Eq. (2.13) is only valid during the mud spurt at the beginning of the experiment and it is again valid at the end of the experiment when the cake formation is dominant. In the latter situation, the flow resistance in the cake is much higher than in the sand and the k_b determined then is the permeability of the cake in the centimetre of cake above the sand.

Table 3.2. Permeabilities found in the tests.

Concentration of bentonite (g/l)	k_w (m/s)	k_b (m/s)	
		Setup 1	Setup 2
40	4.40×10^{-4}	8.00×10^{-5}	6.00×10^{-5}
50	4.40×10^{-4}	5.00×10^{-5}	3.00×10^{-5}
60	4.20×10^{-4}	3.00×10^{-5}	2.00×10^{-5}

The values of k_w (the permeability of sand for water) and k_b are summarised in Table 3.2. It can be seen that the values of k_b for both setups are very comparable. Figs 3.3 to 3.5 show the variations in the permeability of sand for slurries with different concentrations of bentonite as tested with Setup 2. Specifically, for 40 g/l bentonite slurry k_w is around 4.40×10^{-4} m/s (see k3-4 at the very beginning). k_b is more or less 6.00×10^{-5} m/s (k2-3 after 3 cm of infiltration and k3-4 after 5 cm of infiltration). k1-2 is the permeability in the upper part of the sand and 1 cm above the sand. After 6 cm of the slurry infiltration in the sand, k1-2 becomes lower,

because now the cake formation starts at the sand surface. It is very clear that this cake formation is at the sand surface because the permeability between k2 and k4 is not affected by this cake formation. After 10 cm of infiltration, the discharge becomes low and the results will be unreliable. The tests with the 50 and 60 g/l slurries show the same trend but lower values of k_b.

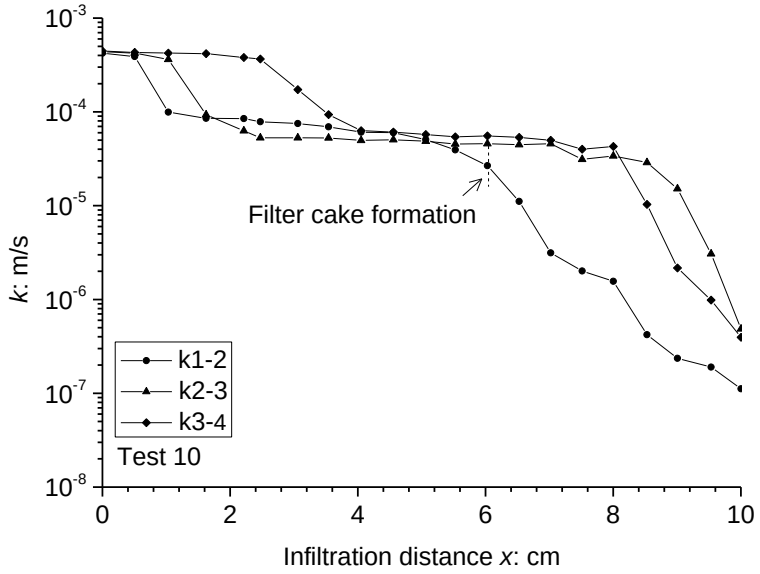

Fig. 3.3. Permeability of sand for 40 g/l Colclay bentonite slurry.

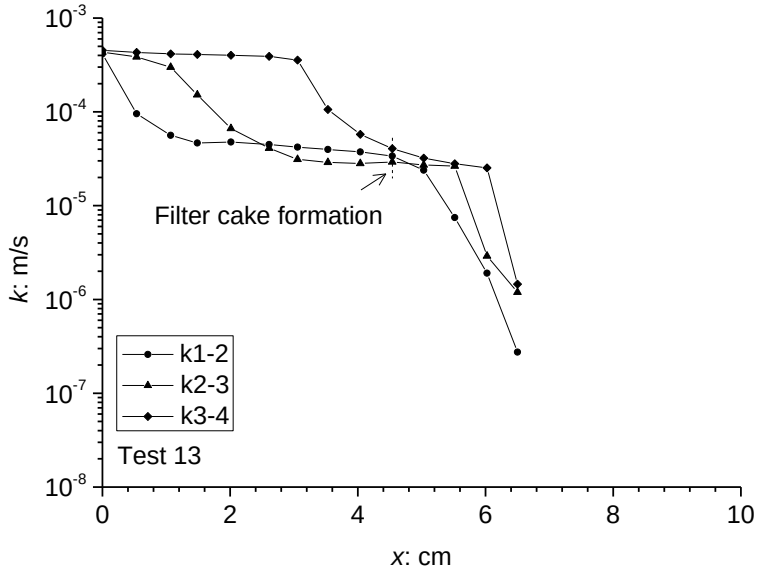

Fig. 3.4. Permeability of sand for 50 g/l Colclay bentonite slurry.

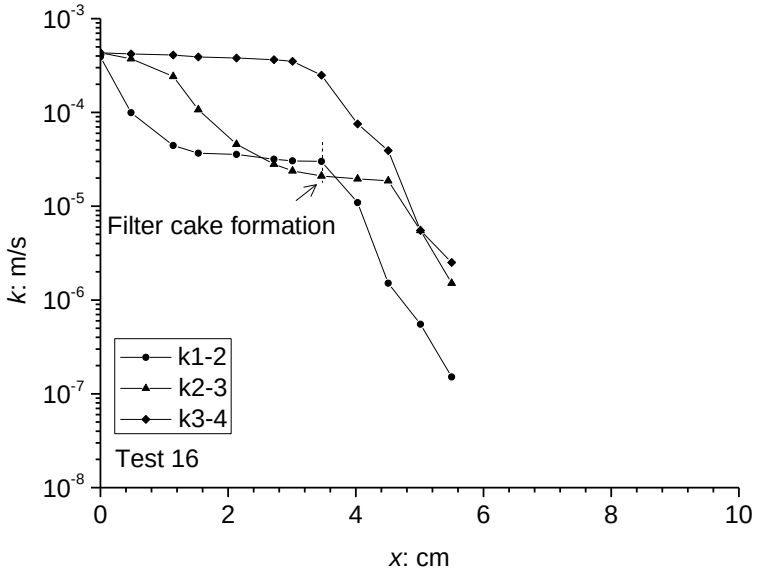

Fig. 3.5. Permeability of sand for 60 g/l Colclay bentonite slurry.

The Peclet number describes when the flow velocity is low enough that clay particles in the can move with respect to the fluid. However, to move with a different speed, there has to be a driving force on the particles that is not present on the fluid. This is only the case when clay particles start to clog at the sand grains.

3.3. SUMMARY

Three tests of infiltration of slurries with different concentration of bentonite have been presented in both a conventional setup (Setup 1) and in a setup that imposes flow velocities comparable to what could be expected at the front of a slurry TBM of 10 m diameter (Setup 2). From these tests it can be concluded:

(a) The experiments are in line with the results published by Talmon et al. (2013). Mud spurt and cake formation are two different processes. The pore pressure measurements and the resulting permeabilities give an additional proof. The external cake formation leads to a significant reduction of the permeability close to the sand surface. The permeability of the internal cake remains more or less constant.

(b) The Peclet number was not the determining number for the onset of the external cake formation. In the tests with the same slurry and sand, the Peclet number only depends on

the pore fluid velocity, but cake formation starts at much lower pore velocities in Setup 2 compared to Setup 1.

(c) Final infiltration distances in the two test setups are similar, therefore not dependent on the flow velocity, contrary to hypothesised at outset. However, the Peclet number is only a threshold, allowing water to move differently than clay fabric of the bentonite. External filter cake might not form immediately.

CHAPTER 4 FILTER CAKE FORMATION UNDER VARIOUS CONDITIONS

(This chapter is based on the article: Xu, T., Bezuijen, A., 2019. Bentonite slurry infiltration into sand, filter cake formation under various conditions. Géotechnique.)

This chapter presents two series of experiments of bentonite slurry infiltration into saturated sand performed in the modified laboratory setup. Series 1 investigates the characteristics of mud spurt and filter cake formation during water-bentonite slurry infiltration, before and after removing the external filter cake formed on the original boundary between the slurry and the sand. Series 2 examines the conditions of filter cake formation during infiltration of water-bentonite-sand slurry (slurry containing sand). The experimental results of Series 1 indicate that, in the second infiltration, a new external filter cake will be formed for low concentrations of slurries (40 and 50 g/l), whereas hardly any new external filter cake formed for high concentration of slurry (60 g/l) due to an internal filter cake formed in the sand during the first infiltration. Due to the internal filter cake formation, the infiltration distance was much smaller for the second infiltration than that in the first for 60 g/l slurry. The experimental results of Series 2 with a water-bentonite-sand slurry showed no external filter cake formation, but deep filtration was observed for high-density slurries (1300 and 1500 kg/m^3). For low density slurries (1050 and 1100 kg/m3), a thicker external filter cake, but with a higher permeability, than that in Series 1 was observed on the sand surface because the cake consisted to a large extent of sand particles.

4.1. INTRODUCTION

Chapter 3 shows that under a hydraulic gradient comparable to that in real tunnels, the filter cake was formed relatively slowly (~ 3 minutes). This means that in a field condition of TBM tunnelling the filter cake will be damaged by the cutting wheel during the drilling because the

rotation speed of the cutting wheel is normally faster than 1/3 rpm. Chapter 2 indicated that even during standstill of the TBM, the filter cake at the tunnel face is very vulnerable to damage because the thickness of the filter cake is only ~ 1mm. Therefore, the first aim of this chapter is to investigate the infiltration characteristics before and after removing the external filter cake that has formed on the original boundary between the slurry and the sand after an infiltration test.

The second aim of this chapter is to investigate the infiltration characteristics of slurry containing sand, since in a field situation the cutting wheel of a TBM carries the excavated soil into the excavation chamber, such that the slurry in front of the tunnel face becomes a mixture of water, bentonite and excavated soil. Therefore, the density of this slurry mixture will be higher than the initial slurry density. The different composition of the slurry mixture may affect the infiltration of the slurry in front of the tunnel face. Tests on the water-bentonite-sand slurries were thus performed to identify the effect of slurry density on the infiltration behaviour of slurry. In these tests the ratio between bentonite and water remains the same (6% bentonite), but the density was increased by adding sand to the mixture. Although similar tests of infiltration of water-bentonite-sand slurry has been performed by others (e.g. Talmon et al., 2013), the differences in infiltration behaviour compared to tests on water-bentonite slurry has not been fully explained. The results of this two test series will be compared with results of a new concept for mud spurt to calculate the mud spurt considering the permeability of sand for bentonite slurry and the theory of deep filtration.

4.2. EXPERIMENTAL STUDY

4.2.1. MODIFICATIONS TO SETUP

Two slurry infiltrations were performed in one test on the same sand sample to simulate the infiltration process before and after removing the external filter cake, as is done in the field by a tooth of the cutting wheel. After the first infiltration the remaining slurry and external filter cake were removed and the same amount of fresh bentonite slurry as for the first test was added on the infiltrated sand surface. The duration of the new infiltration process is the same as the first one: 1 hour. In this case, the infiltration distance is expected to exceed the length of

the sand column in the cylinder (0.17 m) as used in the experiments in Chapter 2 and 3, and hence the sand column was increased up to 0.35 m. Correspondingly, the layout of PPTs was modified as shown in Fig. 4.1.

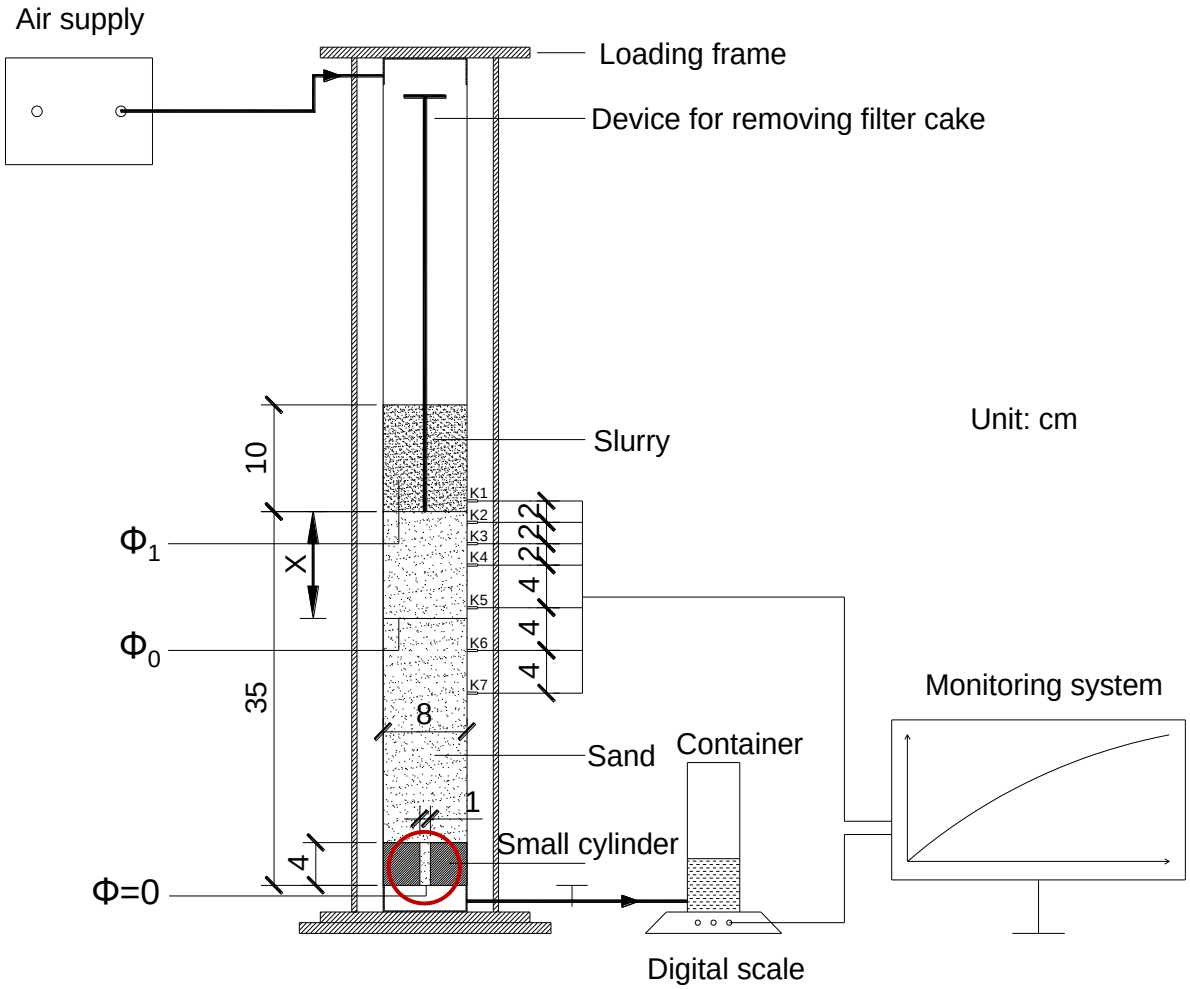

Fig. 4.1. Scheme of the modified setup and principle of pressure infiltration of bentonite slurry. Sand sample filling according to Series 1.

4.2.2. Experimental procedure

4.2.2.1. Series 1: clean slurry

Three commonly used concentrations, 40 g/l, 50 g/l and 60 g/l Colclay D90 bentonite, were adopted for this experimental study. Slurries were prepared by mixing the Colclay D90 bentonite and water in a high shear Fann mixer for 20 minutes and stiffened for 24 hours as

specified by API (2003). The slurry was mixed for 5 minutes, with the same mixer, before use. The properties of these slurries were determined using a Fann Model 35 roto viscometer, see Table 4.1. Data points were obtained for 3, 6, 100, 200, 300 and 600 rpm, corresponding to shear rates between 5.1 and 1021 1/s. In the experiments, assuming that the slurry is a Newtonian fluid, then the shear rates estimated according to the Blake-Kozeny equation in Bird et al. (1960) are between 125 and 234 1/s, which are very comparable to the range of shear rates of the viscometer. The sand used in this experiment is Mol 32 sand.

The infiltration of bentonite slurry started after the valve at the bottom was opened. One hour later, the valve was closed and the air pressure was released. Different from the conventional experiments for bentonite slurry infiltration, we did not stop the experiment after the bentonite slurry infiltrated, but carefully took out the remaining slurry by a low power pump so that the sample was not disturbed. Next, the cake was scraped away by rotating the wire mesh (see Fig. 2.4) and picked up very carefully, and again 10 cm length of fresh slurry was added above the sand surface. The time interval between the end of the first infiltration and the beginning of the second infiltration, is within 5 minutes. The same procedure as the first infiltration was performed again, in order to see if the slurry infiltrates further into the sand. Throughout the test, the amount of discharged water was measured simultaneously with an electronic balance, and the pore water pressures were measured with seven Honeywell-26PCCFG6G PPTs with pressure range of 0 - 100 kPa with a frequency of 1 Hz.

Table 4.1. Thicknesses of bentonite slurry and sand sample in each test.

Parameter / Test No.	Bentonite Concentration: g/l water	Thickness of slurry: cm	Thickness of sand: cm
1: 1st/2nd	40	10	35
2: 1st/2nd	50		
3: 1st/2nd	60		
4 ~ 7	60	20	33
8		30	

4.2.2.2. SERIES 2: SLURRY CONTAINING SAND

The values of the density of the slurry with soil during drilling of the Second Heinenoord Tunnel in the Netherlands were determined from the vertical gradient in the excavation chamber. These values ranged from 1260 to 1450 kg/m^3 (COB, 2001). On the other hand, the maximum density predicted for boring in sand (in a density current on the face of the TBM) is 1495kg/m^3 (COB, 2001). On the basis of the density range measured in the Second Heinenoord Tunnel, the densities of 1050, 1100, 1300 and 1500 kg/cm^3 were adopted for the Series 2. A bentonite concentration of 60 g/l was adopted as the basic slurry due to the minimum shear strength requirement for suspending the sand, which was estimated by:

$$\tau_f = 0.7 \frac{2}{3\pi} d_{particle} \left(\gamma_{particle} - \gamma_{suspension} \right) \tag{4.1}$$

Where $d_{particle}$ is the mean diameter of sand (m); $\gamma_{particle}$ the specific weight of sand particle (N/m^3); $\gamma_{suspension}$ the specific weight of slurry suspension (N/m^3).

This formula was developed on the basis of the table provided by a manufacturer of the 'ball harp' to evaluate the measurements, where balls of different dimensions are lowered in bentonite and is written down which ball infiltrates into the slurry (Leutert, datasheet, 2016). Eq. (4.1) is used to calculate the necessary yield strength for the slurry, so that a grain will not fall through the slurry. The yield strength depends on the weight and diameter of the grain and on the density of the slurry. For the Mol 32 sand with a mean diameter of 150 μm, the required minimum shear strength of the slurry is 1.16 Pa. It can be seen from Table 4.1 that the 60g/l bentonite slurry meets the requirement and thus was used in the tests of Series 2.

Unlike the filter cake formation in Series 1, there will be a sand 'bed' formed as the sand particles in the slurry deposit on the original boundary between the water-bentonite-sand slurry and the sand in Series 2. In order to see the process of how hydraulic conductivity of the sand 'bed' changed, we installed the PPTs k1 and k2 above the original boundary between the slurry and the sand sample with a length of 33 cm. In that case, k2-3 in Series 2 should correspond with k1-2 in Series 1. After making the same 60 g/l bentonite slurry as in the Series 1, the Mol 32 sand was added to the slurry and mixed in a low speed mixer for 5

minutes. The amount of water, bentonite and sand for four densities of slurry are summarised in Table 4.2. Each test lasted one hour. But for 1500 kg/m^3 of slurry containing sand, due to the high discharge during infiltration the period of infiltration of a 20 cm length of slurry suspension will be shorter than 1 hour, therefore the test was repeated with a 30 cm length of slurry suspension.

Table 4.2. Amount of ingredients in mixture of slurry.

Test No.	Density (kg/m^3)	Water (kg)	Bentonite (kg)	Sand (kg)
1: 1st/2nd	1025	1000	40	0
2: 1st/2nd	1031		50	
3: 1st/2nd	1037		60	
4	1050		60	22
5	1100			110
6	1300			530
7	1500			1090
8	1500			1090

4.2.3. Results and discussion

4.2.3.1. Series 1: clean slurry

Test Series 1 consists of six tests of water-bentonite slurries with bentonite concentrations: 40, 50 and 60 g/l. Fig. 4.2 shows the discharged volumes of water-bentonite slurries against the square root of time. The results shown are the results of one test with those conditions, but all the tests have been repeated three times and showed similar results. The full lines are the results of the 1st infiltration, the dashed lines of the 2nd after scraping away the filter cake. As shown in this figure, the slope of the curve during the 1st mud spurt is larger than the slope during the 2nd mud spurt for all bentonite concentrations. With the increase of the bentonite concentration, the slope of the curves flattens. For a bentonite concentration of 40 g/l, the total amounts of water displaced during the 1st and 2nd infiltration are very similar. However, for a bentonite concentration of 50 g/l and 60 g/l, the total amount of water displaced during the 1st

infiltration is larger than during the 2nd. The difference between the amount of water displaced during the 1st and 2nd infiltration is much larger for the bentonite concentration of 60 g/l than for the 50 g/l concentration.

In Fig. 4.2 the time from mud spurt to external filter cake formation is easily distinguished during 1st infiltration for all bentonite concentrations, since there is a clear change in the slope of the lines. For the bentonite concentration of 40 g/l, the time where the external filter cake starts during the 2nd infiltration is also easily observed. For the bentonite concentration of 50 g/l, there is a more gradual change in slope indicating that there is also a gradual change between mud spurt and external filter cake formation and this is even more the case for the 60 g/l concentration. This indicates that the 2nd infiltration depends significantly on the bentonite concentration. Higher bentonite concentration will result in a lower velocity of the 2nd mud spurt and a less clear transition to the external filter cake formation.

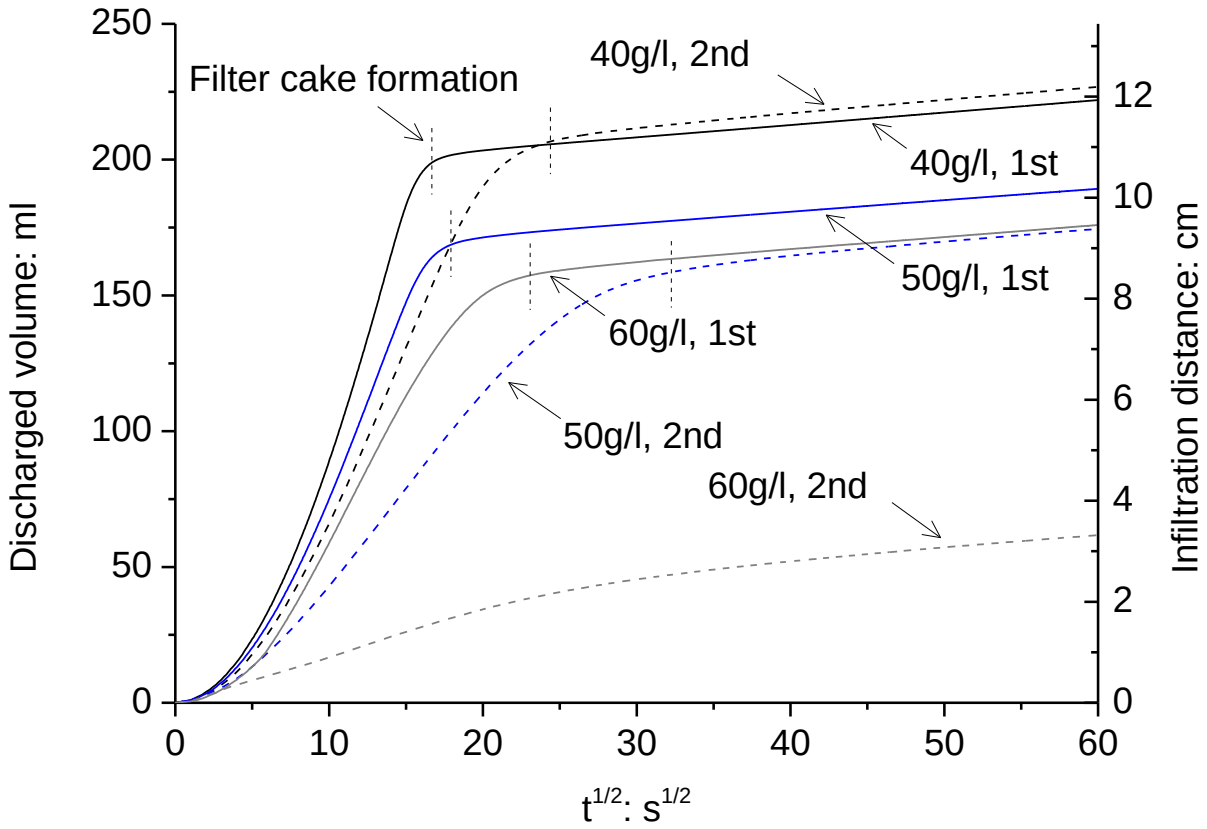

Fig. 4.2. Discharged volume against linear time and square root of time for tests on water-bentonite slurries. The vertical lines indicate start of filter cake formation.

The 40 g/l bentonite slurry has the same or even a bit higher infiltration in the second test (thus with the filter cake removed), for the other tests, the results are more as expected: the infiltration is less in the second test.

For the 40 g/l bentonite slurry: In the theoretical case that there would have been only mud spurt, the infiltration length during mud spurt L (see Table 2.3 in Chapter 2) would have been 4.17 m. However, the external filter cake formation stops the infiltration at around 0.12 m. After removing the cake and starting the test again, the mud spurt goes on, because the internal cake is not yet a limiting factor. The slurry that has infiltrated into the sand during the 1st infiltration will have a higher yield strength due to the thixotropic behaviour of the slurry and therefore the infiltration speed will be lower. The gel strength after one hour will be around 4 times higher than the yield strength for these bentonite slurries (Den Hamer, 2015).

Table 4.3. Input parameters for the concept for mud spurt.

Parameter / Test No.		n	L_s: m	$\Delta\phi$: m	L: m calculated ($\alpha = 3$)	L: m measured	k_w: m/s	k_b: m/s
1	1st	0.37	0.35	5	4.17	0.119	4.00×10^{-4}	2.00×10^{-5}
	2nd					0.122		1.00×10^{-5}
2	1st				2.08	0.102		5.00×10^{-6}
	2nd					0.094		2.50×10^{-6}
3	1st				1.04	0.095		1.00×10^{-6}
	2nd					0.033		-
4			0.33		1.04	0.085		
5						0.130		
6						0.197		
7						-		
8						0.288		

For the other 'extreme', the 60 g/l slurry test, the mud spurt according to Eq. (2.5) is still longer than the realized mud spurt before cake formation starts, see Table 4.3. If also here we assume that due to thixotropic behaviour the gel strength after one hour is 4 times higher than the initial yield strength, then the L according to Eq. (2.5) is comparable to the measured infiltration depth. Consequently, the 2nd infiltration will not result in a further mud spurt in the sand because it is stopped by the gel strength of the slurry. It can be seen in Fig. 4.2 that the slope of the line for the 60 g/l bentonite slurry during the 1st infiltration of Test 3, already decreases before the cake formation starts, indicating that the mud spurt is slowing down. Removing the cake and starting the experiment again will lead to only a limited further infiltration because the experiment is already at the 'mud spurt infiltration limit'. The 50g/l slurry test results are between the extremes described above.

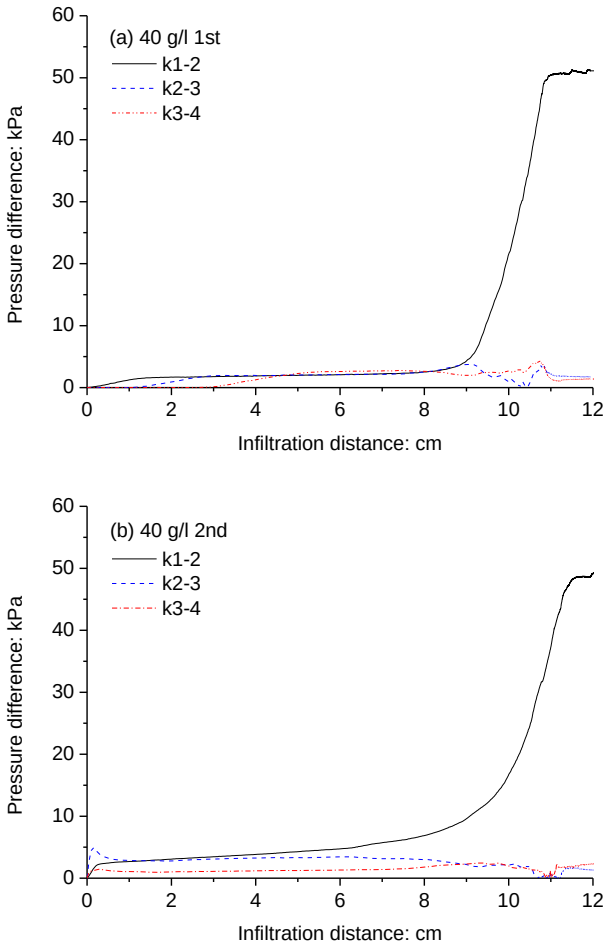

Fig. 4.3. Pressure difference between two PPTs with infiltration distance.

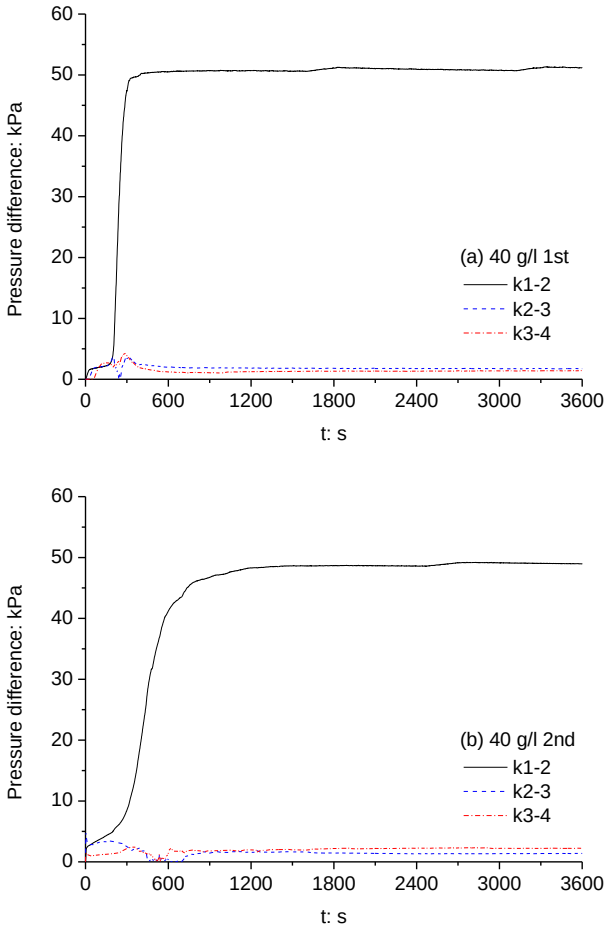

Fig. 4.4. Pressure difference between two PPTs with time.

Figs 4.3 to 4.4 show plots of the pressure difference between two adjacent PPTs as function of infiltration distance and also as function of time for the test of 40 g/l slurry. It is shown that during mud spurt the pressure differences were relatively small and approached to each other. After filter cake formation, the pressure difference k1-k2 (~ 50 kPa) became much higher than k2-k3 and k3-k4 (~ 2 kPa, clearer in Fig. 4.4). When an external filter cake was formed, the slurry pressure was transferred as effective stress onto the soil skeleton and hence pore water pressures at k2-k4 drop to hydrostatic pressures because they were located beneath the filter cake, whereas the pore water pressure at k1 maintained constant as it was located above the filter cake. The pressure difference k1-k2 therefore became relatively high. At the start of filter cake formation, there was a sharp increase in pressure difference k1-k2. Moreover, the

increase rate was higher for 1st infiltration than for 2nd infiltration, which is consistent with the result of discharged volume (Fig. 4.2).

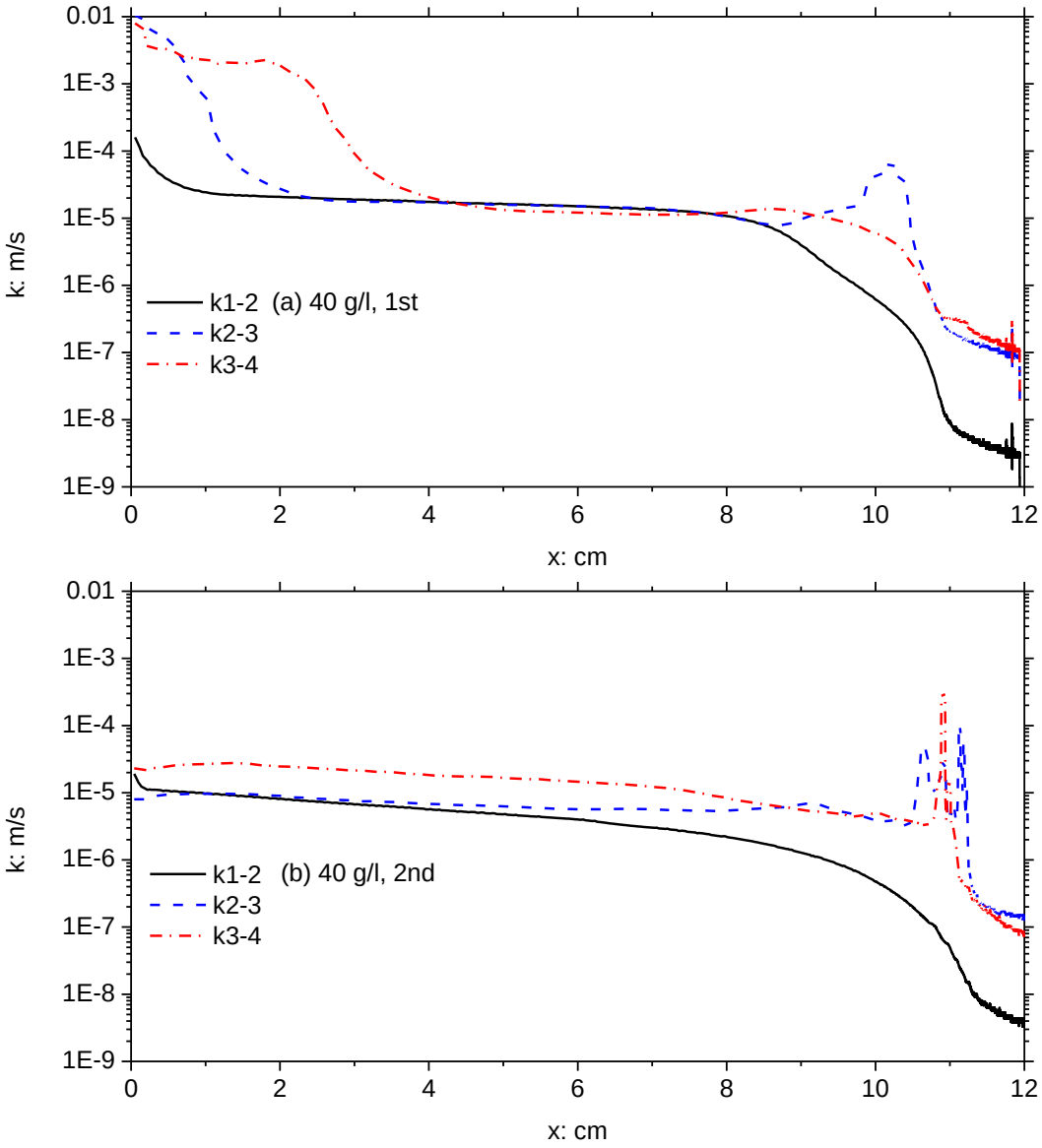

Fig. 4.5. Permeability of sand against infiltration distance for 40 g/l slurry.

The permeabilities of sand for the bentonite slurry (k_b) are determined with Eq. (2.13). The calculated values of k_w and k_b at the end of the test are summarised in Table 4.3. Figs 4.5 to 4.8 show more details in variations in the permeability of sand for fluids in all tests. The experimental data of permeability was smoothed by using a moving average of 17 data points. Due to the large differences in permeability, the high values will have limited accuracy when

the permeability is low in one part of the tube. The part with low permeability will reduce the water flow through the tube and consequently the pressure differences will be small over the areas with higher permeability. In these figures k1-2 represents the permeability determined by the data from PPTs k1 and k2, and so on. It should be noted that k1-2 is the permeability in the upper part of the sand and 1 cm above the sand. It can be seen from the top plot of Fig. 4.5 that the value of k_b for 40 g/l bentonite slurry is ~ 2.00 × 10^{-5} m/s for 1st infiltration. (the k1-2 after 1 cm of infiltration, the k2-3 after 3 cm and the k3-4 after 4 cm of infiltration). After 8 cm of infiltration of the bentonite slurry in the sand, the values for k1-2 become lower, because now the filter cake formation starts at the sand surface. It is very clear that this cake formation is at the sand surface because the permeability k1-2 decreased, but the permeability between k2 and k4 is not affected by this cake formation.

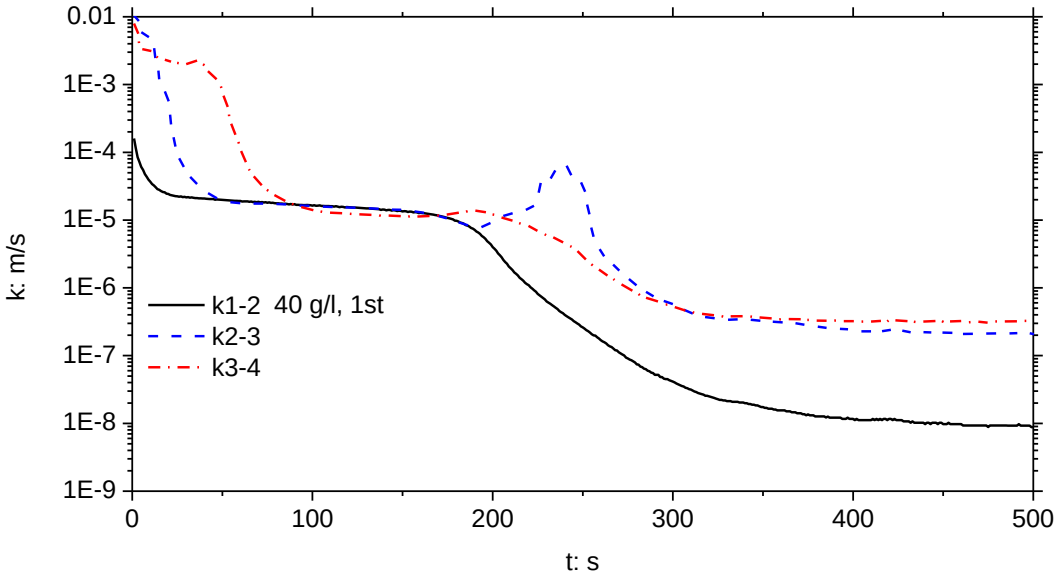

Fig. 4.6. Permeability of sand against time for 40 g/l slurry.

Fig. 4.6 shows the same experimental data of k_b for 40 g/l bentonite slurry as a function of time. As shown in this figure, after 180 s, the value of permeability became very low, ~ 10^{-9} m/s. After approximately 10 cm of infiltration and after 500 s in Fig. 4.4, the external filter cake takes most of the pressure and the mud spurt in the sand has stopped. The permeability that is measured for k2-4, is then the permeability of the water that percolates through the bentonite particles, because, due to the external filter cake, the pressure gradient in this part of

cylinder (k2 to k4) is too low to push the bentonite particles further into the sand. This permeability is in the order of 10^{-7} m/s, higher than the permeability for the filter cake, due to the lower density of the bentonite particles outside the filter cake, but much lower than the permeability during mud spurt.

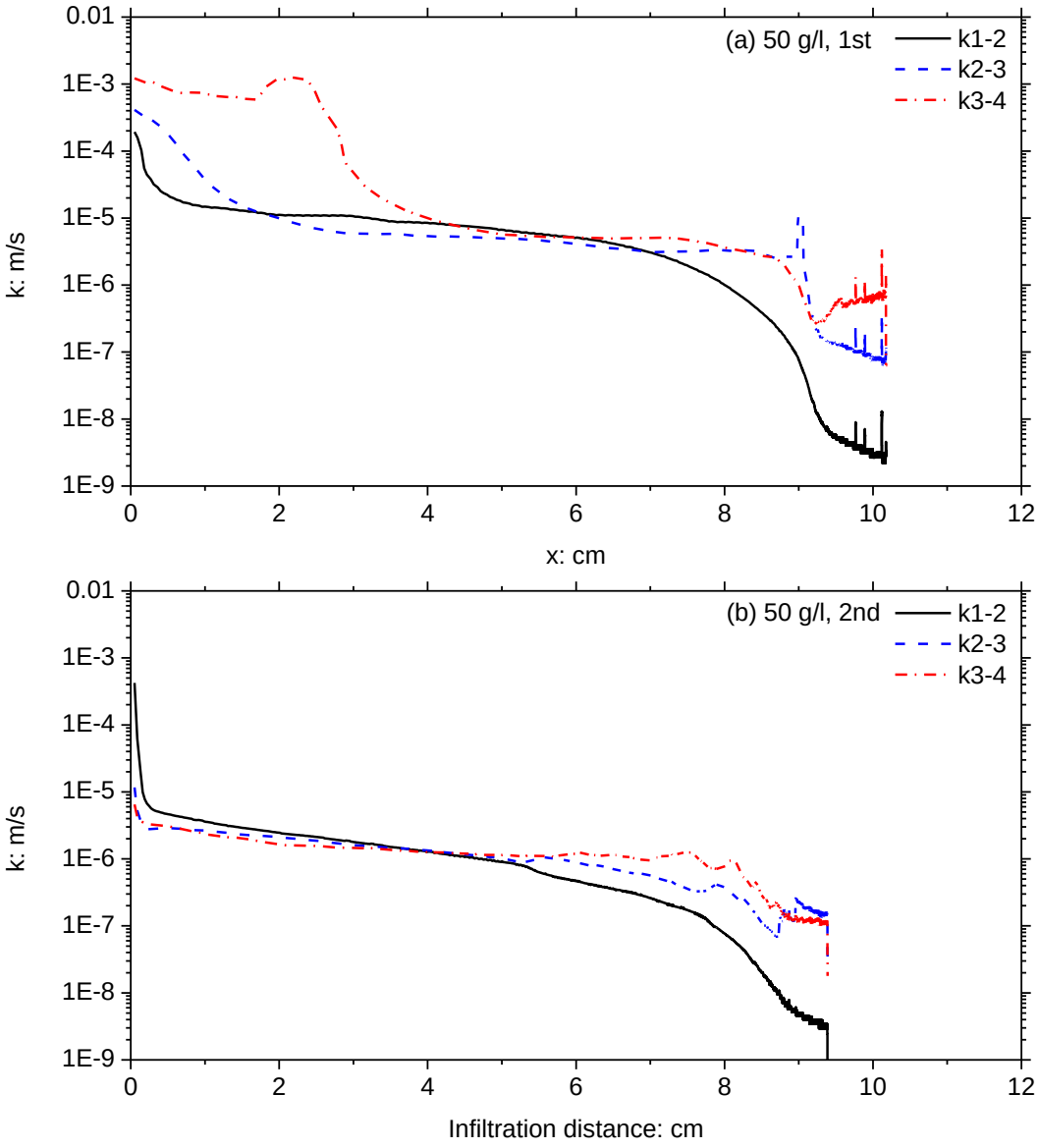

Fig. 4.7. Permeability of sand against infiltration distance for 50 g/l slurry.

The permeabilities (k1-2, k2-3 and k3-4) were found to be less than 1.00×10^{-5} m/s for 2nd infiltration in Test 1 (40 g/l), which was half the values of the 1st infiltration of Test 1. This indicated that after 1st infiltration the pores in the sand at the location of the PPTs were filled

with slurry rather than with water. More significantly, since the yield strength is too low to prevent this mud spurt, the higher pressure gradient leads to additional mud spurt, followed by the build-up of an external filter cake afterwards.

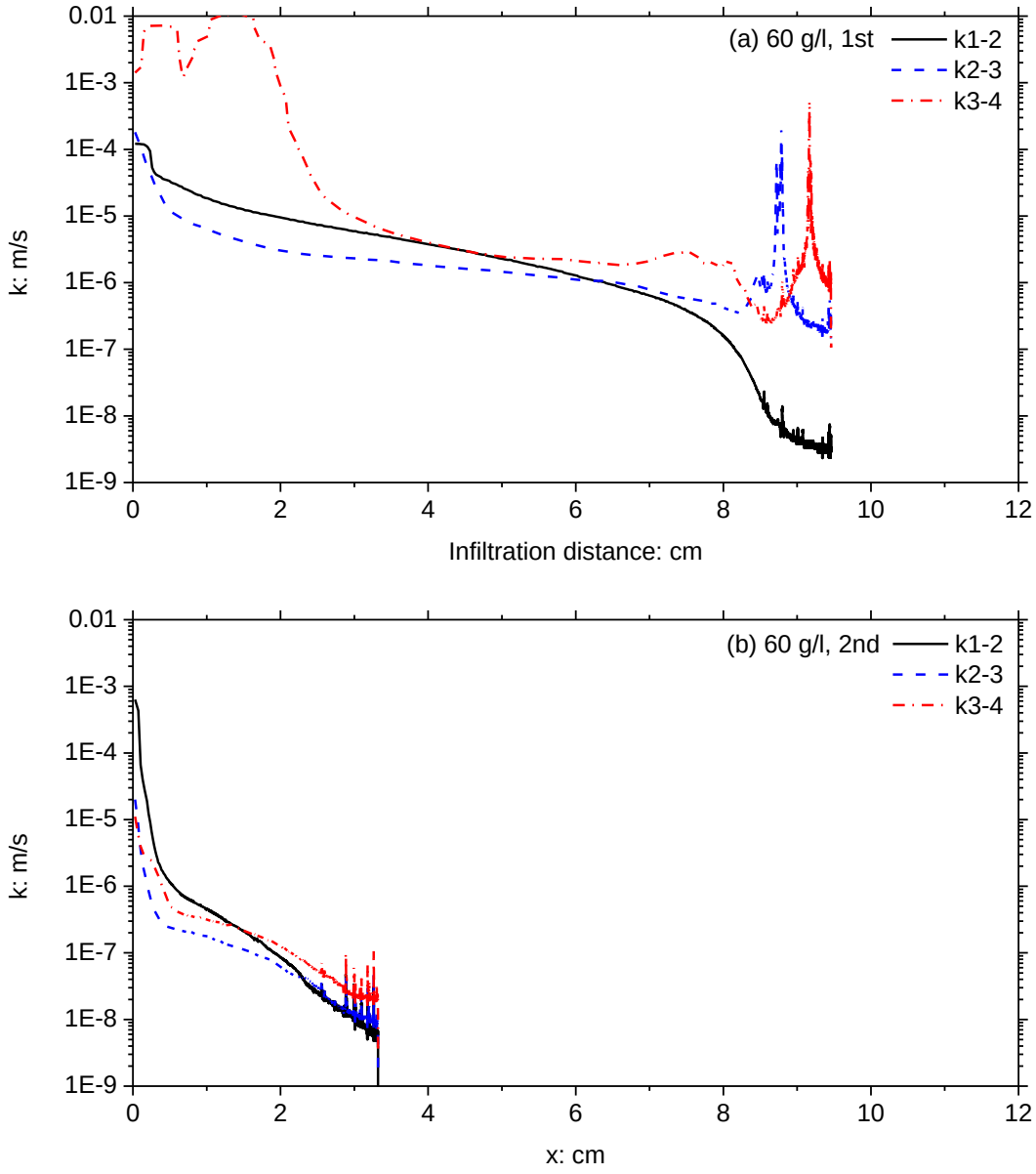

Fig. 4.8. Permeability of sand against infiltration distance for 60 g/l slurry.

For 50 g/l bentonite slurry (Test 2), the value of k_b during 1st mud spurt was 5.00×10^{-6} m/s and 2.50×10^{-6} m/s during 2nd mud spurt. For 60 g/l bentonite slurry (Test 3), the value of k_b during 1st mud spurt was 1.00×10^{-6} m/s, whereas no apparent mud spurt was observed during

2nd infiltration because now the pressure gradient is not high enough to create a 2nd mud spurt. The permeability is now determined by the water that percolates around the bentonite particles and fine sand grains that are more or less fixed to the sand particles. During the 2nd infiltration the permeability further decreases (Fig. 4.8b). It is likely that this is caused by 'deep filtration' (Ripperger et al., 2012), which will be interpreted in Section 4.2.3.2, in which this phenomenon is the most important finding. Additional bentonite particles that infiltrate into the sand with the percolating water and filling the larger pores in the sand, leading to the internal filter cake formation.

In the case of 60 g/l bentonite slurry, the values of permeability of sand for slurry of k1-2 at very beginning of the 2nd infiltration were large. This might be caused by disturbing the sand surface by the wire mesh. However, the values of k1-2 immediately decreased to the values during steady mud spurt. Moreover, the values of permeabilities are much lower than for the 40 g/l bentonite slurry. The result demonstrated that the yield strength of the slurry in the sand is sufficient high to prevent further mud spurt. The situation of 50 g/l bentonite slurry was between 40 and 60 g/l bentonite slurries.

There are still some parts where the permeability is much higher than the permeability of k1-2, e.g. there was a peak in k2-3 at 10 cm in Fig. 4.5. At further infiltration of the slurry, the high permeability disappears and k2-3 is again in line with k3-4. That is also the case in Figs 4.7 to 4.8. Figs 4.3 to 4.4 show that there was a drop in pressure difference between k2 and k3 at the start of filter cake formation. A possibility is that we get Peclet or consolidation effect in the slurry. The pressure drop is low in that phase of the experiment and small deviations can have a large effect.

With the determined parameters in Table 4.3, the infiltration distance during mud spurt can be calculated by Eq. (2.12). It should be noted that the measured values of L in Table 4.3 are the values of the infiltration distances only taking into account the mud spurt. Figs 4.9 to 4.10 show the calculated values with the experimental data. Eq. (2.12) is not valid, when cake formation starts. For this reason, the bending in the measured curves (blue lines) is much steeper than in the calculated curves using the measured value of L (and thus determined by the onset of cake formation). It is clear that the mud spurt versus time calculated by Eq. (2.12)

with the measured L is a little larger than that from the experimental result. Even though, the theoretical curves coincide well with the experimental data at the early period of mud spurt. If the theoretical values of L are used, the measured and calculated values of the infiltration agree more until cake formation starts. There is no mud spurt in 2nd infiltration of Test 3 (60 g/l) and hence Eq. (2.12) is not valid.

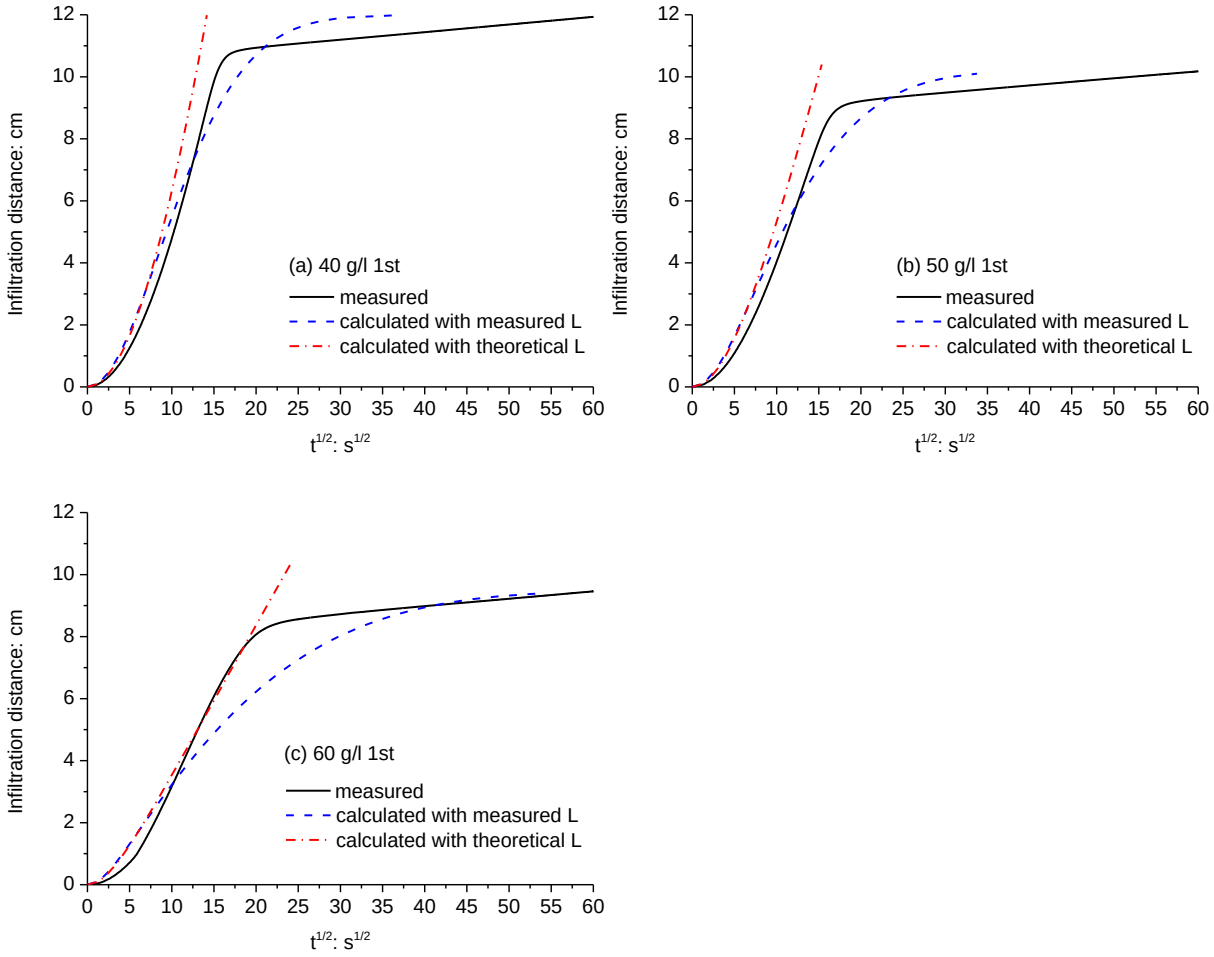

Fig. 4.9. Infiltration distance against square root of time for tests on clear slurries.

Fig. 4.11 interprets the process of the 1st and 2nd infiltration. The initial state is as shown in Fig. 4.11a. The second phase 'mud spurt' (Fig. 4.11b), is defined as the process that fluid passes through the filtration medium before filter cake is formed. In the third phase 'external filter cake formation' (Fig. 4.11c), the bentonite particles will be deposited on the sand surface and hence the discharge is reduced dramatically. At the end of the external filter cake

formation, there will be a only tiny water flow through the bentonite particles. After removal of the cake and start a 2nd infiltration, for low concentrations of bentonite (e.g. 40 and 50 g/l Colclay D90 bentonite), mud spurt will start again (Fig. 4.11d) followed by again external filter cake formation (Fig. 4.11e). The depth of the infiltrated zone is now higher (2 times the thickness after the first infiltration for the 40 g/l slurry). For high concentrations of bentonite (e.g. 60 g/l Colclay D90 bentonite), the process is different (Fig. 4.11f). The bentonite particles will be deposited in the pores between the sand particles and hence an internal cake is formed. In this case, the discharge in the 2nd infiltration will be much lower than that in the 1st infiltration.

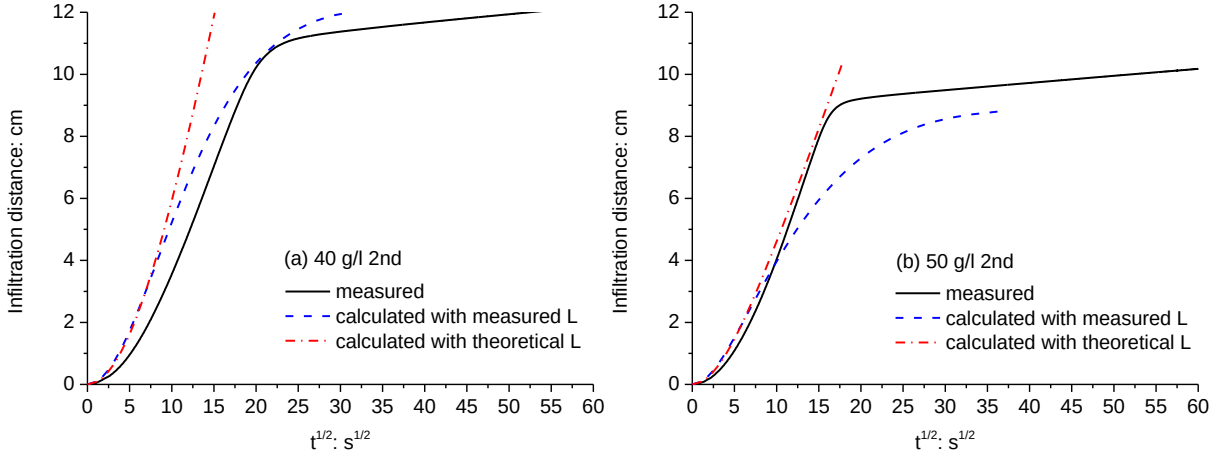

Fig. 4.10. Infiltration distance against square root of time for tests on slurries containing sand.

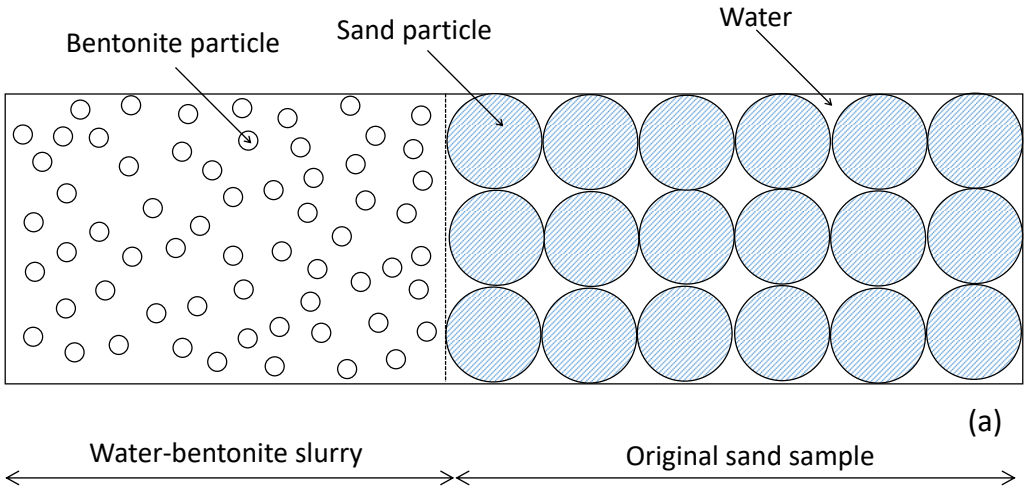

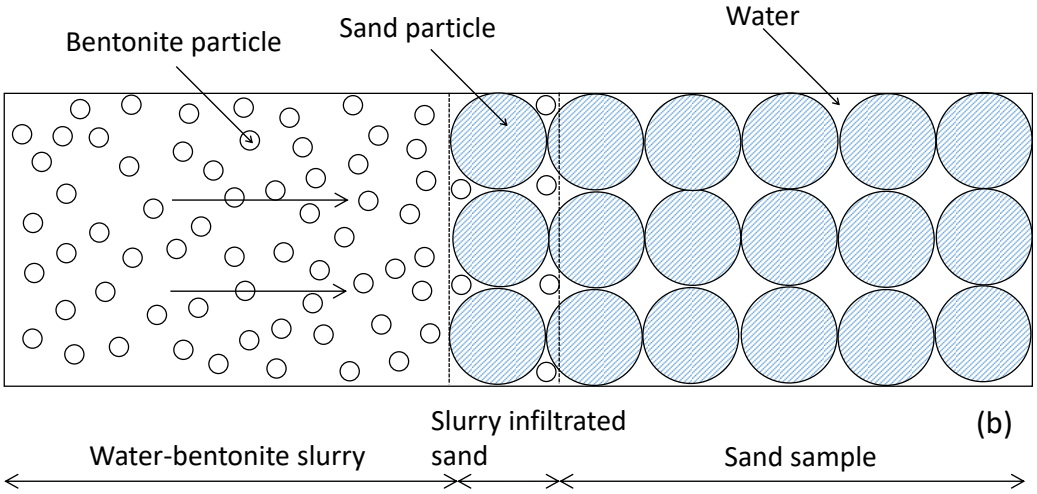
Bentonite particle
Sand particle
Water
Slurry infiltrated sand
(b)
Water-bentonite slurry
Sand sample

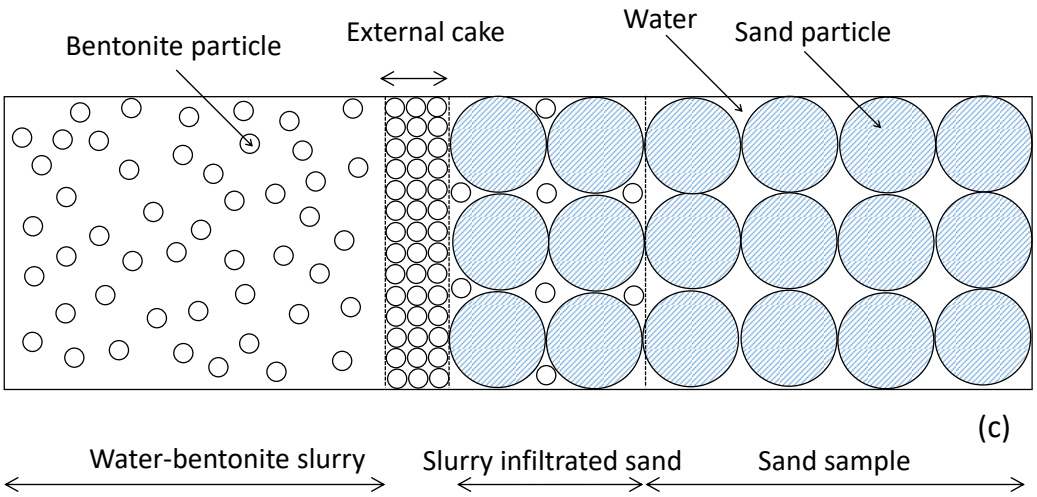
Bentonite particle
External cake
Water
Sand particle
(c)
Water-bentonite slurry
Slurry infiltrated sand
Sand sample

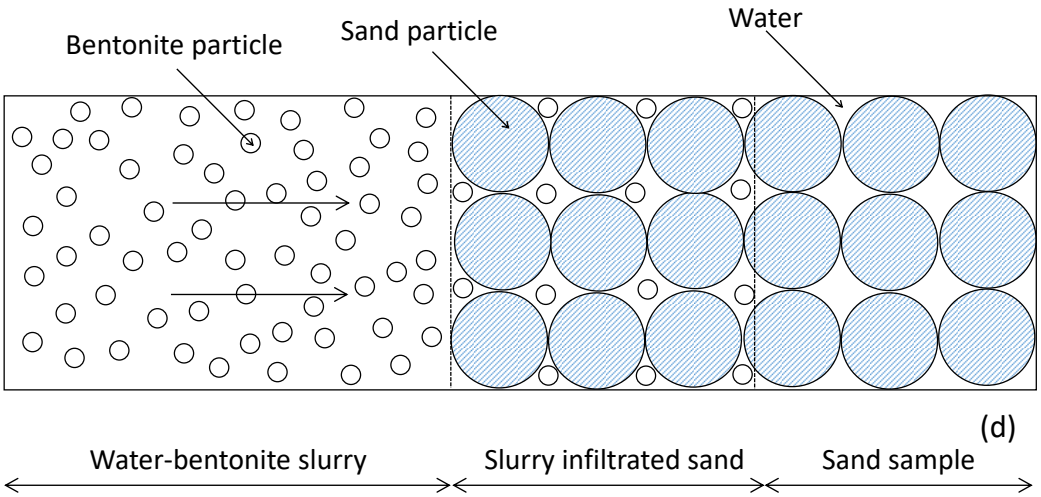
Bentonite particle
Sand particle
Water
(d)
Water-bentonite slurry
Slurry infiltrated sand
Sand sample

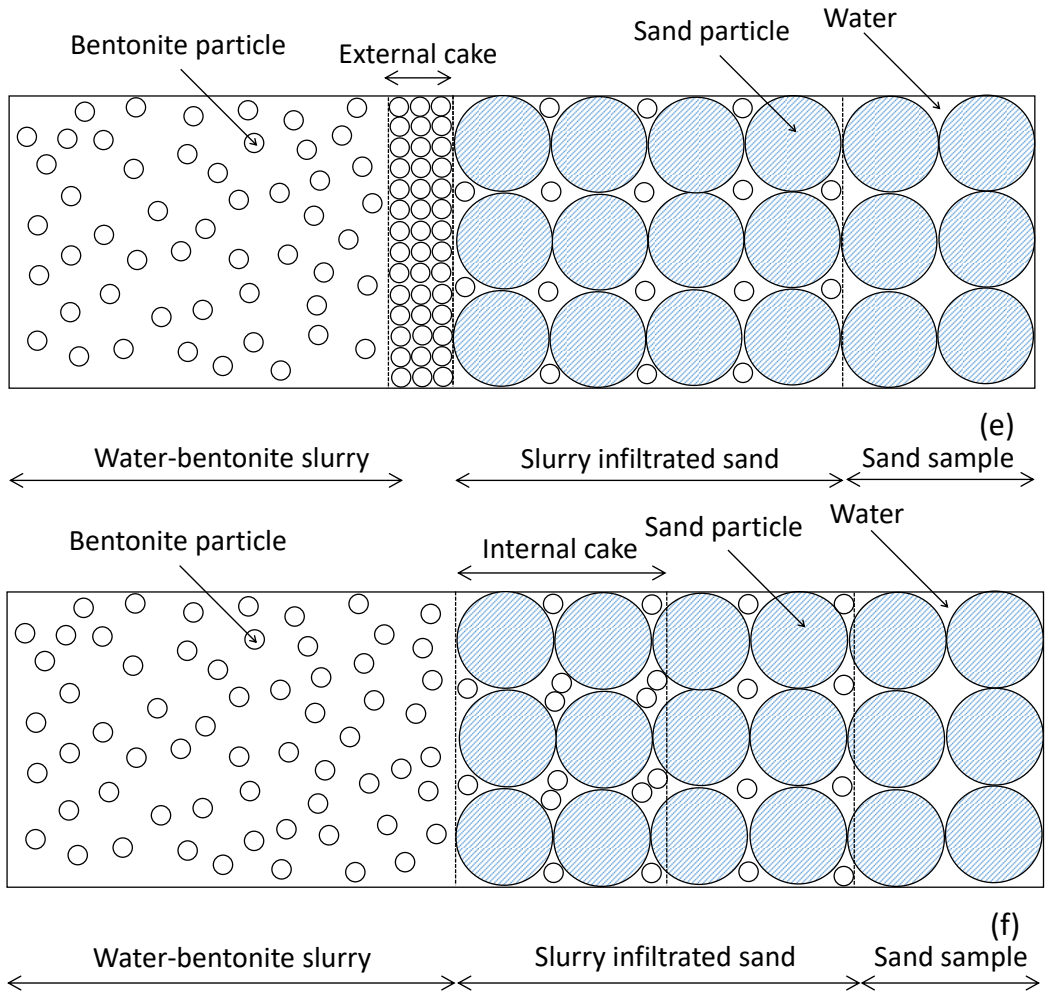

Fig. 4.11. Sketch of process of infiltration: (a) Initial state; (b) Mud spurt in 1st infiltration; (c) External cake formation in 1st infiltration; (d) Mud spurt in 2nd infiltration; (e) External cake formation in 2nd infiltration; (f) Internal cake formation in 2nd infiltration.

4.2.3.2. SERIES 2: SLURRY CONTAINING SAND

Test Series 2 consists of four tests on water-bentonite-sand slurries with 60 g/l bentonite and added the same Mol 32 sand to reach various densities: 1050, 1100, 1300 and 1500 kg/m^3. See also Table 4.2. Fig. 4.12 shows the volumes of water discharged from the sand column against the square root of time. For the slurry with density of 1050 kg/m^3, mud spurt and filter cake formation can be distinguished. The infiltration rate reduces significantly after around 25

√s, as indicated in the figure. However, such a distinction cannot be observed for the slurries with higher densities.

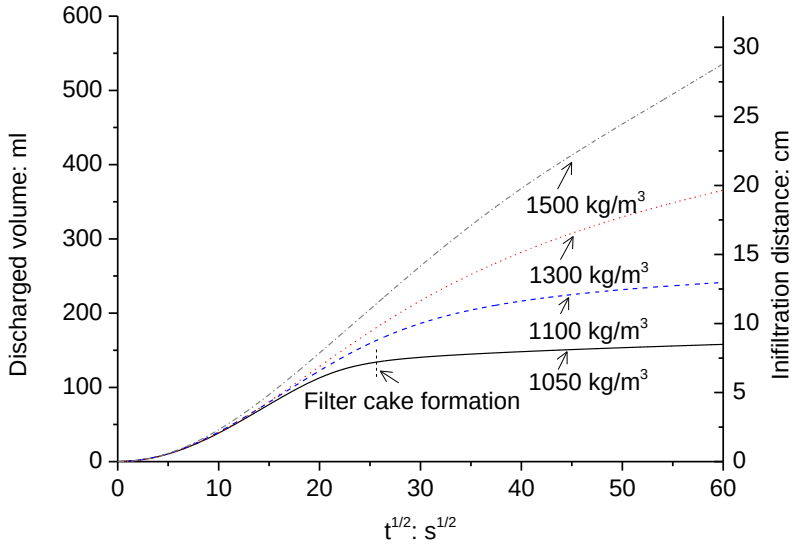

Fig. 4.12. Discharged volume against square root of time for tests on slurries containing sand. The vertical lines indicate start of filter cake formation.

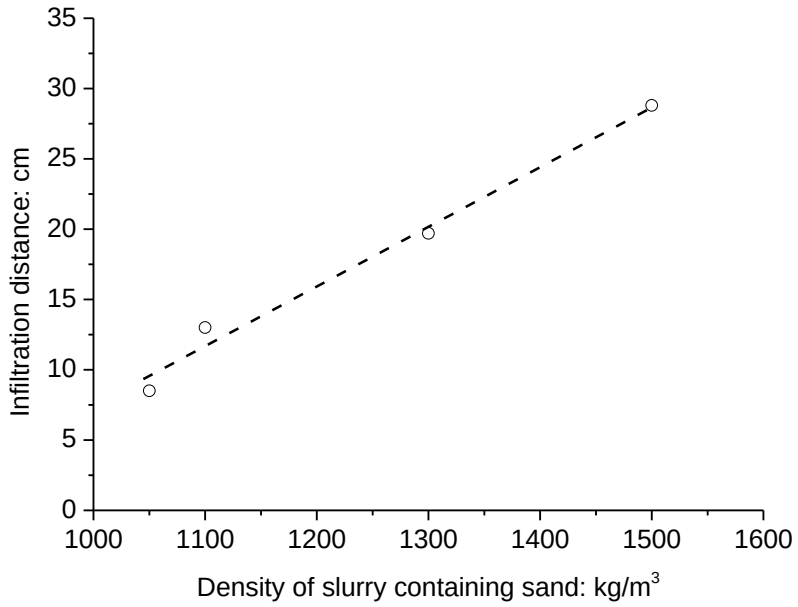

Fig. 4.13. Infiltration distance with density of slurry containing sand after one-hour infiltration.

From Fig. 4.13 it can also be seen that the infiltration distance after one hour of infiltration increases more or less linearly with increasing density of the slurry. The formation of an

external filter cake is hampered by the sand grains. The sand grains take the effective stress and therefore the external filter cake cannot form, see Fig. 4.14. It shows the formation of a 'filter cake' with sand filled slurry. There is no real filter cake with the bentonite. Since the infiltration depth without external filter cake is much larger than the ones measured with clean slurry, if an external filter cake is avoided, then the infiltration will be more. The more sand is added the more effective is this sand to prevent an external filter cake and thus the larger the infiltration depth. This result is remarkably different from results given in literature (Talmon et al. 2013) where fine sand is mixed in the slurry, much finer than the original sand that is excavated. This was done to simulate the slurry after it had passed the slurry regeneration plant. In an infiltration experiment using slurry with relatively fine sand, the fines block the pores leading to less infiltration.

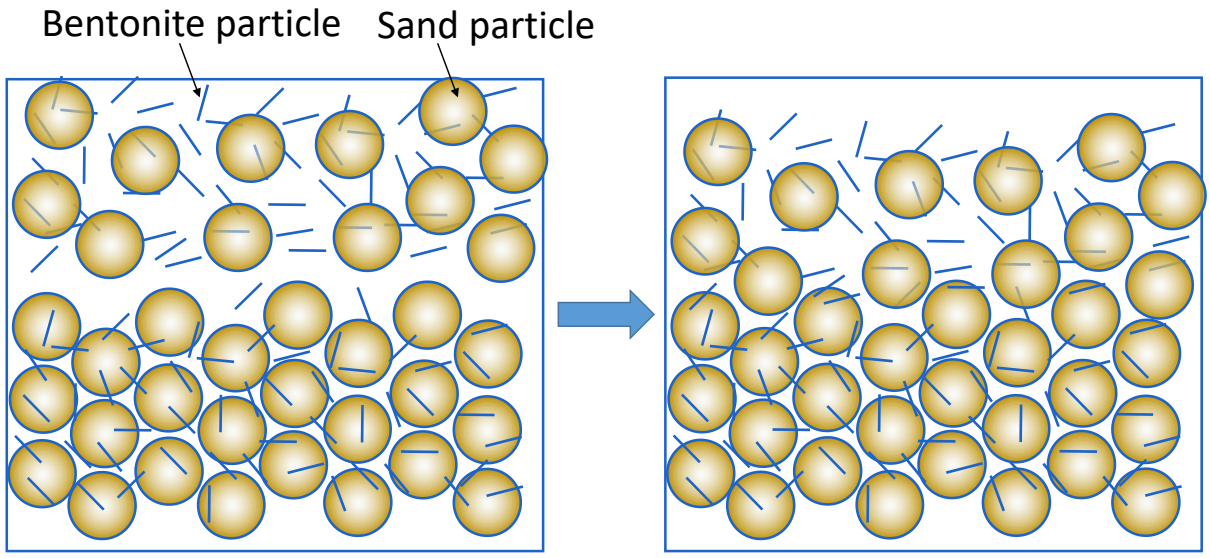

Fig. 4.14. Evolution of 'deep filtration'.

Fig. 4.15 shows the results of the permeabilities of sand for slurry. In the cases of 1050 and 1100 kg/m^3 slurries there is still some cake forming between k1 and k2 (3 and 1 cm above the original sand sample surface respectively), resulting in a low permeability. However, from the measurements, this seems not to be the case. The pressure drop between k1 and k2 (k1-2) is about 10^3 times lower than the pressure drop between k2 and k3 (k2-3). The reason is that there is only a sand layer deposited between k2 and k3. By 'deep filtration' a lot of bentonite

particles deposit in this sand layer between k2 and k3 where the lower porosity stops them and causes some blockage over there. In the cases of 1300 and 1500 kg/m^3 slurries, this 'blocking' between k2 and k3 does not occur, because with enough sand from the water-bentonite-sand slurry the top level of the sand layer deposited on the original sand sample surface will exceed the level of k1. Consequently, bentonite particles and also more sand particles are captured in the sand layer deposited, which has a lower permeability.

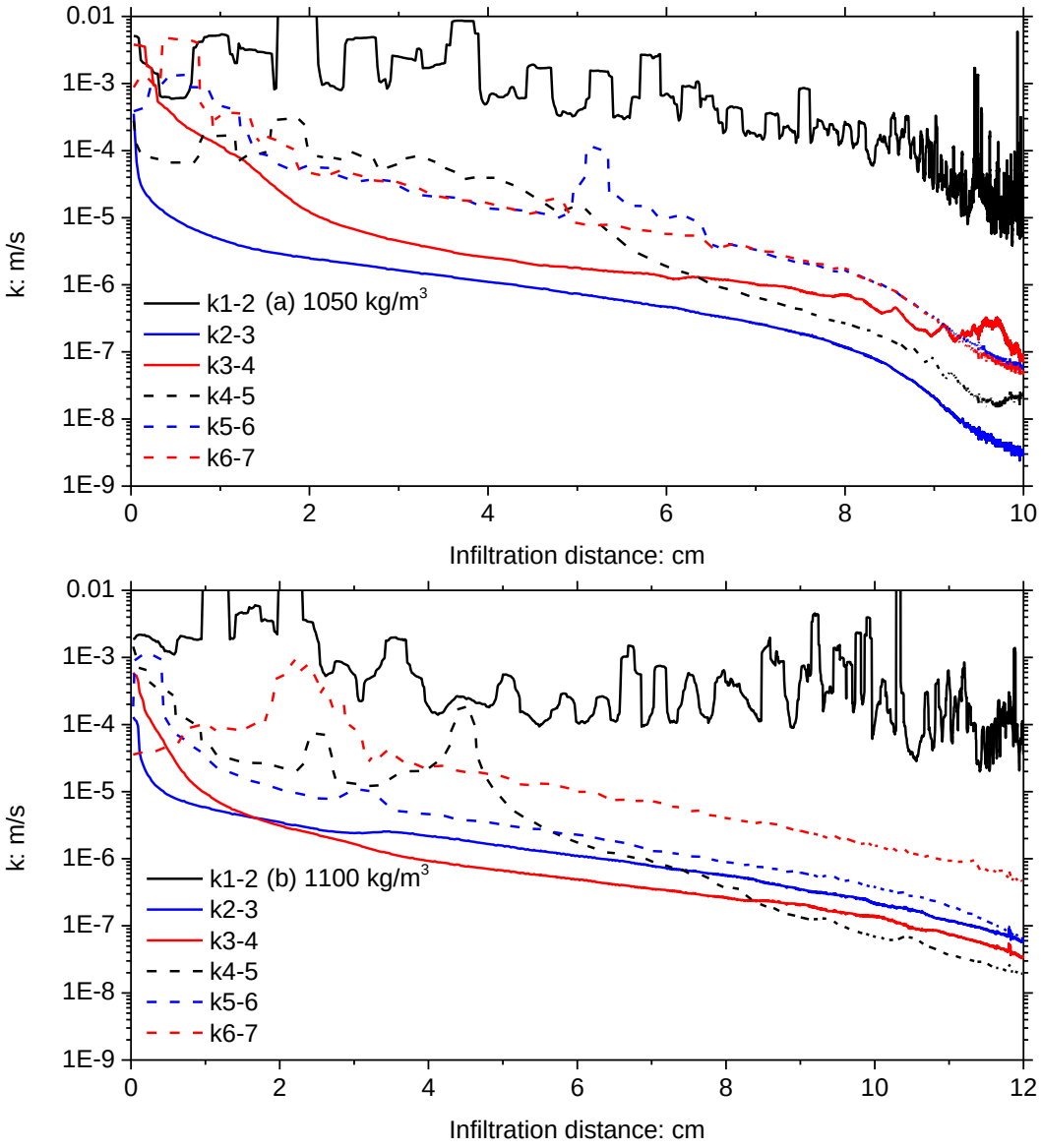

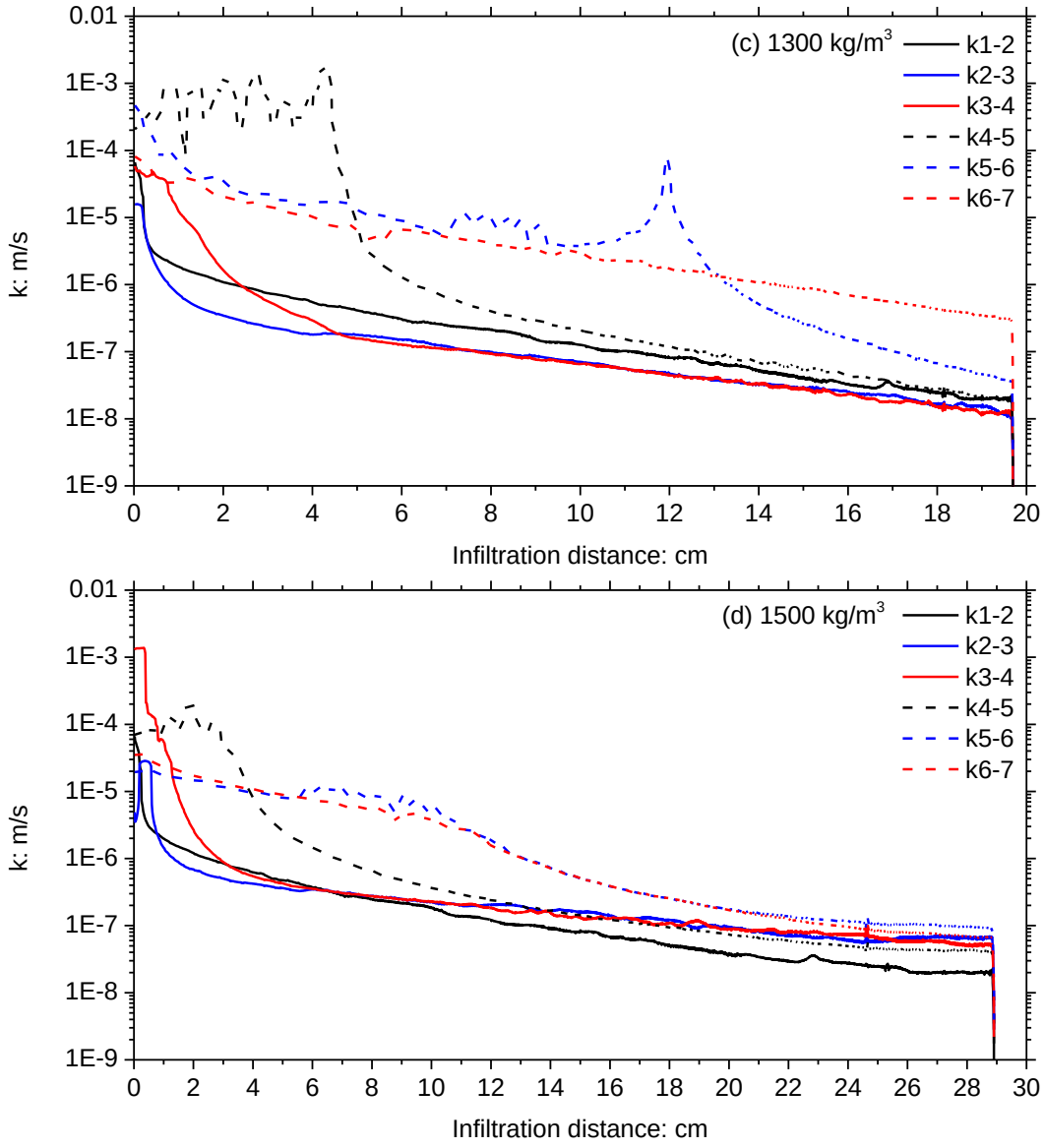

Fig. 4.15. Variations in the permeability of sand for fluids during infiltration of slurries containing sand.

In cases of 1050 and 1100 kg/m^3 slurries, k3-4 and k4-5 remain more or less constant when the filter cake has formed. But in the cases of 1300 and 1500 kg/m^3 slurries, k3-4 showed a continuous decrease and there appeared to be no filter cake formation. The external filter cake is created because bentonite particles are blocked by the sand grains and are pressed to a lower void ratio by the pressure difference over the slurry. However, in a slurry-sand mixture, the deposited sand grains create a grain skeleton and the pressure difference is taken by this

grain skeleton and not by the bentonite particles. The bentonite particles will stick to the sand grains and therefore do not deform to the same low void ratio.

The sand works as a 'deep filtration' for the bentonite particles. This is not the same process as can be seen from the measurements of the clean slurry. Mud spurt means that the slurry carrying bentonite particles moves into the sand. In case there is external cake formation there is hardly any pressure difference over the bentonite slurry in the mud spurt and as a consequence the mud spurt stops and only some water percolates through the bentonite particles. However, there is no feed of bentonite particles in the sand, so the permeability remains high. With deep filtration, there is no external filter cake, which means that there is a continuous feed of bentonite particles in the sand reducing the permeability continuously. The same process was noticed during the 2nd infiltration test of the 60 g/l slurry where there was also no external filter cake formation.

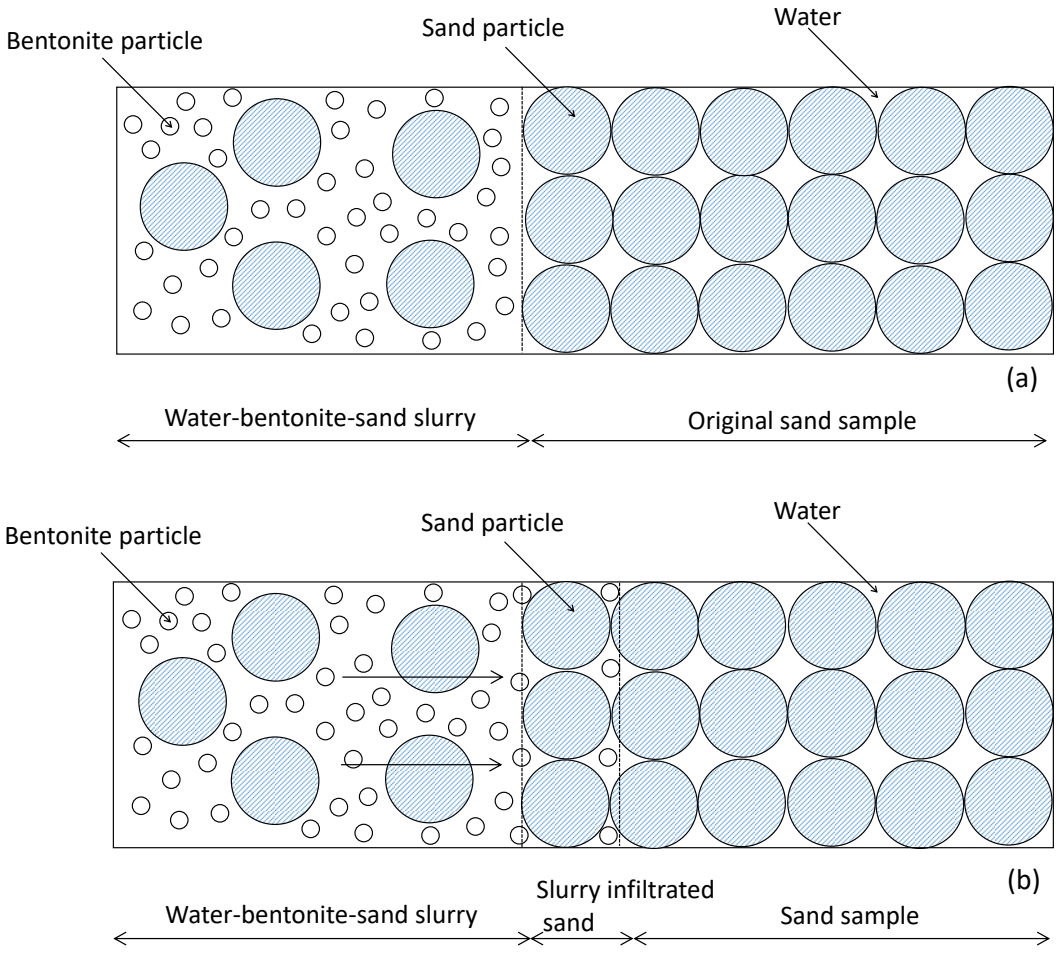

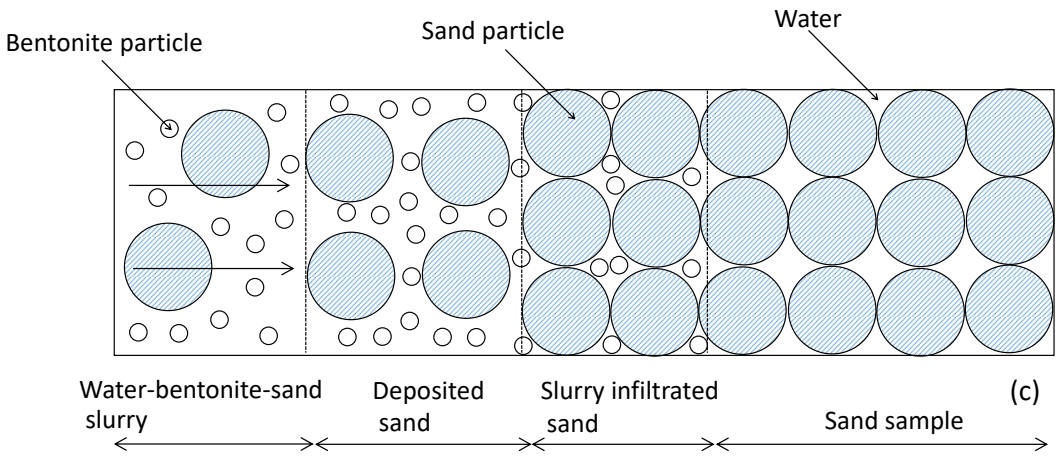

Fig. 4.16. Sketch of process of deep filtration: (a) Initial state; (b) Mud spurt/high and constant discharge; (c) Sand deposition.

'Deep filtration' is described for other disciplines than tunnelling, but the principles are the same. Fig. 4.16 shows a sketch of process of deep filtration, the initial state (Fig. 4.15a) is shown together to make the process clear. At the very beginning, the infiltration is the same as the clean slurry, the discharge is high and constant, but this process is very short, see Fig. 4.16b. Afterwards, as opposed to cake formation, solid particles (here bentonite particles) are retained in the pores of a deep filter layer (here deposited sand, or called 'sand bed', see Fig. 4.16c). This takes place for example in sand filters for clarification of drinking water, which retain even colloidal particles. The typical effect of deep bed filtration is adhesion of solids (here the bentonite particles) to the particles of the filter layer. Only rather big particles are retained by the screening effect. During deep filtration, the coarse material (the sand) becomes more and more clogged by the fine material (the bentonite). Consequently, the permeability in the sand decreases slowly.

For slurry without sand, cake formation occurs because when the pressure gradient presses water from the slurry, the bentonite particles get in contact and consolidate due to the pressure gradient over the particles creating effective stresses between the bentonite particles. In case of slurry with sand there are always incompressible sand particles these sand particles take most of the effective stresses in this way avoiding that the bentonite particles become a cake.

In case of 1300 kg/m^3 slurry, the permeability measured between k6 and k7 shows a continuous decrease, although theoretically the slurry has not yet reached that area. This may be due to the error of PPT k7. It can be seen from Fig. 4.17 that the pressure difference between k6 and k7 maintained more or less constant when the slurry has reached that area. The distance between the calculated infiltration locations, at which the pressure difference between k4-k5 and k5-k6 start to increase is more than 4 cm (the distance between the PPTs k4 and k5). It can be a consequence of the deep filtration. There is no mud spurt, but bentonite particles are captured on their way through the sand. This means, there is no direct slurry front. Water will move faster than the bentonite and consequently the pressure will not increase when the water from the slurry arrives but only when the bentonite particles arrive. Consequently, the bentonite concentration in the sand will be higher than in the slurry in the tests with deep filtration. During mud spurt there is, only one infiltration front of the slurry (seen as one component bentonite and water 'traveling' together). In case of deep filtration, the slurry has still infiltrated over that distance but in the sand, the 'far' front is only water from that slurry (what cannot be seen in the test) and indeed the bentonite particles stay behind and infiltrate less.

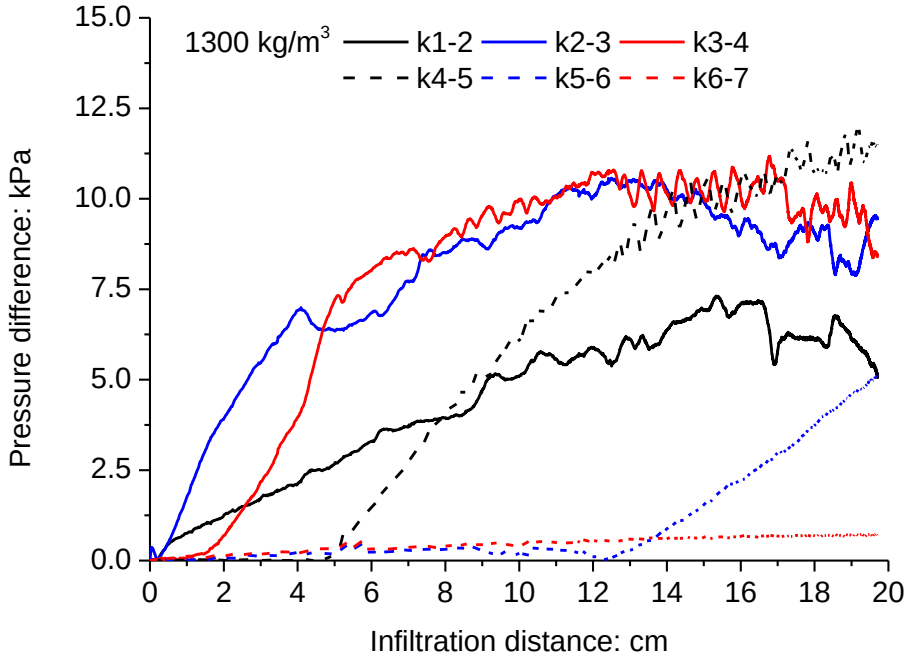

Fig. 4.17. Pressure difference with infiltration distance: slurry of 1300 kg/m^3.

Fig. 4.18 shows the comparison between the measured permeabilities in the first centimetres of sand for slurry with a density of 1500 kg/m^3 during the infiltration test in both a 20 cm and 30 cm thick slurry containing sand. The result looks very consistent. The very good agreement between the two curves indicated that the values of the permeability during infiltration of a 30 cm thick slurry containing sand are comparable to the values of permeability during infiltration of a 20 cm thick slurry containing sand.

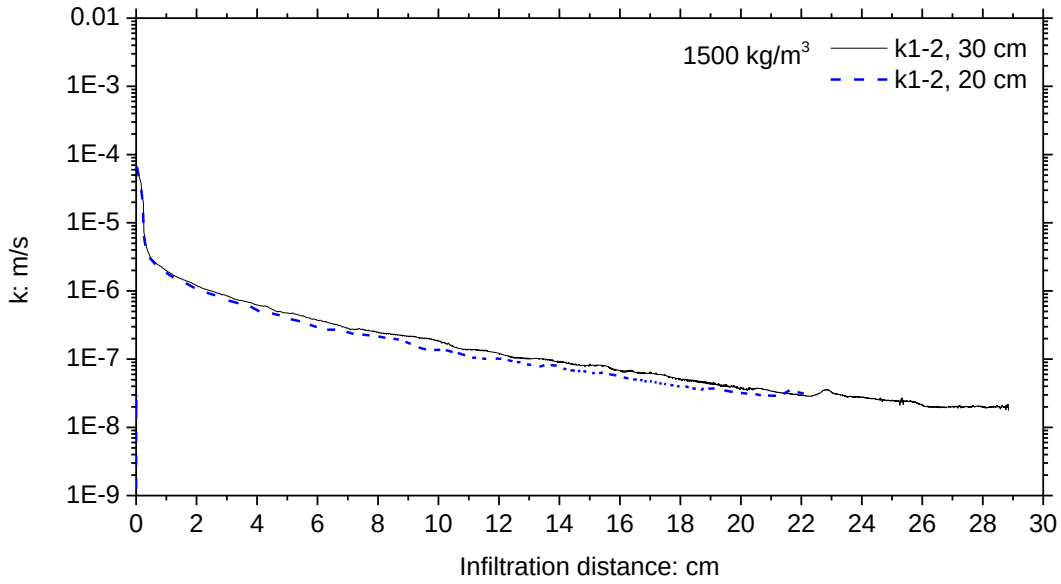

Fig. 4.18. Comparison between permeabilities of sand for fluids during infiltration of slurry of 1500 kg/m^3 with thicknesses of 20 and 30 cm, determined between PPTs k1 and k2.

4.3. CONSEQUENCES FOR TUNNELLING

The experimental results presented in this chapter have consequences for our understanding of plastering at the front of a slurry TBM. In the 1st series it was shown that the removal of an external filter cake can lead to the formation of a new one, but that it is also possible that no external filter cake is formed anymore when drilling of TBM is slower than infiltration, because the internal filter cake has become very impermeable due to gelling of the bentonite slurry. In that case the excess pore water in front of the tunnel face may have a steep increase just after ring building when the drilling has started and the ‘gelled’ internal filter cake is

removed. The increase will be much steeper when there is an external filter cake that is removed. This could be a typical moment that a blow-out occurred.

The period of mud spurt may be more significant for the face stability of slurry shield tunnels when the drilling velocity of TBM is faster than the mud spurt velocity, e.g. at GHT. In this case, the later period of mud spurt will only be relevant during standstill.

The 2nd series showed that with sufficient production (enough sand in the slurry) there will be no or hardly any external filter cake and only an internal one. It is likely that this will be present over a considerable larger distance than measured in 'traditional' slurry infiltration tests performed with slurry without sand. This last finding is positive for the safety of tunnelling when air intervention is necessary at the tunnel face, because it means that a low permeable slurry-sand mixture is present over a larger thickness in front of the tunnel face than up to now anticipated.

4.4. SUMMARY

A modified setup with a reduced permeability and a device available to remove the external filter cake has been presented. This modified setup can lead to pressure gradients and flow velocities that are comparable to what could be expected at the front of a slurry TBM of 10 m diameter. The process of cutting off the filter cake formed at the tunnel face by the cutting wheel is simulated by removing the filter cake formed on the original boundary between the slurry and the soil. In this modified setup, two series of infiltration tests with bentonite slurries have been performed: water-bentonite slurry and water-bentonite-sand slurry. The analysis and discussion of the experimental data with the new concept for mud spurt allowed the following conclusions to be drawn:

(a) After removing the external filter cake formed during the 1st infiltration, the external filter cake would be formed again during the 2nd infiltration for low concentrations of slurries (40 and 50 g/l) in fine sand as used in these tests. However, no new external filter cake formed for high concentration of slurry (60 g/l) due to an internal filter cake formed in the sand. For coarser sand it is likely that also for higher slurry concentrations there will be an external filter cake.

(b) The mud spurt before and after removing the filter cake is more or less the same during infiltration with low concentrations of bentonite, e.g. 40 g/l Colclay D90 slurry. For high concentrations of bentonite, e.g., 50 g/l Colclay D90 slurry, the mud spurt after removing the filter cake is much slower than that before removing the filter cake. There is no mud spurt anymore for 60 g/l Colclay D90 slurry after removing the filter cake.

(c) The filter cake is expected to be formed during infiltration with low densities of water-bentonite-sand slurry, e.g. 1050 and 1100 kg/m^3 for basic Colclay D90 slurries. In contrast, due to solid particles being retained in the pores of a deep filter layer, deep filtration appears to the high densities of water-bentonite-sand slurry, e.g. 1300 and 1500 kg/m^3 for basic Colclay D90 slurries.

(d) Because the permeability of sand for slurry k_b is a variable in infiltration of water-bentonite-sand slurries, the new concept for mud spurt (Eq. (2.12)) is not valid for these slurries, but can be used as an approximation only.

(e) The excess pore water pressure in front of the tunnel face may have a steep increase just after ring building when the drilling has started and the 'gelled' internal filter cake or external filter cake is removed. This could be a typical moment that a blowout occurred in front of the tunnel face.

(f) With sufficient sand in the slurry, there will be no or hardly any external filter cake and only an internal one. In that case, there will a considerable larger infiltration distance than that measured in the conventional slurry infiltration tests performed with slurry without sand. This is positive for the safety of TBM tunnelling when air intervention is necessary at the tunnel face, since a low permeable slurry-sand mixture is present over a larger thickness in front of the tunnel face than up to now anticipated.

PART III EXPERIMENTS ON FOAM INFILTRATION

EPB (Earth Pressure Balance) shield was first used in tunnelling in clayey soils, where an adequate consistency is given and thus additional soil conditioning was unnecessary (Budach and Thewes, 2015). With additional soil conditioning including chemical additives (e.g. foam), EPB shields have also be used in tunnelling in sandy soils, e.g. Botlek Rail Tunnel in the Netherlands, Port of Miami Tunnel in America, Metro Rio Line 4 in Brazil and Tehran Metro, Line 7 in Iran (Bezuijen, 2002; Merritt et al., 2013; Maidl and Pierri, 2014; Amoun et al., 2017). Soil conditioning with foam is important for an improvement of the excavated soil used for stabilising the tunnel face during closed-mode tunnelling with an EPB shield in sands because it conditions the soil. This improves the workability and the compressibility of the support muck in the excavation chamber, the material transport with the screw conveyor and reduces the permeability of the soil, preventing uncontrolled groundwater inflow to the excavation chamber. The pressurised soil-foam-mixture counteracts the natural earth pressure and groundwater flow towards the excavation chamber. However, the application of EPB shield in sandy soils up to now is based on experience with former tunnelling projects, the standardized experimental investigations and comparable standardized test methods were not commonly used (Budach and Thewes, 2015).

On one hand, many experimental studies have been carried out to investigate the properties of the foam and foam conditioned soil, and their effects on the performance of the cutting wheel and the pressure balance in the excavation chamber of an EPB shield (Maidl, 1995; Quebaud et al., 1998; Bezuijen et al., 1999; Peña, 2003; Merritt and Mair, 2006; Peila et al., 2007; Mooney et al., 2017; Bezuijen, 2012; Budach and Thewes, 2015). Quebaud et al. (1998) comprehensively presented the consistency test, the half-lifetime test and the compressibility test of the foam as a conditioning agent for EPB tunnelling. It was shown that the foam contributes to the fluidification and the lubrication of the soil-foam-mixture. They also recommended the slump test to determine the quality of the conditioned soil. This test is said to be efficient to find easily a suitable FER (foam expansion ratio) and FIR (foam injection ratio) value for a first assessment for the design and operation of TBM (Peila, 2009). Budach

and Thewes (2015) gave a useful range of additives used in EPB tunnelling for different soils based on laboratory tests. In their study, different conditioning agents were tested to examine their properties, an overview of qualitative influence of different parameters on the quality of foam as well as the properties of conditioned coarse-grained soils were presented. In addition to foam, experimental investigations on the properties of soil-foam-mixtures were also carried out in different laboratories (Bezuijen et al., 1999; Mair et al., 2003; Borio et al., 2011; Bezuijen, 2011; Mori et al., 2018). The experiments from Mori et al. (2018) demonstrated that void ratio and effective stress are the main factors that influence the performance of foam-conditioned soil. It was determined that a certain ratio of the void ratio to the maximum void ratio was required to prevent the development of appreciable effective stress and thus, high shear strength and low compressibility. Furthermore, model tests with a small scale screw conveyer, which simulates the extraction of the spoil from a pressure chamber in a similar way as in EPB tunnelling have also been conducted by Bezuijen and Schaminée (2001), Merritt and Mair (2006), Peila et al. (2007) and (Vinai et al, 2008). However, this part is not a research target in this contribution.

On the other hand, only some studies are related to the condition of the tunnel face, e.g. Bezuijen and Schaminée (2001) and Galli (2016). The infiltration of pressurised foam into the soil, which has significance for the tunnel face stability, because due to infiltration the effective support pressure at the tunnel face and thus the tunnel face stability will be reduced. Bezuijen and Schaminée (2001) performed some model tests to examine the effect of pore water in the soil on FIR and FER_m, more comprehensive findings from these model tests were given by Bezuijen (2011, 2012). It was found out that FER_m is more important than the original FER to predict the properties of the soil-foam-mixture in saturated sand. Residual pore water significantly decreases the FER_m resulting in wet foam. Almost complete replacement of the pore water by foam is necessary to have a FER_m that is comparable to the original FER. Due to the pore water in the soil-foam-mixture, the FER_m (Effective Foam Injection Ratio) of the soil-foam-mixture will be much lower than the FER of the foam. Bezuijen (2012; 2013) found out that, for the situation of a soil-foam-mixture with a FER_m of 6 or lower and sufficient FIR, there is no effective stress on the bore front, the front will be stabilised due to an outward directed pore water gradient and a gradual build-up of effective

stress (as sketched in Fig. 6.1). Such stabilization is less effective than when directly an effective stress is present and therefore higher face pressures will be needed for such a situation. Just recently, Galli (2016) carried out some experiments on infiltration of foam into saturated sand and found out that the infiltration process can be evaluated quantitatively by a regression analysis. Though a flow model for porous media to the foam infiltration process would be needed to provide a sound description of the processes, a power-law equation $x = a \cdot t^{0.166}$ (x (m) is the infiltration distance, a (m·s$^{-0.166}$) the fitting factor and t (s) the time) with intercept zero showed a good agreement with the experimental results. The emphasis of his research was on the short term foam infiltration behaviour during excavation and hence his tests were run up to 180 seconds. To improve our understanding of the mechanism of foam infiltration at the tunnel face in EPB shield tunnelling, e.g. the infiltration characteristics, the scale effect and the consequences of foam infiltration for EPB TBM tunnelling etc., further experimental research is necessary.

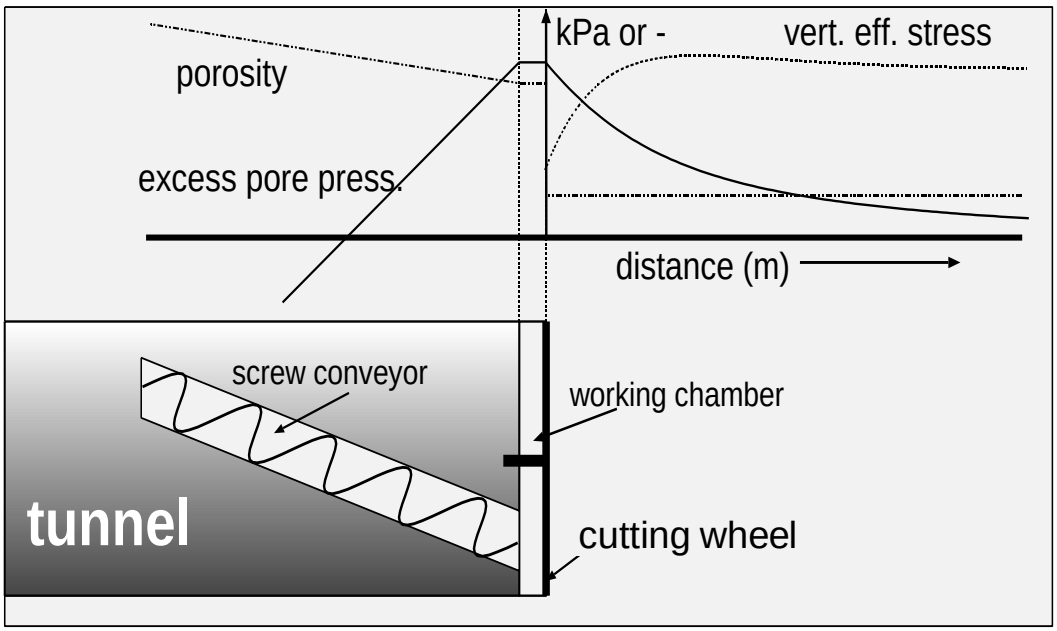

Fig. III.1. Sketch of course pore pressure, porosity and effective stress in front of an EPB shield (after Bezuijen and Schaminée, 2001).

CHAPTER 5 PRESSURE INFILTRATION OF FOAM

Chapter 5 presents the experiments of pressure infiltration of foam into saturated sand in the modified setup. Four different phases were identified in the infiltration: foam bubble infiltration, water flow permeability reduction, water flow permeability increase and residual phase. It appears that the infiltration depth of foam into sand decreases with increasing Foam Expansion Ratio (FER) of the foam until a limit FER (approximately 15 for the foaming agent and sand used in this experiment). For higher FERs the permeability remains more or less constant. It was found out that a 'dry' foam (FER = 20) is not essential for formation of a low permeable layer in the sand, even a 'wet' foam (FER = 5) can form a low permeable layer. A foam-infiltrated zone is essential to achieve a low permeable layer. In some of these tests, the flow velocities were less than the normal excavation velocity of a TBM. Then there will be no foam-infiltrated zone and consequently no zone with low permeability during drilling. Through comparing the pore pressures measured with Pore Pressure Transducers (PPTs) with and without hydrophilic filter papers, capillary pressure was found in the foam-infiltrated sand. In this chapter, experiments of infiltration of foam with various FERs and at different air pressure have been conducted.

5.1. DEFINITIONS

In this chapter, the following definitions are used:

FER: $FER = \frac{Q_F}{Q_L} \cdot \%$ (%)

This parameter indicates how much air is used for each volume of water and foaming agent.

FER_m: $FER_m = \frac{Q_{FM}}{Q_L + Q_{RW}} \cdot \%$ (%)

Normally this is less than the FER due to the residual pore water in the soil (Bezuijen, 2012).

FIR: $FIR = \frac{Q_F}{Q_S} \cdot \%$ (%)

Q_F: Flow rate of foam (m^3/s);

Q_L: Flow rate of foaming liquid (foaming agent +water) (m^3/s);

Q_{FM}: Flow rate of foam in the excavated soil (foaming liquid + residual pore water) (m^3/s);

Q_{RW}: Flow rate of residual pore water in the excavated soil (m^3/s);

Q_S: Flow rate of excavated soil (m^3/s). Q_S can be calculated from the advance rate v_{TBM} (m/s) and the face area A_f (m^2): $Q_S = v_{TBM} \cdot A_f$.

5.2. EXPERIMENTAL STUDY

5.2.1. TEST MATERIALS

5.2.1.1. FOAM

A foam generator FG3 (Budach and Thewes, 2015) at Ruhr University Bochum, which is a reproduction of an original foam generator of an EPB shield but suitable for low flow rates, was used to generate foam for these experiments. Budach (2012) describes the possibilities of influencing the foam properties by the variability in the generator parameters, the parameters of the foam ingredients and the properties and the variability in the parameters of the foaming system. Since the influence of the foaming agent is not a topic in the present study, one surfactant, Condat CLB F5/TM, in one concentration of 3 Vol% was used in all tests. This surfactant and concentration is recommended to be used predominantly in highly permeable sands (Condat Lubrifiants, 2015). Properties of the foam itself used in this experimental study have been reported by Budach (2012) and Galli (2016).

5.2.1.2. SAND

The Euroquarz S80 sand was used for the experiments. The characteristic grain diameters d_{10}, d_{50}, d_{60}, d_{90} are 0.11, 0.16, 0.17 and 0.24 mm, respectively. The minimum and maximum dry densities of the sand are 1550 and 1950 kg/m^3. The permeability of the sand at a saturated

density of 2060 kg/m^3 is 1.00 × 10^{-4} m/s. The saturated density of the sand varied between 2050 and 2080 kg/m^3 in the various tests.

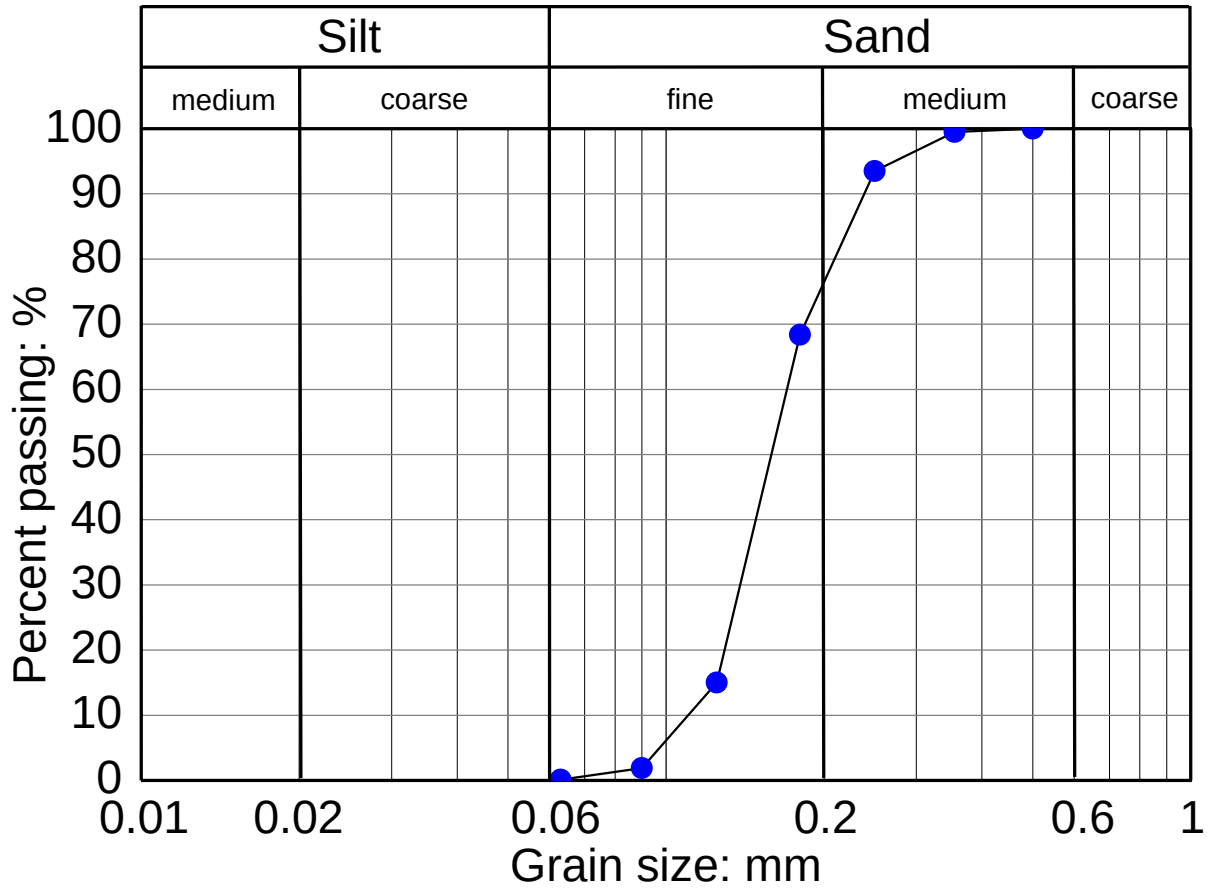

Fig. 5.1. Grain size distribution of S80 sand.

5.2.2. Setup and procedure

The setup used for these experiments is shown in Fig. 5.2, which has been described in detail in Chapters 3 and 4. Four PPTs, numbered k1 to k4, are used to measure the pore water pressures in the foam and sand during the test. To ensure the sufficiency of foam, the foam was brought up to a certain height, 30 cm, above the sand surface at atmospheric pressure. Because foam normally collapses after about 40 minutes (Budach, 2012), this process has to be performed rather quickly (less than 5 minutes) to avoid separation of the air and the liquid. When the pressure is increased but the valve below is still closed, the volume and thus the

height of the mixture will decrease, because the volume of the air is pressure dependent. The FER, thus is related to the absolute pressure. The value of FER_p is calculated by:

$$FER_p = \frac{p_a}{p}(FER_a - 1) + 1 \tag{5.1}$$

Where FER_p is the *FER* at the desired air pressure; FER_a the *FER* at atmospheric pressure; p_a the atmospheric pressure (kPa) and p the desired air pressure (kPa).

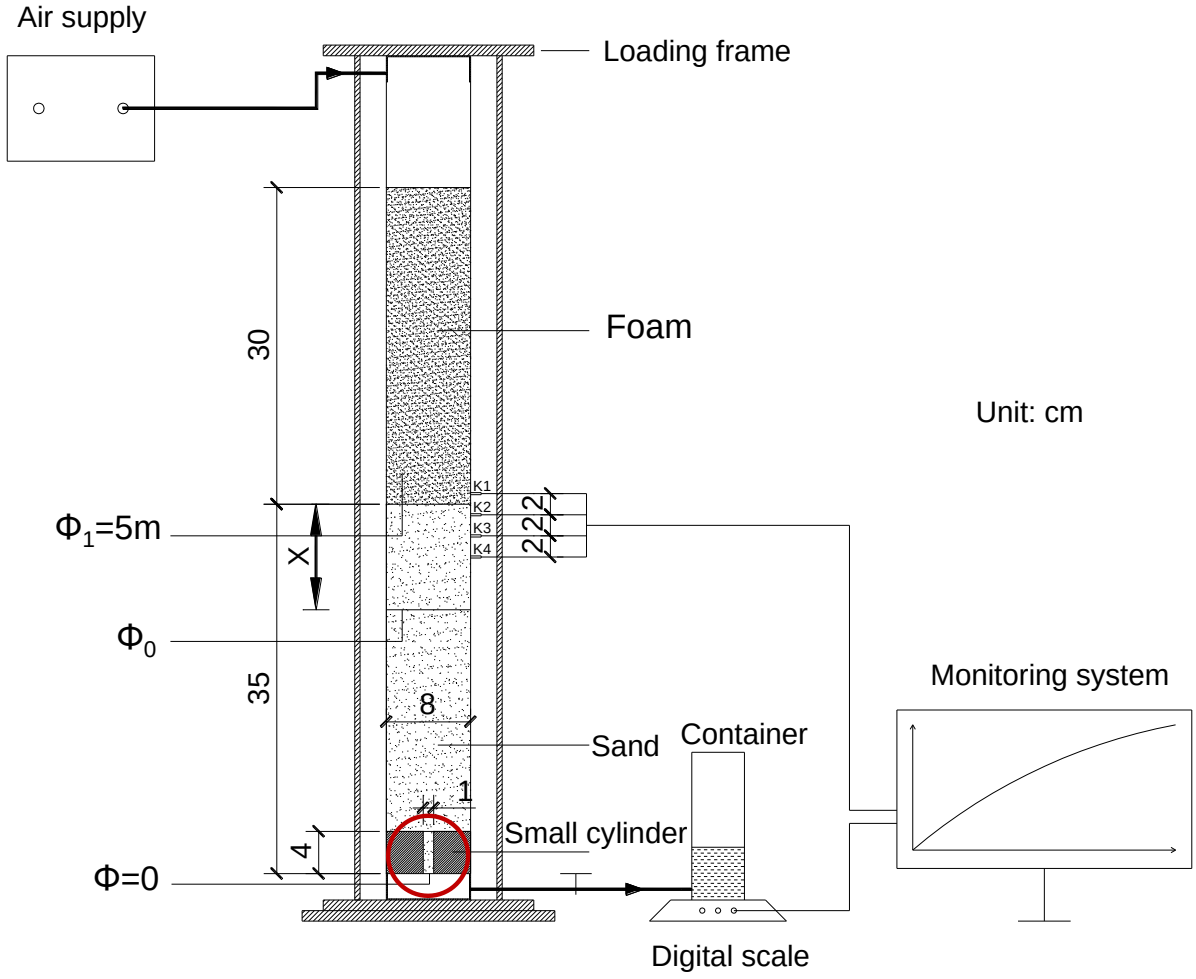

Fig. 5.2. Scheme of the setup and principle of pressure infiltration of foam.

In these experiments, the foam is produced at atmospheric pressure and pressurised in the setup at the desired air pressure of 0.5 bar above atmospheric pressure. Therefore, FER at atmospheric pressure has to be roughly 1.5 times higher than the FER at the desired air

pressure at which the experiment will be performed. For example, to get a foam of FER = 20 at 1.5 bar (absolute pressure), FER should be 29.5 at atmospheric pressure.

Depending on the permeability of the sand and the drilling speed, foam in tunnelling could be wet or dry (Bezuijen and Schaminée, 2001; Bezuijen, 2012). Tests therefore were performed with a 'dry' foam (FER = 20) but also a rather 'wet' foam (FER = 5). Other FER (10, 15) were also tested. It is also realized that there is a scale effect on the behaviour of foam. Although it is hard to reach perfect scaling, it is of importance to get some ideas on dependencies. If there is a tunnel at 20 m below the groundwater table, then the absolute pressure will be around 3.5 bar (atmospheric pressure + 2 bar pore pressure + 0.5 bar 'excess pressure' to stabilise the face). Now the FER in the soil after infiltration, on the relatively low pressure side (atmospheric pressure + 2 bar pore pressure) is only 23 instead of 30 in the test. This situation, a FER of 20 on the high-pressure site and 23 at the low-pressure site, can be simulated by using a smaller pressure in the tests, 1.15 bar instead of 1.5 bar. In this test, the foam expansion will be in agreement with the expansion that can be expected for a tunnel 20 m below the groundwater table, but the pressure gradient and consequently the infiltration will be less compared to the field situation.

5.2.3. Experimental results

5.2.3.1. Discharges and properties of foam-infiltrated soil

Fig. 5.3 presents the water discharges against time for different FERs at a pressure of 1.5 bar. As shown in the figure, in theory, various situations can be expected at the tunnel face in EPB shield tunnelling:

1) The first phase is 'foam bubble infiltration' (Fig. 5.4a). The flow is determined by the 'foam bubble infiltration'. The term 'foam bubble infiltration' is analogous to 'mud spurt' in experiments of slurry infiltration into saturated sand. In this phase, foam bubbles will replace the pore water in the sand. The discharge at the beginning is high and will decrease to a small value at the end of foam bubble infiltration, see Fig. 5.3. In this phase, the overall permeability of sand for foam flow (with foam of a constant defined quality) can be calculated by Darcy's Law:

$$k_f = Q\frac{x}{\Delta\phi_f \pi (D_1/2)^2} \tag{5.2}$$

Where Q is the discharge (m^3/s); x the thickness of the foam-infiltrated sand or the foam infiltration depth (m); $\Delta\phi_f$ the difference in piezometric head over the foam-infiltrated sand (m); D_1 (m) the diameter of the large cylinder.

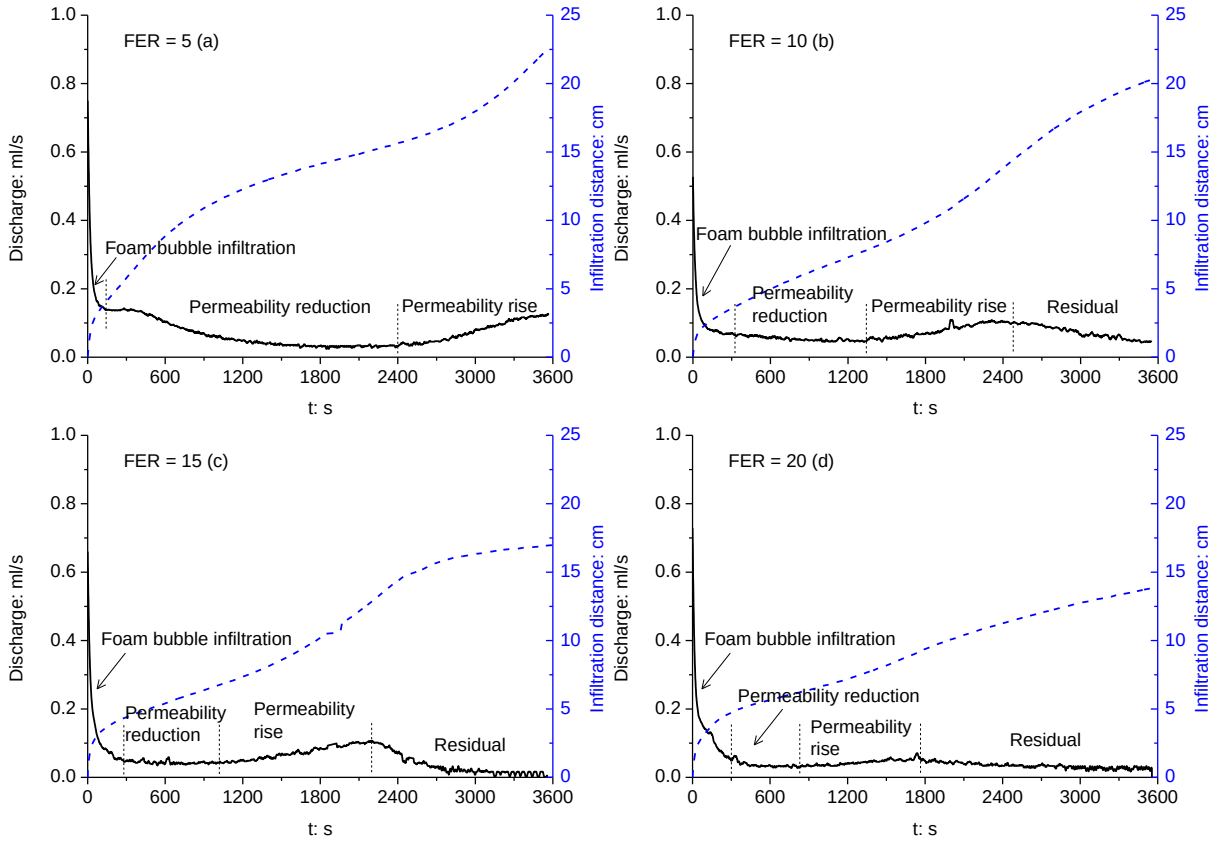

Fig. 5.3. Discharges and infiltration distances against time.

Table 5.1. Final infiltration depths for various FERs.

FER	5	10	15	20
Observed depth (cm)	10	9.5	9	8
Calculated depth (cm)	25	20	17	14

Eq. (5.2) is only valid if the flow is incompressible. For the foam flow, deviations are possible because the entrenched air inside the foam lamellae is compressible. A sketch of this situation can be seen in Fig. 5.5. In the case of foam bubble infiltration, x and $\Delta\phi_f$ are time-dependent

variables. After the foam bubble infiltration, water will continue to infiltrate, but with a much slower velocity. Table 5.1 shows that the roughly observed final infiltration depths are smaller than the calculated values For instance, the calculated depth is 25 cm for FER = 5, whereas the observed depth is only 10 cm (see Fig. 5.6). That means the visual observation of foam infiltration might be wrong and that foam is infiltrating deeper that it can be seen outside the cylinder. Another reason could be that there was slightly more water in the cylinder before adding the foam than is needed to saturated the sand sample. Therefore, it is essential to define 'infiltration' in this thesis as the replacement of the original pore water, rather than the visual foam bubble front. In the foam bubble infiltration, it was observed that the foam flow front was consistent with the water front.

2) The second phase is 'water flow permeability reduction' (Fig. 5.4b). Since the foam bubbles are blocked by the sand grains, there will be a low permeability layer formed within these sand grains. The foam bubbles will not infiltrate further into the soil, only the pore water flows around the bubbles and the sand grains. In this phase, the discharge is very small. From the foam bubble infiltration phase, it is known how far the foam will come during foam bubble infiltration and this value can be used to calculate the overall permeability. Here, Eq. (5.2) will also be used. Since the foam front has not been observed directly, 'x' is assumed to be the final thickness of the infiltrated sand at the end of the foam bubble infiltration (L_f). $\Delta\phi_f$ is the difference in piezometric head over the infiltrated sand at the end of the foam bubble infiltration (here 50 kPa). The permeability of the sand, determined by Eq. (5.2), is the permeability of the foam-sand-mixture. This permeability should be much lower, than that during the foam bubble infiltration. This phenomenon is clearer for low FER = 5, see Fig. 5.3a.

3) The third phase is 'water flow permeability increase' (Fig. 5.4c). The discharge slightly increases (Fig. 5.3). Probably the size of bubbles decreases due to the dissolving of air in the water or some further migration of air bubbles in the sand leading to an increase of the saturation in the original infiltration zone of the foam bubble infiltration. Consequently, there is an increase in the permeability of sand.

4) The fourth phase is ‘residual phase’ (Fig. 5.4d). Again, the discharge and the overall permeability decreases probably due to a process comparable to deep filtration of slurry containing sand, in which there is some slurry leaving the area of infiltrated sand to settle again further in the deeper sand (Chapter 4). Analogously, in the surface sand, which has been infiltrated by foam, deep filtration could cause small bubbles to infiltrate into the pore canals in between the sand grains and the block these pore canals, leading to a decrease in permeability.

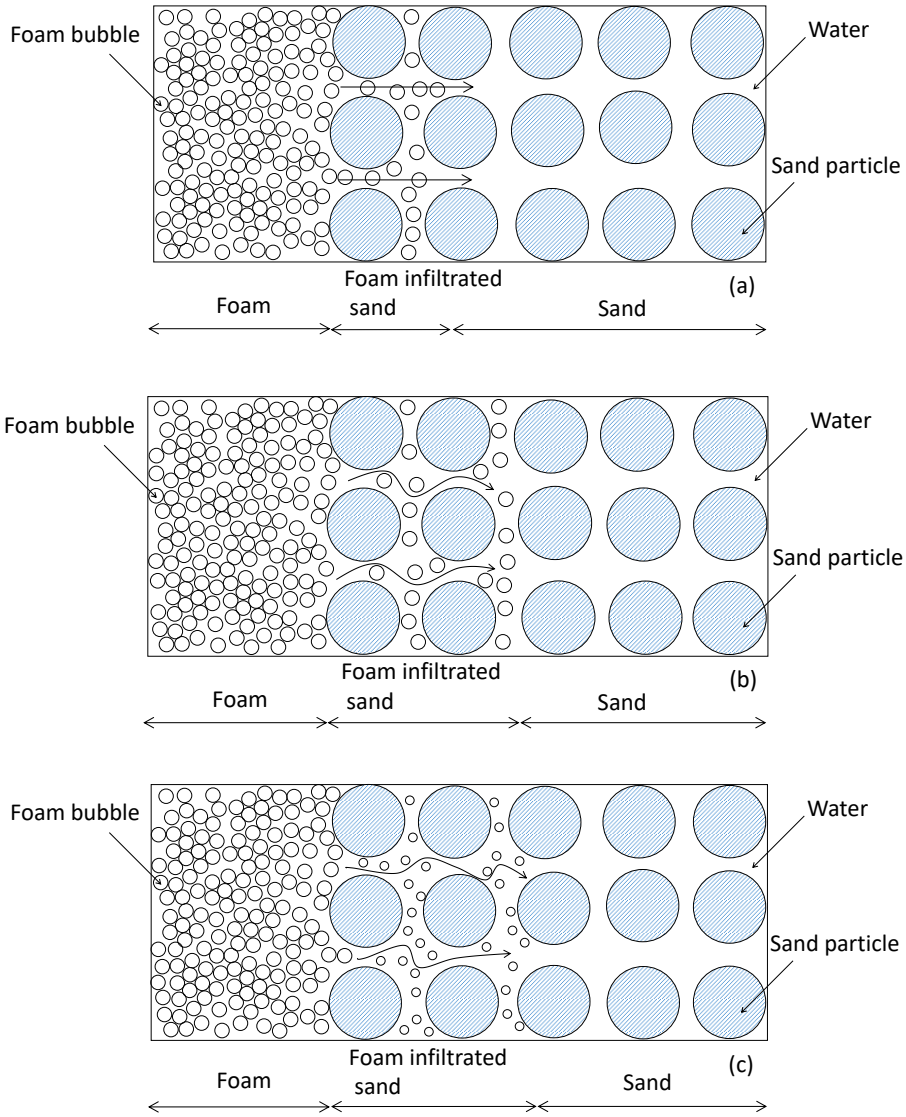

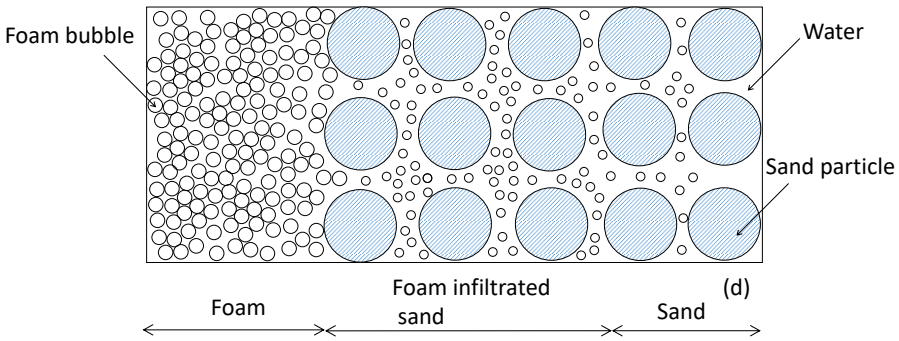

Fig. 5.4. Sketch of various phases of foam infiltration: (a) Water flow and foam bubble infiltration, (b) Water flow permeability reduction, (c) Water flow permeability increase; (d) Residual phase.

In some of these tests, the discharges were less than the corresponding excavation velocity of a TBM, e.g. 6.60×10^{-4} (measurement location MQ1 South) or 7.50×10^{-4} m/s (measurement location MQ4 South) in the Botlek Rail Tunnel (Bezuijen, 2002). Then there will be no foam bubble infiltration and consequently no zone with low permeability, as already found by Bezuijen and Schaminée (2001).

From the results of permeability tests in Section 5.2.3.3, it can be seen that the drop of k3-4 is the largest in this phase, indicating a low permeable layer probably was formed in the deep layer. Correspondingly, k1-2 and k2-3 also decreased slightly, leading to the decrease in discharge (see Figs 5.3b – 5.3d). This phase was not observed in the test on the foam with FER = 5 because it was delayed by a longer duration of the fourth phase.

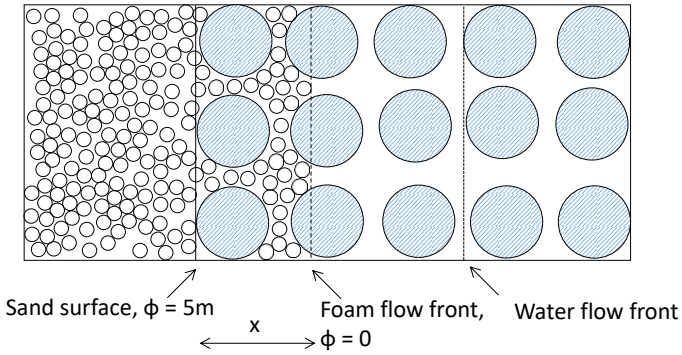

Fig. 5.5. Sketch for calculation of permeability from discharge (Eq. (5.2)). *x* is the infiltration depth (the same as the '*x*' in Fig. 5.1).

A certain pressure gradient is needed to push the bubbles through the pores between the grains. When the bubbles are pushed further into the grain skeleton, the gradient decreases since the total pressure drop remains constant. At a certain moment, the gradient is too small to push the bubbles further into the soil skeleton and only the foaming liquid around the bubbles will 'travel' further into the soil, which leads to a reduction of the infiltration velocity. The process is comparable to the mud spurt described for infiltration of slurry. During mud spurt, it is the yield stress of the slurry that stops the bentonite infiltration, during foam bubble infiltration, it is the pressure drop over a bubble that is necessary to push it through the pore channels.

Fig. 5.6. Photo of the infiltrated soil in the test on foam with FER = 5 after 1 hour.

After a test, the residual water plus foaming liquid content of the soil was determined by taking out the top 1 cm foam-infiltrated sand; determine its weight and drying it in an oven at 105 ^{o}C for 24 hours and determine the weight again. Fig. 5.7 shows the measured residual pore water plus foaming liquid contents of soil together with the theoretical values assuming

that the pore water was completely replaced by foam bubbles. It is clear from the figure that the measured values are higher than the theoretical values because not only foaming liquid, but also residual pore water remain in the pores in soil. Moreover, for different FERs, the differences between the measured and the theoretical values are very similar. Consequently, FER_m in the zone in which the foam has infiltrated will be much lower than the original FER, see Fig. 5.8.

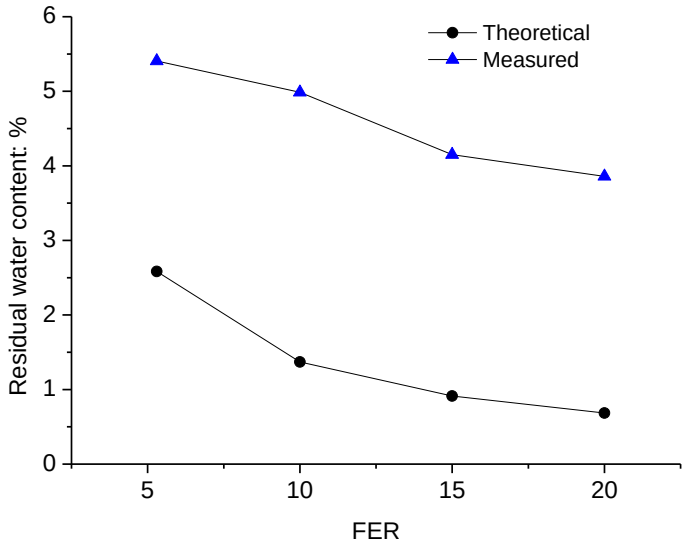

Fig. 5.7. Measured and theoretical residual pore liquid content in the top 1 cm of foam-infiltrated soil.

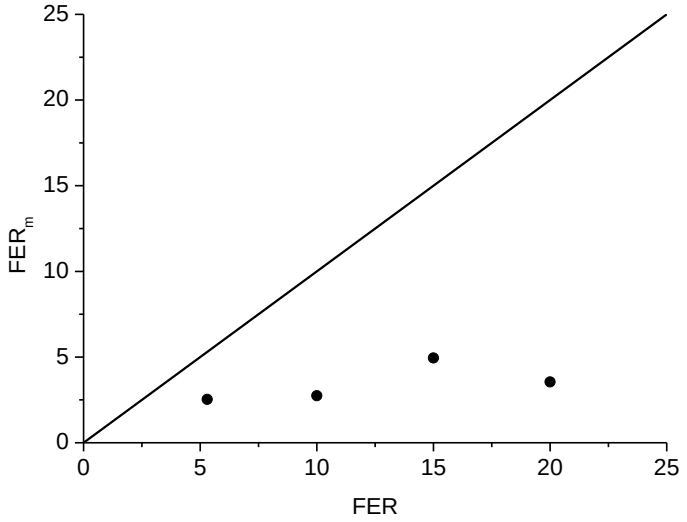

Fig. 5.8. Comparison of measured FER_m and FER of the foam.

5.2.3.2. PRESSURE MEASUREMENT

Fig. 5.9 show the variations in pore water pressure at various sections. The pressures in the foam (k1) above the sand are more or less constant. Due to the flow caused by the infiltration of foam, the pressures in the sand (k2 to k4) decrease to hydrostatic pressure. For FER = 10, 15 and 20, k2 to k4 start to increase gradually, after about 1800 seconds. This increase in pressure may be caused by a water flow in the sand due to the dissolving of air in the water or some further migration of air bubbles in the sand.

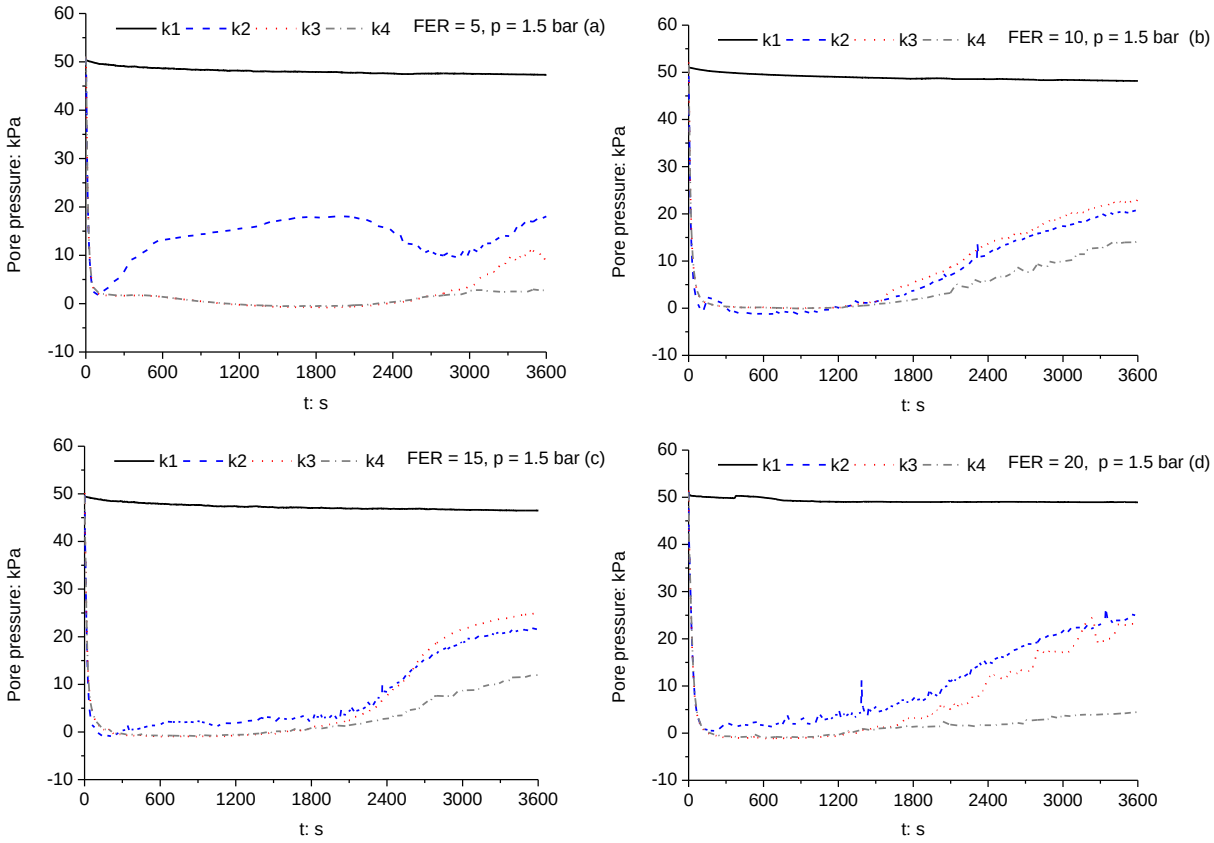

Fig. 5.9. Pore water pressure variations with time, PPTs without hydrophilic filter papers.

As can be seen in Fig. 5.9, there are sometimes irregularities of the measurements (e.g. k2 in Fig. 5.9a) that are difficult to explain. The reason could be: The foam front has passed k2 (1 cm below the sand surface), and hence the PPTs are measuring air pressure instead of water pressure. Therefore, the pore pressures probably cannot be measured as straight forward as in a slurry infiltration test. Since the foam-water mixture is a two-phase mixture, there are also

two ‘pore pressures’, the pressure of the pore water and the pressure of the air. The difference between these two is the capillary pressure. The difference between these two pressures can be measured with selective pressure gauges (Oung and Bezuijen, 2003). With a hydrophilic filter paper, only the water will pass the filter paper and the pressure measured is the water pressure. However, with a hydrophobic filter paper, the filter paper will be filled with air, or silicone oil and the air pressure is transmitted, if there is air available. Without air, in the beginning of our tests, the pore water pressure is measured. Within the limits of this research, it was not possible to test different filter papers. Most tests were done without any filter papers, only a few could be performed with hydrophilic filter papers to measure the pore water pressures.

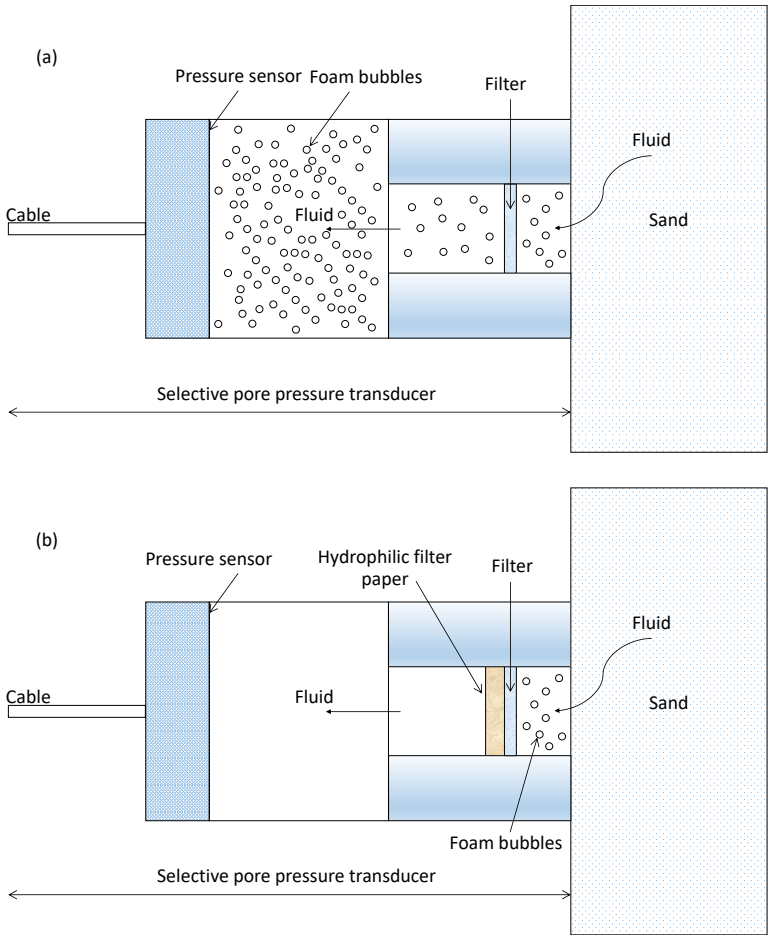

Fig. 5.10. Pore pressure transducer: (a) Without hydrophilic filter paper and (b) With hydrophilic filter paper.

The construction details of the PPTs are shown in Fig. 5.10a and pore pressures were measured with the PPTs with or without hydrophilic filter papers, which were installed in front of the PPTs to filter the foam bubbles, see Fig. 5.10b. Fig. 5.9 shows the pore water pressure variations with time, PPTs with hydrophilic filter paper. It can be seen from Fig. 5.9a and Fig. 5.11 that the hydrophilic filter papers indeed make a difference. After a sharp decrease due to foam infiltration at the beginning of the test, the curve of k2 without hydrophilic filter paper in Fig. 5.9a increases because the foam bubbles enter the tube where the PPTs are installed and thus the measured pressures are at least also influenced by the pore air pressures. For k2 with hydrophilic filter paper, the filter paper prevents the foam bubbles from entering the tube where the PPTs are installed, the measured pressures are thus the pore water pressures. This phenomenon (the capillary pressure) is known for decades in agriculture and oil industry (Davidson et al., 1965; Hammervold et al., 1998), but seemingly this has not yet been considered for TBM tunnelling. The air pressures are higher than the pore water pressures, because the air pressure has also to overcome the surface tension of the water just around the bubble. This has to be taken into account when in the next section permeabilities are determined using pressure measurements without hydrophilic filter paper.

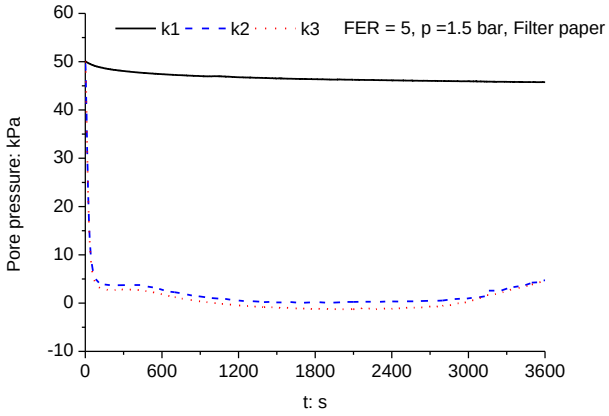

Fig. 5.11. Pore water pressure variations with time, PPTs with hydrophilic filter paper.

Comparing Fig. 5.9a to Fig. 5.11, k2 increased after 2.5 cm of infiltration distance because the foam front had passed it and thus foam bubbles injected into it. There is also some increase in k4 after 18 cm of infiltration distance, where the infiltration distance is larger than the depth of k4 itself. The reason is that after foam bubble infiltration, the water flow was faster than the

foam flow, thus compared to the water flow the time when the foam bubbles injected into k4 was delayed. Unfortunately, PPT k4 with hydrophilic filter paper was broken during test and couldn't be replaced and hence it is not presented in Fig. 5.11.

5.2.3.3. PERMEABILITY

Using the method in Section 5.2.3.1, the permeability of sand for foam flow or water flow through sand and foam bubbles is calculated, which is called 'permeability calculated with discharge'. The values of Q, x and $\Delta\phi_f$ in Eq. (5.2) can be derived from Figs 5.3, 5.9 and 5.10. In the foam bubble infiltration, L_f will be a time dependent variable. As mentioned above, after foam bubble infiltration, the calculated infiltration depths will be larger than the visual ones and hence the depths were assumed to be the infiltration depth of foam bubble infiltration: L_f = 3, 3, 4 and 5 cm in the infiltration of the foams with FER = 5, 10, 15 and 20, respectively. The differences in piezometric head over the foam-infiltrated sand, k1-k3 (FER =5 and 10), k1-k4 (FER = 15 and 20), can be obtained from Figs 5.9 and 5.11 for the foam bubble infiltration. After the foam bubble infiltration, $\Delta\phi$ = 5 m at a pressure of 1.5 bar and 1.5 m at a pressure of 1.15 bar.

Eq. (5.2) can be also used to calculate the permeability of sand for foam flow with pore pressures, through replacing the item 'x' by 'ΔL_s' (the thickness of sand between two adjacent PPTs) and '$\Delta\phi_f$' by '$\Delta\phi_p$' (the corresponding difference in piezometric head over the sand between two adjacent PPTs); this is called 'permeability calculated with pore pressures'. For the water with foaming liquid, deviations are possible because the pore water (with the foam) is compressible. The permeability of sand for foam or water flow calculated with pore pressures, can be compared with the overall permeability determined with discharge.

Fig. 5.12 shows the permeabilities calculated with pore pressures together with the overall permeabilities calculated with discharges. The curve of 'permeability calculated with discharge' is divided into 'foam bubble infiltration' and 'after foam bubble infiltration' by the vertical line in Fig. 5.12 (and also Figs 5.13 and 5.17). The permeabilities calculated with pore pressures k1 and k2 (FER = 5, 10, 15), or k2 and k3 (FER = 20) are consistent with the overall permeabilities calculated with discharges. This indicates that the theory associated with Figs 5.5 and 5.6 is correct, the highest flow resistance is present in the first few

centimetres of the sand column where the foam bubble infiltration occurs. Although later during the experiment the foam infiltrated deeper (see Fig. 5.6), the permeability in these deeper layers remains higher and do not really contribute to the total flow resistance (see also the measured permeability between the PPTs k3 and k4 for FER = 5, Fig. 5.12a). If the infiltration depth in the foam bubble infiltration is larger, e.g. for FER = 20, the foam front passed PPTs k3 and k4 and hence the permeability calculated with discharge was consistent with k3-4 calculated with pore pressures.

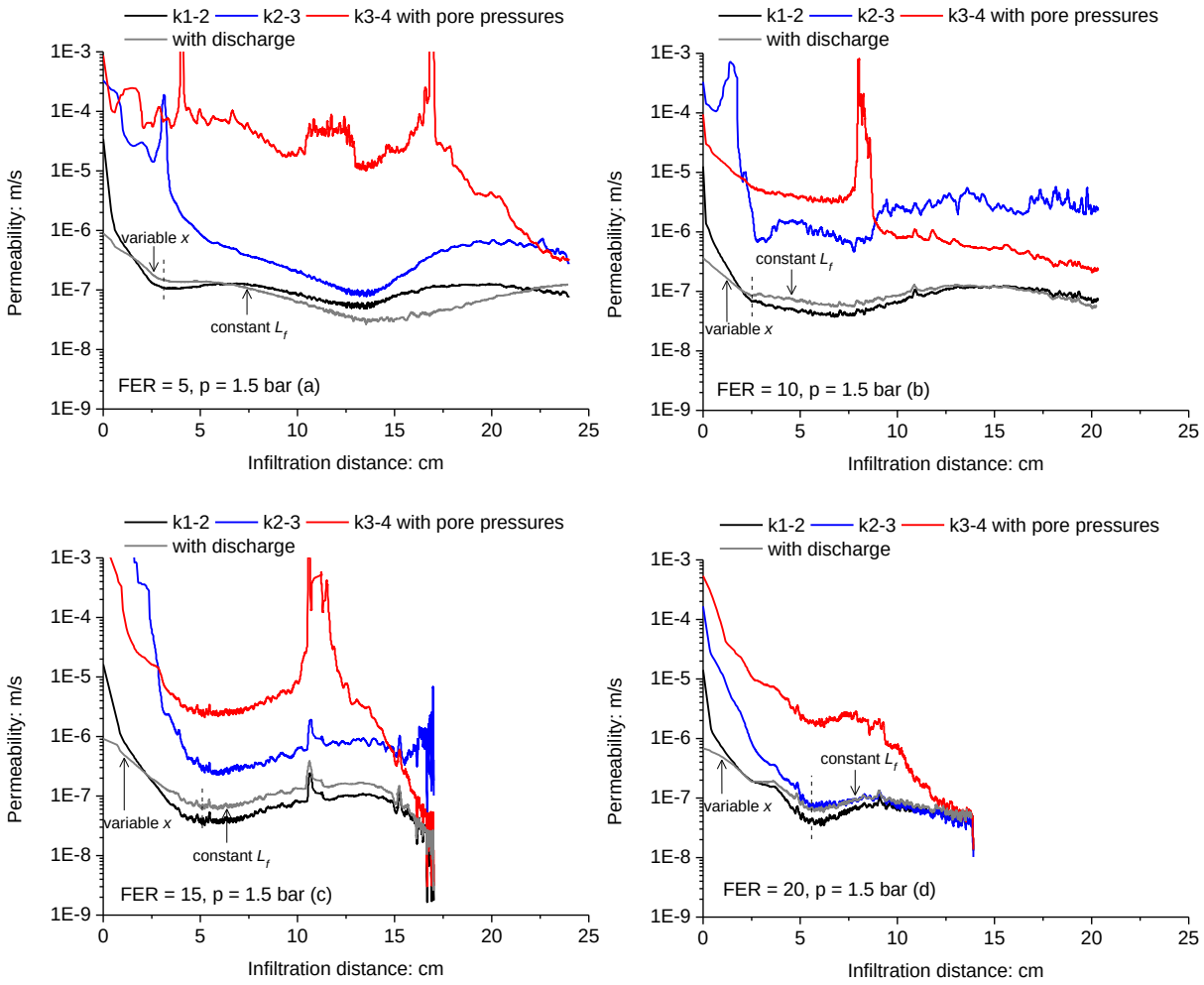

Fig. 5.12. Permeabilites of sand for foam with various FERs and at a pressure of 1.5 bar.

More specifically, for the foam with FER of 5, k_f is ~ 1 × 10^{-7} m/s (k1-2, the permeability in the upper part of the sand and 1 cm above the sand, after 3 cm of infiltration). After 3 cm of foam infiltration in the sand, k1-2 remains constant, because the pores between the PPTs k1

and k2 are completely filled with foam. Now the foam infiltrated in the sand between PPTs k2 and k3, leading to a decrease of permeability until 16 cm of infiltration. After 16 cm of infiltration, k2-3 increased.

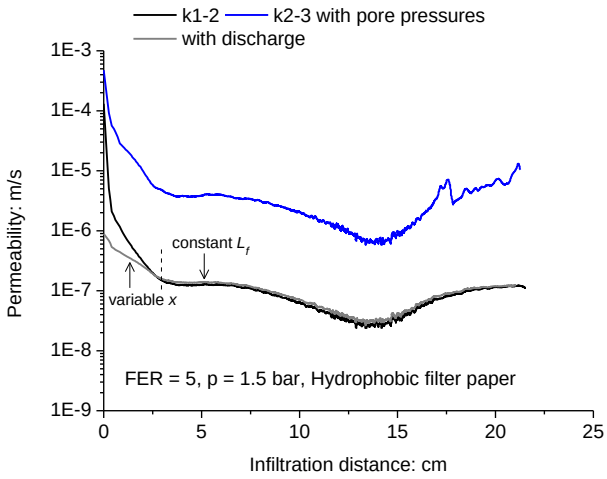

Fig. 5.13. Permeability of sand for foam from PPTs with hydrophilic filter papers at pressure of 1.5 bar.

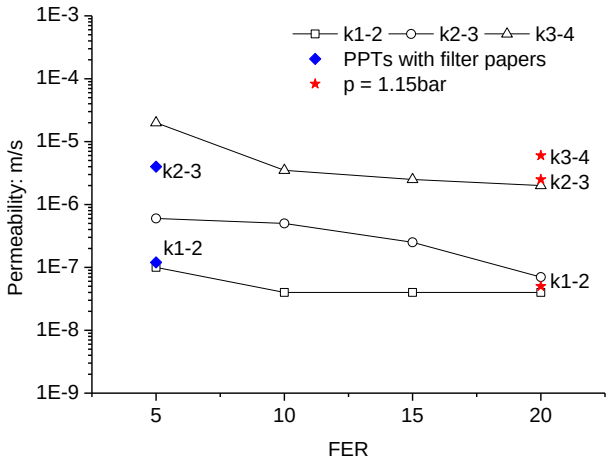

Fig. 5.14. Permeability of sand for foam (average values at the end of tests) changes as function of the FER.

For FERs of 10, 15 and 20, k2-3 decreased until 3, 4 and 5 cm foam infiltration, respectively. k1-2, k2-3 and k3-4 started and stopped to decrease at the same time point. After 7.5 cm of infiltration, k3-4 started to decrease again. This indicates that foam further infiltrated into the layer between k3 and k4. The average values of k_f as measured at the end of the test are

summarised in Table 5.2. Fig. 5.13 shows the permeabilities calculated with the pore pressures measured with hydrophilic filter papers. The result of k1-2 is similar to k1-2 calculated with the pore pressures measured without hydrophilic filter papers because the pressure differences between PPTs k1 and k2 with and without hydrophilic filter papers are very similar. Nevertheless, there is a big difference between k2-3 calculated with and without hydrophilic filter papers. After the foam bubble infiltration there is a large rise in pressure of PPT k2 without hydrophilic filter papers, leading to a higher calculated permeability (see also Fig. 5.14). The permeability of sand for foam decreases with FER, see Fig. 5.14. More significantly, there is a limit of FER, where the permeability is at once much lower. For the foaming agent, sand and pressures used in these tests, it is ~ 15.

Table 5.2. Values of k_f at the end of tests in different FERs.

FER	PPTs with hydrophilic filter paper	Absolute pressure (bar)	k1-2 (m/s)	k2-3 (m/s)	k3-4 (m/s)
5	No	1.5	1.00×10^{-7}	6.00×10^{-7}	2.00×10^{-5}
5	Yes	1.5	1.20×10^{-7}	4.00×10^{-6}	-
10	No	1.5	4.00×10^{-8}	5.00×10^{-7}	3.50×10^{-6}
15	No	1.5	4.00×10^{-8}	2.50×10^{-7}	2.50×10^{-6}
20	No	1.5	4.00×10^{-8}	7.00×10^{-8}	2.00×10^{-6}
20	No	1.15	5.00×10^{-8}	2.50×10^{-6}	6.00×10^{-6}

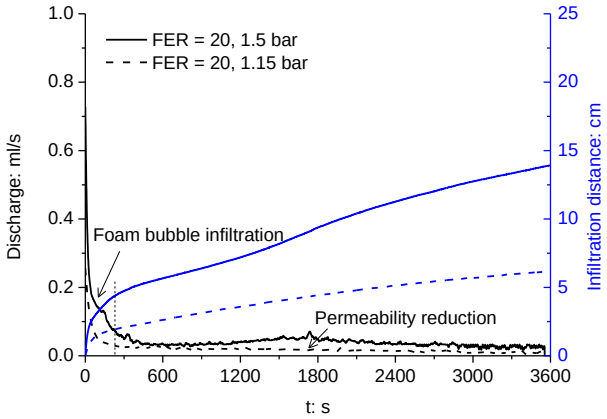

Fig. 5.15. Discharges against time for FER = 20 foam at pressures of 1.5 and 1.15 bar.

3. DISCUSSIONS AND CONSEQUENCES FOR TUNNELLING: THE SCALE EFFECT OF PRESSURE

Fig. 5.15 shows that the water discharge at a pressure of 1.15 bar was smaller than that at a pressure of 1.5 bar. Furthermore, the phase of water flow permeability increase was not observed. Fig. 5.16 shows a plot of pore water pressure changes in time for tests on foam of FER = 20 at pressures of 1.5 and 1.15 bar. The pressures beneath the boundary between the foam and the sand suddenly drop at the starting seconds because of the infiltration, whereas the pressure above the boundary decreased slightly and was constant more or less after some minutes. After a fast drop, the pore pressure of k2 and k3 started to increase to the loading pressure 0.5 bar above the atmospheric pressure. In contrast, this phenomenon was not observed at pressure of 0.15 bar above the atmospheric pressure.

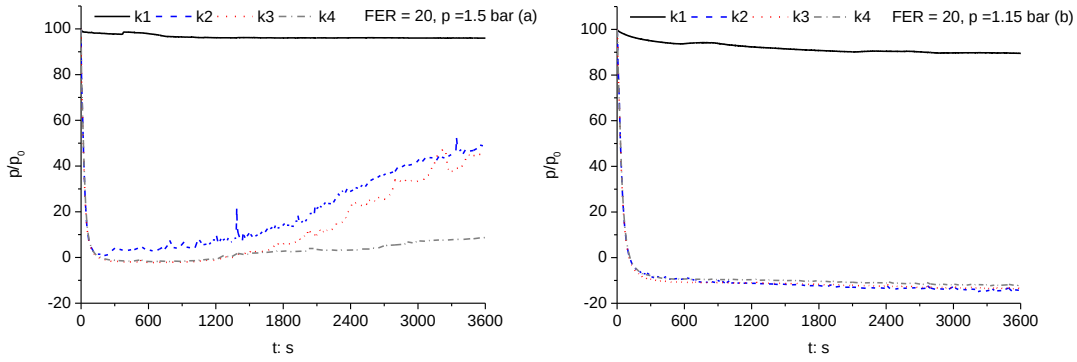

Fig. 5.16. Pore water pressure changes at different air pressures: (a) 1.5 bar and (b) 1.15 bar.

Fig. 5.17 shows that Eq. (5.2) is suitable for various pressures. After foam bubble infiltration, the permeability decreases to a relatively low value and kept constant after foam bubble infiltration. At the end of test, the permeability of sand for foam, k1-2 = 7.00×10^{-8} m/s at pressure of 1.15 bar, is comparable to k1-2 = 1.00×10^{-7} m/s at pressure of 1.5 bar (see Fig. 5.14). The difference in permeability is so small that this difference could also be caused by difference in compaction.

The comparison of the results indicates that a relatively low excess pressure at the tunnel face leads to a low permeable face. However with a low support pressure, the stability of the tunnel face will be reduced. In contrast, in the ground deep below the groundwater table

where the water pressure is high, a higher pressure has to be applied to the foam to balance this water pressure. In this case, the permeability in the foam-infiltrated sand will increase.

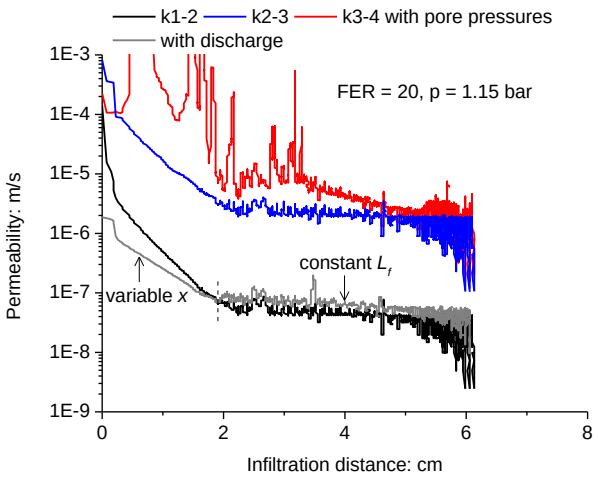

Fig. 5.17. Permeability of sand for foam with FER of 20 and at air pressure of 1.15 bar.

5.4. SUMMARY

The experiments of infiltration of foam into saturated sand have been presented in a setup that imposes flow velocities comparable to what could be expected at the front of an EPB shield of 10 m diameter. From these experiments, it can be concluded:

(a) The infiltration behaviour of foam not only depend on the FER but also on the pressure. Four different characteristics were clearly identified from the experimental results at pressure of 1.5 bar: early high discharge, 'foam bubble infiltration', water flow permeability reduction and water flow permeability increase. However, no regime of water flow with increased permeability was observed for the foam at pressure of 1.15 bar. In the ground deep below the groundwater table, the high pressure difference applied to the foam probably leads to a water flow with increased permeability in the foam-infiltrated sand.

(b) The low permeable layer formed within the sand surface leads to a significant reduction of the permeability close to the sand surface. Contrary to what is mentioned in literature (Bezuijen, 2012), in our experiments a 'dry' foam (FER = 20) is not essential for formation of a low permeable layer in the sand, even a 'wet' foam (FER = 5) could form a

low permeable layer (permeability is about 10^3 times lower than that of normal sand). More significantly, a foam bubble infiltration is essential to get a low permeable face. In some of these tests the discharges were less than the corresponding excavation velocity of a TBM (e.g. in the Botlek Tunnel). Then there will be no foam bubble infiltration and consequently no zone with low permeability.

(c) The permeability of sand for foam decreased with increasing FER of the foam until FER of approximately 15 in these experiments. For higher values of FER, the permeability remains more or less constant.

(d) The air pressure in the bubbles is slightly different from the pore water pressure. This difference, known from theory of partially saturated soil, probably influenced the pore pressure measurements. In future experiments with foam infiltration, PPTs with hydrophilic and hydrophobic filter papers are recommended to use for the measurement of pore water pressures.

CHAPTER 6 PRESSURE INFILTRATION OF SOIL-FOAM-MIXTURE

Chapter 6 presents the experiments on infiltration of pressurised soil-foam-mixture into saturated sand in the modified setup. The soil-foam-mixture used was comparable to the excavated soil (soil-foam-mixture) that can be expected in the excavation chamber of an Earth Pressure Balance shield (EPB shield). It appears that a higher effective Foam Expansion Ratio (FER_m) is more effective to form a low permeable layer in the sand. Since there will be an interaction between air, water and sand in the soil-foam-mixture, the infiltration characteristics of soil-foam-mixture is a bit different from that of the foam. It was shown that a larger air fraction at a given solid fraction reduces the mobility of foam flow in the sand. The water permeability of foam-infiltrated sand decreases with an increasing air fraction and a decreasing liquid fraction for a given solid fraction, and also decreases with an increasing air fraction and a decreasing solid fraction for a given liquid fraction. The situation with high sand fraction should be avoided in the field because there will be no impermeable or low permeable layer formed at the tunnel face. Furthermore, the water permeability of foam-infiltrated sand decreases with the FIR (foam injection ratio) and a FIR of 35 – 40 Vol% larger than a recommendation of 30 – 40 Vol% by EFNARC (2005) is recommended for EPB shield tunnelling in saturated sand. The permeabilities obtained from the experiments are comparable to the values predicted by a close-form equation for predicting the permeability of unsaturated soils (the VG model). Smaller volumetric water content (water fraction) in the soil-foam-mixture will result in a lower water permeability of foam-infiltrated sand.

6.1. INTRODUCTION

On the jobsite, the cutter head will cut away the soil and there is a gap between cutter head and the ground. Consequently, the excavated soil-foam-mixture (containing pore water) will be present in the gap (Maidl, 1995; Galli, 2016). In this case, the foam will infiltrate from that

mixture into the soil and hence the mechanism of infiltration of soil-foam-mixture can be different from infiltration of foam, as it appeared to be different for infiltration of slurry.

As a natural extension to Chapter 5, this chapter presents the experiments on infiltration of pressurised soil-foam-mixture into saturated sand. The experimental results will be discussed with the results of foam infiltration tests. A micro scale sketch of the infiltration process and a micro scale theory of soil-foam-mixture will be used to explain the mechanism of the infiltration. Furthermore, the calculated permeabilities of sand for water through foam from the experiments will be compared to those calculated using the VG model for unsaturated soil (Van Genuchten, 1980). Like the previous work of Budach (2012) and Galli (2016), this experimental study is also a work in order to establish a standardized and comparable test method to estimate performance of the foam conditioning for EPB shield tunnelling in saturated sand.

In Chapter 5, three basic definitions are used: FER, FER_m and FIR. These definitions are used in this chapter too. In these experiments the soils are not excavated, and we calculate the FIR of the soil-foam-mixture as the volume of the foam at 1.5 bar divided by the volume that the sand would have at the same porosity as the sand column in the test.

6.2. EXPERIMENTAL STUDY

6.2.1. FOAMING AGENT, SAND AND SOIL-FOAM-MIXTURE

Measurements at the Botlek Rail Tunnel during construction have shown that the porosity of the muck in the excavation chamber is just a bit higher than the maximum porosity of the sand. Fig. 6.1 shows a graph of fractions of air, water and sand in foam conditioned soil excavated in Botlek Rail Tunnel (Bezuijen, 2006). In this study, the fractions of air, water and sand, and the FIR of the soil-foam-mixtures refer to these measurements, see Table 6.1.

The foaming agent and sand are the same as those used in Chapter 5. The Euroquarz S80 sand was used to make the sand column as well as in the sand-foam mixture, since also in a field situation the sand in the foam will be the same as the sand in front of the tunnel face. The foam was first made at atmospheric pressure and was then added to the sand sample with desired water content in a beaker. Afterwards, the foam and sand sample were mixed very

carefully by hand until the mixture was homogeneous. During mixing it was assumed that no bubbles collapsed. In this study, this mixture of sand-water-air is called ‘soil-foam-mixture’, in which the sand particles were suspended by the foam.

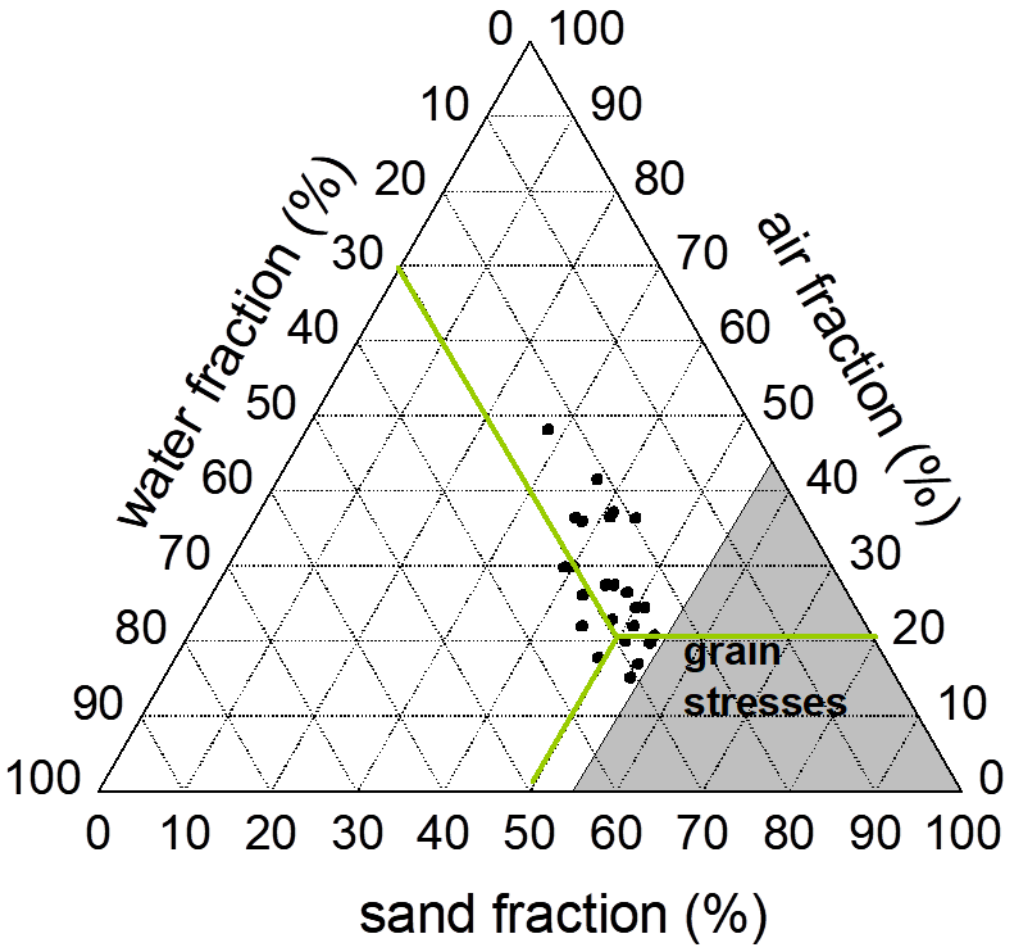

Fig. 6.1. Volume fractions in excavation chamber at the Botlek Rail Tunnel in the Netherlands (Bezuijen, 2012).

When producing the foam, the FER at atmospheric pressure has to be roughly 1.5 times higher than the FER at which the experiment will be performed. Consequently, FER should be 29.5 at atmospheric pressure to be 20 at 1.5 bar (absolute pressure). Bezuijen and Schaminée (2001) and Bezuijen (2012) showed that the foam in tunnelling can be wet or dry, depending on the water permeability of soil and the drilling speed. Tests were performed using soil-foam-mixture with foams ranging from ‘dry’ (FER = 20), to ‘wet’ foam (FER = 5) with FER

= 10 and 15 as intermediate values. Details of the tests are summarised in Table 6.1. The FER, FER_m, FIR and the fractions refer to the conditions in the soil-foam-mixture.

Table 6.1. Properties of foam and soil-foam-mixture used in the tests.

Test No.	FER	FER_m	FIR (Vol%)	Air fraction (Vol%)	Water fraction (Vol%)	Sand fraction (Vol%)	Density (kg/m^3)
1		1.5	22	15	30	55	1757.5
5-2		1.7	32	20	30	50	1625
5-3	5	2	40	25	25	50	1575
5-4		2	54	30	25	45	1442.5
5-5		2.4	70	35	25	40	1310
5-6		3	80	40	20	40	1260
10-1		1.5	20	15	30	55	1757.5
10-2		1.7	29	20	30	50	1625
10-3	10	2	36	25	25	50	1575
10-4		2	48	30	25	45	1442.5
10-5		2.4	63	35	25	40	1310
10-6		3	71	40	20	40	1260
15-1		1.5	19	15	30	55	1757.5
15-2		1.7	28	20	30	50	1625
15-3	15	2	34	25	25	50	1575
15-4		2	46	30	25	45	1442.5
15-5		2.4	60	35	25	40	1310
15-6		3	69	40	20	40	1260
20-1		1.5	18	15	30	55	1757.5
20-2		1.7	27	20	30	50	1625
20-3	20	2	34	25	25	50	1575
20-4		2	45	30	25	45	1442.5
20-5		2.4	59	35	25	40	1310
20-6		3	68	40	20	40	1260

6.2.2. SETUP AND PROCEDURE

The setup used for this experiment is the same as that used in Chapter 5, see Fig. 6. 3. It has been described in detail in Chapters 2 to 4. The soil-foam-mixture was brought up to a certain

height of 30 cm, above the sand surface at atmospheric pressure. The FER_m of the soil-foam-mixture that has the original foaming liquid and the pore water can be calculated. Then when the pressure is increased to 50 kPa but the valve below is still closed, the volume and thus the height of the mixture will decrease. The air volume will decrease to 1/1.5 the original volume. Sand and water in the soil-foam-mixture will keep the same volume. The amount of air in the soil-foam-mixture therefore can be calculated when the volume change was measured. It was found out that the ratios of the air fraction at atmospheric pressure to the air fraction at atmospheric pressure plus the applied pressure of 0.5 bar are between 0.96/1.5 and 1/1.5, which are more or less the same as the theoretical value of 1/1.5. It can therefore be said that hardly any bubbles collapsed during the mixing with sand and pressurising mixture. The test started by opening the bottom valve and lasted one hour or was stopped when all the foam in the soil-foam-mixture had infiltrated into the sand.

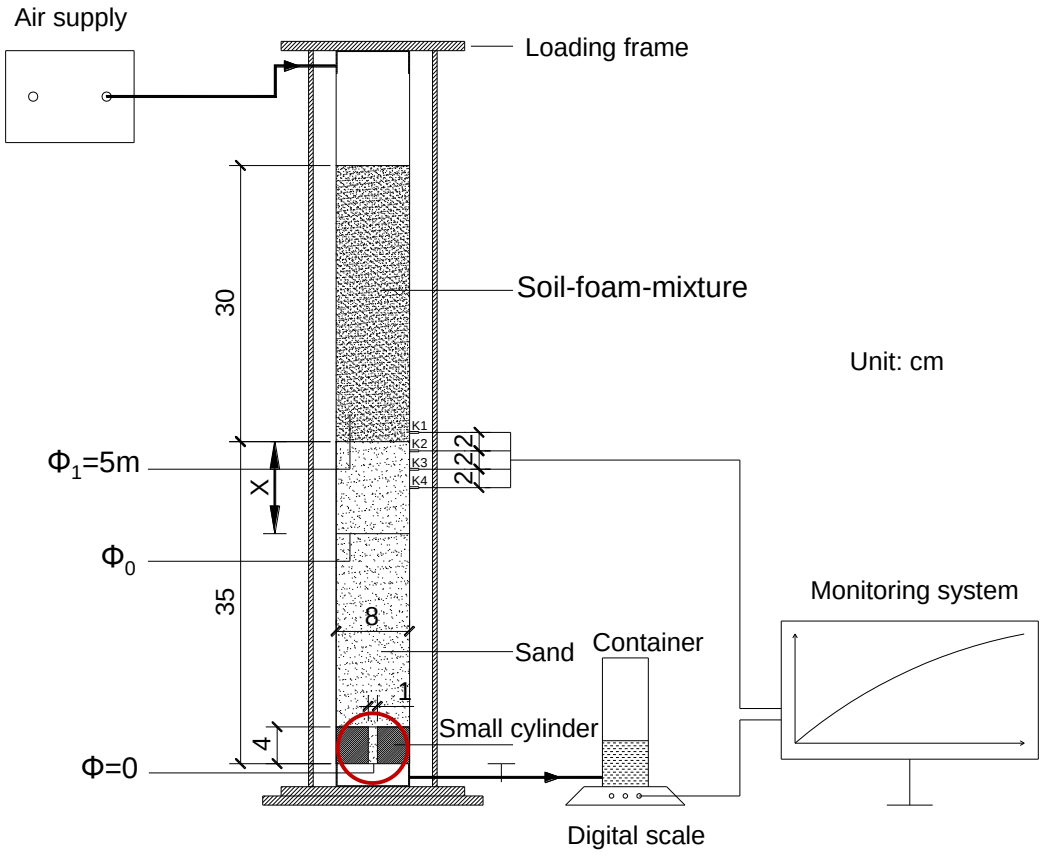

Fig. 6.2. Scheme of the setup and principle of pressure infiltration of soil-foam-mixture.

6.2.4. Experimental results

6.2.4.1. Volume of expelled water

Fig. 6.3 shows the volumes of water expelled from the saturated sand column during infiltration. Generally, more water was expelled during infiltration of the soil-foam-mixture with a lower FIR. As mentioned before, the curves with low FIRs stop when all foam has infiltrated. The curves of relatively low FIRs are very similar, and the flow seems a water flow until FIR = 45 Vol% When FIR ≥ 45 Vol%. The volume of expelled water obviously decreases with increasing FIR. Like the infiltration of foam, phases of 'foam bubble infiltration' (Fig. 6.4a) and water permeability reduction (Fig. 6.4b) were observed. The process is clearer in the courses of discharge, see Fig. 6.5. The foam bubble infiltration is only ~ 2.5 cm into the sand, which is the same as the value in infiltration of foam (Chapter 5).

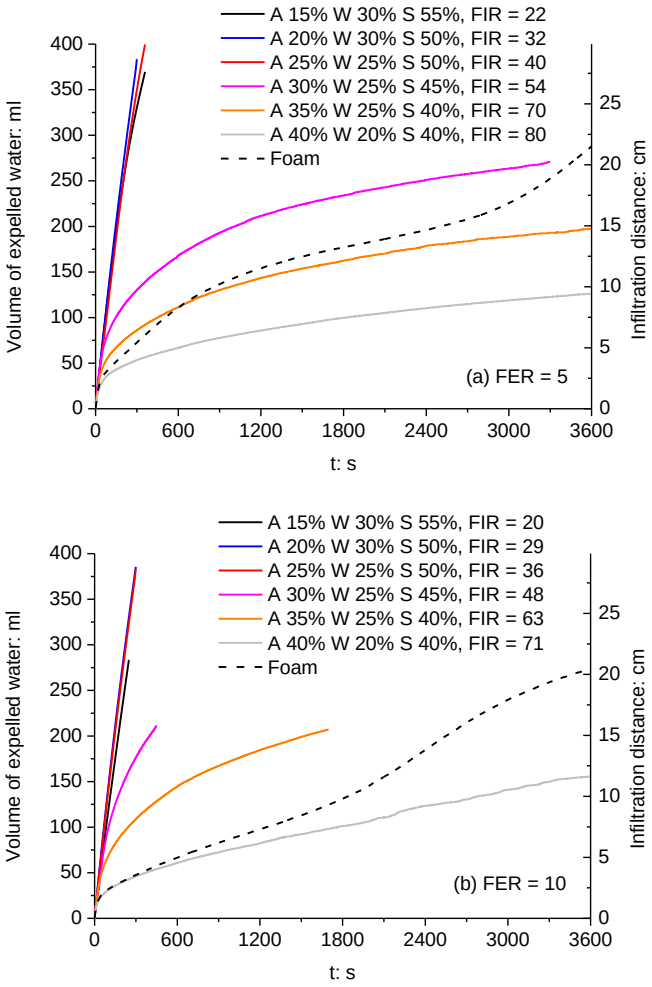

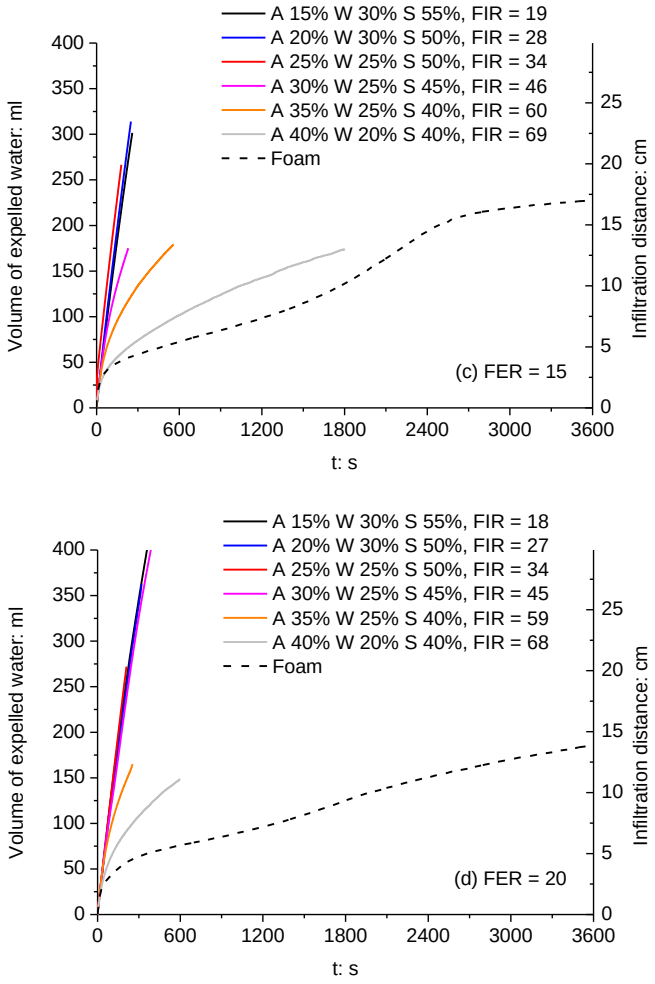

Fig. 6.3. Volumes of water expelled from the saturated sand for various fractions. In this plot and later plots, 'A Vol%, W Vol%, S Vol%' indicates the volume fractions of air, water and sand in the original soil-foam-mixture.

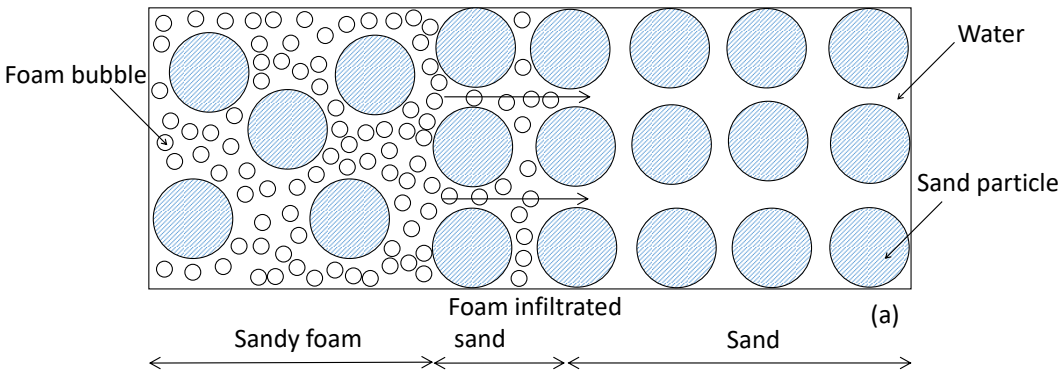

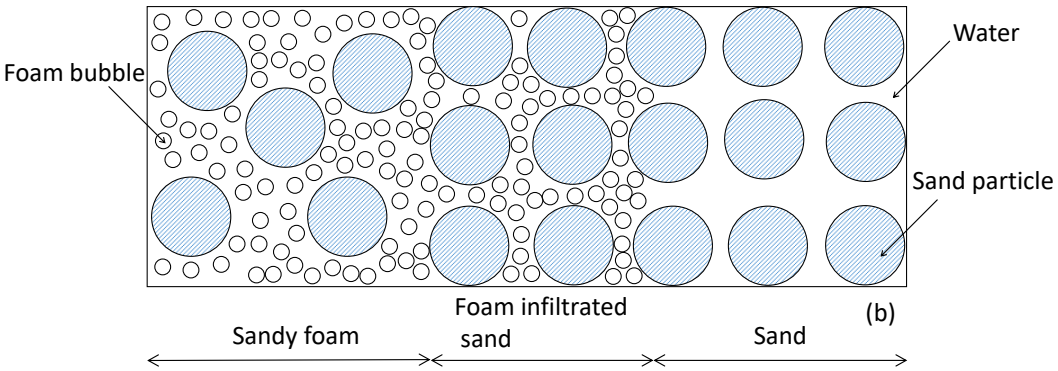

Fig. 6.4. Sketch of foam infiltration into saturated sand: (a) Foam bubble infiltration, and (b) Water permeability reduction.

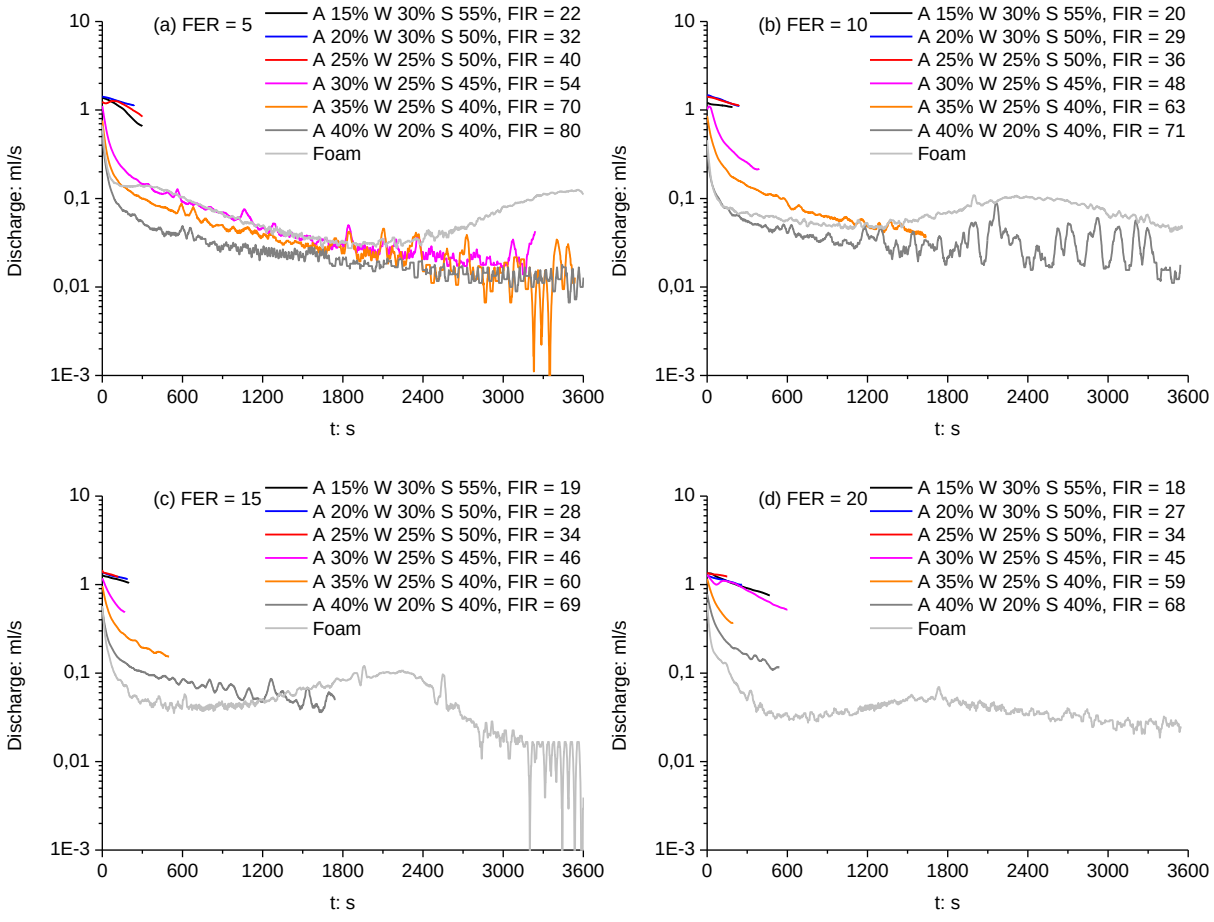

Fig. 6.5. Discharges against time for different FERs and FIRs.

From Fig. 6.5, it can be seen that at the very beginning the discharges with relatively low FIRs (≤ 40 Vol%) are a bit higher than those with relatively high FIRs (> 40 Vol%). For high

FIRs, the discharges dropped to very small values. On the one hand, for low FIRs, there is enough foaming water around the foam bubbles so that a finite permeability remains and the flow will go on. On the other hand, due to faster infiltration for low FIRs, there will be more foam that injects into the sand and forms a low permeable layer in the sand. The infiltration of foam also depends on the dimensions of the bubbles whether they can infiltrate. Large bubbles cannot infiltrate even at a low FIR.

The results show that a FIR of 46 Vol% is needed to have a considerable reduction of the discharge. For lower FIRs there is a continuous water flow from the soil-foam-mixture to the saturated sand. This is in agreement with the field data analyzed by Bezuijen and Dias (2017). They showed that the pressure decrease in the excavation chamber during standstill of an EPB shield could be attributed to this groundwater flow.

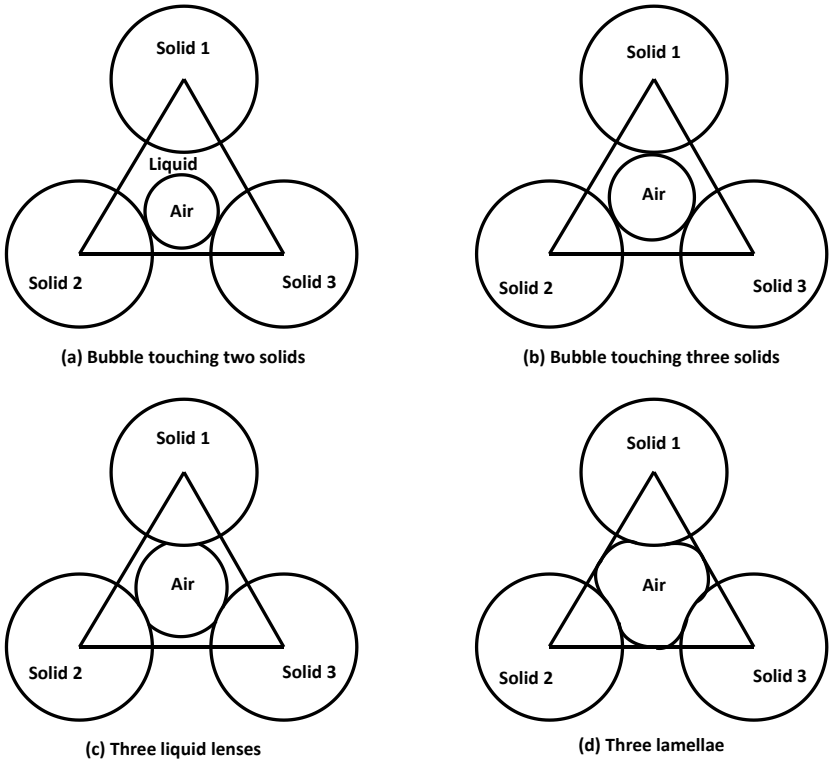

Fig. 6.6. Different air fractions at a given solids fraction. (Modified after Kam et al., 2002)

A qualitative explanation for the FIR dependency of the water permeability of foam-infiltrated sand can be given with the model of Kam et al. (2002). See Fig. 6.6, if there is no contact between solid particles in soil-foam-mixture, there can be four cases of interaction between

bubble and sand particles. In these cases, there are only forces from lamellae and lenses. But in this study, the minimum water fraction tested is 20%, which means that there is too much water to form lamella. Consequently, a pressure gradient will create a water flow in the lenses and water transport is possible. Only at a high FIR, the air bubbles will allow only small lenses that result in only a limited water flow through the tunnel face.

No effective stresses will be transmitted by the air bubbles in the first and second situation of Figs 6.6a and 6.6b, but this will be the case in for the situation shown in Figs 6.6c and 6.6d. The mobility of the foam depends on the bubble size but also the volume fractions. Kam et al. (2002) showed that, the mobility of foam decreases with increasing air fraction at a given solid fraction, and with the solid fraction at a given air fraction. At the tunnel face the situation will be different that there will be grain to grain contact and a reduced water permeability of foam-infiltrated sand, because the foam bubbles are blocked by the grains.

In case of an air fraction ≤ 25 Vol%, the curves of volume of expelled water are more or less the same. In that case, the air fraction is relatively small and thus the water flow is dominant. In case of air fraction ≥ 30 Vol%, the foaming liquid will only be present in thin layers around the grains or between the bubbles (lamellae). Consequently, the flow mobility decreases. This depends also on the water fraction. The water permeability of foam-infiltrated sand is reduced because the small bubbles act as small grains in the sand. If the gradient becomes too high, the bubbles probably also deform blocking the pores even further. A possible mechanism for the influence of pressure gradient on the soil-foam-mixture infiltration is presented in Fig. 6.7. Large bubbles are blocked at the boundary between the soil-foam-mixture and the original sand sample, while small bubbles and water will flow into the sand. This leads to a zone with a lot of bubbles just above the sand the pressure gradient in this zone will squeeze the bubbles. This zone has a low water content (because as mentioned the water will flow through the bubbles and the sand) and thus a low permeability. Consequently, the pore pressure drops at the boundary.

See Table 6.1 again, for FIR = 40, 54 and 70.3 Vol%, the sums of air and solid fractions are the same. With increasing air fraction, the flow mobility decreases. In contrast, with

increasing solid fraction, the mobility of foam decreases. Similar results can be found for other FERs in Table 6.1.

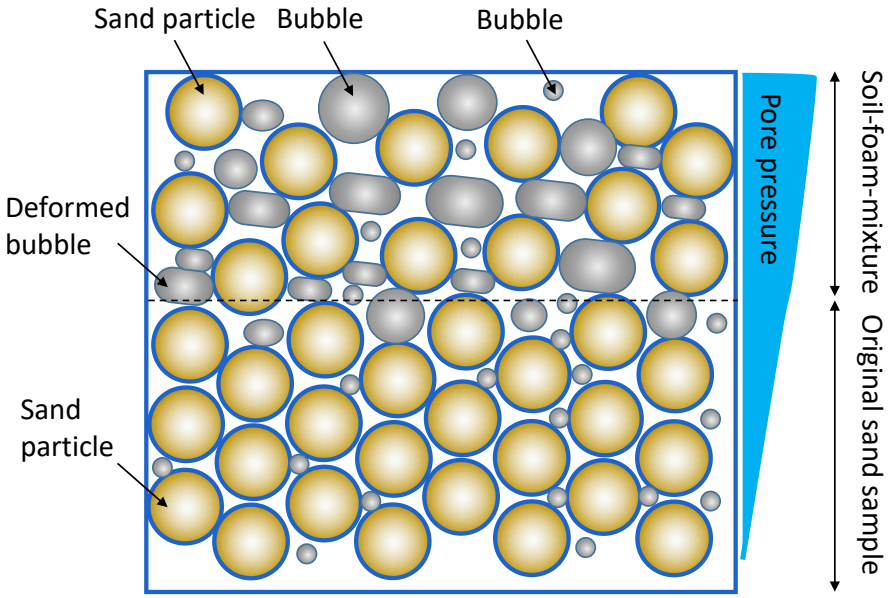

Fig. 6.7. Mechanism for the influence of pressure gradient on the soil-foam-mixture infiltration.

6.2.4.2. PORE PRESSURES

Figs 6.8 – 6.11 show the measured pore pressures from the Pore Pressure Transducers (PPTs). They are numbered k1, k2 and k3 and where places 1 cm above, and 1 and 3 cm beneath the surface of the sand sample, respectively. When the air fraction is low, the water flow is dominant. The air fraction in the mixture does not depend on the FER, but on the amount of air. It depends more on the FIR, see Table 6.1. With the increasing air fraction at a given solid fraction, the yield stress of soil-foam-mixture increases to a relatively high value (Kam et al., 2002). In this case, the foam flow is dominant. In Figs 6.10d – 6.10f, due to reduction of flow, the value of k1 reached a steady value. This indicates that there is an impermeable layer formed between k1 and k2. Some errors were found in the measurements from PPT k1 in Fig. 6.10d because k1 should be higher than k2 and k3, and also PPT k2 in Figs 6.11e and 6.12f. This could be caused by the injection of bubbles into the PPT k2. The same error had also

been found in infiltration test of foam (Chapter 5). Depending on the fractions and thus the FIRs of the soil-foam-mixture, the pressure varies, see Figs 6.9 – 6.11.

There is already a pressure drop between the top of the soil-foam-mixture and k1 (1 cm above the original sand surface). In the cases of low FIRs (≤ 36 Vol%), the pressure drop (~ 20% of the applied pressure) over the infiltrated soil is limited. In this case, the permeability below the infiltrated soil is still high and the pressure drop is over the constriction in the small cylinder. This models the situation in the field of a TBM with permeable tunnel face where the groundwater flow determines the infiltration and the reduction of the permeability by the foam is limited.

In the cases of high FIRs (≥ 70 Vol%), most of the pressure drop (~ 80% of the applied pressure) is above k1 at the end of the test, which is probably caused by the sand from the soil-foam-mixture that comes on top of the sand sample. There is a pressure drop at k1. This is due to sand from the soil-foam-mixture that has 'rained' on the original sand bed. The pressure drop between k2 and k3 is small, this means that the permeability of the original sand is still there. The pressure drop between k1 and k2 is large, so there is a foam layer between these two PPTs.

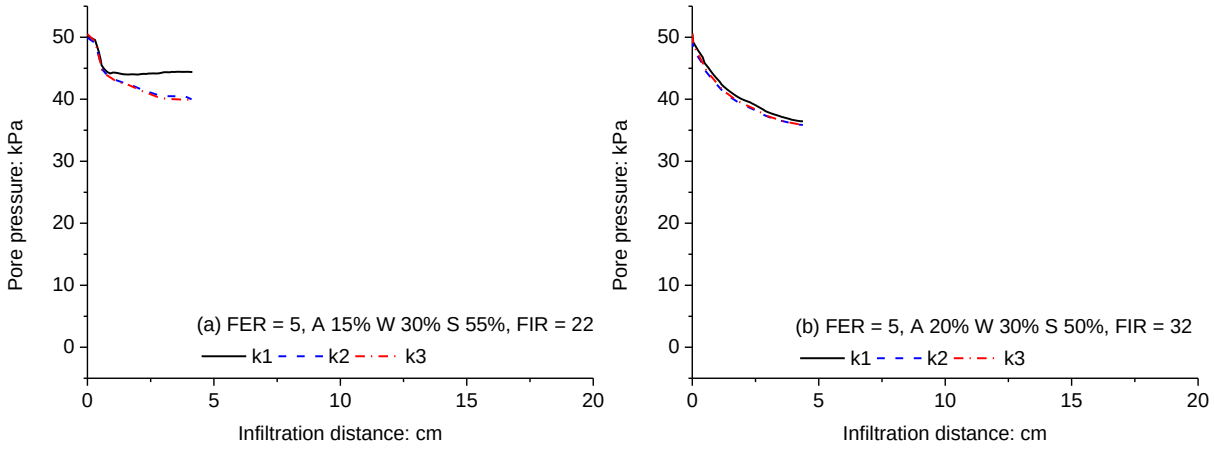

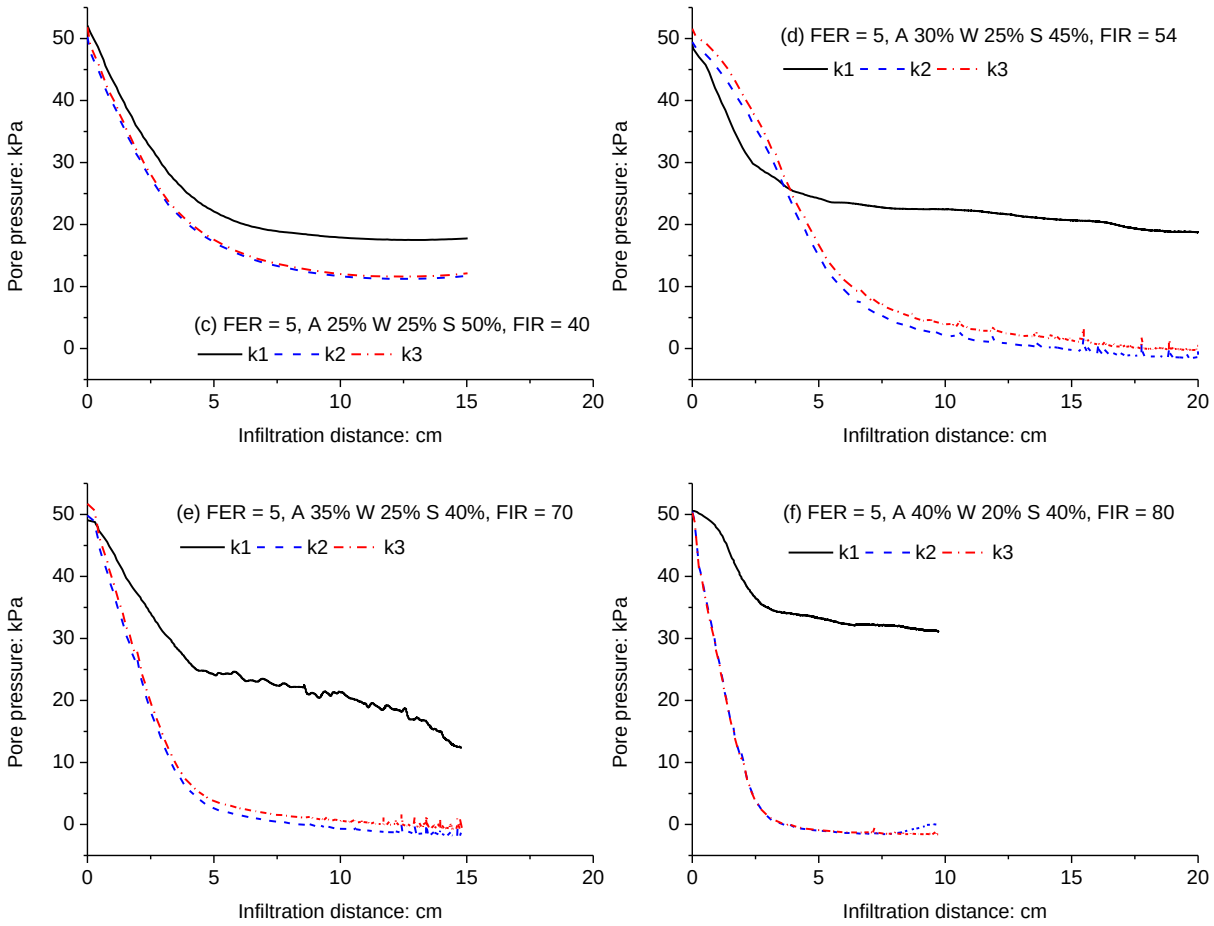

Fig. 6.8. Pore pressure change for FER = 5 foam.

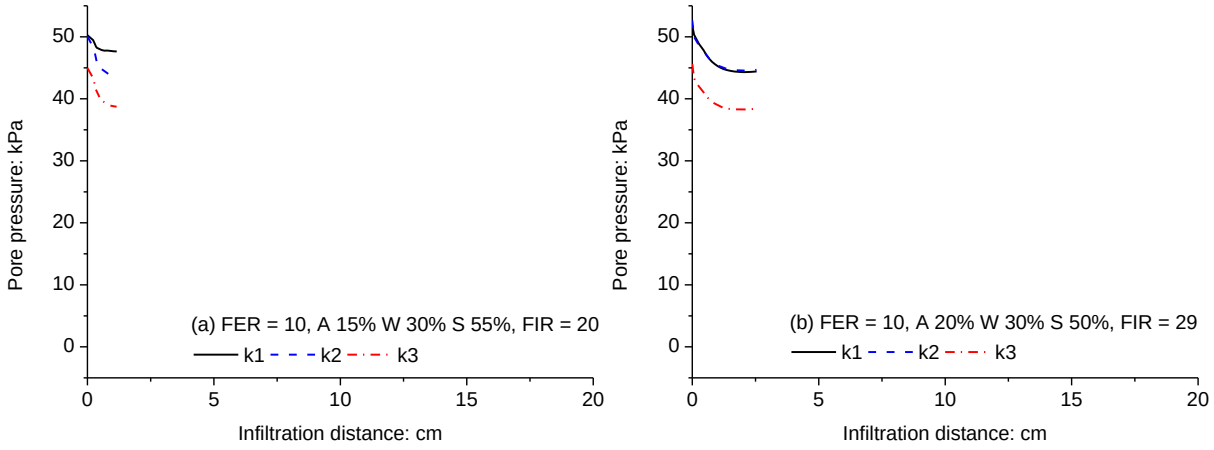

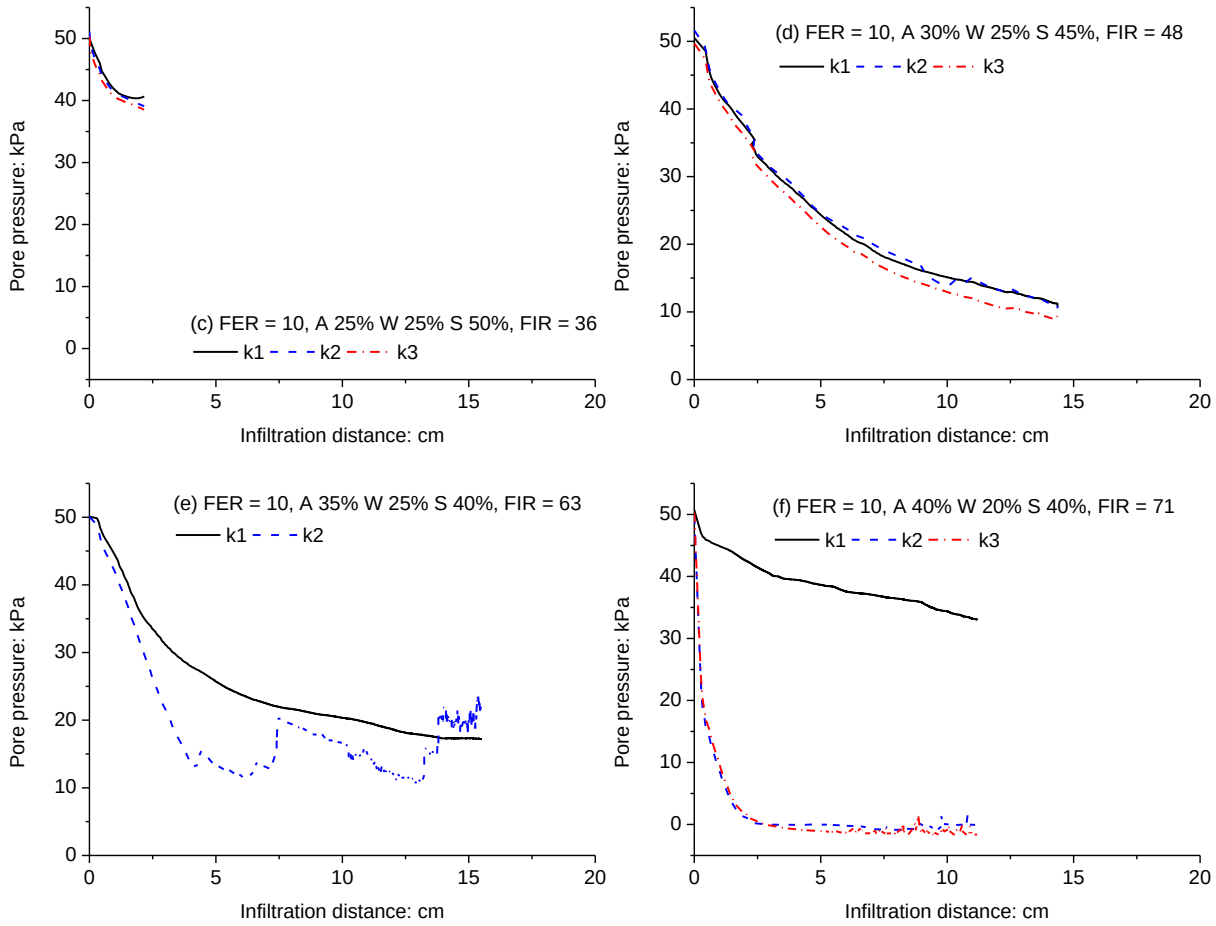

Fig. 6.9. Pore pressure change for foam of FER = 10.

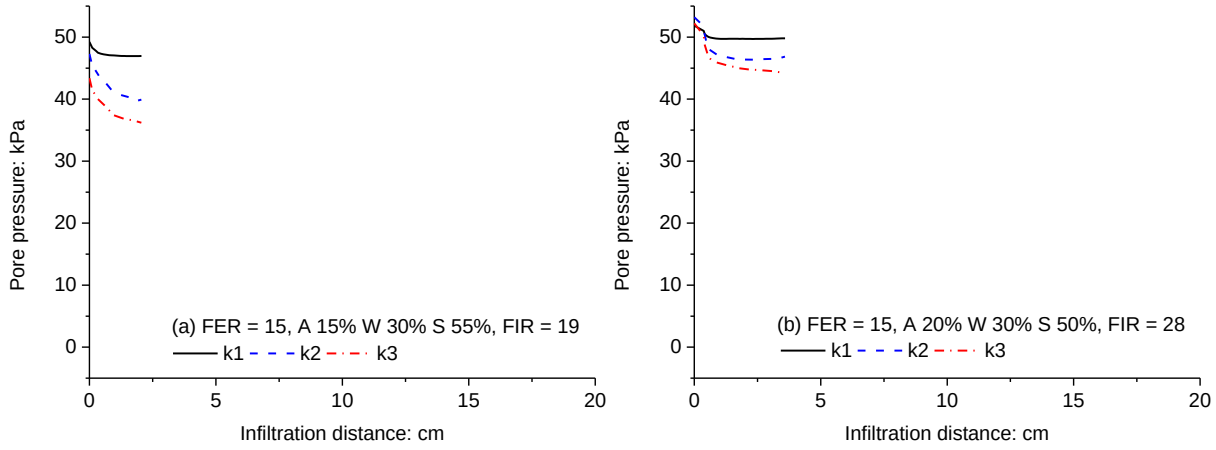

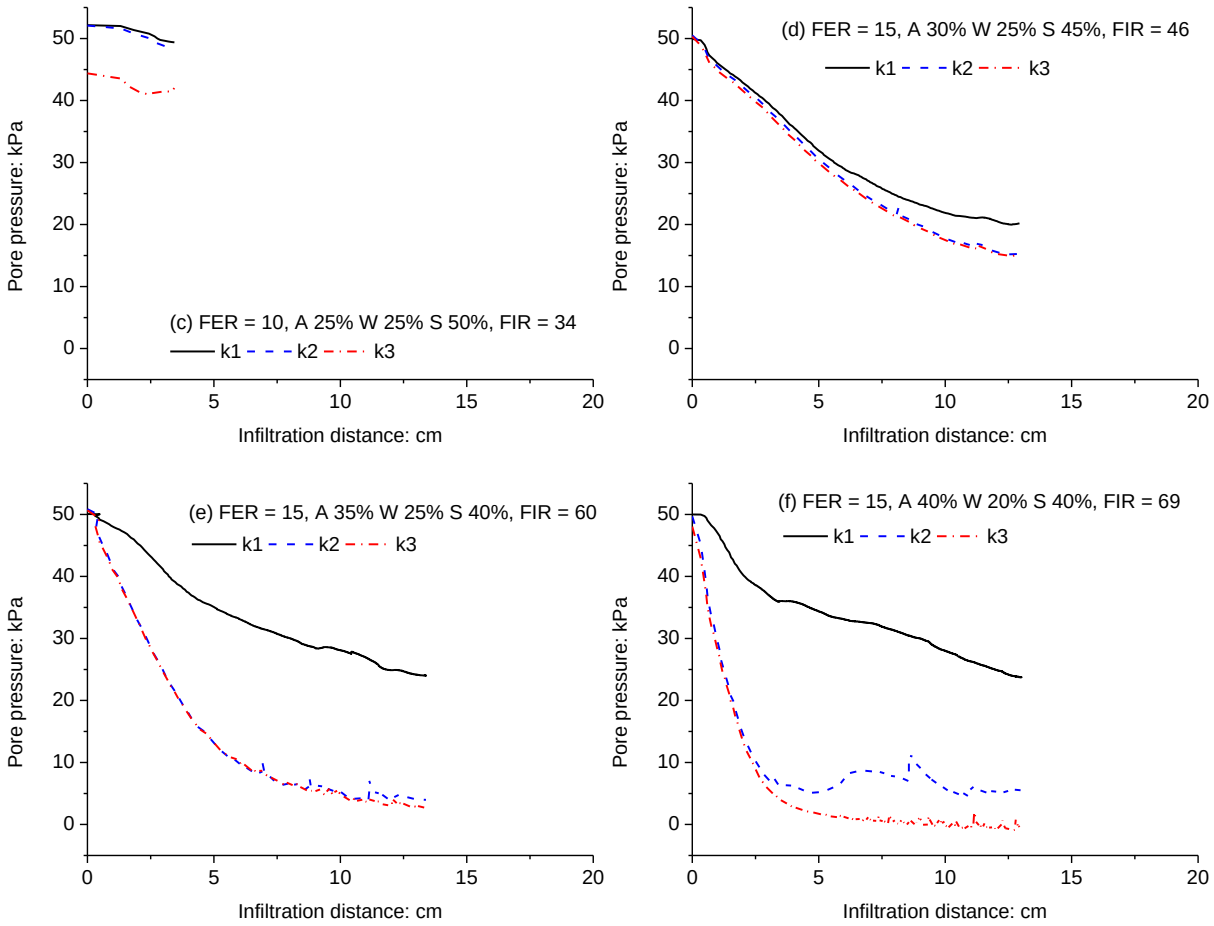

Fig. 6.10. Pore pressure change for foam of FER = 15.

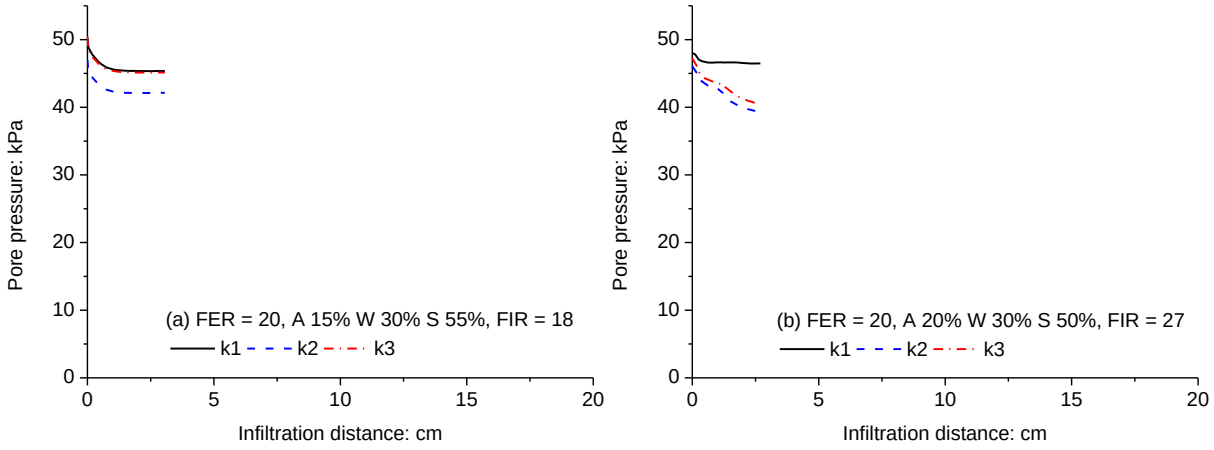

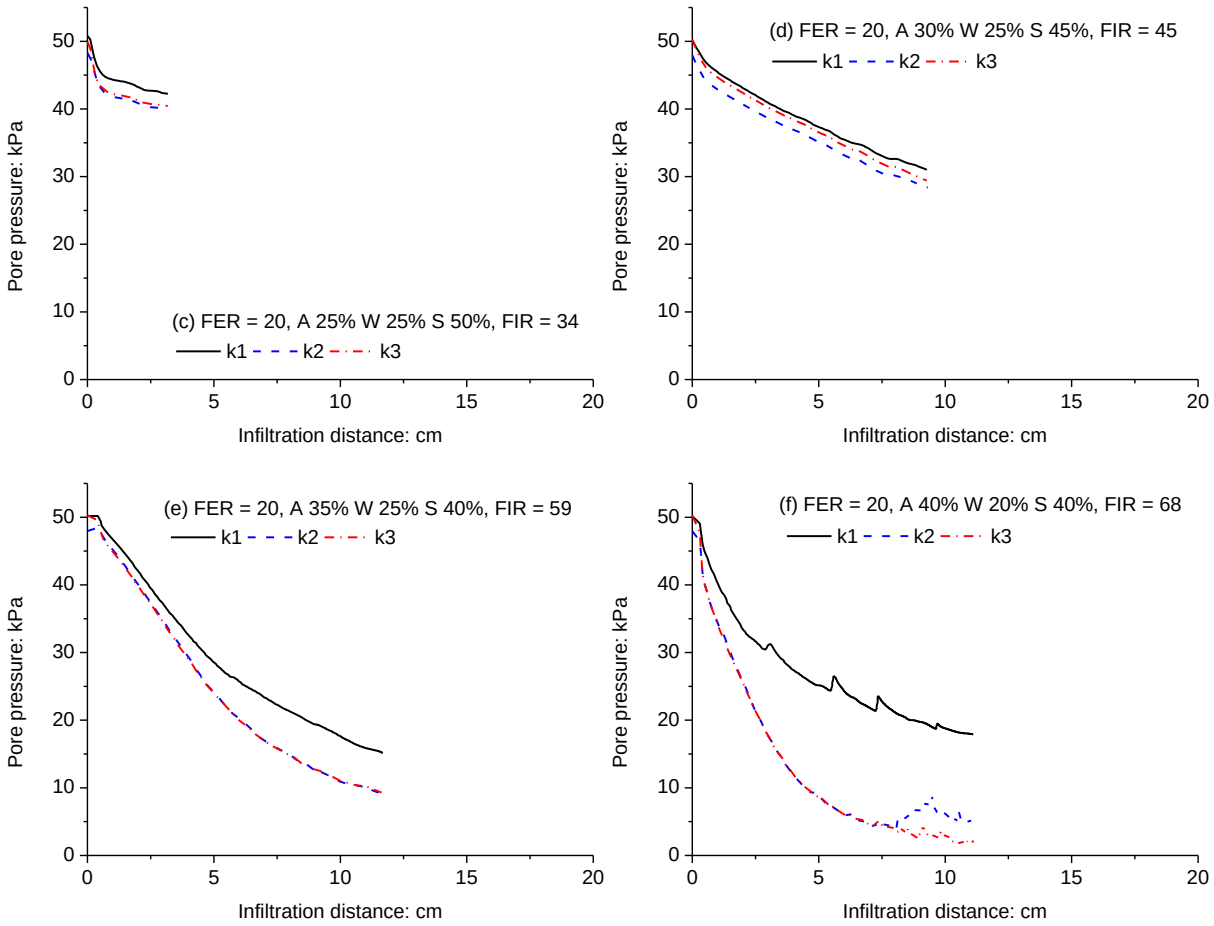

Fig. 6.11. Pore pressure change for foam of FER = 20.

6.2.4.3. PERMEABILITY OF THE INVESTIGATED SOIL

With the data of discharges and pore pressures, the water permeability of foam-infiltrated sand k_f (m/s), can be determined with Eq. (5.2). Fig. 6.12 shows the calculated permeabilities of sand for foam flow for various fractions under different FERs. As shown in Figs 6.12a and 6.12b, for relatively low FIRs (≤ 40 Vol%) or air fractions, the permeability of the sample between k1 and k2 (defined as k1-2, the permeability in the upper part of the sand and 1 cm above the sand surface) decreased due to foam infiltration in the sand. The permeability of the sample between k2 and k3 (defined as k2-3), relatively high at the very beginning of the test. By then, the foam flow had not reached k2 and thus the flow is water flow, the values of k2-k3 are the water permeability of sand. Afterwards, when the foam flow reached k2, the values of k2-3 decreased. For relatively high FIRs (> 40 Vol%) or air fractions, the permeability

decreases more during the test indicating that the foam blocks the groundwater flow, see Figs 6.12c and 6.12d. For a certain solid fraction of 40 Vol%, the value of k_f of an air fraction of 40 Vol% is smaller than for an air fraction of 35 Vol%. For a certain fraction of liquid of 25 Vol%, the value of k_f of air fraction of 35 Vol% is smaller than of an air fraction of 30 Vol%. It seems that the water permeability of foam-infiltrated sand decreases with increasing air fraction and decreasing liquid fraction for a given solid fraction or decreases with increasing air fraction and decreasing solid fraction for a given liquid fraction. Table 6.2 gives the summary of the average permeability, measured at the end of each test.

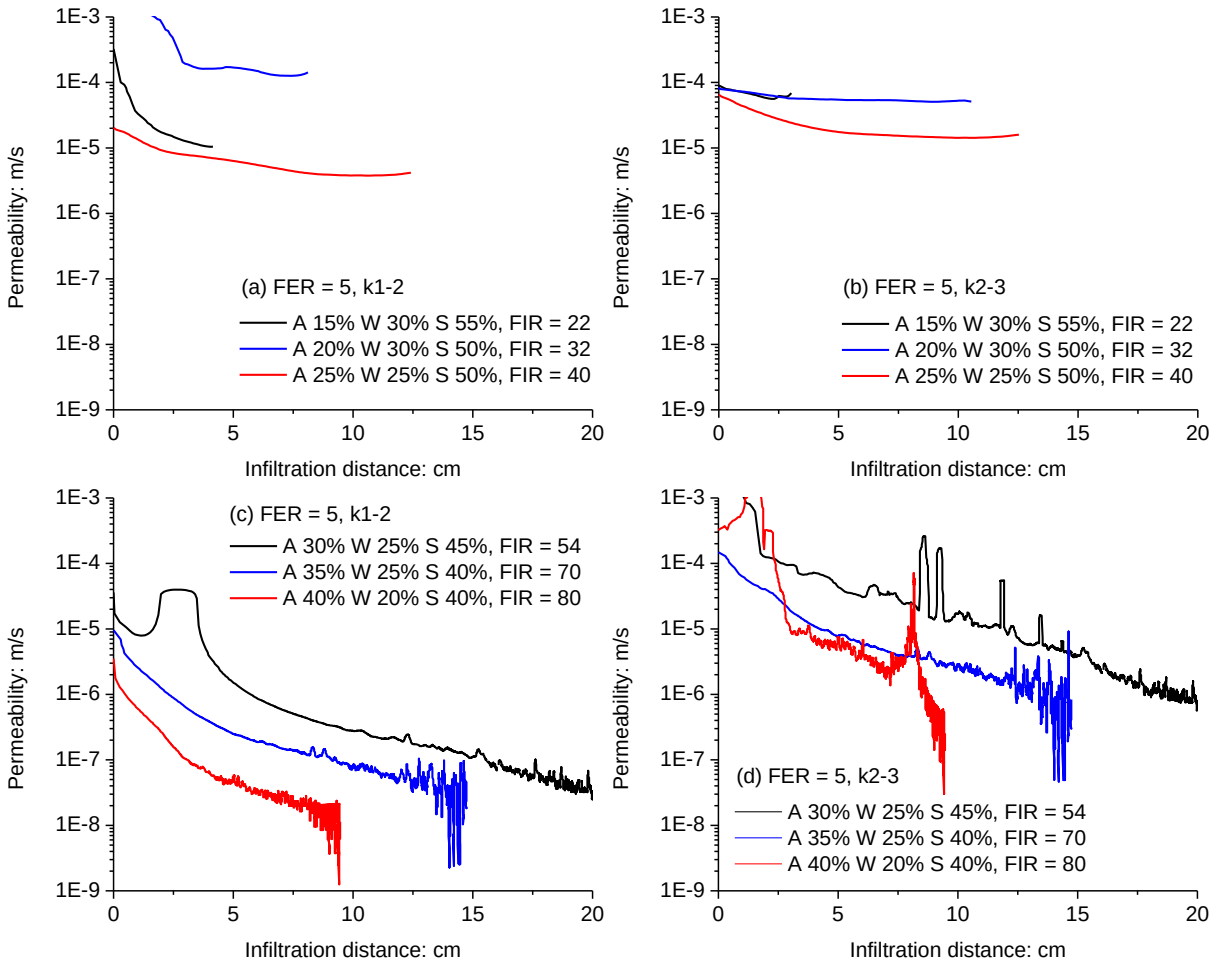

Fig. 6.12. Permeabilities of sand for foam with FER = 5: Low FIR in (a) and (b), high FIR in (c) and (d).

Table 6.2. Permeabilities of sand for foam for various fractions of soil-foam-mixture with different FERs, taken at the end of the tests.

Test No.	FER	FER_m	FIR (Vol%)	k1-2 (m/s)	k2-3 (m/s)
5-1	5	1.5	22	1.00×10^{-5}	2.40×10^{-5}
5-2		1.7	32	5.00×10^{-6}	2.40×10^{-5}
5-3		2	40	3.80×10^{-6}	5.30×10^{-5}
5-4		2	54	3.50×10^{-8}	1.30×10^{-6}
5-5		2.4	70	3.00×10^{-8}	2.90×10^{-6}
5-6		3	80	2.00×10^{-8}	4.80×10^{-6}
10-1	10	1.5	20	1.50×10^{-4}	8.00×10^{-4}
10-2		1.7	29	1.00×10^{-4}	1.00×10^{-5}
10-3		2	36	4.00×10^{-5}	4.00×10^{-4}
10-4		2	48	1.00×10^{-5}	1.00×10^{-5}
10-5		2.4	63	4.50×10^{-7}	-
10-6		3	71	2.50×10^{-8}	3.00×10^{-7}
15-1	15	1.5	19	1.60×10^{-4}	1.00×10^{-5}
15-2		1.7	28	1.40×10^{-4}	4.80×10^{-5}
15-3		2	34	6.00×10^{-5}	7.10×10^{-6}
15-4		2	46	3.60×10^{-6}	2.90×10^{-4}
15-5		2.4	60	2.90×10^{-7}	7.00×10^{-8}
15-6		3	69	5.00×10^{-8}	2.70×10^{-7}
20-1	20	1.5	18	1.00×10^{-4}	1.00×10^{-4}
20-2		1.7	27	4.00×10^{-5}	1.50×10^{-5}
20-3		2	34	2.80×10^{-5}	1.80×10^{-5}
20-4		2	45	2.00×10^{-5}	3.00×10^{-5}
20-5		2.4	59	2.60×10^{-6}	3.60×10^{-7}
20-6		3	68	3.70×10^{-7}	1.50×10^{-6}

6.3. DISCUSSIONS AND CONSEQUENCES FOR TUNNELLING

6.3.1. EFFECT OF SAND FRACTION ON INFILTRATION BEHAVIOUR

Analogous to the deep filtration of slurry containing sand, there will be a sand layer formed on the boundary of the sand and the soil-foam-mixture. On the one hand, with a high sand

fraction, there will be a dense sand layer formed, the foam bubbles thus will be blocked by the grains and the foam flow will be reduced. On the other hand, with a lower sand fraction, there will be loose sand layer formed, and thus more foam bubbles will flow out from the soil-foam-mixture into the sand, resulting in a low permeable layer formed close the boundary between the soil-foam-mixture and the sand sample. This means the sand fraction is of importance for the plastering at the tunnel face.

In the extreme case there is 55 Vol% of sand in the soil-foam-mixture. This means that the porosity of the soil-foam-mixture is only 45% thus close to the porosity of loosely packed sand (0.45). For these situations (55 or 50 Vol% sand fractions), there will be a grain skeleton very quickly and there is no foam available to create a low permeable area between k1 and k2. The tests end very quickly, because there is no foam above the newly formed sand skeleton. At lower sand fractions, more foam can flow from the soil-foam-mixture into the sand and this can form a low permeable layer between k1 and k2, the discharge reduces and the pressure drop over k1-2 increases. In all cases the pressures measured at k2 and k3 are the same, thus the foam does not reach this layer.

6.3.2. Effect of FIR on permeabilities

Fig. 6.13 shows the result of permeability change with FIR. It is shown that the fit curves are likely ‘S’ lines. The drop of permeability is between FIR of 35 – 70 Vol%. When FIR < 35 Vol%, the water permeability of foam-infiltrated sand is more or less equal to the water permeability of sand except for the FER = 5. This indicates that the water permeability of foam-infiltrated sand depends on properties of the original foam. It is likely that a minimum FIR of 35 Vol% is required before a less permeable face is formed. This is comparable to the recommendation of a FIR of 30 – 40 Vol% by EFNARC (2005) for EPB shield tunnelling in sandy soils.

Consequently, in the case of tunnelling a low permeable soil, since a large amount of pore water remains in the soil, the FIR in the excavated soil (soil-foam mixture) will be small. To reduce the permeability of the face, a higher FIR is necessary than to just prevent grain to grain contact. From Fig. 6.13 it can be seen that FIR = 70 Vol% is enough for a nearly

impermeable face to be formed. Refer to the recommendation by EFNARC (2005), therefore a FIR of 35 – 40 Vol% is recommended for EPB shield tunnelling in sandy soils.

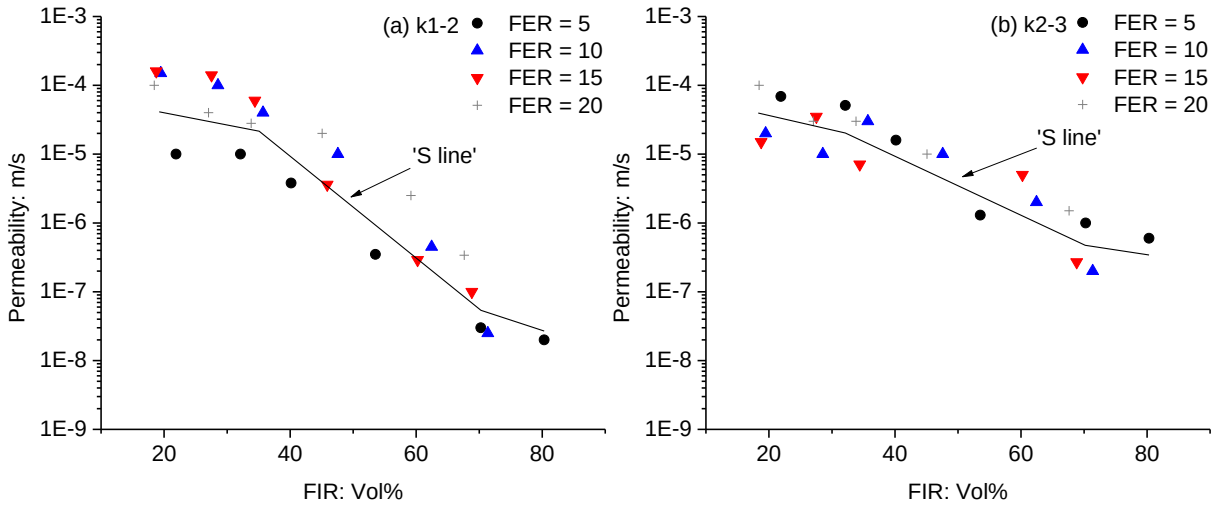

Fig. 6.13. Permeability change with the ratio of air fraction/sand fraction.

6.3.3. Comparison of permeabilities obtained from experiments and VG model

The permeabilities determined from the experiment can be compared with the permeability predicted by the VG model (Van Genuchten, 1980):

$$K_r = \frac{\{1-(ah)^{n-1}[1+(ah)^n]^{-m}\}^2}{[1+(ah)^n]^{m/2}} \tag{6.1}$$

Where K_r is the relative permeability (-); h the matric potential (cm); a (1/cm); n (-) and m (-) yet undetermined parameters. The parameters can be gained by fitting a known soil-water retention curve (SWRC) using below equation:

$$\Theta = \left[\frac{1}{1+(ah)^n}\right]^m \tag{6.2}$$

With Θ the volumetric water content (-).

For S80 sand, the input parameters in Eq. (6.2) were determined by fitting a SWRC based on the modified Kovács model (MK model) from Galli (2016), see also Fig. 6.14, and came to the values mentioned in Table 6.3. With these determined parameters, the permeabilities can be calculated with Eq. (6.1).

Table 6.3. Determined parameters for the VG model for S80 sand.

Parameter	*a* (1/cm)	*m* (-)	*n* (-)
Value	0.01271	0.74314	3.89323

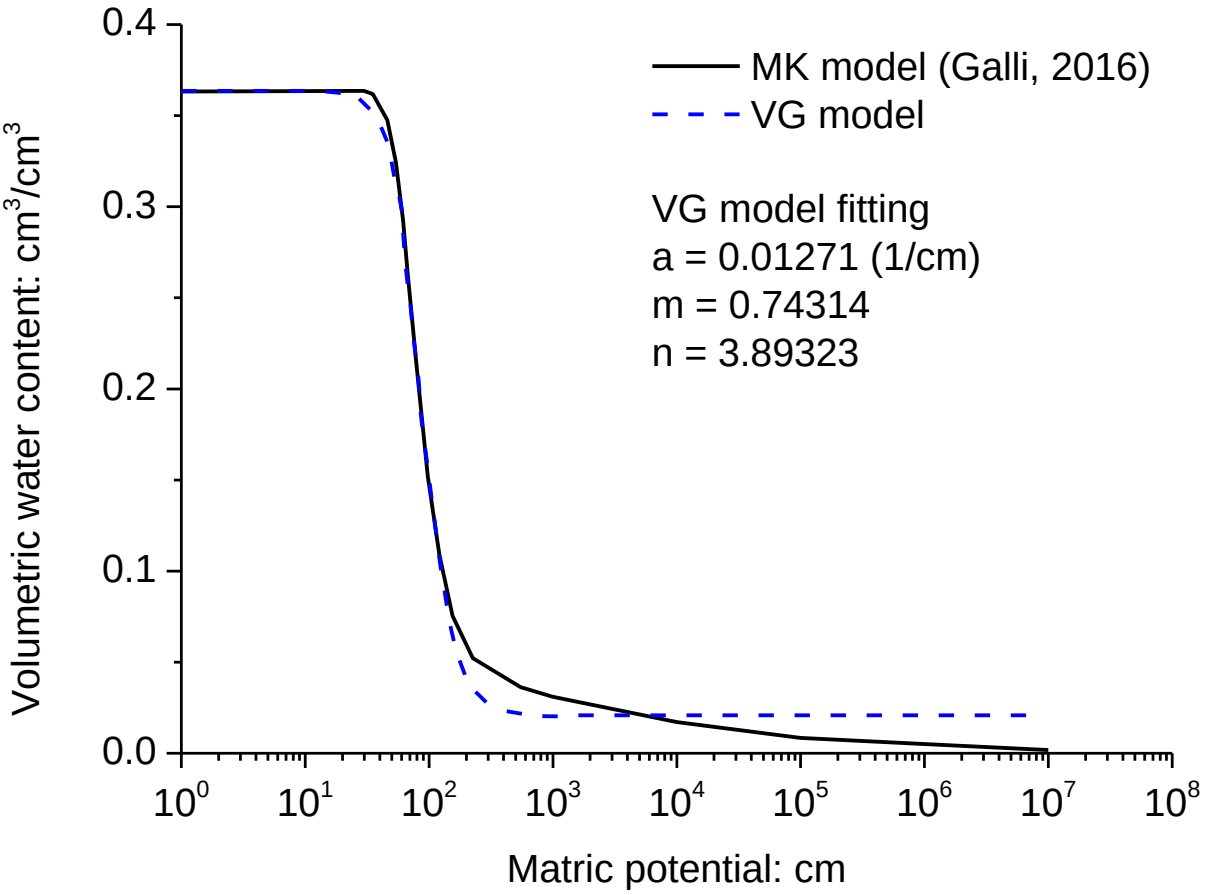

Fig. 6.14. Soil-water retention curves based on the modified Kovács model (MK model) (Galli, 2016) and predicted by VG model.

Fig. 6.15 shows the comparison of permeabilities from the experiment and the prediction by the VG model. The results for soil-foam-mixture and unsaturated soil are comparable. The measured permeabilities correspond to the VG model. For volumetric water content (water fraction) of 30 Vol%, most points are around the permeability line by the VG model. For a volumetric water content (water fraction) of 25 Vol%, about 1/2 points are around the line. For a volumetric water content (water fraction) of 20 Vol%, one point is around the line, rest points are on the right side of the line. The big difference may be led by the smaller porosity

of the foam-infiltrated sand than the soil-foam-mixture. The volumetric water contents in the plot are the ones in the original soil-foam-mixture. Assume that the pore water in the original sand sample has been fully replaced by the foam from the soil-foam-mixture, the foam-infiltrated sand will have a lower volumetric water content than the original soil-foam-mixture and thus a higher matric potential. This larger matric potential leads to a lower permeability. This point needs further information of the foam-infiltrated sand, e.g. matric potential, volumetric water content and degree of saturation etc. to prove.

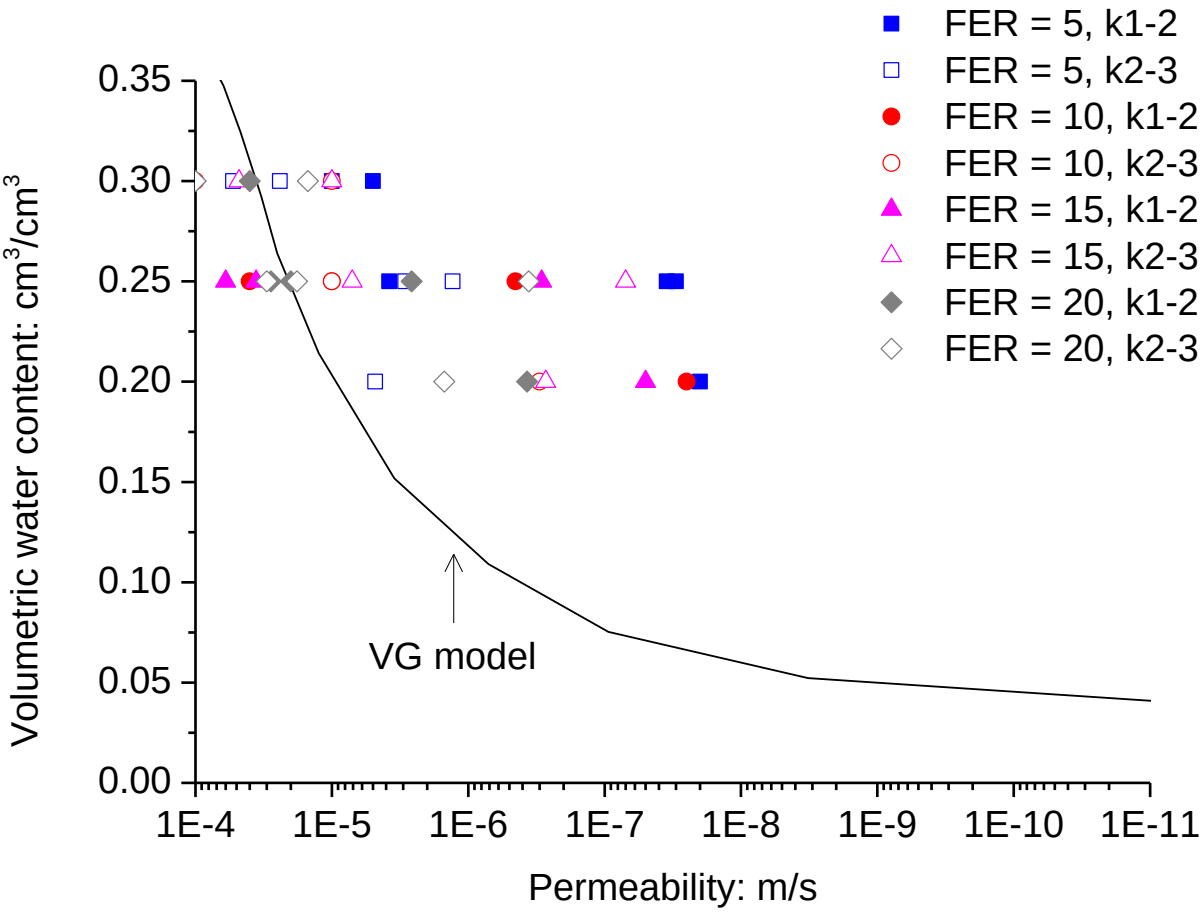

Fig. 6.15. Comparison of permeabilities from the experiment and prediction by VG model (Van Genuchten, 1980).

Because the total volume of soil-foam-mixture is known and the volume of sand is constant, if the volume of foam is assumed to be constant, then the volume of water and thus the volumetric water content can be determined. With a low FER there may be water lost by the

water flow, then the amount of air becomes higher and thus the water permeability of foam-infiltrated sand lower. The water permeability of foam-infiltrated sand is determined by the water film that is around the bubbles.

6.4. SUMMARY

The experiments of infiltration of soil-foam-mixture into saturated sand have been presented and discussed together with the experiment of foam infiltration. The following conclusions may be drawn:

(a) The mobility of foam flow depends on FIRs, but also the fractions of air, water and solid in the soil-foam-mixture. Relatively high FIRs lead to a higher mobility of foam flow than relatively low FIRs. On one hand, with relatively high FIRs, larger air fractions at given solid fraction reduces the mobility of foam flow. On the other hand, with relatively low FIRs (≤ 40 Vol%), the difference in the mobility of foam flow between different fractions is small.

(b) The water permeability of foam-infiltrated sand decreases with increasing air fraction and decreasing liquid fraction with a given solid fraction, or decreases with increasing air fraction and decreasing solid fraction with a given liquid fraction.

(c) Foam infiltration results in a lower water permeability of foam-infiltrated soil between k1 and k2. For the foams with FER = 10, 15 and 20 the results are more or less the same. No clear trend was found for the permeabilities of the sand measured between k2 and k3.

(d) Analogous to deep filtration of the slurry containing sand, high sand content of the soil-foam-mixture will interfere the impermeable or low permeable layer formation on the boundary between the soil-foam-mixture and the sand.

(e) The water permeability of foam-infiltrated sand decreases with FIR. The line (Fig. 6.13) is assumed, without a physical meaning. Based on this line, a FIR of 35 – 40 Vol% is recommended for EPB shield tunnelling in sandy soils.

(f) The measured foaming liquid permeabilities of foam-infiltrated sand correspond to the VG model for unsaturated soil. With increasing volumetric water content (water fraction),

the water permeability of foam-infiltrated sand decreases. The permeability is determined by the water film that is around the bubbles.

(g) To further understand the mechanism of infiltration of foam from soil-foam-mixture into saturated sand, yield stress and surface tension of the foam and size of the foam bubble have to be determined. Based on these determined parameters, it is expected to gain some more physics of soil-foam-mixture, like the minimum pressure gradient and the maximum size of the foam bubble for the mobility of foam bubbles, other than a simple line (Fig. 6.13). Further information of the foam-infiltrated sand, e.g. matric potential, volumetric water content and degree of saturation etc. will also be important to estimate the permeability of foam-infiltrated sand by the VG model.

PART IV COMPUTATIONAL MODELS

Chapters 2 to 6 have presented the experiments of drilling fluids (slurry and foam) and the mechanisms of infiltration of slurry and foam. On the basis of the mechanisms, a steady state model for predicting the excess pore water pressure in front of a slurry shield will be developed. An existing transient model will also be shown. Both models will be validated with the field measurements at Green Heart Tunnel and Amsterdam North/South Metro Line. The differences between two models will also be discussed too.

CHAPTER 7 COMPUTATIONAL MODELS OF EXCESS PORE WATER PRESSURES

(This chapter is based on the article: Xu, T., Bezuijen, A., 2018. Analytical methods in predicting excess pore water pressure in front of slurry shield in saturated sandy ground. Tunnelling and Underground Space Technology.)

During mechanized tunneling with a slurry shield in saturated sand, excess pore water pressures will generate in front of slurry shield. These excess pore water pressures can influence the stability of the tunnel face. The magnitude of the excess pore water pressures thus becomes of importance for the stability of the tunnel face. In this chapter, two analytical solutions are presented to describe the development and decline of the excess pore water pressures in front of slurry shield in saturated sandy ground. The first theory considers transient flow in a semi-confined aquifer with elastic storage, while the second one assumes different conditions of unconfined steady-state flow governed by the infiltration of slurry into the soil in front of the tunnel face. Both methods are tested at different positions around the tunnel, during both drilling and standstill and compared with measurements performed at the Green Heart Tunnel (GHT) and Amsterdam North/South Metro Line (N/S Line) in the Netherlands. It is shown that both analytical theories can predict the excess pore water pressures in front of slurry shield. The second one seems more appropriate because it reflects the effect of slurry infiltration. Furthermore, the measurements seem to indicate that the influence of elastic storage is not as big as assumed in the first theory.

7.1. INTRODUCTION

The experience on shield tunnelling, started in the Netherlands only two decades ago (Bezuijen & Bakker, 2008). Because of the limited knowledge of shield tunnelling in permeable saturated sandy ground, a series of in-situ measurements and studies have been carried out during the construction of early shield tunnels in Netherlands. One of the findings

of that research was that there is an excess pore pressure present in the soil in front of the TBM during drilling, which influences the stability of the tunnel face (Bezuijen et al., 2006; Broere, 2003; Broere & van Tol, 2000, 2001). This excess pore pressure disappears during standstill of the TBM, see Fig. 7.1. In Netherlands, excess pore pressures were measured during the tunnel driving at various projects, such as the Second Heinenoord Tunnel, the Botlek Tunnel, Green Heart Tunnel (GHT) and Amsterdam North/South Metro Line (N/S Line) (Bezuijen, et al., 2006; Bezuijen et al., 2016; Broere, 2003; Kaalberg, et al., 2014).

To predict the excess pore water pressure in front of a TBM, some analytical methods have been developed (Bezuijen et al., 2006; Bezuijen et al., 2016; Broere & van Tol, 2001). Broere & van Tol (2001) proposed a model to predict these excess pore water pressures assuming that drilling takes place in a semi-confined aquifer and that equilibrium is not achieved immediately due to elastic storage, so that transient conditions must be considered. The excavation is modelled through its discharge, which is estimated considering that the amount of water displaced by the infiltrating slurry is roughly equal to the pore volume in the excavated soil. Bezuijen et al. (2006) and Bezuijen et al. (2016) developed a model where the pore water pressure variations are governed by the properties of the slurry that infiltrate into the soil during drilling and the excavation is set in a homogenous unconfined thick soil layer where steady-state conditions can be considered. The dissipation of the hydraulic head through the infiltrated zone defines the piezometric head in front of the tunnel, which sets the new pore water pressure distribution based on an assumption of radial flow. Unlike the model of Broere, Bezuijen assumed that the influence of elastic storage is negligible, thus there must be no phase shift between pore pressure responses taken at different positions. As explained by Talmon et al. (2013), the infiltration of slurry can be distinguished into two processes: mud spurt and filter cake formation. When mud spurt starts, the slurry (water with bentonite particles) infiltrates into the soil. After some time, the bentonite particles are blocked in the soil pores and only water from the slurry flow into the soil, the filter cake thus forms at the surface of soil. Because the cutting wheel will constantly remove the filter cake, however, there will be no formation of filter cake at the tunnel face during drilling of TBM. Hence, the effect of filter cake is not taken into account. The piezometric head drops because of

infiltration during standstill of TBM, and rises due to removal of the infiltrated soil by cutting wheel during drilling.

In this chapter, the two analytical models are introduced and the differences between them are interpreted. The calculated results from these two models are compared with the pore pressures measured around the construction of the GHT and the N/S Line in the Netherlands.

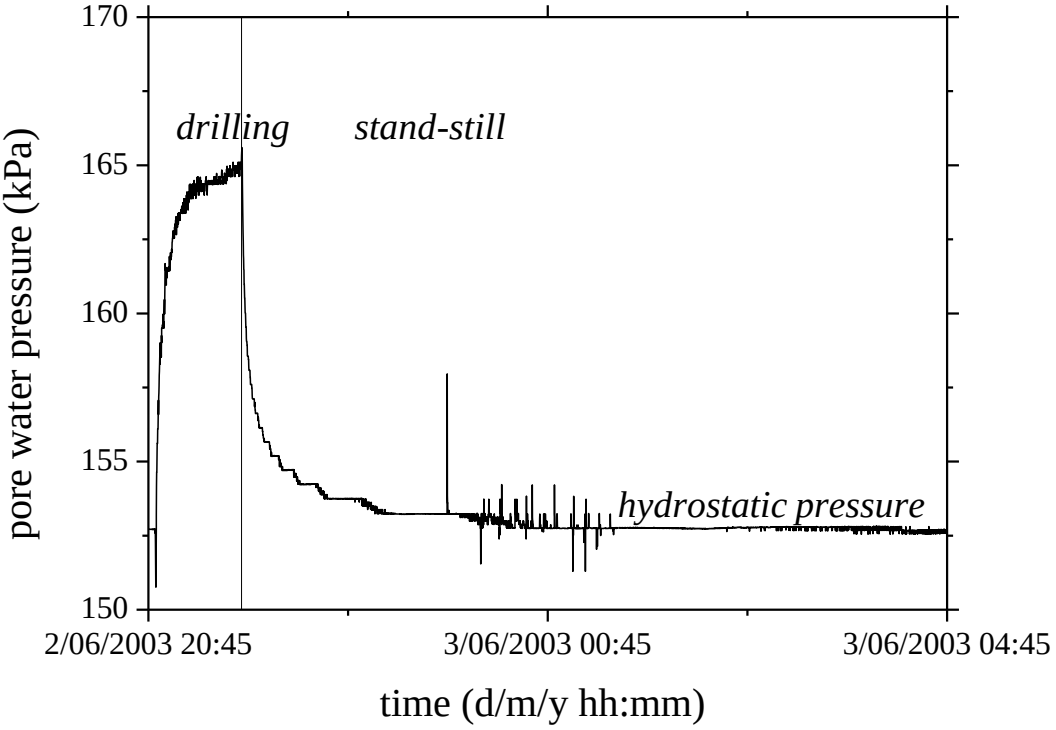

Fig. 7.1. Pore water pressure during the process of tunneling at GHT: drilling and standstill.

7.2. FIELD MEASUREMENTS AT GHT AND N/S LINE

The GHT is located approximately 20 km southwest of Amsterdam. The tunnel is constructed through a saturated sand layer, where the overburden consists of peat and clay. Hydro-geotechnical conditions are described by Aime et al. (2004) and tunnel design by Aristaghes et al. (2002). Eight pore pressure transducers (PPTs) were installed in the soil around the tunnel in advance of the TBM passing. The location of PPTs around the tunnel cross-section can be seen in Fig. 7.2. The two instruments further away from the TBM are just marked at their

depth (WR1, WR2). All instruments were placed in the ground along the tunnel chainage 4219 m, with the exception of WB0 (4221 m) and WC0 (4223 m). This layout allows the pore pressures to be evaluated both in time and space. The records of the shield position are only available after the face of the TBM had passed the instrumentations section. However, other cases (Kaalberg et al., 2014; Aime et al., 2004) reveal that the increments of pore pressure are more or less symmetric regarding the distance between the face and the instruments. Therefore, the distances after the section can be considered equivalent to distances before the section.

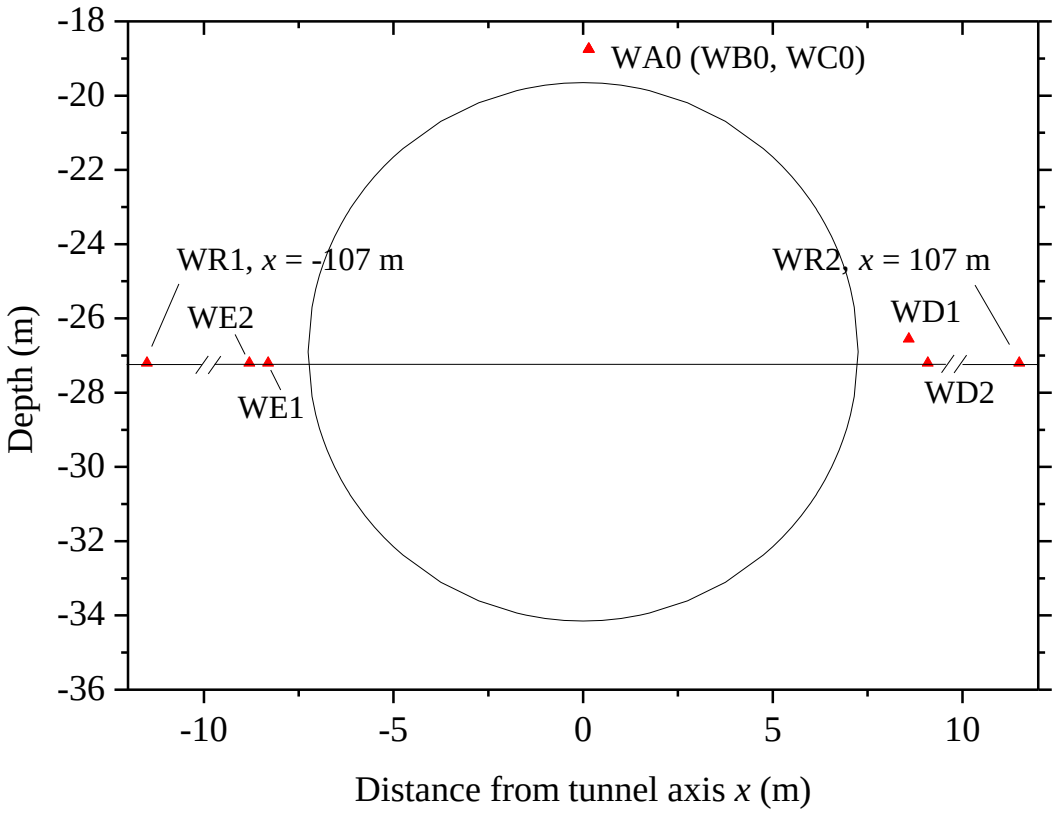

Fig. 7.2. Sketch of pore pressure transducers at ring 2117 at GHT.

The tunnels of N/S Line in Amsterdam are constructed through a saturated sand layer, where the overburden consists of very soft soil. It is a challenging project in an unfavourable urban environment with over 1000 historical buildings founded on wooden piles close to the tunnels (Kaalberg et al., 2014). The diameter of the two bored tunnels is 6.5 m. At a historic bridge "Bridge 404", both tunnels pass the bridge at a different depth (see Fig. 7.3). The East tunnel

is constructed only 1.5 m below the pile tips of the bridge. Unfortunately, details of instruments at N/S Line are unavailable.

7.3. TRANSIENT MODEL

In the Netherlands, the sandy layers used for tunnelling are normally overlain with soft soil layers of peat and clay with a low permeability. In such a situation, the pressure distribution in the soil can be evaluated as a semi-confined aquifer. A time-dependent method for build-up and dissipation of excess pore pressures in a semi-confined aquifer was proposed by Broere et al. (2001). While the TBM is drilling, the excess pore pressure is given by:

$$\phi - \phi_\infty = \frac{Q\lambda}{4k_s H}\left[erfc\left(\frac{xu}{2\sqrt{t}} + \frac{\sqrt{t}}{u\lambda}\right)\exp\left(\frac{x}{\lambda}\right) - erfc\left(\frac{xu}{2\sqrt{t}} - \frac{\sqrt{t}}{u\lambda}\right)\exp\left(-\frac{x}{\lambda}\right)\right] \qquad (7.1)$$

Where ϕ is the piezometric head (m) at a distance x (m) in front of the tunnel face; ϕ_∞ the piezometric head far from the tunnel in the soil (m); Q the discharge (m^3/s) at $x = 0$; the leakage length $\lambda = \sqrt{k_w H \dot{c}}$ (m), with $\dot{c}$ the hydraulic resistance of the confining layer (s); k_w the permeability of aquifer (m/s); H the height of aquifer (m); $u = \sqrt{S_s/k_w}$, with S_s the coefficient of specific storage (m^{-1}); t the time (s).

According to Mohkam (1985), volume of the water discharged by the infiltrating slurry is roughly equal to total pore volume of the excavated material. Hence, the specific discharge at the tunnel face could be estimated by:

$$q = -nv_{TBM} \qquad (7.2)$$

With n the porosity of the excavated soil (-) and v_{TBM} the advance rate of the TBM (m/s).

The value of Q then can be determined by Eq. (7.2). This is in fact a one dimensional transient model assuming flow from the tunnel front into a semi confined aquifer. The model implicitly takes into account the influence of slurry infiltration. The pore pressure build up at the beginning of drilling is according to this model governed by elastic storage, as well as the pressure decay. Eq. (7.1) is only valid when the drilling velocity is smaller than the infiltration velocity of the slurry. When the drilling velocity is larger than the infiltration velocity the

piezometric head will be overestimated by Eq. (7.1). In this case, therefore, the Eq. (7.1) needs to be rewritten as:

$$\phi - \phi_\infty = \frac{\Delta p_p}{2\gamma_w}\left[-erfc\left(\frac{xu}{2\sqrt{t}} + \frac{\sqrt{t}}{u\lambda}\right)\exp\left(\frac{x}{\lambda}\right) + erfc\left(\frac{xu}{2\sqrt{t}} - \frac{\sqrt{t}}{u\lambda}\right)\exp\left(-\frac{x}{\lambda}\right)\right] \tag{7-3}$$

Where Δp_p is the remaining excess pore pressure (Pa); and γ_w the specific weight of water (kg/m^3). For a large t, the Eq. (7.3) can be written as:

$$\phi - \phi_\infty = \frac{\Delta p_p}{\gamma_w}\exp(-\frac{x}{\lambda}) \tag{7.4}$$

This equation can be used to estimate the maximum pore water pressure distribution at some distance in front of a TBM, or, if the distance between the pore pressure measurement and the tunnel face is known, it can be used to estimate the leakage length (λ).

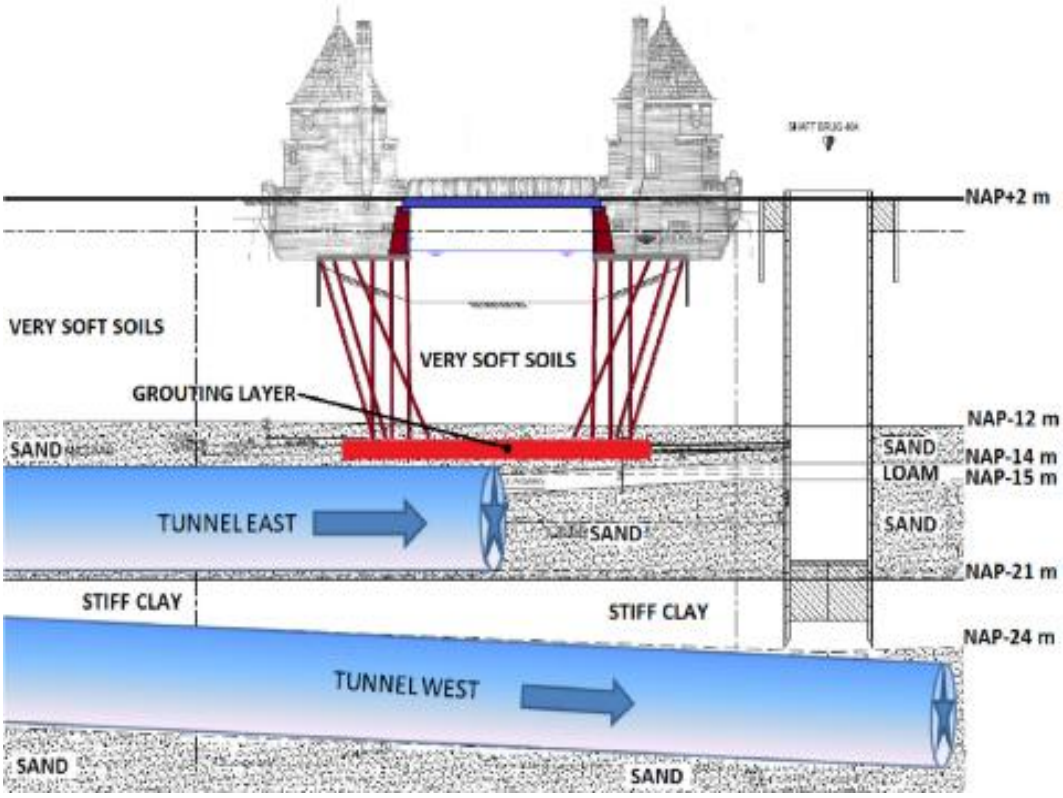

Fig. 7.3. Sketch of N/S Line beneath Bridge 404 (after Kaalberg, 2014).

At the GHT, the excess pore pressure at the tunnel face Δp_p was estimated to be 22 kPa from the available field data. The permeability of the aquifer was about 4×10^{-4} m/s (Aime, et al., 2004), and the thickness is $H = 35$ m. Combining the results from Eq. (7.4) and the measured pore pressure as a function of the distance in front of the TBM, the leakage length λ can be estimated as 50 m. Fig. 7.4 shows the pore water pressures measured in the transducer WA0 (see Fig. 7.2 for its position) and predicted with Eq. (7.4) and Eq. (7.6) (in Section 7.4) for the maximum pore pressures. The TBM passed the instrument section at ring 2117 where is 4204 m from the start of the tunnel. For the situation of steady groundwater flow, it is clear that the semi-confined aquifer in which the GHT is drilled is better modelled with a semi-confined aquifer model than with a model that assumes outflow in all directions.

During the standstill of TBM process, the decreasing excess pore pressure is calculated by:

$$\phi - \phi_\infty = \frac{\Delta p_p}{2\gamma_w}\left[erfc\left(\frac{xu}{2\sqrt{t}} + \frac{\sqrt{t}}{u\lambda}\right)\exp\left(\frac{x}{\lambda}\right) + erfc\left(-\frac{xu}{2\sqrt{t}} + \frac{\sqrt{t}}{u\lambda}\right)\exp\left(-\frac{x}{\lambda}\right)\right] \tag{7.5}$$

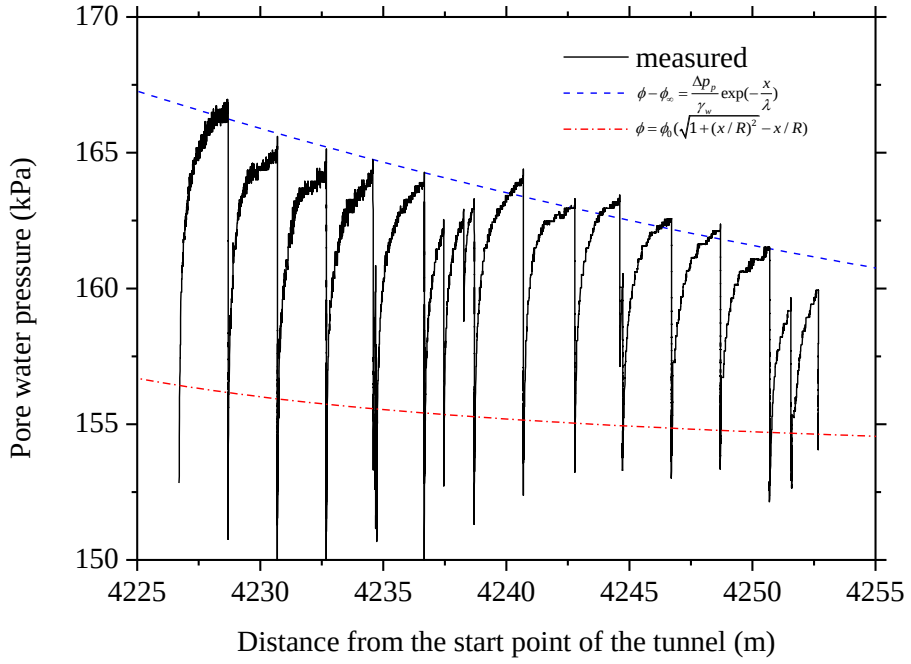

Fig. 7.4. Pore water pressure in front of slurry shield as a function of the distance from the TBM front at GHT.

7.4. STEADY STATE MODEL

The pore water pressure in front of a TBM has already been described as a function of the distance from the TBM front more than a decade ago (Bezuijen et al., 2006):

$$\phi = \phi_0(\sqrt{1+(x/R)^2} - x/R) \tag{7.6}$$

Where ϕ_0 is the piezometric head (m) at the tunnel face; ϕ the piezometric head (m) at a distance x (m) in front of the tunnel face and R the radius of the tunnel (m), assuming a piezometric head of zero far from the tunnel in the pore water, see Fig. 7.5.

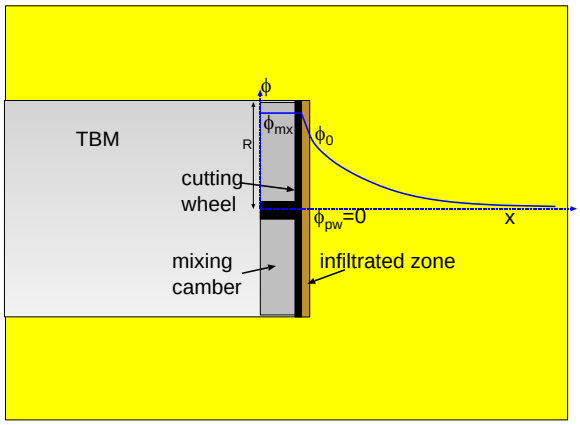

Fig. 7.5. Definition sketch. TBM, infiltration zone and piezometric head.

The formula is valid for situations where the permeability of soil around the tunnel is constant, thus not if the tunnel is drilling in a semi-confined aquifer. The formula is derived for the axis of the tunnel. Numerical calculations by Zizka et al. (2017) have shown that at the outer ring there is a larger pressure drop as a function of x than according to this formula. This means that the formula needs to be modified when it is used to calculate the pore water pressure at outer ring. Fig. 7.6 shows measured pore pressure in front of a slurry shield as a function of distance measured at the axis in front of the TBM. The model of Bezuijen et al. (2006) assumes that plastering occurs during standstill, resulting in a pressure of 120 kPa (the hydrostatic pressure) in the soil. Higher pore pressures were measured during drilling, because the TBM's cutter head removes the cake before it can form at the tunnel face. Fig. 7.7

shows the same phenomenon measured in front of an EPB shield. Here, only the maximum pressure during drilling was recorded.

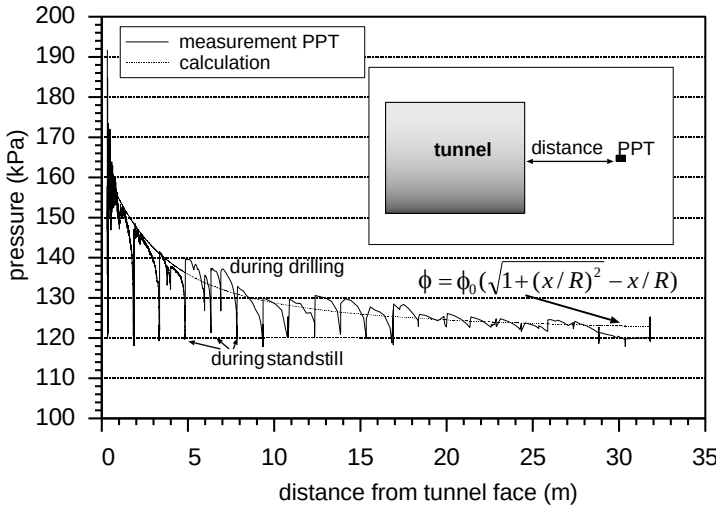

Fig. 7.6. Measured excess pore pressure in front of a slurry shield and approximation (after Bezuijen et al., 2006).

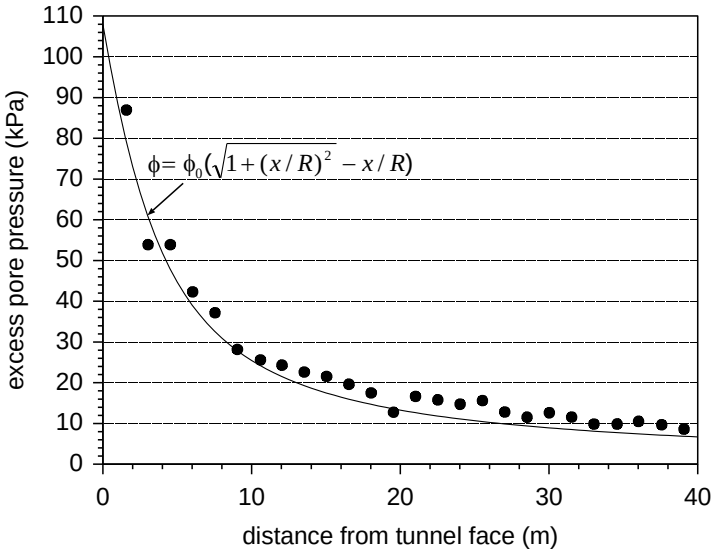

Fig. 7.7. Measured excess pore pressure in front of an EPB shield (●) and approximation at Botlek Rail Tunnel, MQ1 South (after Bezuijen, 2006).

This model assumes that the drilling speed is higher than the slurry infiltration velocity and consequently there is no influence of the infiltrated zone. The infiltrated zone only has an

influence during stand still. The situation that the drilling speed is lower than the slurry infiltration velocity is described by Bezuijen et al. (2016). This model also describes the pressure increase when drilling starts and the decrease during standstill (using for the last item the same principles as in Bezuijen et al. (2006). In this chapter the model described by Bezuijen et al. (2016) will be used.

7.4.1. THE EFFECT OF INFILTRATED ZONE

Different from Broere's model Bezuijen assumes that there is no elastic storage and that the pore water pressure buildup and decrease is governed by the infiltration of slurry into the soil and the removal of this infiltrated zone during drilling. When slurry infiltrates into the soil in front of slurry shield, the piezometric head will drop dramatically over the infiltrated zone. This was measured during construction of the N/S Line in the Netherlands (Kaalberg et al., 2014). It appeared that the piezometric head ϕ_0 in soil around the tunnel was not equal to the slurry pressure in the excavation chamber but has a lower value. It means that the slurry infiltrated into soil during TBM tunnelling. To reflect the effect of infiltrated zone, a value of α was introduced and defined as:

$$\phi = \alpha(\phi_{mx} - \phi_{\infty}) \tag{7.7}$$

Where ϕ_{mx} is the piezometric head in the excavation chamber (m) and ϕ_{∞} the piezometric head far from the tunnel in the soil (m).

The value of α depends on the infiltration velocity of the slurry for a slurry shield and thus of the permeability of the soil. If the infiltration velocity of the slurry is lower than the drilling velocity, there will be no effective plastering and α will be close to 1. If on the other hand the infiltration velocity of the slurry is larger than the drilling velocity, then α will be smaller than 1.

Differentiation of Eq. (7.6) to x results in the hydraulic gradient for $x = 0$, thus at the tunnel face:

$$i = \phi_0 / R \tag{7.8}$$

The flow velocity of water in pore channels which follows Darcy's law, can be written:

$$v = k_w h / L \tag{7.9}$$

Where k_w is the permeability of soil for water (m/s); h the total head difference (m) and L the length of seepage path (m). Considering the pore channel is an irregular path, the actual length of seepage path by which water flows through the pores of soil is longer than L. As v in Eq. (7.9) is defined as $v = Q/A$, in which A is the entire cross-sectional area of sand, the actual velocity of water in the voids is $v_p = v/n$, where n is the sand porosity. With Darcy's law considering the porosity and the relation between filter velocity and pore velocity (v_p), this leads to:

$$v_p = \frac{k_w \phi_0}{nR} \tag{7.10}$$

When α =1, this relation can be used to calculate the infiltration rate of the slurry, which will be equal to the pore velocity. If for α = 1 the calculated infiltration velocity of the slurry is larger than the drilling velocity of the TBM, the slurry will infiltrate further into the soil in front of the TBM. Due to the higher viscosity of the slurry than the viscosity of water and the yield stress of the slurry, the infiltration rate will slow down and after some infiltration the infiltration rate will be equal to the drilling velocity. Now Eq. (7.10) in combination with Eq. (7.7) can be used again, but with the pore water velocity v_p that is equal to v_{TBM}, the drilling velocity, because after the initial faster infiltration, the slurry infiltration in the soil will have the same velocity as the drilling velocity of the TBM. This allows to calculate α (Steeneken, 2016):

$$\alpha = \frac{nRv_{TBM}}{(\phi_{mx} - \phi_\infty)k_s} \tag{7.11}$$

This result makes it possible to estimate whether excess pore water pressures can be expected in front of a tunnel face when drilling in homogeneous saturated sandy soil. When α calculated with Eq. (7.11) is larger than 1 then v_{TBM} is larger than v_p and the equality $v_p = v_{TBM}$

is not valid anymore. In that case v_p has to be determined by Eq. (7.10) with $\phi_0 = \phi_{mx} - \phi_\infty$ leading automatically to $\alpha = 1$.

For an alternate expression of the partial pressure drop over the infiltration zone, see Broere (2001), which is based on the average period between passages of the cutting teeth and the infiltration velocity according to Krause (1987).

7.4.2. PORE WATER PRESSURE AFTER DRILLING

During standstill, for example because of ring building, the infiltration of slurry in the soil will continue until the maximum infiltration distance is reached. Assume the situation that there is hardly any slurry infiltration during drilling. When drilling stops, the slurry starts to infiltrate into the soil. The maximum infiltration distance is L (m). Assume again a piezometric head that is zero far from the tunnel. In that case the relation between the piezometric head in the soil just in front of the slurry and the piezometric head in the excavation chamber can be written as:

$$\phi_{mx} = \phi_0 + \frac{n v_p}{k_b} x + \frac{\phi_{mx}}{L} x \tag{7.12}$$

With k_b is the permeability of the soil for the slurry (m/s).

If a situation at the end of the slurry infiltration process is considered, L is input in the equation for x. The infiltration will be impeded due to the filter cake formation and thus the slurry pressure will be applied onto the soil skeleton rather than the pore water in the soil. In this case, hence, the values of v_p and ϕ_0 will tend to zero.

Since $v_p = dx/dt$ this leads to the equation:

$$\frac{\mathrm{d}x}{\mathrm{d}t} = \frac{\phi_{mx}\left(1 - x/L\right)}{\left(nR/k + nx/k_b\right)} \tag{7.13}$$

Eq. (7.12) is a non-linear differential equation. This can be solved numerically starting at $x = 0$ if there is no slurry infiltration during drilling and starting with a certain value of x if there

had been slurry infiltration during drilling. When $v_p = dx/dt$ is determined, Eq. (7.10) can be used to determine ϕ_0 as a function of time.

Again, the empirical formula suggested by Krause (1987) is used to estimate the infiltration distance:

$$x(t) = \frac{t}{a+t} L \tag{7.14}$$

Where a (s) is the timespan to reach half of the final infiltration depth ($0.5L$). The value of a can be of importance in tunnelling because it determines the time span until the cake in front of the TBM is fully formed. This is important when air pressure has to be applied at the tunnel face. In literature this parameter is often determined by slurry infiltration tests. However, it also depends on the flow conditions in front of the tunnel. Although the integration of Eq. (7.13) leads to a different formula as Krause's equation, it can be used to make an estimate for a and to see what parameters determine its value. Differentiation of Eq. (7.14) results in:

$$\frac{\mathrm{d}x}{\mathrm{d}t} = \frac{a}{(a+t)^2} L \tag{7.15}$$

For $t = 0$ and $x = 0$ this can be compared with Eq. (7.10) leading to:

$$a = \frac{nRL}{\phi_{mx} k_w} \tag{7.16}$$

The parameter a as defined by Krause can thus be estimated with parameters in Section 7.5.1. It shows that the timespan a is not only a function of the bentonite properties, but also of the diameter of the tunnel and permeability of the soil. Bezuijen et al. (2016) have shown that a will have a much smaller value in a model test than in a real TBM.

7.4.3. Pore pressure build up when drilling starts

The principle of pore pressure during standstill can also be used to predict the increase in excess pore water pressure when drilling starts. Again Eq. (7.13) can be used, but it should be realized that during drilling the cutting wheel takes some soil in which the slurry is infiltrated.

And therefore to calculate x at various time steps the reduction x due to drilling has to be added:

$$x_{i+1} = x_i + (\frac{\mathrm{d}x}{\mathrm{d}t} - v_{TBM})\Delta t \tag{7.17}$$

Where the suffixes i and $i+1$ refer to different times in a numerical solution and Δt is the time step between them.

For this analytical method, because the calculation of x_{i+1} starts after the first standstill, the pore pressure is calculated started from first standstill. For the first time step, this leads Eq. (7.17) to:

$$x_{i+1} = L + (\frac{\mathrm{d}x}{\mathrm{d}t} - v_{TBM})\Delta t \tag{7.18}$$

Because also the dx/dt is close to zero, the Eq. (7.18) can be rewritten:

$$x_{i+1} = L - v_{TBM} \cdot \Delta t \tag{7.19}$$

7.5. RESULTS AND DISCUSSIONS

7.5.1. COMPARISON OF PREDICTED AND MEASURED RESULTS

The two analytical theories of predicting the excess pore pressure in front of a TBM have been presented in Sections 7.3 and 7.4. The pore water pressures measured during drilling and stand-still are compared with the values calculated based on the two theories.

Starting with the pressure drop at the end of drilling, the transient model is applied with the same parameters calibrated in Section 7.4 and compared with the measurements from the GHT. The value of the coefficient of specific storage S_s = 4.00 × 10^{-8} m^{-1} is calibrated by fitting the calculated results with Eqs (7.1) and (7.3) to the measured values, see Figs 7.8a and 7.8b. For the steady state model, the procedure from Sections 7.4.2 and 7.4.3 is used, assuming the following parameters: k_b = 2.00 × 10^{-5} m/s, k_w = 4.00 × 10^{-4} m/s, L = 0.07 m, ϕ_{mx} = 4.16 m, n = 0.35, and R = 7.25 m, v_{TBM} = 6.60 × 10^{-4} m/s, v_p = 5.60 × 10^{-4} m/s. Because the

types of soil and bentonite used at GHT and N/S Line are different from the experiments in this thesis, the parameters k_b, k_w and L determined by the infiltration experiments using the same types of soil and bentonite as those used on the jobsite were used (Steeneken, 2016). $v_{TBM} > v_p$, thus $\alpha = 1$.

Fig. 7.8a shows the comparison of measured and calculated results when the TBM stops at about 26 m from the PPT WA0. It can be seen that the pressures predicted by both theories fit the measured values well, but the transient model underestimate the excess pore pressure after about 500 s. To simulate the pressure increase during drilling, Eq. (7.17) can be used with the parameters listed above. Fig. 7.8b shows the results of both theories compared with the measured pressure increase. Both theories predict the excess pore pressure well, but again the steady state model shows a more reasonable agreement, but the difference is only small.

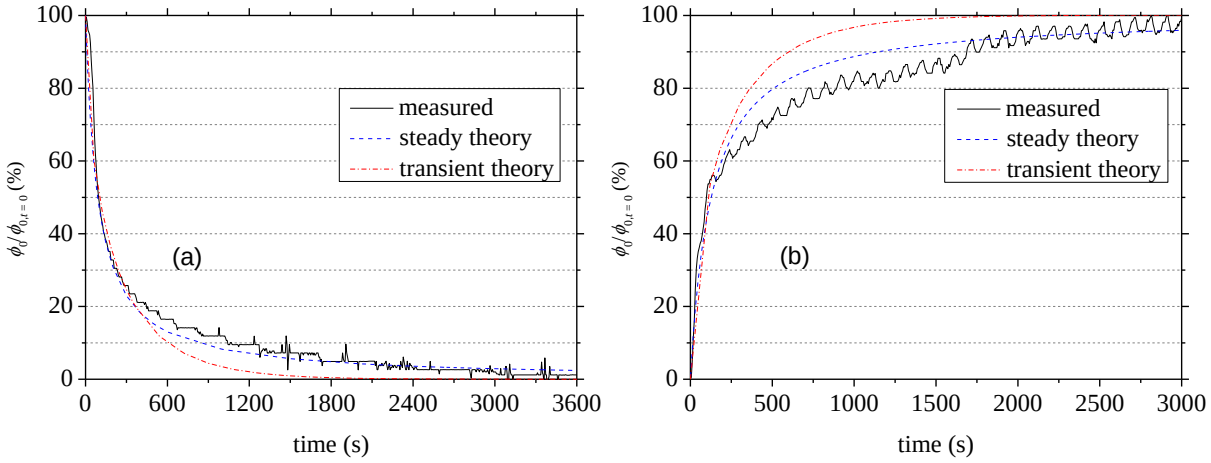

Fig. 7.8. Pore pressure decline when drilling stops at GHT (a). Pore pressure increase when drilling starts at GHT (b).

The pore pressure in PPT WA0 at ring 2117, during the course of three days, was plotted in Fig. 7.9. More than 36 cycles of pore water pressure increase and decrease can be seen. The range of the cycles increased from 10 kPa to 20 kPa during the first and second days and then decreased from about 20 kPa to less than 10 kPa during the third and fourth days.

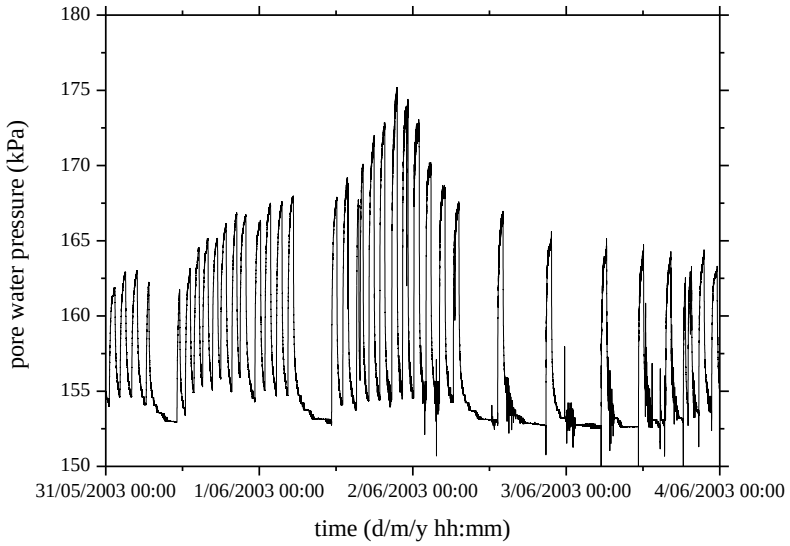

Fig. 7.9. Pore pressure in WA0 with time at GHT.

To explore this mechanism in more detail, four cycles were analyzed, reflecting different distances between the TBM face and the instrumentation section. The period of these cycles were: 2/6 13:15 to 20:50; 3/6 15:32 to 18:17; 3/6 20:42 to 22:42 and 4/6 04:28 to 06:22, during which the TBM was drilling around the chainages of: 4227, 4235, 4239, and 4247 m, respectively. It is worth to recall that PPT WA0 was installed at 4219 m. For each of the cycles the magnitude of the water pressures was different. Therefore, the values are scaled between 0 and 100% for the range between the minimum and the maximum pressures at each cycle.

The resultant curves for the pressure development can be seen in Fig. 7.10a. For all the relative positions of the TBM face, the curves closely resemble one another. This was expected according to the steady state model because the effect of distance from the TBM front is eliminated with this normalization. However, the transient model from Broere predicts that the excess pore water pressures, when drilling starts, depend on the distance x (see Eq. (7.3)). Fig. 7.10b shows the predicted pressure development according to Eq. (7.3), calculated with the parameters listed in Section 7.3. The pressures at a larger distance increased at a lower rate than those at shorter distances, but the difference was quite small.

The corresponding curves for the pressure decline are plotted in Fig. 7.10c. For all the relative positions of the TBM face, the curves closely resemble one another, with the exception of x = 4227 m. As the figure shows, the dissipation at this position was slower. According to the transient model from Broere, the course of the excess pore water pressures during standstill, also depends on the distance x (see Eq. (7.3)). Fig. 7.10d shows the calculated pressure decline according to Eq. (7.5) with parameters listed in Section 7.4. Similar to the curves for pressure development, when the distance was higher, the dissipation was slower.

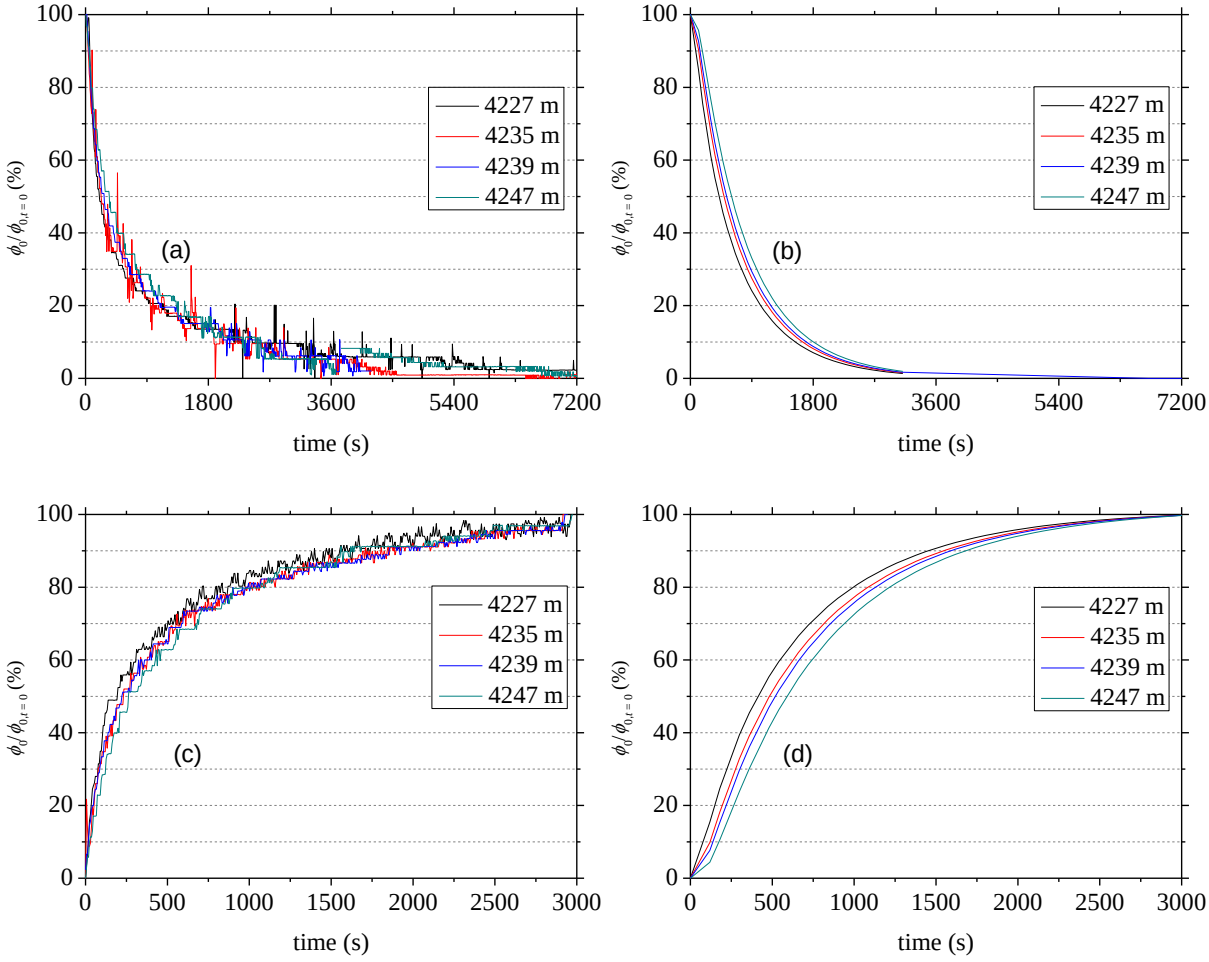

Fig. 7.10. Pore pressure at different time in front of slurry shield at GHT. Measured pore water pressure increase in WA0 (a). Calculated pore water pressure increase in WA0 according to transient model (b). Measured pore water pressure decline in WA0(c). Calculated pore water pressure decline in WA0 according to transient model (d).

7.5.2. PARAMETRIC ANALYSIS

For N/S Line, by measuring the piezometric head close to the TBM during drilling, it was determined that α was 0.60. It means that there is always some slurry that is infiltrated into the soil in front of the TBM also during drilling. Thus the integration should not start with x = 0 m, but with the value of x that corresponds with a piezometric head that is 0.6 times the piezometric head in the excavation camber. This appeared to be x = 0.0534 m. Assuming the following parameters: $k_b = 5.00 \times 10^{-6}$ m/s, $k_w = 1.00 \times 10^{-4}$ m/s, L = 0.25 m extrapolated from laboratory tests of bentonite slurry infiltration in saturated sand (Steeneken, 2016), ϕ_{mx} = 14.30 m, n = 0.35, and R = 3.44 m, $v_{TBM} = 5.10 \times 10^{-4}$ m/s, $v_p = 1.20 \times 10^{-3}$ m/s in west tunnel and $v_p = 1.48 \times 10^{-3}$ m/s in east tunnel. $v_{TBM} < v_p$, thus $\alpha < 1$. With measured ϕ_{mx} and ϕ_0, Eq. (7.7) resulted in α = 0.60. On the other hand, with determined parameters, Eq. (7.11) gave another value: α = 0.43. This value is somewhat comparable to α = 0.60. It delivers that the excess pore water pressure is not depending on the piezometric head in excavation chamber, but the piezometric head just in front of the infiltrated zone, if some plastering during excavation occurs. Fig. 7.11 shows the comparison of results measured and calculated with α = 1.00 and α = 0.60. It is shown that the curve with α = 0.60 matches the curve of measured values better than α = 1.00.

Fig. 7.11a also indicates that a longer time is needed for dissipation of the calculated piezometric head. This is probably caused by the assumption that ϕ_∞ the piezometric head far from the tunnel is zero. If we assume the ϕ_∞ as approximately 1 m, for instance, 0.7 m, the curves from calculation show a better agreement with the measured curve, see Fig. 7.11b.

It was mentioned that Eq. (7.15) is an empirical formula to describe the infiltration of the slurry and that following the theory of steady model, the pore velocity v_p can be estimated with Eq. (7.13). Both formulas are compared in Fig. 7.12. For the GHT, both the calculated results show a good agreement with the measured result. But for the N/S Line, the curve from calculation with Eq. (7.15) only approximates the curve from measurement within about 300 s. Afterward, although the value is also overestimated by the calculation with Eq. (7.13), the curve made with Eq. (7.13) shows a better agreement with the curve from measurement.

Again the difference is not very large, but using a as determined in a laboratory test would result in a significant mismatch (Steeneken, 2016).

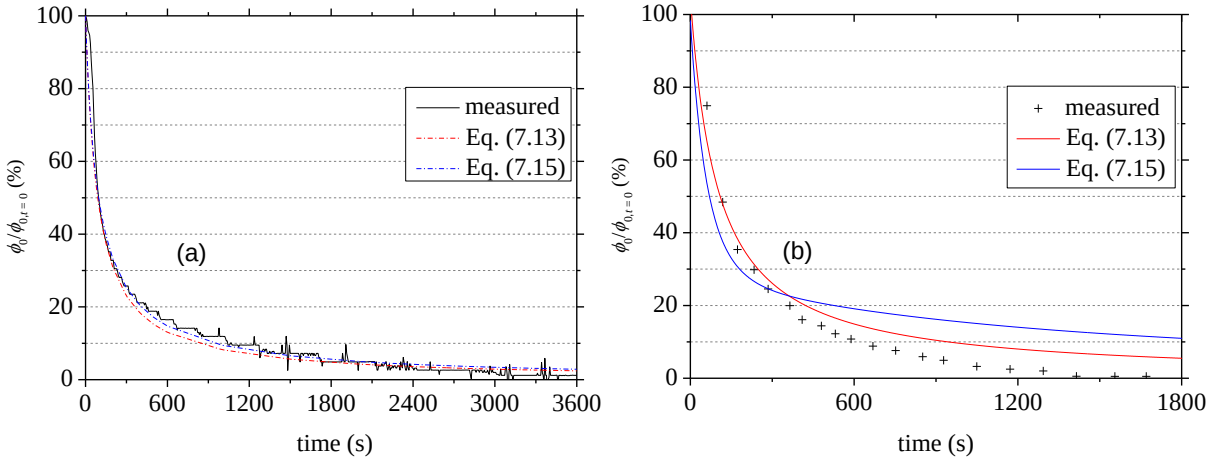

Fig. 7.12. Calculated results with different v_p compared with measured results at GHT (a) and N/S Line (b).

Fig. 7.13 shows that the value of the coefficient of specific storage (S_s) has significant influence on the calculated results. In other words, the results are sensitive to this parameter. Compared to the input value of 4.00×10^{-8} m^{-1}, a higher value of S_s will result in too fast change of pore water pressure, whereas a smaller value of S_s will lead to too slow change of pore water pressure. Therefore, this parameter needs a careful calibration for the calculation.

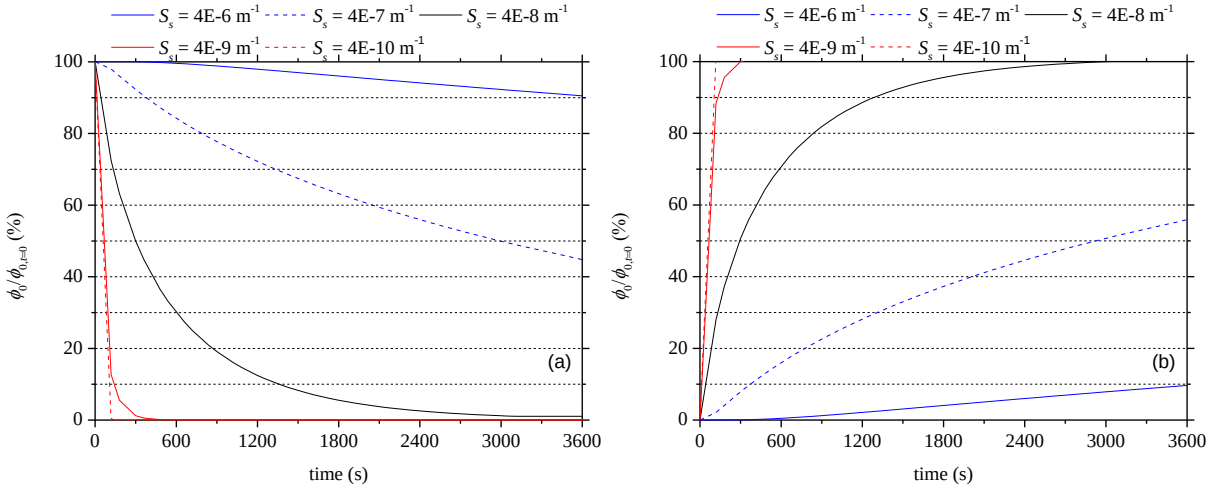

Fig. 7.13. Influence of the storage coefficient on the calculated results.

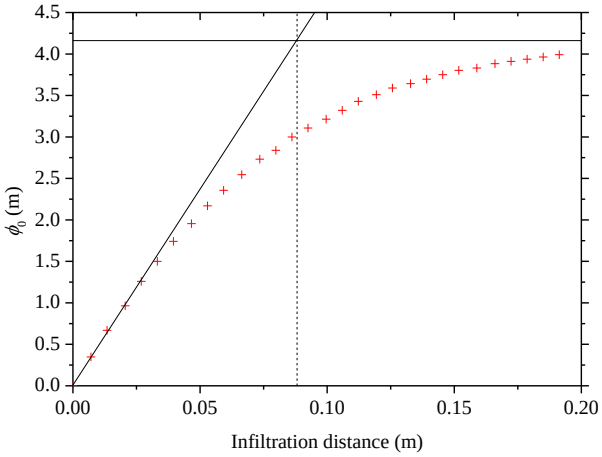

Fig. 7.14. Estimated infiltration distance.

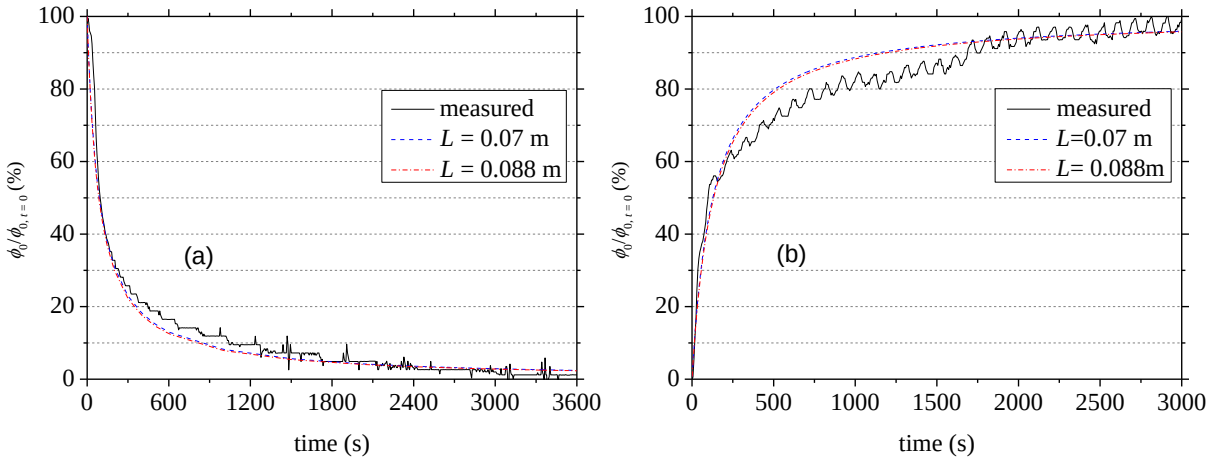

Fig. 7.15. Calculated results with different L compared with measured result.

It also presents an interesting possibility to make an estimate of the distance the slurry has infiltrated into the soil for the situation that the pore pressures are measured but there is no information on the infiltration distance. In the first calculation steps using Eq. (7.17), dx/dt will be close to zero and thus x will shorten each time step with $v_{TBM} \cdot \Delta t$. This allows for a graphical solution to determine L, see Fig. 7.14. To test this procedure, the data for the GHT simulation were used and a infiltration distance of 0.088 m is found, while 0.07 m was used as input data. Fig. 7.15a shows the decline of the pore water pressure measured and calculated with L = 0.07 m and L = 0.088 m and Fig. 7.15b the development of the pore water pressure measured and calculated with L = 0.07 m and L = 0.088 m. It is also possible to estimate the

infiltration distance using the pressure decrease at the end of drilling, but then you need also data on the permeability of the sand layer, which introduces some uncertainty.

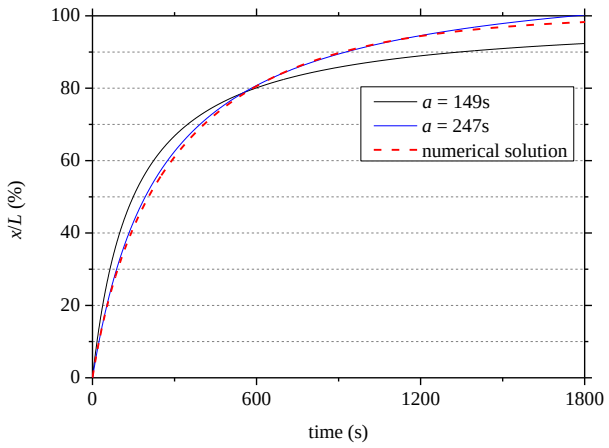

Fig. 7.16. Numerical solution compared with curve proposed by Krause (1987) at N/S Line.

The value of a is of importance in slurry shield tunnelling because it determines the time span until the cake in front of the TBM is fully formed. This is important when air pressure has to be applied at the tunnel face. Eq. (7.16) indicates that the parameter a as defined by Krause depends on porosity and permeability of the soil, radius of the tunnel, infiltration distance and piezometric head in the excavation chamber. Since integration of Eq. (7.13) will lead to another equation than the empirical Eq. (7.14), it is possible that also dx/dt at $t = 0$ is different. To check this x in function of t was determined using numerical integration of Eq. (7.13). With non-linear regression this curve was fitted to Eq. (7.14), see Fig. 7.15. There appears to be only a reasonable agreement. At larger values of t, the infiltration is underestimated by Eq. (7.14). For the N/S Line, the a that follows from the non-linear regression, 149 s, is also in reasonable agreement with a calculated from Eq. (7.16), 210 s. A better agreement is possible by assuming that the L as defined by Krause can be different from the L used in the numerical calculation. Thus in the non-linear regression analysis L in Eq. (7.14) is replaced by $c{\cdot}L$ where c can vary, but should be approximately 1. This allows a much better agreement, see also Fig. 7.16 and the resulting a from non-linear regression is now 247 s also in better agreement with the 210 s calculated with Eq. (7.16). Therefore Eq. (7.16) can be used to have a first

estimation of a for the situation in front of a TBM drilling in saturated sand if L is determined as a function of ϕ_{mx}, in an infiltration test.

7.6. SUMMARY

Two theories with analytical solutions are presented to describe the development and decline of excess pore water pressures in front of slurry shield in saturated sand. Based on the above calculations and comparative analyses, the following conclusions are possible from the measurements and theory presented in this chapter.

(a) The assumptions to come to the two different theories are quite different. The steady state groundwater flow is different (Eq. (7.4) and (7.6) in the transient model and the steady state model, respectively). The way the influence of the slurry is taken into account by the elastic storage in the transient model and the infiltrated zone in the steady state model. Yet, this chapter showed that the results are quite comparable and for both cases can be fitted to the measurements.

(b) For the situation of steady groundwater flow, it is clear that the semi-confined aquifer in which the GHT is drilled is better modelled with a semi-confined aquifer model than with a model that assumes outflow in all directions. A way to improve the semi-confined aquifer model, would be to take into account the influence of radial flow in the horizontal plane, but this is not studied further.

(c) The way the slurry infiltration is taken into account in Broere's model, seems quite a simplification of the real process. This is more or less 'compensated' by introducing the elastic storage in the soil.

(d) The overall conclusion must be that agreement between theory and measurements is no guarantee that the theory is right. This chapter shows that with two quite different theories such agreement can be reached. Therefore the real issue is whether or not the theory is based on the right physics.

PART V CONCLUSIONS AND RECOMMENDATIONS FOR FUTURE RESEARCH

CHAPTER 8 CONCLUSIONS AND RECOMMENDATIONS FOR FUTURE RESEARCH

8.1. INTRODUCTION

This thesis about infiltration and excess pore water pressure in front of a TBM analysed the mechanisms of infiltration of slurry and foam in front of a TBM, compared the two analytical models of excess pore water pressure induced by shield tunnelling in an aquifer with two field measurements. The study improved our understanding of the infiltration of slurry and foam in front of a TBM, and showed how the elastic storage and the infiltration determine the excess pore water pressure.

Thirteen model experiments of slurry infiltration and thirty model experiments of foam infiltration were carried out. The measured pore pressures and discharges in a number of these scaled model experiments guided the development of ideas underlying the newly developed concept for mud spurt (Section 2.3) and the micro scale explanations for the movement of slurry and foam in the saturated sand. The two analytical models were validated using the measurements of pore water pressures from two tunnel projects. The correlation between the analytical models and the experimental data and its consequences for practice will be discussed in this chapter.

8.2. EXPERIMENTS OF INFILTRATION OF SLURRY

8.2.1. CONVENTIONAL SETUP

From the experiments of infiltration of clean bentonite slurries into saturated sand in the conventional setup, it was found out that mud spurt and filter cake formation are two different

processes as already noticed by Talmon et al. (2013). The measurements of pore pressure and discharge and the resulting permeabilities give an additional proof. A filter cake will be formed at the sand surface within a short time (~ 3 mins). The mud spurt will stop when this cake formation starts. These results confirm ideas developed by Talmon et al. (2013): the cake formation does not start when the mud spurt stops, but the cake formation creates an impermeable layer on top of the sand and consequently the driving force for the mud spurt (the pressure gradient over the sand) decreases and the mud spurt stops. The excess pore water pressures will decrease because of the build-up of the effective stress onto the soil skeleton due to formation of the filter cake. Since the hydraulic gradient and thus the flow velocity at the tunnel face are much smaller than those in this small-scale setup, the decrease of pore water pressure is a slower process in front of a TBM compared to the decrease measured in this setup.

The external cake formation leads to a significant reduction of the permeability close to the sand surface. The permeability of sand for bentonite slurry (k_b) and the permeability of the filter cake for water (k_c) differ with several orders of magnitude, slightly depending on the concentration of bentonite. Both of the permeability of sand for bentonite slurry and the permeability of the filter cake for water slightly decrease with the increasing concentrations of the bentonite.

Adding bentonite decreases the infiltration in the mud spurt, but has minimal influence on the filter cake formation. The experiments also showed that the estimated Peclet number (Pe) is a bit higher than the expected value ($Pe < 10$) at the initiation of the filter cake formation.

For clean bentonite slurry, the cake just on the surface of the sand has a permeability that is at least 3 orders of magnitude lower than the permeability of the slurry in the sand. This layer is very thin (~ 1 mm). Consequently, the filter cake at the tunnel face is very vulnerable to damage even during standstill of the TBM. If it is damaged mud spurt will start again and causes excess pore water pressure in the ground, leading to a reduction of effective support pressure at the tunnel face and thus reduction of the tunnel face stability.

8.2.2. MODIFIED SETUP

To get a hydraulic gradient and thus a flow velocity comparable to what could be expected at the front of a tunnel with diameter of 10 m, the conventional setup was modified. A small cylinder was added in the bottom of the original cylinder and hence the hydraulic gradient over the sand column in the modified setup was reduced to 1.7, which is very comparable to the value of 1 in a tunnel with diameter of 10 m in a homogeneous soil (Chapter 3).

From the comparison of the experiments of infiltration of slurries in both a conventional and in the modified setup, it was found out that, like the infiltration in the conventional setup, mud spurt and cake formation can also be observed. The final infiltration distances in the two test setups are similar, therefore not dependent on flow velocity, contrary to hypothesised at outset.

The Peclet number was not the determining number for the onset of the external cake formation. In the tests with the same slurry and sand, the Peclet number only depends on the pore fluid velocity, but cake formation starts at 15 times lower pore fluid velocities in the modified setup compared to the conventional one.

8.2.3. FILTER CAKE REMOVAL

Through removing the filter cake formed on the original boundary between the slurry and the soil, the process of cutting off the filter cake formed at the tunnel face by the cutting wheel was simulated. There are two infiltrations (1^{st} and 2^{nd}) before and after removing the filter cake. The slurry that infiltrated into the sand during mud spurt was not removed.

After removing the external filter cake formed during the 1^{st} infiltration, the external filter cake would be formed again during the 2^{nd} infiltration for low concentrations of slurries (40 and 50 g/l). The external cake formation in the 2^{nd} infiltration also leads to a significant reduction of the permeability close to the sand surface. However, no new external filter cake formed for high concentration of slurry (60 g/l) due to the internal filter cake formed in the sand during the mud spurt at the first infiltration. For coarser sand it is likely that also for higher slurry concentrations there will be an external filter cake.

The mud spurts before and after removing the filter cake are more or less the same during infiltration with low concentrations of bentonite, e.g. 40 g/l Colclay D90 slurry. For high concentrations of bentonite, e.g., 50 g/l Colclay D90 slurry, the mud spurt after removing the filter cake is much slower than that before removing the filter cake. There is no mud spurt anymore for 60 g/l Colclay D90 slurry after removing the filter cake.

8.2.4. SLURRY-SAND-MIXTURE

In a field situation the cutting wheel of a TBM carries the excavated soil into the excavation chamber, such that the slurry in front of the tunnel face becomes a mixture of water, bentonite and excavated soil. Therefore, the density of this slurry mixture will be higher than the initial slurry density. The densities used were comparable to the ones measured at the 2nd Heinenoord Tunnel (Bakker and Bezuijen, 2008). Experiments of infiltration of water-bentonite-sand slurry (or slurry containing sand), therefore were also carried out in the modified setup. Only 60 g/l slurry was used to obtain a stable sand-slurry mixture.

An external filter cake is formed during infiltration with low densities of water-bentonite-sand slurry, e.g. 1050 and 1100 kg/m^3 the basic Colclay D90 60 g/l slurry. In contrast, due to solid particles being retained in the pores of the sand layer, deep filtration appears to the high densities of water-bentonite-sand slurry, e.g. 1300 and 1500 kg/m^3 for basic Colclay D90 slurries. In an infiltration experiment with a high density slurry, the sand grains will get deposited on the sand surface, this prevents a steep pressure gradient at the slurry-sand boundary and it is this steep pressure gradient that causes the external filter cake.

The excess pore water pressure in front of the tunnel face may have a steep increase just after ring building when the drilling has started and the ‘gelled’ internal filter cake is removed. This could be a typical moment that a blowout occurred in front of the tunnel face.

With sufficient sand in the slurry, there will be no or hardly any external filter cake and only an internal one. In that case, there will a considerable larger infiltration distance than that is measured in ‘conventional’ slurry infiltration tests performed with clean slurry. This is positive for the safety of TBM tunnelling when air intervention is necessary at the tunnel face, since a low permeable slurry-sand mixture is present over a larger thickness in front of the tunnel face than up to now anticipated.

The influence of the excavation on the infiltration process was a new aspect in this study. As described above the excavation has a significant influence. The very low permeable external filter cake will not be present when the excavation creates a high-density slurry. The mud spurt is stopped by the external cake formation, which means that a mud spurt over a larger depth is possible when the external cake is removed, depending on the bentonite concentration of the slurry. It likely that this also depends on the pressure difference, but this was not tested, since all experiments were performed with one pressure difference.

8.3. EXPERIMENTS OF INFILTRATION OF FOAM

8.3.1. FOAM

Compared to the experiments of infiltration of clean slurry, it appears that there will be no external filter cake formed on the sand surface, but an impermeable layer will be formed in the sand. This impermeable layer is about 5 to 10 cm, depending on the FER of the foam. Like the infiltrated sand in the infiltration of slurry, the permeability of the impermeable layer is ~ 2000 times lower than the permeability of the original soil. According to the measurements there is a lot of difference in the permeability of first 2 cm and the permeability of the foam infiltrated sand at larger depth. The permeability of the first 2 cm layer is up to 2 orders of magnitude lower than the permeability of the 3 to 5 cm layers. The experiments show that also here a thin layer close to the surface determines the flow resistance of the column. This layer is formed after ~ 150 - 300 seconds (after the foam bubble infiltration). A possible explanation is presented in Fig. 8.1.

The figure shows a sketch of the boundary between the foam bubbles and the sand surface. When the foam is pressurised and the valve at the low end of the sand is opened the foam-water mixture will start to flow, however, large bubbles are blocked at the boundary, while small bubbles and water will flow into the sand. This leads to a zone with a lot of bubbles just above the sand the pressure gradient in this zone will squeeze the bubbles. This zone has a low water content (because as mentioned the water will flow through the bubbles and the sand) and thus a low permeability. The course of the pressure is sketched on the right hand side of the figure. This shows the pressure drop at the boundary.

From the experiments of infiltration of foam themselves, more findings are given:

The infiltration behaviour of foam not only depends on the FER but also on the pressure. Four different characteristics were cleanly identified from the experimental results at pressure of 1.5 bar: early high discharge, 'foam bubble infiltration', water flow with reduced permeability and water flow with increased permeability. However, no regime of water flow with increased permeability was observed for the foam at pressure of 1.15 bar. A scale effect of pressure applied to the foam on the infiltration behaviour was noticed in these tests. In the ground deep below the phreatic line, the high pressure applied to the foam probably leads to a water flow with increased permeability in the infiltrated sand and hence there will be a risk of collapse of the tunnel face.

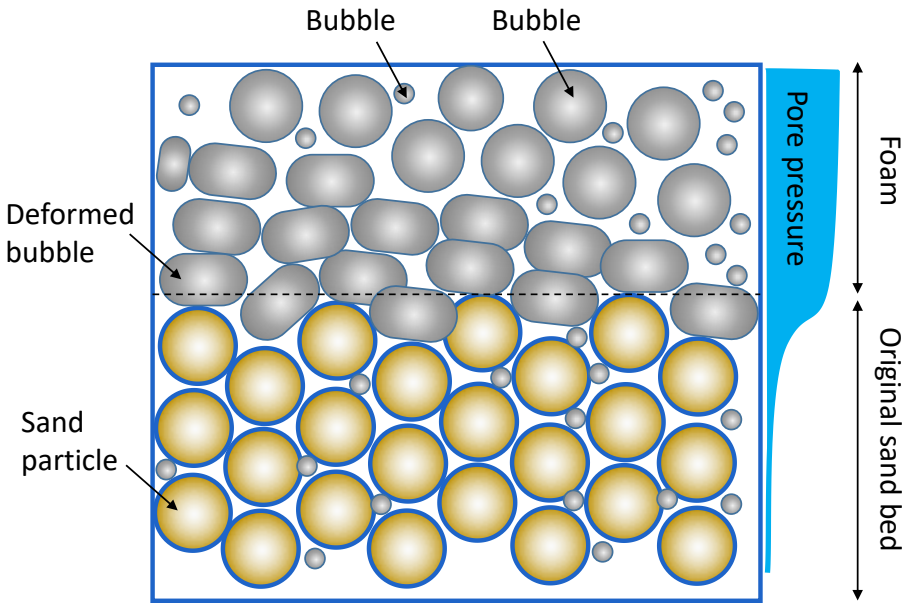

Fig. 8.1. Sketch of the boundary between the foam bubbles and the sand surface.

The impermeable layer formed within the sand surface leads to a significant reduction of the permeability close to the sand surface. Contrary to what is mentioned in literature (Bezuijen, 2012), a 'dry' foam (FER = 20) is not essential for formation of an impermeable muck, even a 'wet' foam (FER = 5) could form an impermeable layer. Important is that there is sufficient flow from the excavation chamber to the ground, allowing the foam bubbles to make a low permeable layer on top of the sand (see above).

The permeability of sand for foam decreased with increasing FER of the foam until FER of approximately 15 in this study. For higher FERs the permeability remains more or less constant.

The air pressure in the bubbles is a bit different from the pore water pressure. This difference, known from theory of unsaturated soil, probably influenced the pore pressure measurements. In the future experiments of foam infiltration, PPTs with filter papers are recommended to use in the measurement of pore water pressures. In one test using PPTs' with hydrophilic filter papers the influence of these papers on the results could be demonstrated.

8.3.2. SOIL-FOAM-MIXTURE

Analogous to 'deep filtration' of slurry containing sand, in the infiltration of soil-foam-mixture solid grains will also be deposited on the surface of the sand 'bed'. The permeability of the low permeable layer formed close to the sand surface depends on sand fractions of the soil-foam-mixture. From the experiments on infiltration of soil-foam-mixture, the following conclusions can be drawn:

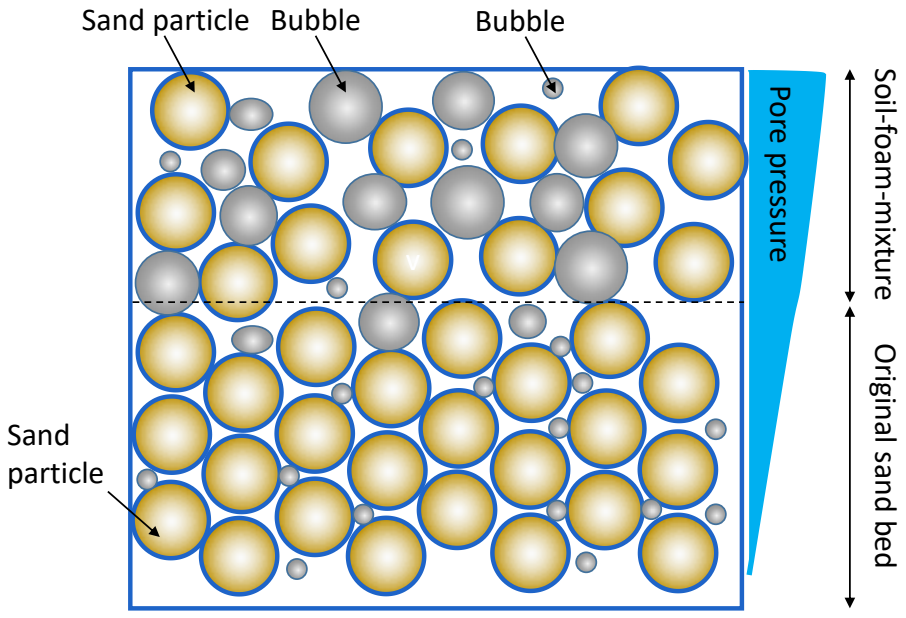

Fig. 8.2. Mechanism for the influence of the FIR for the soil-foam-mixture experiments.

Apart from the flow through the sand, there will be an extra water flow through the foam. The permeability of sand for water flow through the foam decreases with the increasing gas

fraction and the decreasing liquid fraction with a given solid fraction, or decreases with the increasing gas fraction and the decreasing solid fraction with a given liquid fraction. Furthermore, the permeability of sand for water flow through the foam decreases with FIR and a FIR larger than 40 is recommended for a sandy ground. A possible mechanism for the influence of the FIR for the soil-foam-mixture experiments is presented in Fig. 8.2. Again the lower grains indicates the original sand sample. The upper halve is the soil-foam-mixture for a low FIR.

With a low FIR, only a limited water flow will cause that there is a skeleton of loosely packed grains above the original sand bed. This is difficult to draw in a 2D picture, but in 3D the grains of the upper halve are more or less connected or there is effective stress because bubbles are trapped in between the sand grains. The trapped larger bubbles can now not migrate to the sand surface to form a low permeability layer. There can be some reduction of the sand permeability due to small grains invading into the sand. But a clean pressure drop as for foam is not observed. With a higher FIR there will not be enough sand to prevent all migration of the bubbles.

The mobility of foam flow depends on the fractions of gas, water and solid in the soil-foam-mixture. On one hand, with relatively high FIRs, larger gas fractions at given solid fraction reduces the mobility of foam flow. On the other hand, with relatively low FIRs, the difference in the mobility of foam flow between different fractions is small.

Foam infiltration results in a lower water permeability close to the sand surface for a constant FIR compared with experiments with a higher FER for FIRs below 50. For the foams with FER = 10, 15 and 20 the results are more or less the same. No clean trend was found for the permeabilities of the relatively deeper layers.

The measured permeabilities sand for water flow through the foam correspond to the model of Van Genuchten for unsaturated soil. With increasing volumetric water content (water fraction), the permeability decreases. It can be said that, therefore, after the ‘foam bubble infiltration’ the air is more or less immobile. The permeability is determined by the water film that is around the bubbles.

This finding agrees with the model explained above that the foam bubbles are after some flow trapped in the sand skeleton in the soil-foam-mixture. These trapped bubbles will have a concentration in the mixture, which depends on the original air concentration. In case of foam the bubbles migrate and there is a region (at the boundary with the sand) with a much higher air concentration and, again according to Van Genuchten, a much lower permeability.

8.4. COMPUTATIONAL MODEL ANALYSIS

Two analytical models of excess pore water pressure induced by TBM tunnelling in an aquifer were presented. The transient model simplifies the impact of slurry infiltration. It assumes that as soon as drilling stops immediately an impermeable filter cake is formed and the pressure decay that is measured in the ground is caused by elastic storage, and the steady state model takes into account the cake formation but not elastic storage. In steady state during drilling the transient model assumes a 1-dimensional flow in a semi-confined aquifer. The steady state model assumes circular flow in a permeable aquifer not taking into account possible low permeable top layers.

Even though the assumptions for the two models are quite different and the steady state solutions for the groundwater flow are different, the calculated results are quite comparable and for both cases can be fitted to the field measurements from the pore pressure transducers close to the tunnel. The predictions by the transient model are in a good agreement with the field measurements even at 100 m from the tunnel as are measured at the GHT, since the leakage length and elastic storage parameters are unknown and have to be fitted on the field measurements. But the steady state model cannot explain these pore water pressure fluctuations at 100 m from the tunnel, because it only considers the situation at the tunnel face. Based on the comparative analysis of the calculated results and the field measurements, it can be concluded:

The excess pore water pressure increases with drilling of the TBM because the cutter head of TBM cut off the infiltrated soil and then decreases during the standstill of TBM because the TBM stops.

For the situation of steady state groundwater flow, it is clear that the semi-confined aquifer in which the GHT is drilled is better modelled with a semi-confined aquifer model than with a model that assumes outflow in all directions. However, a 1D semi-confined aquifer model seems to be too simple and therefore a cylindrical symmetric model needs to be developed.

The way the infiltration of bentonite slurry is taken into account in the transient model, is quite a simplification of the real process. This is more or less 'compensated' by introducing the elastic storage in the soil.

The overall conclusion must be that agreement between theory and field measurements is no guarantee that the theory is right. This study shows that with two quite different theories such agreement can be reached. Therefore, the real issue is whether the theory is based on the right physics.

In addition to above conclusions, further general conclusions and consequences for practice can be gained from the discussion on the correlation between the steady state model (see also Chapter 7) and the experimental results in this study.

In the steady state model, it is assumed that, there is an infiltrated zone in the ground during the standstill of TBM and the thickness of this infiltrated zone is reduced linearly with time when drilling starts drilling with a constant velocity. This is the case of the infiltration of soil-foam-mixture in Chapter 6, where an infiltrated zone is formed in the soil. However, in the case of infiltration of clean slurry in Chapters 2 to 4, there will be an external filter cake formed on the soil surface and then most of the slurry pressure is transferred onto the soil skeleton through this cake rather than the infiltrated soil. Though the infiltration will further proceed after the cake formation, the slurry pressure will not drop with this further infiltration. The development of the excess pore water pressure after drilling starts will therefore be faster than that in the situation assumed in the steady state model in Chapter 7 that the excess pore water pressure decreases linearly with the increasing thickness of the infiltrated zone.

The input parameters for the steady state model are gained from the experiments performed in the conventional setup, thus the infiltration velocity is much higher than that in real tunnels. The development rate of excess pore water pressure therefore will be too high.

Chapter 4 also shows that after removing the filter cake, the slurry will further infiltrate into the soil. Though the removal of the impermeable layer in the foam infiltration tests in Chapter 5 has not been achieved, it can be expected that if this layer was removed, the foam will further infiltrate into the soil too. As mentioned in Chapter 2, the filter cake is vulnerable to damage even during the standstill. If this happens, the final infiltration distance will be much larger than the value assumed in the steady state model. The drop of piezometric head at the tunnel face will be larger than that predicted by the steady state model.

More significantly, in Chapter 5, 'deep filtration' was found in the infiltration of water-bentonite-sand slurry, which is also expected in the excavation of the TBM. In deep filtration, the infiltration distance and the pore fluid velocity will be much higher than in the infiltration of clean slurry and no filter cake will be formed. A similar situation was also found in the infiltration of soil-foam-mixture. It seems that such a situation is comparable to the assumption of an infiltrated zone in the steady state model. But the infiltration velocity and the infiltration distance determined by the conventional experiments on infiltration of clean slurry or foam probably are too low, since a filter cake or impermeable/low permeable layer will be formed after mud spurt.

General comment is:

In most field situations there is not 'clean foam' or 'clean slurry'. In these situations there is no filter cake or 'foam cake' and the 'old theory' (Bezuijen et al., 2016) applies. Only the infiltration length have to be determined differently and we have a much better understanding how these mechanism works.

For deep filtration in case of slurry containing sand, most of the low permeability soil is located in the original sand. However, for the foam the bubbles are trapped in the sand grains of the soil-foam-mixture mixture. Thus, the low permeability range is above the original sand layer. If this is the case this has consequences when drilling starts after stop. For foam most of the low permeable soil would be immediately removed when the cutter head starts drilling.

To better predict the excess pore water pressure by the steady state model, therefore, experiments of infiltration of slurry containing sand or soil-foam-mixture in the modified setup are recommended.

8.5. FUTURE WORK

In the experiments of infiltration of either bentonite slurry or foam, only one type of fine sand was used to make the sand sample. To investigate the range of applicability of the conclusions in this research experiments sand samples made of other types of sand, especially the coarse sands are highly recommended.

In the experiments of infiltration of foam, the capillary pressure was measured with the pore pressure transducers with filter papers. However, due to time limit, only few tests were carried out using such pore pressure transducers with hydrophilic filter papers. In the further research, such pore pressure transducers with both hydrophilic and hydrophobic filter papers are highly recommended to measure the pore pressures. New findings are anticipated.

To further understand the mechanism of infiltration of foam from soil-foam-mixture into saturated sand, yield stress and surface tension of the foam and size of the foam bubble have to be determined. Based on these determined parameters, it is expected to gain some understanding of the behaviour of soil-foam-mixture, like the minimum pressure gradient and the maximum size of the foam bubble for the mobility of foam bubbles, other than a simple line (Fig. 6.14).

In the experiments of infiltration of foam, the foam was placed on the sand surface at atmospheric pressure and was then pressurised to a desired pressure. In real tunnels, however, the foam is produced under a constant pressure. A modification to the setup shall be made to achieve the same condition of pressure as in the field.

Even though the computational model of the excess pore water pressures with considering the infiltration has been proposed in a homogenous ground, there is still some work to do in the case of a semi-confined aquifer. A model of cylindrical groundwater flow that takes into account the influence of radial flow in the horizontal plane, rather than a 1-D flow model therefore has to be developed. In a semi-confined aquifer, the way the infiltration affects the pore water pressure can be different too. Moreover, how to determine the input parameters for such a model based on the experiments shown in this thesis is also a key question.

BIBLIOGRAPHY

Amoun, S., Sharifzadeh, M., Shahriar, K., Rostami, J., Azali, S. T., 2017. Evaluation of tool wear in EPB tunneling of Tehran Metro, Line 7 Expansion. Tunnelling and Underground Space Technology, 61, 233–246.

Anagnostou, G. and Kovári, K., 1994. The Face Stability of Slurry-shield-driven Tunnels, Tunnelling and Underground Space Technology, 9 (2), 165–174.

API (American Petroleum Institute). 2003. Recommended Practice Standard Procedure for Field Testing Water-Based Drilling Fluids, 13B–1, 3rd ed., American Petroleum Institute, Washington, DC.

ASTM (American Society for Testing and Materials International), 2006. Standard test method for classification of soils for engineering purposes (Unified Soil Classification System). D2487–90.

Bakker, K. J., Bezuijen, A., 2008. 10 years of bored tunnels in the Netherlands. Proceeding 6th Int. Symposium on Underground Construction in Soft Ground, Shanghai.

Bezuijen, A., Schaminée, P. E. L., and Kleinjan, J. A., 1999. Additive testing for earth pressure balance shields. Proc. 12th Eur. Conf. on Soil Mech. and Geotech. Engrg., Amsterdam, Balkema, Rotterdam, 1991–1996.

Bezuijen, A., Schaminée, P. E. L., 2001. Simulation of the EPB-shield TBM in model tests with foam as additive, Proc. Int. Symp. on Modern Tunneling Science and Techn. Kyoto.

Bezuijen, A., 2002. The influence of permeability on the properties of a foam mixture in a TBM. 4th Int. Symp. on Geotechnical Aspects of Underground Construction in Soft Ground, Toulouse.

Bezuijen, A., Pruiksma, J. P., et al., 2006. Pore pressures in front of tunnel , measurements , calculations and consequences for stability of tunnel face. Tunnelling. A Decade of Progress. GeoDelft 1995-2005, 35–41.

Bezuijen, A., Talmon, A. M., 2008. Processes around a TBM. Proceeding 6th Int. Symposium

on Underground Construction in Soft Ground, Shanghai, 3–13.

Bezuijen, A., Sanders, M. P. M., den Hamer, D., 2009. Parameters that influence the pressure filtration characteristics of bentonite grouts. Géotechnique 59 (8), 717–721.

Bezuijen, A., 2010. Compensation grouting in sand: experiments, field experiences and mechanisms. Doctoral thesis. Delft University of Technology, Netherlands.

Bezuijen, A., 2011. Foam used during EPB tunnelling in saturated sand, description of mechanisms. Proceedings WTC 2011, Helsinki.

Bezuijen, A., 2012. Foam used during EPB tunnelling in saturated sand, parameters determining foam consumption, Proceedings WTC 2012, Bangkok.

Bezuijen, A., 2013. Foam parameters in saturated sand, theory and model tests. In: Proceedings of the ITA-AITES World Tunnel Congress, Geneva.

Bezuijen, A., Dias, T. G. S., 2017. EPB, chamber pressure dissipation during standstill. Proceeding IV International Conference on Computational methods in tunnelling and subsurface engineering. 1. 225–231.

Bezuijen, A., Steeneken, S. P., et al., 2016. Monitoring and Analysing Pressures Around a TBM, In: Proceeding of the 13th International Conference Underground Construction, Prague.

Bird, R. B., Stewart, W. E. and Lightfoot, E. N., 1960. Transport Phenomena. John Wiley & Sons, New York.

Bolton, M. D. and McKinley, J. D., 1997. Geotechnical properties of fresh cement grout pressure filtration and consolidation. Géotechnique 47 (2), 347–352.

Broere. A., 2001. Tunnel face Stability & New CPT applications. PhD thesis. Delft University of Technology, Netherlands.

Broere, W., 2003. Influence of Excess Pore Pressures on the Stability of the Tunnel Face. Reclaiming the Underground Space ITA, Amsterdam, 759–765.

Broere, W., van Tol, A.F., 2000. Influence of infiltration and groundwater flow on tunnel face stability. In: Proceeding of 3rd International Symposium on Geotechnical Aspects of

Underground Construction in Soft Ground, Tokyo, 339–344.

Broere, W., van Tol, A.F., 2001. Time-dependant infiltration and groundwater flow in a face stability analysis. In: Proceedings of International Symposium on Modern Tunnelling Science and Technology, Kyoto, 629–634.

Broere, W., 2016. Urban underground space: Solving the problems of today's cities. Tunnelling and Underground Space Technology 55, 245–248.

Budach, C., 2012. Extended application ranges of EPB-Shields in coarse grained soils. Dissertation, Ruhr-Universität Bochum.

Budach, C., Thewes, M., 2015. Application ranges of EPB shields in coarse ground based on laboratory research. Tunnelling and Underground Space Technology, 50, 296–304.

CURTA (China Urban Rail Transit Association), 2016. Statistics and analysis of urban rail transit in 2015. Urban Rapid Rail Transit, 29(4): 6–11. (In Chinese).

COB (Centre for Underground Contruction), 2000. Second Heinenoord Tunnel Evaluation Report, COB report K100-06. Gouda, Netherlands.

Condat Lubrifiants, 2015. New high-tech foaming agent for TBM. https://www.condat-lubricants.com/product/sealant-foam-lubricant-tunnel-boring/foaming-agents-epb/.

Davidson, J. M., Nielsen, D. R., Biggah, J. W. 1965. The Dependence of Soil Water Uptake and Release Upon the Applied Pressure Increment. Soil Science Society of America Journal, 30 (3), 298–304.

Den Hamer, D. A., Di Emidio, G., Bezuijen, A., Flores D. V., 2015. Preliminary test on modified clays for seawater resistant drilling fluids. Proceedings of the XVI ECSMGE Geotechnical Engineering for Infrastructure and Development, 1267–1272.

Dias, T. G. S., Bezuijen, A., 2016. A different view on TBM face equilibrium in permeable ground. ITA World Tunnel Congress 2016 – Uniting an Industry, San Francisco, USA.

EFNARC (ed.) (2005), Specification and guidelines for the use of specialist products for mechanised tunnelling (TBM) in soft ground and hard rock.

Galli, M., 2016. Bochum Rheological characterisation of Earth-Pressure-Balance (EPB) support medium composed of non-cohesive soils and foam. Doctoral thesis, Ruhr-Universität, Germany.

Hitachi Zosen Cooperation, 2017. 17.45 m Earth pressure balance shield tunneling machine for Seattle. http://www.hitachizosen.co.jp/english/products/products024.html.

Hammervold, W. L., Knutsen, Ø., Iversen, J. E., Skjæveland, S. M., 1998. Capillary pressure scanning curves by the micropore membrane technique. Journal of Petroleum Science and Engineering, 20. 253–258.

Huisman M. 1998. Static plastering, Theory and experiments, BTL – report 34, WL | Delft Hydraulics J1384. (In Dutch).

Kaalberg, F.J., Ruigrok, J.A.T. et al., 2014. TBM face stability & excess pore pressures in close proximity of piled bridge foundations controlled with 3D FEM. In: Proceeding of 8th International Symposium on Geotechnical Aspects of Underground Construction in Soft Ground, Seoul.

Kam, S. I., Gauglitz, P. A., Rossen, W. R. 2002. The yield stress of foamy sands. Colloids and Surfaces A: Physicochemical and Engineering Aspects, 202, 53–62.

Krause T., 1987. Schildvortrieb mit flüssigkeits- und erdgestützter Ortsbrust. PhD thesis, Technischen Universität Carolo-Wilhelmina, Braunschweig. (In German).

Maidl, U., 1995. Erweiterung der Einsatzbereiche der Erddruckschilde durch Bodenkonditionierung mit Schaum. Doctoral thesis, Ruhr-Universität Bochum, AG Leitungsbau und Leitungsinstandhaltung, Germany. (In German).

Maidl, U., Pierri, J., 2014. Innovative hybrid EPB tunnelling in Rio de Janeiro. Geomech. Tunn. 7, 55–63.

Merrit, A., Jefferis, S., Storry, R., Brais, L., 2013. Soil conditioning laboratory trials for the Port of Miami Tunnel, Miami, Florida, USA. In: Proceedings of the ITA-AITES World Tunnel Congress, Geneva.

Merritt, A. S., Mair, R. J. (2006). Mechanics of tunnelling machine screw conveyors: model tests. Géotechnique 56 (9), 605–615.

McKinley, J. D., Bolton, M. D., 1999. A geotechnical description of fresh cement grout: filtration and consolidation behaviour. Magzine of Concrete Research, 51 (5), 295–307.

Mooney, M. A., Wu, Y., Parikh, D., Mori, L., 2017. EPB granular soil conditioning under pressure. Keynote Paper. In: Proc. 9th Intl. Symp. Geotechnical Aspects of Underground Construction in Soft Ground, Sao Paulo.

Mori, L., Mooney, M., Cha, M., 2018. Characterizing the influence of stress on foam conditioned sand for EPB tunnelling. Tunnelling and Underground Space Technology, 71, 454–465.

Oung, O., Bezuijen, A., 2003. Selective pore pressure transducers for use in model tests to study two-phase flow in porous media. International Journal of Physical Modelling in Geotechnics 3 (4), 31–41.

Quebaud, S., Sibai, M., Henry, J.P., 1998. Use of chemical foam for improvements in drilling by earth pressure balanced shields in granular soils, Tunnelling and Underground Space Technology, 13(2), 173–180.

Peila, D., Oggeri, C., Vinai, R., 2007. Screw conveyor device for laboratory tests on conditioned soils for EPB tunneling operations, Journal of Geotechnical and Geoenvironmental Engineering, ASCE, 133, 1622–1625.

Peila, D., Oggeri, C., Borio, L., 2009. Using the slump test to assess the behaviour of conditioned soil for EPB tunnelling, Environmental & Engineering Geoscience, XV (3), 167–174.

Peña, M., 2003. Soil conditioning for sands, Tunnels & Tunnelling international, July, 40–42.

Quebaud, S., Sibai, M., Henry, J. P., 1998. Use of chemical foam for improvements in drilling by earth pressure balanced shields in granular soils, Tunnelling and Underground Space Technology, 13(2), 173–180.

Ripperger, S., Gösele, W., Alt., C., 2012. Filtration, 1. Fundamentals, Ullmann's Encyclopedia

of Industrial Chemistry.

Steeneken, S. P., 2016. Excess pore pressures near a slurry tunnel boring machine: modelling and measurements. MSc Thesis, Delft University of Technology, Netherlands.

Talmon, A. M., Bezuijen, A., 2009. Simulating the consolidation of TBM grout at Noordplaspolder. Tunnelling and Underground Space Technology, 24, 493–499.

Talmon, A. M., Mastbergen, D. R., and Huisman, M. 2013 Invasion of pressurised clay suspensions into granular soil. Journal of Porous Media, 16, 351–365.

Thewes, M. and Budach, C., 2010. Soil conditioning with foam during EPB tunnelling, Geomechanics and Tunnelling, 3(3), 256–267.

Thewes, M. and Budach, C., 2011. Soil Conditioning for EPB Shields: New Results from Research on Foams and Soil-Foam-Mixtures. Proceedings WTC 2011, Helsinki.

Van Genuchten, 1980. A closed-form equation for predicting the hydraulic conductivity of unsaturated soils. Soil Science Society of American Journal, 44, 892–898.

Vinai, R., Oggeri, C., Peila, D., 2008. Soil conditioning of sand for EPB applications: a laboratory research, Tunnelling and Underground Space Technology, 23 (3), 308–317.

Winterwerp, J. C. and van Kesteren, W. G. M., 2004. Introduction to the Physics of Cohesive Sediment in the Marine Environment, Developments in Sedimentology, 56, Elsevier, New York.

Xanthakos, P., 1979. Slurry Walls, 622. New York: McGraw Hill.

Xu, T., Bezuijen, A., Dias, T. G. S., 2017. Slurry infiltration ahead of slurry TBM's in saturated sand: laboratory tests and consequences for practice. 9th International Symposium on Geotechnical Aspects of Underground Construction in Soft Ground, Sao Paulo.

Zizka, Z., Thewes, M., 2016. Recommendations for Face Support Pressure Calculations for Shield Tunnelling in Soft Ground, Deutscher Ausschuss fuer unterirdisches Bauen e. V. German Tunnelling Committee (ITA-AITES).

Zizka, Z., Schoesser, M., Thewes, M., 2017. Excavation cycle dependent changes of hydraulic

properties of granular soil at the tunnel face during slurry shield excavation, Proceedings of 9th International Symposium on Geotechnical Aspects of Underground Construction in Soft Ground, Sao Paulo.